

Heat Structure (HS) Package Reference Manual

The MELCOR Heat Structure (HS) package calculates heat conduction within an intact, solid structure and energy transfer across its boundary surfaces. The modeling capabilities of heat structures are general and can include pressure vessel internals and walls, containment structures and walls, fuel rods with nuclear or electrical heating, steam generator tubes, piping walls, etc.

This document provides detailed information about the models, solution methods, and timestep control that are utilized by the HS package. Section 1 is an introduction to heat structure modeling and the calculation procedure. Section 2 provides details on the heat and mass transfer models. The solution methods utilized are discussed in Section 3, and timestep control is summarized in Section 4.

Information which is necessary to execute the HS package with other packages in the MELCOR code is found in the HS Users' Guide.

Contents

1.	Introduction	5
2.	Detailed Models	9
2.1	Finite-Difference Equations for Interior.....	10
2.1.1	Nodalization at Interior Temperature Nodes	11
2.1.2	Difference Approximation at Interior Nodes	14
2.1.3	Finite-Difference Equations at Interior Temperature Nodes.....	15
2.2	Finite-Difference Equations at Boundary Surfaces	16
2.2.1	Boundary Condition Coefficients.....	17
2.2.2	Nodalization at Boundary Temperature Nodes	19
2.2.3	Difference Approximation at Boundary Nodes	23
2.3	Power Sources	27
2.3.1	Internal Power Sources.....	27
2.3.2	Surface Power Sources	28
2.3.3	Energy Transferred by Other Packages.....	28
2.4	Pool Fractions	29
2.4.1	Rectangular Geometry.....	31
2.4.2	Cylindrical Geometry.....	31
2.4.3	Spherical Geometry	33
2.4.4	Hemispherical Geometry	33
2.5	Thermal Properties.....	33
2.5.1	Thermal Conductivity and Volumetric Heat Capacity.....	33
2.5.2	Modifications for Degassible Materials.....	33
2.6	Heat Transfer	34
2.6.1	Atmosphere Convection Heat Transfer.....	38
2.6.2	Radiation Heat Transfer.....	47
2.6.3	Pool Convection Heat Transfer.....	49
2.6.4	Pool Boiling Heat Transfer	52
2.6.5	Energy Transfer to Control Volumes.....	58
2.7	Mass Transfer	59
2.7.1	Sherwood Number for Diffusion Mass Transfer.....	60
2.7.2	Condensation and Evaporation with Noncondensibles.....	61
2.7.3	Mass-Energy Transfer to Control Volumes	62
2.8	Liquid Film Modeling	64
2.8.1	Film Models.....	64
2.8.2	Film Tracking Model.....	65
2.9	Stored Energy of a Heat Structure	66
2.10	Degassing Model.....	68
2.11	Ice Condenser Model	70
2.12	Steel Melt Model.....	71
2.13	Communication with Other Packages	71

HS Package Reference Manual

3.	Solution Methods	72
3.1	Iteration Strategy	73
3.2	Steady-State Convergence Criteria	75
3.3	Transient Convergence Criteria.....	76
4.	Timestep Control.....	77
	APPENDIX A: Sensitivity Coefficients	78
	References	86

List of Figures

Figure 1.1	Heat Structure in a Control Volume	6
Figure 2.1	Nodalization in Interior of a Heat Structure	12
Figure 2.2	Nodalization at Boundary Surfaces of a Heat Structure	20

List of Tables

Table 2.1	Surface and Volume Weights in Interior	13
Table 2.2	Surface and Volume Weights at Boundary Surfaces.....	20
Table 2.3	Constants for HS Package Heat Transfer Correlations	39

1. Introduction

The Heat Structure (HS) package calculates heat conduction within an intact, solid structure and energy transfer across its boundary surfaces into control volumes. This document is the reference manual for the HS package. It contains the following information for this package:

- (1) detailed models,
- (2) solution methods, and
- (3) timestep control.

This section describes the modeling of a heat structure in the MELCOR code and provides a discussion of the calculation procedure which is used to obtain the temperature distribution and energy transfer for each heat structure and to calculate its interactions with structures in other packages.

A heat structure is an intact, solid structure which is represented by one-dimensional heat conduction with specified boundary conditions at each of its two boundary surfaces. The modeling capabilities of heat structures are general and can include pressure vessel internals and walls, containment structures and walls, fuel rods with nuclear or electrical heating, steam generator tubes, and piping walls.

Figure 1.1 illustrates a heat structure between two control volumes. A heat structure is inclined at some angle with respect to the vertical and is partially immersed. Although the geometry shown here is rectangular, a heat structure may have a rectangular, cylindrical, spherical, or hemispherical geometry.

The heat structure in Figure 1.1 is nodalized with N temperature nodes. The nodalization is specified by user input and may be nonuniform, i.e., the distance between temperature nodes need not be the same. Node 1 is the temperature node at the left boundary surface for a rectangular geometry or at the inside boundary surface for a cylindrical, spherical, or hemispherical geometry. Node N is the temperature node at the right boundary surface for a rectangular geometry or at the outside boundary surface for other geometries.

The region between two adjacent temperature nodes is called a mesh interval. Each mesh interval may contain a different material. The material in each mesh interval is specified by user input. The Material Properties package provides thermal properties for each material through an interface with the HS package. Most materials commonly found in PWRs and BWRs are included in the Material Properties package default database, and properties for materials which are not included can easily be defined through Materials Properties package user input (refer to the MP package documentation).

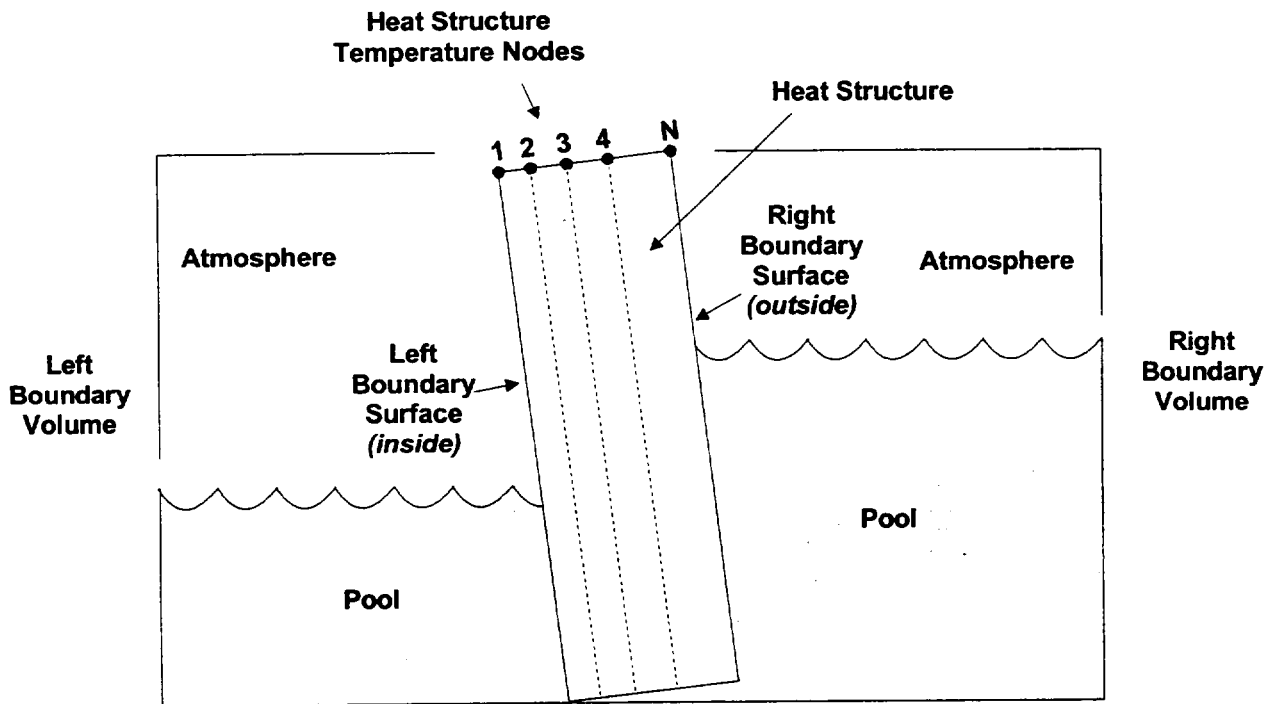


Figure 1.1 Heat Structure in a Control Volume

An internal power source may be specified for a heat structure. Its spatial dependence is specified by user input and may vary for each mesh interval. Its time dependence is given by a user-specified tabular function or control function.

Each heat structure has two boundary surfaces—left and right for rectangular geometries or inside and outside for cylindrical, spherical, or hemispherical geometries. At each boundary surface one of the following boundary conditions is specified:

- (1) symmetry (adiabatic)
- (2) convective with calculated heat transfer coefficient,
- (3) convective with calculated heat transfer coefficient and a specified surface power source function,
- (4) convective with specified heat transfer coefficient function,
- (5) specified surface temperature function, and
- (6) specified surface heat flux function.

If a convective boundary condition is selected for a boundary surface, a control volume must be specified as its boundary volume. Furthermore, the entire boundary surface must

fit within its boundary volume—that is, the bottom of the surface (user value HSALT) must equal or exceed the elevation of the bottom of the control volume specified in the CVH user input, and the top of the surface (calculated from HSALT and the surface length and orientation) must not exceed the elevation of the top of the control volume. No boundary volume is permitted for a symmetry or specified surface temperature boundary condition and a boundary volume for the specified heat flux boundary condition is a user option.

If a boundary volume is specified for a surface, then some additional data are required through user input. For each boundary surface with a boundary volume, these data are its

- (1) surface area,
- (2) characteristic length (the dimension used in calculating the Reynolds, Grashof, Nusselt, and Sherwood numbers),
- (3) axial length (length of structure along boundary surface, used to determine pool fraction),
- (4) type of flow over the surface (internal or external; used in calculating the Nusselt number), and
- (5) critical pool fractions for pool and atmosphere heat transfer.

The pool fraction of a heat structure boundary surface is the fraction of its surface area in the pool of its boundary volume. Pool fractions and critical pool fractions permit a weighting of heat and mass transfer to the boundary volume atmosphere and pool. These are discussed in detail in Section 2.4.

If a convective boundary condition with calculated heat transfer coefficient is specified, then an extensive set of correlations is available for calculating natural or forced convection to the pool and atmosphere. Pool boiling heat transfer is calculated if the temperature of a heat structure surface is above the boundary volume saturation temperatures by utilizing correlations for nucleate boiling, critical heat flux, film boiling, and transition boiling.

Radiation heat transfer from a heat structure surface to the boundary volume pool is calculated during boiling. Radiation heat transfer can also be specified between a heat structure surface and the boundary volume atmosphere. Note, however, that radiation heat transfer to the atmosphere will occur only if the atmosphere contains water vapor (steam) and/or carbon dioxide; all other gases are considered to be non-absorbing by MELCOR. Two options, an equivalent band model and a gray gas model, are currently available. Radiation between user-specified pairs of surfaces may also be modeled, as described in Section 2.6.2.2. Radiation heat transfer between the COR structures and HS structures is discussed in the COR package documentation.

HS Package Reference Manual

Mass transfer between a heat structure surface and the boundary volume atmosphere is modeled using correlations or expressions for calculating mass flux. Models include condensation and evaporation in the presence of noncondensibles with an appropriate limit for pure steam, and flashing in any environment. Liquid films on heat structure surfaces are also modeled so that condensate transferred from the boundary volume atmosphere and liquid deposited by other packages can be treated. An optional film tracking model is available to track condensate film drainage from structure to structure. The film tracking model is activated when the user defines one or more network(s) of connected structures, such as stacked cylindrical sections to represent the steam generator tubes and/or cylindrical shells capped by a hemisphere to represent a containment dome. The user also specifies a drainage pattern for each network, which consists of drainage destinations and fractions for the drainage from each structure in the network. Drainage from a structure surface may be partitioned between three destination types:

- (1) the surface of one or more additional structures in the network,
- (2) "rain" which is passed to the MELCOR Containment Sprays (SPR) package via the Transfer Process (TP) package, and/or
- (3) the pool of the CVH volume associated with the surface.

The user may also designate an external source of water for any structure in the network via tabular function input or a control function. External sources are primarily intended to allow the user to model the source for a passive containment cooling system or some such similar cooling device. When the film tracking model is active, the film thickness is calculated as a function of the condensate flow rate throughout the network.

Mass transfer affects the temperature distribution within a heat structure by its energy flux at the surface. This energy flux due to mass transfer is included in the boundary conditions for the conduction calculations, and film/atmosphere interfacial temperatures are calculated simultaneously with the structure node temperatures. The volume occupied by liquid films affects the virtual volume tracked by the CVH package, and the presence of liquid films also affects the rate and accumulation of radionuclides deposited on the surfaces by the RN package (see RN documentation). Decay heat from deposited radionuclides is treated as power source at the surface in the equation for the surface temperature.

Finite-difference equations are used to advance the temperature distribution of a heat structure in time during MELCOR execution or to obtain its steady-state temperature distribution during MELGEN execution if specified by user input. These equations are obtained from an integral form of the one-dimensional heat conduction equation and boundary condition equations utilizing a fully implicit numerical method. The finite-difference approximation is a tridiagonal system of N equations (or $N + 1$ or $N + 2$ if there is a liquid film on one or both surfaces of the structure) for a heat structure with N temperature nodes (or $N + 1$ or $N + 2$ temperature nodes if there is liquid film on one or

both surfaces of the structure). The solution of this system is obtained using the standard solution algorithm for a tridiagonal system of linear equations.

A degassing model is provided for the release of gases from materials which are contained in heat structure mesh intervals. Input may be provided, for example, to represent the release of water vapor or carbon dioxide from concrete as its temperature increases. The HS package calculates a constant gas release rate over the degassing temperature range and modifies the thermal properties over this range to account for the energy associated with the gas production and release. The degassing model is also used in a modified form to treat ice condensers.

Communication of mass and energy changes to other packages is achieved through well-defined interfaces.

The remainder of the reference manual amplifies this calculation procedure. An enumeration and description of all models employed in the HS package calculations are included in Section 2. The solution methods used by the HS package are discussed in Section 3. Section 4 elaborates on the timestep control use by this package.

The references for the HS Package Reference Manual are found in Section 5. Appendix A contains information on the sensitivity coefficients used in the HS package.

2. Detailed Models

The modeling of a heat structure in the MELCOR Code System and the calculation procedure for the HS package are discussed in Section 1. This section provides a detailed description of the models that are utilized by the HS package in the calculation procedure.

Heat conduction within a heat structure is modeled by the heat conduction equation in one spatial dimension. This equation and the specification of boundary conditions constitute a well-defined mathematical problem for the temperature distribution of a heat structure. However, the generality of boundary conditions, the inclusion of surface power sources and mass transfer at each boundary surface, temperature-dependent thermal properties, spatial-dependent materials, and the variety of geometries preclude the possibility of analytic solutions for the temperature distribution. Therefore, the HS package utilizes numerical methods for the determination of the temperature distribution for each heat structure. The description of detailed models in the HS package begins in Section 2.1 with a presentation of the finite-difference equations that approximate the heat conduction equation within a heat source. The finite-difference equations that approximate the heat conduction equation at the boundary surfaces are presented in Section 2.2.

The finite-difference equations of Sections 2.1 and 2.2 require specification or calculation of the following:

HS Package Reference Manual

- (1) power sources,
- (2) pool fractions,
- (3) thermal properties,
- (4) heat transfer,
- (5) mass transfer, and
- (6) liquid film modeling.

Sections 2.3 through 2.8 provide the detailed models which specify these items.

Knowledge of the temperature distribution of a heat structure permits the calculation of its stored energy. The definition of stored energy of a heat structure is given in Section 2.9 within the context of the approximations of the HS package.

The thermal interactions between heat structures and control volumes result in the transfer of mass and energy between the CVH and HS packages. The HS package calculates such transfers between modules for the following:

- (1) heat flux,
- (2) liquid film evaporation and condensation, and
- (3) degassing.

The detailed modeling of these phenomena in the HS package is discussed in Sections 2.6, 2.7, and 2.10. The COR package calculates heat transfer from the core to the bounding heat structures and passes the resulting energy transfers to the appropriate heat structures through an interface with the HS package (see COR package documentation for further details).

2.1 Finite-Difference Equations for Interior

The equation that governs conduction heat transfer in the interior of a heat structure is the one-dimensional heat conduction equation. This equation has the form

$$C_p \frac{\partial T}{\partial t} = \frac{1}{A} \frac{\partial}{\partial x} \left(k A \frac{\partial T}{\partial x} \right) + U \quad (2.1)$$

where

C_p	= volumetric heat capacity (product of heat capacity at constant pressure and density)
T	= temperature
$\frac{\partial}{\partial t}$	= partial derivative with respect to time
A	= heat transfer area
k	= thermal conductivity
$\frac{\partial}{\partial x}$	= partial derivative with respect to spatial variable
U	= volumetric power

The heat conduction equation is a parabolic partial differential equation. The HS package must solve it with boundary and initial conditions to determine the temperature distribution at each point in a heat structure. Sections 2.1.1 and 2.1.2 discuss the finite-difference approximation of Equation (2.1) in the interior of a heat structure.

2.1.1 Nodalization at Interior Temperature Nodes

The finite-difference approximation of the heat conduction equation requires a spatial partitioning of the heat structure into a finite number of temperature nodes. Temperature nodes must be located at the boundary surfaces and at interfaces between different materials. Additional nodes may be located at arbitrary locations within individual materials.

The region between two adjacent temperature nodes is called a mesh interval. For rectangular geometries, the node locations are relative to the node at the left boundary; for cylindrical geometries, they are relative to the axis of the cylinder; and for spherical or hemispherical geometries, they are relative to the center of the sphere. The location of the temperature nodes increases in a monotonic manner from the node at the left or inside boundary surface.

Figure 2.1 illustrates the nodalization of the interior of a heat structure near the n -th temperature node. This figure contains three temperature nodes and the mesh intervals for which they are the boundary points. For a rectangular geometry, the HS volume which is depicted in Figure 2.1 is part of a rectangular solid; for a cylindrical geometry, it is part of a cylindrical shell; and for a spherical or hemispherical geometry, it is part of a spherical shell. The quantities represented in Figure 2.1 are:

HS Package Reference Manual

- N = number of temperature nodes in heat structure
 n = interior node number (2, 3, ..., N-1)
 X = location of temperature node
 ΔX_n = $X_{n+1} - X_n$, length of n -th mesh interval
 k = thermal conductivity of material
 C_p = volumetric heat capacity of material
 U = volumetric power source

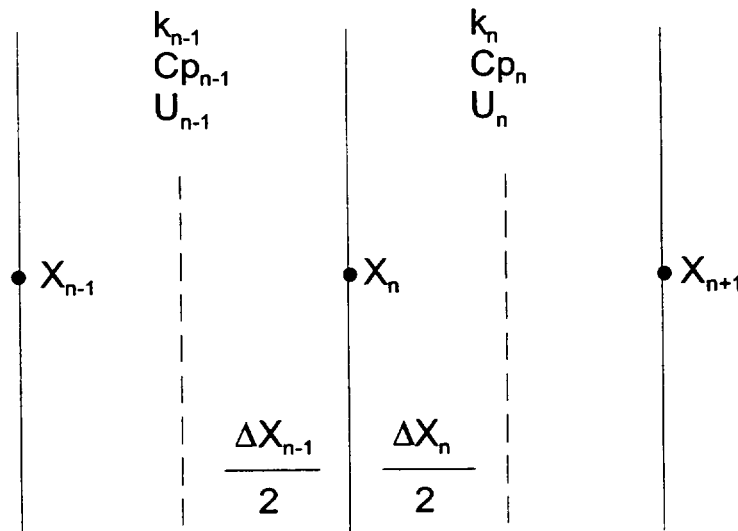


Figure 2.1 Nodalization in Interior of a Heat Structure

This figure also shows thermal properties and volumetric power sources in the mesh intervals adjacent to the n -th temperature node. These quantities are present in the finite-difference equations and are discussed in Sections 2.3 and 2.5.

To allow a more general representation of the equations and to consolidate expressions that define the numerical approximation, the following geometrical quantities are used [1]:

- HSL_n = left surface weight for n -th temperature node
 HVL_n = left volume weight for n -th temperature node
 HSR_n = right surface weight for n -th temperature node

HVR_n = right volume weight for n -th temperature node

Table 2.1 Surface and Volume Weights in Interior

Rectangular Geometries	Equation
$HSL_n = 1/\Delta X_{n-1}$	(2.2)
$HVL_n = \Delta X_{n-1}/2$	(2.3)
$HSR_n = 1/\Delta X_n$	(2.4)
$HVR_n = \Delta X_n/2$	(2.5)
Cylindrical Geometries	Equation
$HSL_n = 2\pi (X_n - \Delta X_{n-1}/2)/\Delta X_{n-1}$	(2.6)
$HVL_n = \pi [X_n^2 - (X_n - \Delta X_{n-1}/2)^2]$	(2.7)
$HSR_n = 2\pi (X_n + \Delta X_n/2)/\Delta X_n$	(2.8)
$HVR_n = \pi [(X_n + \Delta X_n/2)^2 - X_n^2]$	(2.9)
Spherical Geometries	Equation
$HSL_n = 4\pi (X_n - \Delta X_{n-1}/2)^2/\Delta X_{n-1}$	(2.10)
$HVL_n = (4\pi/3) [X_n^3 - (X_n - \Delta X_{n-1}/2)^3]$	(2.11)
$HSR_n = 4\pi (X_n + \Delta X_n/2)^2/\Delta X_n$	(2.12)
$HVR_n = (4\pi/3) [(X_n + \Delta X_n/2)^3 - X_n^3]$	(2.13)
Hemispherical Geometries	Equation
$HSL_n = 2\pi (X_n - \Delta X_{n-1}/2)^2/\Delta X_{n-1}$	(2.14)
$HVL_n = (2\pi/3) [X_n^3 - (X_n - \Delta X_{n-1}/2)^3]$	(2.15)

$HSR_n = 2\pi(X_n + \Delta X_n / 2)^2 / \Delta X_n$	(2.16)
$HVR_n = (2\pi/3)[(X_n + \Delta X_n / 2)^3 - X_n^3]$	(2.17)

The surface and volume weights in the interior of a heat structure are defined in Table 2.1. The interior temperature nodes correspond to $n = 2, 3 \dots, N-1$. The weights for $n = 1$ and N are defined in Section 2.2.1.

The surface and volume weights may be interpreted by considering for each geometry the rectangular solids, cylindrical shells, and spherical shells which are bordered by a temperature node and have thicknesses equal to half the length of the mesh intervals adjacent to this node. For all geometries, each surface weight has a factor that is the reciprocal of the length of the appropriate mesh interval. These weights appear in the gradient terms of the difference equations. For rectangular geometries, the other factors in the surface weight and the volume weight are the surface area and volume per unit area of one of the solids, respectively. For cylindrical geometries, they are the surface area and volume per unit axial length of one of the shells; and for spherical or hemispherical geometries, they are the surface area and volume of one of the shells. By definition, $HSL_{n+1} = HSR_n$ for all geometries, which ensures conservation.

2.1.2 Difference Approximation at Interior Nodes

The finite-difference equations are obtained from an integral form of the heat conduction equation. Consider multiplying Equation (2.1) by the area term and integrating the result over a heat structure. This integral equals the sum of integrals each of which is evaluated over a solid that is bounded by the dashed lines in Figure 2.1. The finite-difference approximation at the n -th interior temperature node is obtained from the integral of this equation over the solid that is bounded by these dashed lines. This approximation has the form

$$G_n (T_n^{m-1} - T_n^m) / \Delta t_m = k_{n-1} HSL_n (T_{n-1} - T_n) + k_n HSR_n (T_{n+1} - T_n) + (U_{n-1} HVL_n + U_n HVR_n) \quad (2.18)$$

where

- T_n^m = temperature of n -th node at time t_m
- G_n = $Cp_{n-1} HVL_n + Cp_n HVR_n$
- U_n = volumetric power for n -th mesh interval

- Δt_m = timestep for m -th computational cycle
 n = quantity at n -th temperature node or mesh interval
 m = quantity at time t_m
 $m+1$ = quantity at time $t_m + \Delta t_m$

The time superscript for most of the terms in this equation is omitted. If all are m , then the finite-difference formulation is fully explicit. If all are $m + 1$, then the formulation is fully implicit. The fully implicit method is used by the HS package, so

$$G_n^{m+1} (T_n^{m+1} - T_n^m) / \Delta t_m = d_n^{m+1} \quad (2.19)$$

where

$$d_n^i = \text{right side of Equation (2.18) at time } t_i$$

For steady-state initialization calculations, the appropriate difference equation is

$$d_n = 0 \quad (2.20)$$

2.1.3 Finite-Difference Equations at Interior Temperature Nodes

The finite-difference equation at each interior temperature node is obtained by expanding Equation (2.19) or (2.20) and collecting the temperature terms at the $m + 1$ time level on the left. This equation is

$$A_{n-1}^{m+1} T_{n-1}^{m+1} + B_n^{m+1} + C_n^{m+1} T_{n+1}^{m+1} = D_n^{m+1} \quad (2.21)$$

where, in addition to previously defined quantities,

$$A_n^{m+1} = -k_{n-1}^{m+1} HSL_n \Delta t_m$$

$$C_n^{m+1} = -K_n^{m+1} HSR_n \Delta t_m$$

$$B_n^{m+1} = A_n^{m+1} - C_n^{m+1} + a G_n^{m+1}$$

$$D_n^{m+1} = a G_n^{m+1} T_n^m + (U_{n-1}^{m+1/2} HVL_n + U_n^{m+1/2} HVR_n) \Delta t_m$$

HS Package Reference Manual

- a = 1 for transient calculations
= 0 for steady-state calculations
- n = 2, 3, ..., $N-1$

The value of the power, U , is evaluated as the average of old and new time values in order to more accurately reflect the desired input energy. The result of applying Equation (2.21) to a heat structure with N temperature nodes is a tridiagonal system of $N-2$ equations for the interior temperature nodes.

2.2 Finite-Difference Equations at Boundary Surfaces

The numerical calculation of the temperature distribution of a heat structure not only requires a finite-difference approximation of the heat conduction equation at interior temperature nodes, but also a finite-difference approximation of this equation and the boundary condition at each boundary surface.

There are two basic cases to consider at the surfaces of a structure:

- (1) the case when there is no liquid film on the surface, and
- (2) the case when there is a liquid film on the surface.

If there is no liquid film, then a boundary condition is applied to the structure surface and used to calculate the structure surface temperature. If a liquid film exists, then an additional mesh interval, consisting of the film bounded by the structure surface temperature node on the inside and the film/atmosphere interfacial temperature node on the outside, is defined, and a conduction equation for the film/atmosphere interfacial temperature is added to the set of N equations for the structure node temperatures. In this case, the equation for the structure surface (i.e., the structure/film interface) temperature is similar to the equations for the temperatures at the interior nodes, except that the half mesh interval on the outside consists of half of the liquid film instead of structure material. Hence, if there is no liquid film on either surface of the structure, the tridiagonal set will consist of N equations ($N-2$ for interior nodes and 2 for the two surface node temperatures), while the set will consist of $N+1$ (or $N+2$) temperature equations, if there is a liquid film on one (or both) surfaces of the structure.

Only certain types of boundary conditions are permitted if mass transfer (liquid film condensation/evaporation) is to be treated; film formation is prohibited if an adiabatic, specified surface heat flux or specified surface temperature boundary condition is imposed.

In the discussion that follows, it is to be understood that the boundary condition is applied at the film/atmosphere interface and not the structure/film interface if a liquid

film exists on the surface of the structure. The general form of the boundary condition at the surface of a heat structure is

$$\alpha T + \beta \frac{dT}{dN} = \gamma \quad (2.22)$$

where

α = first boundary condition coefficient

β = second boundary condition coefficient

γ = third boundary condition coefficient

T = temperature of surface

$\frac{dT}{dN}$ = gradient of temperature in direction of outward normal

This expression is implicit in the surface temperature, which is determined iteratively. All variables in this expression that are part of the heat structure package database (structure temperatures and properties that are functions of the structure temperature) are treated implicitly during the iteration procedure. Variables from other MELCOR packages (CVH temperatures and energy deposited by other packages) must be treated explicitly because of the explicit coupling between all MELCOR packages. All permitted boundary conditions can be put into this form as shown below.

2.2.1 Boundary Condition Coefficients

2.2.1.1 Symmetry (Adiabatic)

The symmetry boundary condition is represented by

$$\frac{dT}{dN} = 0 \quad (2.23)$$

For this boundary condition, the boundary condition coefficients are

$$\alpha = 0$$

$$\beta = 1$$

$$\gamma = 0$$

2.2.1.2 Convective (Calculated or Specified Heat Transfer Coefficients)

The convective boundary condition is represented by

$$-k \frac{dT}{dN} + S = (h_{atm} + h_{atmr})(1 - x_{pool})(T - T_{atm}) + h_{pool}x_{pool}(T - T_{pool}) \quad (2.24)$$

where

- k = thermal conductivity
- S = surface energy flux (flowing into heat structure)
- h_{atm} = atmosphere heat transfer coefficient
- h_{atmr} = atmosphere radiation heat transfer coefficient
- x_{pool} = fraction of surface in pool of boundary volume
- T_{atm} = temperature of atmosphere in boundary volume
- h_{pool} = pool heat transfer coefficient
- T_{pool} = temperature of pool in boundary volume

For these boundary conditions, the coefficients are

$$\alpha = h_{pool}x_{pool} + (h_{atm} + h_{atmr})(1 - x_{pool})$$

$$\beta = k$$

$$\gamma = h_{pool}x_{pool}T_{pool} + (h_{atm} + h_{atmr})(1 - x_{pool})T_{atm} + S$$

2.2.1.3 Specified Surface Heat Flux

For specified heat flux at the surface, the boundary condition is represented by

$$-k \frac{dT}{dN} = q'' \quad (2.25)$$

where

q'' = specified heat flux at surface (positive out)

For these boundary conditions, the coefficients are

$$\alpha = 0$$

$$\beta = k$$

$$\gamma = -q''$$

2.2.1.4 Specified Surface Temperature

The boundary condition for a specified surface temperature is represented by

$$T = T_{surf} = \text{specified surface temperature} \quad (2.26)$$

For these boundary conditions, the coefficients are

$$\alpha = 1$$

$$\beta = 0$$

$$\gamma = T_{surf}$$

2.2.2 Nodalization at Boundary Temperature Nodes

Figure 2.2 illustrates the geometry of a heat structure near the surface temperature nodes of a heat structure. This figure contains two temperature nodes and the mesh intervals for which they are the boundary points at both surfaces. It also depicts the condensate films which may or may not be present on each boundary surface. For all geometries, the volumes which are depicted in this figure are as described in Section 2.1.1. The quantities represented in Figure 2.2 are:

N = number of temperature nodes in heat structure

X = location of temperature node

ΔX_n = $X_{n+1} - X_n$, length of n -th mesh interval

k = thermal conductivity of material

c_p = volumetric heat capacity of material

HS Package Reference Manual

- U = volumetric power
- S = surface power
- δ_f = thickness of liquid film
- m_f = mass of liquid film
- h_f = specific enthalpy of liquid film
- C_p specific heat of liquid film

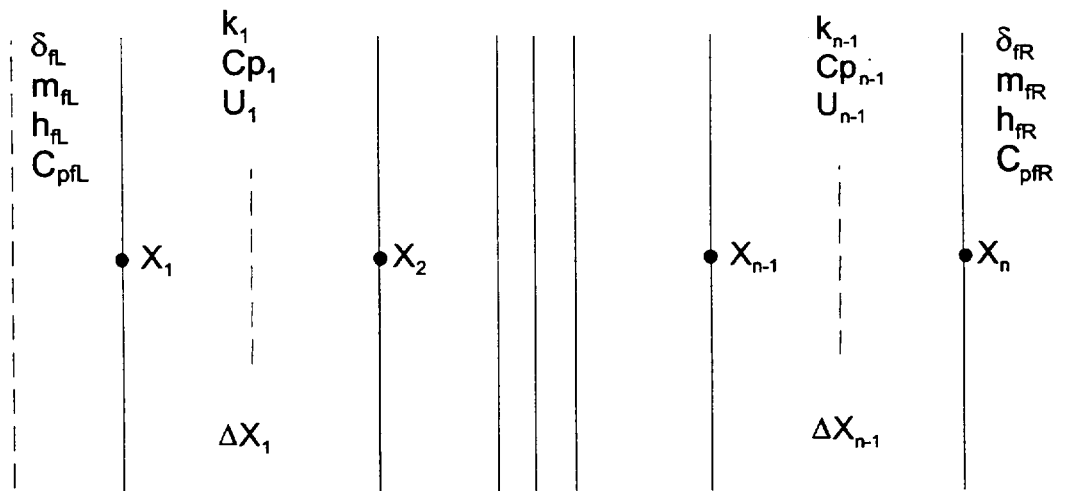


Figure 2.2 Nodalization at Boundary Surfaces of a Heat Structure

Table 2.2 Surface and Volume Weights at Boundary Surfaces

Rectangular Geometries	Equation
$HSL_1 = 1$	(2.27)
$HVL_1 = 0$	(2.28)
$HSR_1 = 1/\Delta X_1$	(2.29)
$HVR_1 = \Delta X_1/2$	(2.30)

$HSL_N = 1 / \Delta X_{N-1}$	(2.31)
$HVL_N = \Delta X_{N-1} / 2$	(2.32)
$HSR_N = 1$	(2.33)
$HVR_N = 0$	(2.34)
Cylindrical Geometries	Equation
$HSL_1 = 2\pi X_1$	(2.35)
$HVL_1 = 0$	(2.36)
$HSR_1 = 2\pi(X_1 + \Delta X_1 / 2) / \Delta X_1$	(2.37)
$HVR_1 = \pi[(X_1 + \Delta X_1 / 2)^2 - X_1^2]$	(2.38)
$HSL_N = 2\pi(X_N - \Delta X_{N-1} / 2) / \Delta X_{N-1}$	(2.39)
$HVL_N = \pi[X_N^2 - (X_N - \Delta X_{N-1} / 2)^2]$	(2.40)
$HSR_N = 2\pi X_N$	(2.41)
$HVR_N = 0$	(2.42)
Spherical Geometries	Equation
$HSL_1 = 4\pi X_1^2$	(2.43)
$HVL_1 = 0$	(2.44)
$HSR_1 = 4\pi(X_1 + \Delta X_1 / 2)^2 / \Delta X_1$	(2.45)
$HVR_1 = (4\pi / 3)[(X_1 + \Delta X_1 / 2)^3 - X_1^3]$	(2.46)
$HSL_N = 4\pi(X_N - \Delta X_{N-1} / 2)^2 / \Delta X_{N-1}$	(2.47)
$HVL_N = (4\pi / 3)[X_N^3 - (X_N - \Delta X_{N-1} / 2)^3]$	(2.48)

HS Package Reference Manual

$HSR_N = 4\pi X_N^2$	(2.49)
$HVR_N = 0$	(2.50)
Hemispherical Geometries	Equation
$HSL_1 = 2\pi X_1^2$	(2.51)
$HVL_1 = 0$	(2.52)
$HSR_1 = 2\pi(X_1 + \Delta X_1/2)^2 / \Delta X_1$	(2.53)
$HVR_1 = (2\pi/3)[(X_1 + \Delta X_1/2)^3 - X_1^3]$	(2.54)
$HSL_N = 2\pi(X_N - \Delta X_{N-1}/2)^2 / \Delta X_{N-1}$	(2.55)
$HVL_N = (2\pi/3)[X_N^3 - (X_N - \Delta X_{N-1}/2)^3]$	(2.56)
$HSR_N = 2\pi X_N^2$	(2.57)
$HVR_N = 0$	(2.58)

The figure also shows thermal properties and volumetric power sources in the mesh intervals adjacent to the boundary nodes. These quantities are present in the finite-difference equations and are discussed in Sections 2.3 and 2.5.

The surface and volume weights are also defined at the boundary surfaces. The definitions are given in Table 2.2 for the case when no liquid film exists on either surface. The surface and volume weights for the case involving liquid films are similar, except there is one additional temperature node on each side that has a liquid film, and the mesh interval (with a thickness equal to that of the liquid film, δ_l) between the additional node (on the outside) and the structure surface node (on the inside) contains the liquid film. The surface and volume weights may be interpreted as discussed in Section 2.1.1 except (a) the left volume weight at the left (inside) temperature node and the right volume weight at the right (outside) temperature node are zero and (b) the left surface weight at the left (inside) temperature node and the right surface weight at the right (outside) boundary surface are the areas of these respective surfaces.

2.2.3 Difference Approximation at Boundary Nodes

The finite-difference equations at boundary nodes are obtained from an integral form of the heat conduction equation. The finite-difference approximation at the boundary temperature nodes is obtained from the integral of Equation (2.1) (multiplied by the area term) over the solid that is bounded by the film surface and the dashed line in Figure 2.2.

2.2.3.1 Finite-Difference Equation at Left (Inside) Boundary

By using Equation (2.22) to eliminate the spatial derivative term, the finite-difference approximation has the following form at the left (inside) boundary surface:

$$G_1^{m+1}(T_1^{m+1} - T_1^m) / \Delta t_m = [k_1(y_L - \alpha_L T_1) / \beta_L] HSL_1 + k_1(T_2 - T_1) HSR_1 + U_1 HVR_1 - m_{f,L}^m \Delta h_{f,L} / f \quad (2.59)$$

If there is no liquid film on that surface (i.e., there was and is no film, or there was film that completely evaporated or was transferred to the pool associated with the boundary volume). If there is a liquid film, then the equations for the film surface temperature and structure surface temperature are:

$$G_{f,L}^{m+1}(T_{f,L}^{m+1} - T_{f,L}^m) / \Delta t_m = HSR_{f,L} H_{f,L} (T_1 - T_{f,L}) + HSL_{f,L} [(1 - x_{pool,L}) \cdot (H_{atm,L} + H_{atm,r,L}) \cdot (T_{atm,L} - T_{f,L}) + x_{pool,L} H_{pool,L} \cdot (T_{pool,L} - T_{f,L})] + [(1 - x_{pool,L}) A_L / f] \cdot [(h_{v,L} - h_{f,L}) \cdot \max(0, \dot{m}_{c,L}) + (h_{v,L} - \bar{h}_{f,L}) \cdot \min(0, \dot{m}_{c,L})] \quad (2.60a)$$

$$(G_1^{m+1} + G_{f,L}^{m+1})(T_1^{m+1} - T_1^m) / \Delta t_m = HSR_1 k_1 (T_2 - T_1) - HSR_{f,L} H_{f,L} (T_1 - T_{f,L}) + [(1 - x_{pool,L}) A_L / f] (h_{f,L} - \bar{h}_{f,L}) \max(0, \dot{m}_{c,L}) + U_1 HVR_1 \quad (2.60b)$$

where

$$G_1^{m+1} = C_{\rho 1}^{m+1} HVR_1$$

f = geometry factor

= surface area of heat structure for rectangular geometries

= axial length of heat structure for cylindrical geometries

= 1.0 for spherical and hemispherical geometries

HS Package Reference Manual

m_f^m	= (old) mass of film evaporated (or transferred) this timestep
Δh_f	= specific enthalpy added to m_f^m before its removal = latent heat of vaporization if film evaporated = 0.0 if film was transferred to pool
HSR_f	= HSR evaluated at film mass median surface
HSL_f	= HSL evaluated at film/atmosphere interface
A	= structure surface area
x_{pool}	= fraction of boundary surface in pool of boundary volume
H_{atm}	= convective heat transfer coefficient to atmosphere
H_{atmr}	= radiative heat transfer coefficient to atmosphere
H_{pool}	= convective heat transfer coefficient to pool
H_f	= convective/conductive heat transfer coefficient through film
T_{atm}	= temperature of atmosphere in boundary volume
T_{pool}	= temperature of pool in boundary volume
m_f	= mass of film
\dot{m}_c	= condensation/evaporation mass flux (+/- for cond/evap)
c_{pf}	= specific heat capacity of film
G_f^{m+1}	= $0.5 m_f^{m+1} c_{pf}^{m+1} / f$
h_v	= specific enthalpy of vapor in boundary volume
$h_{f,L}$	= specific enthalpy of film evaluated at film/atmosphere interfacial temperature
$h_{f,1}$	= specific enthalpy of film evaluated at structure/film interfacial temperature
\bar{h}_f	= $0.5 \times (h_{f,L} + h_{f,1})$

- L = quantity at left (inside) boundary surface
- i = quantity at i -th temperature node or mesh interval
- m = quantity at time t_m
- $m+1$ = quantity at time $t_m + \Delta t_m$

Equation (2.60) does not apply when $\beta = 0$. This corresponds to the specified surface temperature boundary condition, in which case $T_1^{m+1} = T_{surf,L}^{m+1}$ and the presence of surface films and mass transfer is not permitted.

The time superscript for each term on the right side of Equation (2.60) is omitted. If all are m , then the finite-difference formulation is fully explicit. If all are $m+1$, then the formulation is fully implicit. The fully implicit numerical method is used by the HS package. Equation (2.60) is used for both steady-state (MELGEN) and transient (MELCOR) calculations, except that for steady-state calculations the old time values (m) are overwritten with the new time values ($m+1$) after each iteration. Hence, when convergence is achieved in MELGEN, temperatures that do not change with time (steady-state) have been determined. In MELGEN the timestep size is given by the value of sensitivity coefficient C4051(3), which is 10^5 s by default.

The finite-difference equation(s) at the left (inside) boundary temperature node(s) are obtained by expanding Equation (2.60) and collecting the temperature terms at the $m+1$ time level on the left. Equation (2.60) reduces to

$$B_1^{m+1}T_1^{m+1} + C_1^{m+1}T_2^{m+1} = D_1^{m+1} \quad (2.61a)$$

where for β_L not zero,

$$B_1^{m+1} = G_1^{m+1} - C_1^{m+1} + (\alpha_L^{m+1}k_1^{m+1}HSL_1\Delta t_m) / \beta_L^{m+1}$$

$$C_1^{m+1} = -k_1^{m+1}HSR_1\Delta t_m$$

$$D_1^{m+1} = G_1^{m+1}T_1^m + (\gamma_L^{m+1}k_1^{m+1}HSL_1\Delta t_m) / \beta_L^{m+1} + U_1^{m+1/2}HVR_1\Delta t_m - m_{f,L}^m \Delta h_{f,L} / f$$

and for β_L zero,

HS Package Reference Manual

$$B_1^{m+1} = 1$$

$$C_1^{m+1} = 0$$

$$D_1^{m+1} = \gamma_L^{m+1} = T_{surf,L}^{m+1}$$

Equation (2.60a) and (2.60b) reduce to

$$B_L^{m+1}T_L^{m+1} + C_L^{m+1}T_1^{m+1} = D_L^{m+1} \quad (2.61b)$$

$$A_1^{m+1}T_{f,L}^{m+1} + B_1^{m+1}T_1^{m+1} + C_1^{m+1}T_2^{m+1} = D_1^{m+1} \quad (2.61c)$$

where

$$B_L^{m+1} = G_{f,L}^{m+1} - C_L^{m+1} + HSL_{f,L} \left[(1 - x_{pool,L}) (H_{atm,L}^{m+1} + H_{atmr,L}^{m+1}) + x_{pool,L} H_{pool,L}^{m+1} \right] \Delta t$$

$$C_L^{m+1} = -H_{f,L}^{m+1} HSR_{f,L} \Delta t_m$$

$$D_L^{m+1} = G_{f,L}^{m+1} T_{f,L}^m + HSL_{f,L} \left[(1 - x_{pool,L}) (H_{atm,L}^{m+1} + H_{atmr,L}^{m+1}) T_{atm,L} + x_{pool,L} H_{pool,L}^{m+1} T_{pool,L} \right] \Delta t_m \\ + \left[(1 - x_{pool,L}) A_L / f \right] \left[(h_{v,L} - h_{f,L}^{m+1}) \max(0, \dot{m}_{c,L}^{m+1}) + (h_{v,L} - \bar{h}_{f,L}^{m+1}) \min(0, \dot{m}_{c,L}^{m+1}) \right] \Delta t_m$$

$$A_1^{m+1} = C_L^{m+1}$$

$$B_1^{m+1} = G_1^{m+1} + G_{f,L}^{m+1} - A_1^{m+1} - C_1^{m+1}$$

$$C_1^{m+1} = -k_1^{m+1} HSR_1 \Delta t_m$$

$$D_1^{m+1} = (G_1^{m+1} + G_{f,L}^{m+1}) T_1^m + \left[(1 - x_{pool,L}) A_L / f \right] \left[(h_{f,L}^{m+1} - \bar{h}_{f,L}^{m+1}) \max(0, \dot{m}_{c,L}^{m+1}) \right] \Delta t_m \\ + U_1^{m+1/2} HVR_1 \Delta t_m$$

2.2.3.2 Finite-Difference Equation at Right (Outside) Boundary

The finite-difference equation(s) at the right (outside) boundary surface are exactly analogous to those at the left (inside) boundary surface. The subscripts 1, 2 and L are merely replaced by subscripts N, N-1 and R; HSL and HSR are reversed; HVL and HVR are reversed; and matrix elements A and C are reversed.

2.3 Power Sources

Power sources are included in the calculation of the temperature distribution of each heat structure. These sources include the following:

- (1) internal power source,
- (2) surface power source, and
- (3) energy transferred by other packages.

These items are discussed in Sections 2.3.1 through 2.3.3, respectively.

2.3.1 Internal Power Sources

The internal power source is included in the temperature evolution equations as volumetric power terms in each mesh interval. User input specifies the spatial distribution of the power source for each heat structure that contains an internal power source. These data are used to calculate the fraction of power from a tabular function or control function that is applied to each mesh interval. The HS package calculates the volumetric power terms, U , that appear in the equations. For the n -th mesh interval,

$$U_n = x_{P,n} P_{int} / (HVL_{n+1} + HVR_n) / f \quad (2.62)$$

where

n = 1, 2, ..., $N-1$

$N-1$ = number of mesh intervals

x_P = fraction of power from tabular function that is applied to this mesh interval (user input)

P_{int} = average of power from internal source tabular function at old and new times or power from a specified control function for transient calculations and time zero value for initialization calculations

HVL = left (inside) volume weights defined in Sections 2.1.1 and 2.2.2

HVR = right (outside) volume weights defined in Sections 2.1.1 and 2.2.2

f = geometry factor with the following values for different geometries

= surface area of heat structure for rectangular geometries

HS Package Reference Manual

= axial length of heat structure for cylindrical geometries

= 1.0 for spherical and hemispherical geometries

2.3.2 Surface Power Sources

For a convective boundary condition with calculated heat transfer coefficients, a surface power source may be specified by a user-input control function or a tabular function of time. This source is included in Equations (2.24) and (2.25) as energy fluxes which are added to the boundary condition coefficients, γ , in Equation (2.24). The HS package calculates these fluxes, q''_{surf} , prior to calculating the temperature distribution of each heat structure. For each boundary surface, these terms are

$$q''_{surf} = P_{surf} / A_{surf}$$

where

q''_{surf} = energy flux at boundary surface from surface power source

P_{surf} = average of surface power from tabular function at old and new times for transient calculations and zero for initialization calculations

A_{surf} = area of boundary surface

2.3.3 Energy Transferred by Other Packages

The energy which is transferred to a heat structure surface by other packages is obtained from an array in the HS package data base whose elements are updated using an interface subroutine that can be called any package. This energy includes, for example, the radiant energy from a core cell, conduction from debris deposited on the structure surface by the high-pressure-melt-ejection (HPME) model of the FDI package or the decay-heat energy of radionuclides deposited on a heat structure surface. This energy is included in Equations (2.24) and (2.25) as energy fluxes which are added to the boundary condition coefficients γ in Equation (2.24). The HS package calculates these fluxes, q''_{ext} , prior to calculating the temperature distribution of each heat structure. For each boundary surface, these terms are

$$q''_{ext} = E_{ext} / A_{surf} / \Delta t \quad (2.63)$$

where

q''_{ext}	= energy flux at boundary surface from energy which is transferred by other packages
E_{ext}	= energy which is transferred to boundary surface by other packages since the previous call to the HS package for transient calculations and zero for initialization calculations
A_{surf}	= area of boundary surface
Δt	= computational timestep

For each boundary surface, the surface energy flux term S in Equation (2.24) used in determining the boundary coefficient γ is the sum of q''_{surf} and q''_{ext} obtained from the above equations.

2.4 Pool Fractions

When a heat structure with a convective boundary condition is in contact with a CVH volume containing either single-phase liquid or vapor, the implementation of the boundary condition is straightforward. However, if the surface is partially submerged, then it is necessary to partition the heat transfer between the pool and the atmosphere as described in Section 2.2.1.2. In this case, heat transfer is partitioned on the basis of a calculated fraction of the heat structure surface that is submerged as depicted in Figure 1.1. This fraction is called the pool fraction with a range of 0 to 1. This section describes how the pool fraction is calculated for each type of geometry and the controls available to the user.

There are two input parameters for each surface, CPFPL and CPFAL, which allow the user to disable heat transfer to the pool and/or atmosphere as a function of the pool fraction. The range of each is 0 to 1. Heat transfer to the pool is calculated only when the pool fraction exceeds the critical pool fraction CPFPL. Similarly, heat and mass transfer to the atmosphere occur only when the pool fraction falls below the critical pool fraction CPFAL. Note that CPFPL and CPFAL are completely independent. Furthermore, disabling heat transfer to either phase will not affect heat transfer to the other phase directly. Also, when permitted, the heat transfer rates are independent of the values of CPFPL and CPFAL. When heat transfer from either phase is permitted, it occurs over the fraction of the surface area that is in contact with that phase (as given by x_{pool} for the pool and $1-x_{pool}$ for the atmosphere in Equation (2.24)). When heat transfer to either phase is disabled it is as though there is a perfectly insulating layer at the interface.

The primary use of this input feature is to prohibit simultaneous heat transfer to both pool and atmosphere when such an occurrence will generate unrealistic results. The most common situation to be avoided occurs when a vertical structure is in contact with both a cool liquid pool and a hot atmosphere. In this case, if the heat structure is allowed to

HS Package Reference Manual

communicate with both phases simultaneously, the relatively large heat transfer coefficient to the pool pulls the one-dimensional structure surface temperature down to a value much closer to the pool temperature than the atmosphere temperature. Consequently, heat transfer from the atmosphere to the structure is much greater than should be expected. The net effect is an artificially large heat transfer from the atmosphere to the pool via the structure surface. This situation can be avoided by specifying equal values of CPFPL and CPFAL so that structure only communicates to either the pool or atmosphere.

For situations in which the pool and atmosphere temperatures in the boundary control volume are nearly the same and heat transfer to both phases is expected to be significant, the user should enable simultaneous communications with both phases by specifying a value of zero for CPFPL and one for CPFAL. This option is often used for steam generator heat structures. This should also be used for horizontal floors and ceiling for which the pool fraction is specially modified as described in Section 2.4.1.

A value of 0.0 for CPFPL, or of 1.0 for CPFAL, can lead to numerical problems because heat transfer may be calculated to an arbitrarily small fluid mass if the heat structure extends to the bottom or top of the control volume, respectively. To avoid this potential problem, bounds are imposed on the user-input values so that $CPFPL \geq 0.02$ and $CPFAL \leq 0.98$. These bounds are contained in sensitivity coefficient array 4071.

If CPFPL is greater than CPFAL, there will be a dead band with no communication to either the pool or atmosphere. This unlikely situation is not currently treated as a fatal input error.

If CPFPL is less than CPFAL, there will be a band with simultaneous heat transfer to both pool and atmosphere.

If CPFPL is equal to CPFAL, heat transfer will switch from one phase to the other as the pool fraction crosses the critical value. In the special case where the calculated pool fraction is exactly equal to the common value of CPFPL and CPFAL, communication will be to the pool if the value is greater than or equal to 0.5 and to the atmosphere otherwise.

Because of the potential for serious problems when unequal values of CPFPL and CPFAL are specified, MELGEN will generate a warning message to alert the user to the potential for unrealistic results. Nevertheless, if simultaneous heat transfer to both the pool and atmosphere is unlikely to cause serious problems, then CPFPL and CPFAL should be chosen to permit simultaneous heat transfer (i.e., set $CPFPL = 0$ and $CPFAL = 1$).

The pool fraction for a surface is set to 0.0 if its lowest point is above the pool and set to 1.0 if it is completely immersed in the pool. If the pool/atmosphere interface is very close to the top or bottom of a heat structure surface (less than the maximum film thickness), the pool fraction is set to 1.0 or 0.0, respectively. For all other situations, the expressions given below are evaluated for the pool fraction. Sections 2.4.1 through 2.4.4 present these expressions for rectangular, cylindrical, spherical, and hemispherical geometries, respectively.

2.4.1 Rectangular Geometry

The pool fraction for a surface with a rectangular geometry is given by

$$x_{pool} = Z / L \cos(\alpha) \quad (2.64)$$

where

Z = depth of pool in boundary volume of this surface relative to the altitude of the lowest point on this surface

L = axial length of this surface

α = angle between this surface and the vertical

For horizontal surfaces, such as floors and ceilings, where $\cos(\alpha) = 0$ in Equation (2.64), the pool fraction is defined to vary from zero to one as the pool surface ascends through a vertical distance of the maximum of liquid film thickness (see Section 2.8) and 10^{-6} m, which eliminates a step change in pool fraction.

2.4.2 Cylindrical Geometry

The following quantities are used for defining the pool fraction for a surface with a cylindrical geometry:

R = radius of cylinder containing the surface

L = axial length of this surface

α = angle between this surface and the vertical

a = vertical projection of cylinder diameter, $2R \sin(\alpha)$

b = vertical projection of cylinder axial length, $L \cos(\alpha)$

Z = depth of pool in boundary volume of this surface relative to the altitude of the lowest point on this surface

The pool fraction for a vertical surface, $\cos(\alpha)=1$, with a cylindrical geometry is given by

$$x_{pool} = Z / L \quad (2.65)$$

HS Package Reference Manual

The pool fraction for a horizontal surface, $\cos(\alpha)=0$, with a cylindrical geometry is given by

$$X_{pool} = \Theta / \pi \quad (2.66)$$

where

$$\Theta = \cos^{-1}[(R - Z)/R]$$

is in radians and is π for $Z > 2R$.

The pool fraction for a cylinder inclined at an angle α between vertical and horizontal is given as follows:

$$X_{pool} = R \sin(\alpha) [TERML(Z) + TERM(R(Z))] / b \quad (2.67)$$

where $TERML(Z)$ and $TERM(R(Z))$ are functions of Z that are derived by considering whether or not the pool surface intersects the bottom and/or top flat surfaces of the cylinder. Defining

$$XL = 1 - Z / [R \sin(\alpha)] \quad (2.68)$$

it can be shown that, if the pool intersects the bottom surface ($XL > -1$), then

$$TERML = \frac{1}{\pi} \left\{ [1 - XL^2]^{1/2} - \frac{XL}{\cos(XL)} \right\} \quad (2.69)$$

Otherwise, the bottom surface is completely submerged, and

$$TERML = -XL \quad (2.70)$$

Similarly, defining

$$XU = (a + b - z) / [R \sin(\alpha)] - 1 \quad (2.71)$$

It can be shown that

$$TERMR = \frac{1}{\pi} \left\{ \frac{XU}{\cos(XU)} - [1 - XU^2]^{1/2} \right\} \quad (2.72)$$

when the surface intersects the top end ($XU < 1$); otherwise,

$$TERMR = 0 \quad (2.73)$$

2.4.3 Spherical Geometry

The pool fraction for a surface with a spherical geometry is given by

$$x_{pool} = Z / 2R \quad (2.74)$$

2.4.4 Hemispherical Geometry

The pool fraction for a surface with a hemispherical geometry is given by

$$x_{pool} = Z / R \quad (2.75)$$

2.5 Thermal Properties

The conduction equations require the thermal conductivity and volumetric heat capacity (product of heat capacity and density) of the material in each mesh interval. These thermal properties are discussed in Section 2.5.1. Their modification for a degassible material is discussed in Section 2.5.2.

2.5.1 Thermal Conductivity and Volumetric Heat Capacity

The thermal conductivity, heat capacity, and density of the material in each mesh interval are obtained as a function of temperature using an interface with the Material Properties package. They are obtained for the material in each mesh interval at a temperature that is the average of the temperatures of the nodes which are boundaries of this mesh interval.

2.5.2 Modifications for Degassible Materials

The volumetric heat capacity of a degassible material whose temperature is in the degassing temperature range is increased by an amount equal to the product of the heat of reaction and the source density divided by the degassing temperature range. The volumetric heat capacity is therefore replaced by

$$C_p + \Delta h_R \rho_{gas} / \Delta T_{gas} \quad (2.76)$$

where

C_p = volumetric heat capacity from Material Properties package, $\text{kJ/m}^3 \cdot \text{K}$

Δh_R = heat of reaction of gas source, kJ/kg

ρ_{gas} = density of gas in source, kg/m^3

ΔT_{gas} = degassing temperature range of gas source, K

This modification accounts for the energy which is required to produce and release the gas.

2.6 Heat Transfer

The methods of calculating heat transfer at a heat structure surface are discussed in this section for the following:

- (1) specified temperature boundary conditions
- (2) specified heat flux boundary conditions
- (3) convective boundary conditions

If the temperature of a surface is specified by a tabular function, the heat flux is calculated from a finite-difference approximation which expresses the surface heat flux in terms of temperatures at the surface and adjacent nodes and quantities known in the interior of the heat structure. For the left boundary surface, this heat flux is given by

$$q_L'' = \left[-k_1^{m+1} (T_1^{m+1} - T_2^{m+1}) HSR_1 + U_1 HVR_1 - Cp_1^m \frac{T_1^{m+1} - T_1^m}{\Delta t_m} HVR_1 \right] / HSL_1 \quad (2.77)$$

For the right boundary surface, this heat flux is

$$q_R'' = \left[-k_N^{m+1} (T_N^{m+1} - T_{N-1}^{m+1}) HSL_N + U_N HVL_N - Cp_N^m \frac{T_N^{m+1} - T_N^m}{\Delta t_m} HVL_N \right] / HSR_1 \quad (2.78)$$

where

k^m	= thermal conductivity of heat structure at time t_m
C_p^m	= volumetric heat capacity of heat structure at time t_m
HSL	= left (inside) surface weight defined in Section 2.2.1
HSR	= right (outside) surface weight defined in Section 2.2.1
HVL	= left (inside) volume weight defined in Section 2.2.1
HVR	= right (outside) volume weight defined in Section 2.2.1
U^n	= volumetric power source at time t_m
T^m	= node temperature at time t_m
T^{m+1}	= node temperature at time t_{m+1}
Δt	= timestep size, $t_{m+1} - t_m$

If the surface heat flux is specified by a tabular function, the heat flux is known from the value of the tabular function.

If a convective boundary condition is specified, the heat flux is the product of the heat transfer coefficient and the temperature difference between the surface (film surface, if a liquid film is present) and the atmosphere or pool of the boundary volume. The heat transfer coefficient is either calculated or provided by a tabular function of time or temperature.

If a convective boundary condition with calculated heat transfer coefficients is specified, then correlations are available for the following heat transfer regimes:

- (1) atmosphere natural convection
- (2) atmosphere forced convection
- (3) pool natural convection
- (4) pool forced convection
- (5) pool boiling

The HS package calculates convective heat transfer between a heat structure and the boundary volume atmosphere whenever the pool fraction at a boundary surface is less than or equal to its critical pool fraction for atmosphere heat transfer. Atmosphere heat transfer occurs through a gas boundary layer and, if condensate is present on the surface,

HS Package Reference Manual

through a liquid layer between the surface and the boundary layer. Radiation heat transfer also can occur between a heat structure and the boundary volume atmosphere. For this case, radiation and convection for the structure surface (or the film surface, if a liquid film exists) occur in parallel with one another (and in series with conduction/convection through the liquid film to the structure surface).

Heat transfer through the gas boundary layer is accounted for by a heat transfer coefficient obtained from correlations for natural or forced convection heat transfer. User input must specify whether an internal flow or external flow correlation is to be used when calculating atmosphere heat transfer coefficients for each boundary surface. These correlations are given in Section 2.6.1 for atmosphere heat transfer. Section 2.6.1.1 describes the modeling of heat transfer through liquid films when the film tracking model is inactive. The modeling of heat transfer through liquid films flowing over structures included in user-defined film tracking networks is discussed in Section 2.6.1.2.

Radiation heat transfer between a heat structure surface and the boundary volume atmosphere is modeled in either of two ways. The user has the option of employing the equivalent band model or the gray gas model for radiation heat transfer. These models are presented in Section 2.6.2.

At any surface, an arbitrary, user-specified nonnegative scaling factor may be applied to the calculated convective and radiative heat transfer coefficients to the atmosphere. The user may also apply a separate, arbitrary nonnegative scaling factor to the condensation/evaporation mass transfer coefficient. Users are cautioned that the application of significantly different heat and mass transfer scaling factors at the same surface may lead to nonphysical results and numerical problems. The scaling factors are provided primarily for conducting sensitivity studies associated with uncertainties related to surface fouling, local fluid effects, etc.

The HS package calculates heat transfer between a heat structure and the boundary volume pool whenever the pool fraction at a boundary surface is greater than or equal to its critical pool fraction for pool heat transfer. Pool heat transfer can be by natural convection, forced convection, or pool boiling. The HS package uses an extensive set of correlations for natural or forced convection pool heat transfer. User input must again specify whether an internal flow or external flow correlation is to be used when calculating pool heat transfer coefficients for each boundary surface. These correlations are exhibited in Section 2.6.3.

Pool boiling heat transfer is calculated at a surface if its pool fraction is greater than the critical pool fraction and its temperature is greater than the saturation temperature of its boundary volume (at total pressure). In calculating pool boiling heat transfer, the HS package uses a set of correlations for nucleate boiling, critical heat flux, minimum film boiling, and stable film boiling. Radiation heat transfer between a surface and the pool of its boundary volume is calculated during stable film and transition boiling. Correlations for

pool boiling heat transfer as well as models for pool radiation heat transfer are discussed in Section 2.6.4.

The HS package obtains the boiling heat transfer coefficient at a boundary surface as the quotient of the boiling heat flux and the difference between the temperature of this surface and the saturation temperature of its boundary volume (at total pressure).

The correlation of experimental heat transfer data is usually accomplished with dimensionless variables which are obtained by dimensional analysis or physical reasoning. These variables include:

$$\text{Reynolds number (Re)} = \rho V L_c / \mu$$

$$\text{Prandtl number (Pr)} = \mu c_p / k$$

$$\text{Grashof number (Gr)} = g \beta \Delta t L_c^3 \rho^2 / \mu^2$$

$$g | \rho_{sat} - \rho | L_c^3 \rho / \mu^2 \text{ (during condensation)}$$

$$\text{Nusselt number (Nu)} = h L_c / k$$

$$\text{Rayleigh number (Ra)} = Gr \cdot Pr$$

where

$$\rho = \text{density of atmosphere (pool), kg/m}^3$$

$$\rho_{sat} = \text{density of atmosphere evaluated at film surface temperature}$$

$$V = \text{velocity of atmosphere (pool), m/s}$$

$$L_c = \text{characteristic length of surface, m}$$

$$\mu = \text{viscosity of atmosphere (pool), kg/m}\cdot\text{s}$$

$$c_p = \text{heat capacity at constant pressure of atmosphere (pool), J/kg}\cdot\text{K}$$

$$k = \text{thermal conductivity of atmosphere (pool), W/m}\cdot\text{K}$$

$$g = \text{acceleration of gravity, m/s}^2$$

$$\beta = \text{volume coefficient of expansion of atmosphere (pool), K}^{-1}$$

HS Package Reference Manual

Δt = magnitude of difference between temperatures of surface and atmosphere (pool), K

h = atmosphere (pool) heat transfer coefficient, W/m²•K

The HS package uses these variables for selecting the appropriate heat transfer correlation or in expressing the functional form of the correlation for all heat transfer regimes except pool boiling. The pool boiling correlations are not expressed in a dimensionless form.

2.6.1 Atmosphere Convection Heat Transfer

Natural, forced, or mixed convection heat transfer to the atmosphere is determined at a surface by the following criteria:

Region	Criteria	Equation
Natural Convection	$Re^2 < 1.0 Gr$	(2.79)
Forced Convection	$Re^2 > 10.0 Gr$	(2.80)
Mixed Convection	$1.0 Gr \leq Re^2 \leq 10.0 Gr$	(2.81)

where

Re = Reynolds number for atmosphere

Gr = Grashof number for atmosphere

Ra = Rayleigh number for atmosphere

The constants in Equations (2.79) through (2.81) are implemented as sensitivity coefficient array C4060.

The atmosphere natural convection heat transfer correlations have the following form:

$$Nu = C Ra^m + D \quad (2.82)$$

where

Nu = Nusselt number

Ra = Rayleigh number

C, m, D = constants dependent on flow condition and geometry

The constants C , m , and D in Equation (2.82) have been implemented as sensitivity coefficient arrays C4101 – C4112 and are presented in Table 2.3 for the various flow conditions and geometries.

Table 2.3 Constants for HS Package Heat Transfer Correlations

Region	Type of Flow	Geometry	(1)	(2)	(3)	(4)	Ref	SC Array	
ATMOSPHERE									
Natural Convection	Internal	Laminar	Rectangular	0.046	1/3	0	-	[1]	C4101
		Cylindrical	0.046	1/3	0	-	[1]	C4102	
		Spherical	0.228	0.226	0	-	[1]	C4103	
	Turbulent	Rectangular	0.046	1/3	0	-	[1]	C4104	
		Cylindrical	0.046	1/3	0	-	[1]	C4105	
		Spherical	0.228	0.226	0	-	[1]	C4106	
External	Laminar	Rectangular	0.59	0.25	0	-	[1]	C4107	
	Cylindrical	0.59	0.25	0	-	[1]	C4108		
	Spherical	0.43	0.25	2.0	-	[1]	C4109		
Atmosphere	Turbulent	Rectangular	0.10	1/3	0	-	[1]	C4110	
		Cylindrical	0.10	1/3	0	-	[1]	C4111	
		Spherical	0.43	0.25	2.0	-	[1]	C4112	
Forced Convection	Internal	Laminar	Rectangular	8.235	0	0	0	[1]	C4113
		Cylindrical	48/11	0	0	0	[1]	C4114	
		Spherical	48/11	0	0	0	[1]	C4115	
	Turbulent	Rectangular	0.023	0.8	1/3	0	[2]	C4116	
		Cylindrical	0.023	0.8	1/3	0	[2]	C4117	
		Spherical	0.023	0.8	1/3	0	[2]	C4118	
External	Laminar	Rectangular	0.664	0.5	1/3	0	[2]	C4119	
	Cylindrical	0.664	0.5	1/3	0	[2]	C4120		
	Spherical	0.60	0.5	1/3	2.0	[2]	C4121		
Turbulent	Rectangular	0.037	0.8	1/3	0	[2]	C4122		
	Cylindrical	0.037	0.8	1/3	0	[2]	C4123		
	Spherical	0.60	0.5	1/3	2.0	[2]	C4124		
POOL									
Natural Convection	Internal	Laminar	Rectangular	0.046	1/3	0	-	[1]	C4151
		Cylindrical	0.046	1/3	0	-	[1]	C4152	
		Spherical	0.028	0.226	0	-	[1]	C4153	
	Turbulent	Rectangular	0.046	1/3	0	-	[1]	C4154	
		Cylindrical	0.046	1/3	0	-	[1]	C4155	
		Spherical	0.228	0.226	0	-	[1]	C4156	
External	Laminar	Rectangular	0.59	0.25	0	-	[1]	C4157	
	Cylindrical	0.59	0.25	0	-	[1]	C4158		
	Spherical	0.43	0.25	2.0	-	[1]	C4159		
Pool	Turbulent	Rectangular	0.10	1/3	0	-	[1]	C4160	
		Cylindrical	0.10	1/3	0	-	[1]	C4161	
		Spherical	0.43	0.25	2.0	-	[1]	C4162	
		Rectangular	8.235	0	0	0	[1]	C4163	

HS Package Reference Manual

Region	Type of Flow	Geometry	(1)	(2)	(3)	(4)	Ref	SC Array		
Forced Convection	Internal	Laminar	Cylindrical	48/11	0	0	0	[1]	C4164	
			Spherical	48/11	0	0	0	[1]	C4165	
		Turbulent	Rectangular	0.023	0.8	1/3	0	[2]	C4166	
			Cylindrical	0.023	0.8	1/3	0	[2]	C4167	
			Spherical	0.023	0.8	1/3	0	[2]	C4168	
	External	Laminar	Rectangular	0.664	0.5	1/3	0	[2]	C4169	
				Cylindrical	0.664	0.5	1/3	0	[2]	C4170
				Spherical	0.60	0.5	1/3	2.0	[2]	C4171
		Turbulent	Rectangular	0.037	0.8	1/3	0	[2]	C4172	
				Cylindrical	0.037	0.8	1/3	0	[2]	C4173
				Spherical	0.60	0.5	1/3	2.0	[2]	C4174

The atmosphere forced convection heat transfer correlations have the following form:

$$Nu = C Re^m Pr^n + D \quad (2.83)$$

where

Nu = Nusselt number

Re = Reynolds number

Pr = Prandtl number

C, m, n, D = constants dependent on flow condition and geometry

The constants C , m , n , and D in Equation (2.83) have been implemented as sensitivity coefficient arrays C4113 – C4124 and are presented in Table 2.3 for the various flow conditions and geometries.

The Nusselt number in the mixed convection regime is a linear interpolation between the Nusselt numbers for the natural and forced convection regimes, based on the ratio Re^2/Gr . That is,

$$Nu_{mixed} = \left[(Re^2/Gr - 1)/9 \right] [Nu_{forced} - Nu_{natural}] + Nu_{natural} \quad (2.84)$$

The constants in Equation (2.84) are, of course, derived from the sensitivity coefficients that define the limits of natural and forced convection. If the values of these coefficients do not define a proper transition—specifically if the upper limit for natural convection, C4060(1) (default value 1.0) is negative or is greater than or equal to the lower limit for forced convection, C4060(2) (default value 10.0)—no mixed convection regime is considered. Instead, convection heat transfer to the atmosphere is assumed to be given

by the greater of the values defined by the natural and forced convection correlations. This simple and often-used treatment may be specified in MELCOR by deliberate modification of the sensitivity coefficients.

Laminar or turbulent natural convection heat transfer to the atmosphere is determined at a surface by the following criteria:

Region	Criteria	Equation
Laminar Natural Convection	$Ra < 10^9$	(2.85)
Turbulent Natural Convection	$Ra > 10^{10}$	(2.86)
Transition between Laminar and Turbulent Natural Convection	$10^9 \leq Ra \leq 10^{10}$	(2.87)

The constants in Equations (2.85) through (2.87) are implemented as sensitivity coefficient arrays C4061 – C4063 for rectangular, cylindrical, and spherical (hemispherical) geometries.

Laminar or turbulent forced convection heat transfer to the atmosphere is determined at a surface by the following criteria:

Region	Criteria	Equation
Laminar Forced Convection	$Re < 3 \times 10^5$ (rectangular)	(2.88a)
	$Re < 2 \times 10^3$ (cylindrical/spherical)	(2.88b)
Turbulent Forced Convection	$Re > 6 \times 10^5$ (rectangular)	(2.89a)
	$Re > 1 \times 10^4$ (cylindrical/spherical)	(2.89b)
Transition between Laminar and Turbulent Forced Convection	$3 \times 10^5 \leq Re \leq 6 \times 10^5$ (rectangular)	(2.90a)
	$2 \times 10^3 \leq Re \leq 1 \times 10^4$ (cylindrical/spherical)	(2.90b)

The constants in Equations (2.88) through (2.90) are implemented as sensitivity coefficient arrays C4064 – C4066 for rectangular, cylindrical, and spherical (hemispherical) geometries.

The Nusselt number in the transition region is a linear interpolation between the Nusselt numbers for the laminar and turbulent regimes. The interpolation is based on the Rayleigh number for natural convection and the Reynolds number for forced convection. An example is the Nusselt number in the transition region for forced convection with rectangular geometries:

$$Nu_{transition} = \left[(Re - 3 \times 10^5) / 3 \times 10^5 \right] [Nu_{turbulent} - Nu_{laminar}] + Nu_{laminar} \quad (2.91)$$

The constants in Equation (2.91) are, of course, derived from the sensitivity coefficients that define the limits of laminar and turbulent convection. If the values of these coefficients do not define a proper transition—specifically, if the upper limit for laminar convection, C406m(1) is negative or is greater than or equal to the lower limit for turbulent convection, C406m(2)—no transition regime is considered. Instead, convection heat transfer to the atmosphere is assumed to be given by the greater of the values defined by the laminar and turbulent convection correlations. This simple and often-used treatment may be specified in MELCOR by deliberate modification of the sensitivity coefficients.

2.6.1.1 Conduction/Convection through Liquid Films (film tracking inactive)

Liquid film modeling is discussed in detail in Section 2.8. Heat transfer through a liquid film is accounted for by a heat transfer coefficient, H_f , which is used in Equations (2.59) and (2.60a). The value of H_f used when the structure is included in a user-defined film tracking network is discussed in Section 2.6.1.2. When film tracking is inactive, the value of H_f used is the greater of two values:

- (1) a value obtained from a steady-state correlation appropriate for the geometry and film conditions (zero is used if no film exists) and
- (2) the quotient of the thermal conductivity of the liquid and the transient film thickness. Thus, the liquid film heat transfer coefficient is given by

$$H_f = \max(H_{f,corr}, k_f / \delta_f) \quad (2.92)$$

where

k_f = thermal conductivity of liquid film, W/m·K

δ_f = liquid film thickness, m

and $H_{f,corr}$ is a function of surface geometry and film flow conditions. Laminar or turbulent heat transfer through the condensate film is determined by the following criteria:

Laminar if $Re_f < Re_{LOW,m}$

Turbulent if $Re_f > Re_{HIGH,m}$

Transition if $Re_{LOW,m} \leq Re_f \leq Re_{HIGH,m}$

where

Re_f = Reynolds number for the film flow

The laminar heat transfer coefficient through the film, $h_{f,l}$, is given by

$$h_{f,l} = (k_f / L) Nu_{f,l}$$

where the laminar film Nusselt number, $Nu_{f,l}$, is given by

$$Nu_{f,l} = C_{l,m} \left\{ g \rho_f (\rho_f - \rho_v) h_{fg} L^3 \sin(\theta) / [\mu_f k_f (T_{sat} - T_{srf})] \right\}^{et1,m}$$

The turbulent heat transfer coefficient through the film, $h_{f,t}$, is given by

$$h_{f,t} = \left\{ k_f / [(\mu_f / \rho_f)^2 / g] \right\}^{et1,m} Nu_{f,t}$$

where the turbulent film Nusselt number, $Nu_{f,t}$ is given by

$$Nu_{f,t} = (Re_f^{et2,m} + C_{t,m} Re_f^{et3,m} Pr_f^{et4,m})^{et5,m}$$

The transition heat transfer coefficient through the film, $h_{f,tr}$, is given by linear interpolation of Re_f as

$$h_{f,tr} = h'_{f,l} + [h'_{f,t} - h'_{f,l}] \cdot [Re_f - Re_{LOW,m}] / [Re_{HIGH,m} - Re_{LOW,m}]$$

In each of these equations,

k_f = thermal conductivity of film

L = characteristic length of surface

ρ_f = density of film

ρ_v = density of vapor

g = acceleration of gravity

h_{fg} = latent heat of vaporization corrected for sensible heat

$$[h_{fg} + 0.68 c_{p,f} (T_f - T_{srf})]$$

HS Package Reference Manual

- $C_{p,f}$ = specific heat capacity of film
- T_f = temperature of film/atmosphere interface
- T_{sf} = temperature of film/structure interface
- μ_f = viscosity of film
- θ = angle between horizontal and structure surface or axis (cyl.)
- $h'_{f,l}$ = $h_{f,l}$ evaluated with $Re_f = C42m0(1)$
- $h'_{f,t}$ = $h_{f,t}$ evaluated with $Re_f = C42m0(2)$

and

- m = 1 for upward-facing rectangular geometries
= 2 for horizontal cylindrical geometries
= 3 for spherical or hemispherical geometries

$Re_{LOW,m}$, $Re_{HIGH,m}$ and the minimum permissible value of $\sin(\theta)$ ($\cos(\theta)$ for cylindrical geometry) have been implemented as sensitivity coefficients 42m0. $C_{l,m}$ and $e_{l,m}$ have been implemented as sensitivity coefficients 42m1, and $C_{t,m}$ and $e_{t,m}$ have been implemented as sensitivity coefficients 42m2.

For downward-facing rectangular geometries, the laminar/turbulent transition criteria are given by:

Laminar if $Ra_f < Ra_{TRAN}$
Turbulent, otherwise

where

Ra_f = Rayleigh number for the film flow

The heat transfer coefficient through the film is given by

$$h_f = \left(k_f / \left\{ \sigma_f / [g(\rho_f - \rho_v) \cos(\theta)] \right\}^{1/2} \right) Nu_f$$

where the film Nusselt number is given by

$$Nu_f = C_{t,4} [\max(Ra_{MIN}, Ra_f)]^{e_{t,4}}$$

for laminar flow, and by

$$Nu_f = C_{t,4} [\min(Ra_{MAX}, Ra_f)]^{e_{t,4}}$$

for turbulent film flow. Ra_{TRAN} , Ra_{MIN} , Ra_{MAX} and the minimum value of $\cos(\theta)$ have been implemented as sensitivity coefficients 4213, $C_{t,4}$ and $e_{t,4}$ have been implemented as sensitivity coefficients 4214 and $C_{t,4}$ and $e_{t,4}$ have been implemented as sensitivity coefficients 4215.

Early in its formation, the transient film thickness determines the rate of heat transfer, while its steady-state value is limited by the greater of the correlation value or k_f / δ_{max} where δ_{max} is the user-specified maximum film thickness discussed in Section 2.8.1 below. Note, that because the film convective heat transfer correlations are functions of the flow conditions, and the flow conditions are a function of the rate of heat transfer, the convective heat transfer coefficient through the film must be determined iteratively as part of the overall solution for the temperature profile through a heat structure and its associated films. This is implied by use of the new time superscript $(m+1)$, e.g., $H_{f,L}^{m+1}$.

2.6.1.2 Conduction/Convection through Liquid Films (Film Tracking Active)

Section 2.8.2 discusses the film tracking model. This section only describes the correlations used to evaluate heat transfer through films being treated by the film tracking model. The correlations used are the same for all geometries and treat both laminar and turbulent film flow conditions. Laminar or turbulent heat transfer through the condensate film is determined by the following criteria:

Laminar if $Re_f < Re_{LOW}$
 Turbulent if $Re_f > Re_{HIGH}$
 Transition if $Re_{LOW} \leq Re_f \leq Re_{HIGH}$

where

Re_f = Reynolds number for the film flow

The laminar heat transfer coefficient through the film, $h_{f,l}$, is given by

$$h_{f,l} = k_f / \max(\delta_{f,l}, \delta_{min})$$

HS Package Reference Manual

where the laminar film thickness, $\delta_{f,l}$, is obtained from the film tracking model solution, and δ_{\min} is the user-adjustable minimum film thickness implemented as sensitivity coefficient 4251(1) (see Section 2.8.1). The turbulent heat transfer coefficient through the film, $h_{f,t}$, is given by

$$h_{f,t} = \left\{ k_f / \left[(\mu_f / \rho_f)^2 / (g \cdot \sin(\theta)) \right]^{1/3} \right\} Nu_{f,t}$$

where the turbulent film Nusselt number, $Nu_{f,t}$, is given by

$$Nu_{f,t} = \left(Re_f^{et1} + C_t Re_f^{et2} Pr_f^{et3} \right)^{et4}$$

The transition heat transfer coefficient through the film, $h_{f,tr}$, is given by linear interpolation of Re_f as

$$h_{f,tr} = h'_{f,l} + [h'_{f,t} - h'_{f,l}] \cdot [Re_f - Re_{LOW}] / [Re_{HIGH} - Re_{LOW}]$$

In each of these equations,

k_f = thermal conductivity of film

ρ_f = density of film

g = acceleration of gravity

μ_f = viscosity of film

θ = angle between horizontal and structure surface or axis (cyl.)

$h'_{f,l}$ = $h_{f,l}$ evaluated with $Re_f = C4253(5)$

$h'_{f,t}$ = $h_{f,t}$ evaluated with $Re_f = C4253(6)$

Re_{LOW} , Re_{HIGH} , C_t , $et1$, $et2$, $et3$, and $et4$ have been implemented as sensitivity coefficients 4253.

2.6.2 Radiation Heat Transfer

Simple models are available to determine the energy exchanges between a heat structure surface and the surrounding atmosphere and between the surfaces of heat structures. These are discussed below.

2.6.2.1 Atmosphere Radiation Heat Transfer

In addition to the convective boundary condition options, radiative heat transfer between the surface and the boundary volume atmosphere can be specified. Two options are currently available. They are:

- (1) Equivalent band model, and
- (2) Gray gas.

The equivalent band model is based on work by Edwards et al. [3] [4] in which the total radiation properties can be used to adequately calculate radiation heat transfer without resorting to a band model. The equivalent band equation is:

$$q_{EB} = \begin{cases} \sigma(F_g T_g^4 - F_{gw} T_w^4) & \text{for } T_g \neq T_w \\ 0 & \text{for } T_g = T_w \end{cases} \quad (2.93)$$

where

σ = Stefan-Boltzmann constant

$F_g = \varepsilon_w \varepsilon_{g1} / (1 - \rho_w \tau_{gb})$

$F_{gw} = \varepsilon_w \alpha_{gw1} / (1 - \rho_w \tau_{gbw})$

$\tau_{gb} = (\varepsilon_{g2} - \varepsilon_{g1}) / \varepsilon_{g1}$

$\tau_{gbw} = (\alpha_{gw2} - \alpha_{gw1}) / \alpha_{gw1}$

and ε and α are the emissivity and absorptivity, respectively. Subscripts g , w , gw , 1, and 2 refer to the gas, the wall, the gas at the wall temperature, one path length, and two path lengths. The values of the gas emissivity (ε_g) and absorptivity (α_{gw}), obtained from the model in CONTAIN [5], are functions of the gas composition, including the pressure of water vapor, CO, and CO₂ as well as the radiation path length, which is user specified. The wall emissivity ε_w , is given by user input, $\varepsilon_{w,user}$, that is overwritten if a liquid film is present. The emissivity of the film-covered wall becomes

$$\varepsilon_w = 1 - \rho_f - \rho_w \tau_f / (1 - \rho_f \rho_w) \quad (2.94a)$$

where

$$\tau_f = \exp(-1000\delta) \quad (2.94b)$$

$$\rho_f = (1 - \varepsilon_{H2O})(1 - \tau_f) \quad (2.94c)$$

$$\rho_w = 1 - \varepsilon_{w,user} \quad (2.94d)$$

$$\varepsilon_{H2O} = 0.96$$

and δ is the film thickness in meters.

The gray gas model equation is:

$$q_{GG} = \sigma [(1/\varepsilon_g) + (1/\varepsilon_w) - 1]^{-1} (T_g^4 - T_w^4) \quad (2.95)$$

where the gas emissivity is calculated for one path length.

2.6.2.2 Structure-to-Structure Radiation Heat Transfer

Structure-to-structure radiation can be calculated by a simple gray surface model. This optional model assumes that the radiative exchange between pairs of surfaces is independent and decoupled from the exchanges involved with other surfaces or with the intervening atmosphere. This permits sequential processing for each pair and does not require the use of iterative or simultaneous solution techniques. The net radiative heat loads for the surfaces of each heat structure are entered explicitly into the surface nodal energy balances similar to the method described in Section 2.3.2 for surface power sources.

An arbitrary number of heat structure surface pairs may be defined by the user and radiative exchange calculated between the surfaces of each pair by the following relationship:

$$q_{12} = \frac{\sigma(T_1^4 - T_2^4)}{\frac{1 - \varepsilon_1}{\varepsilon_1 A_1} + \frac{1}{A_1 F_{12}} + \frac{1 - \varepsilon_2}{\varepsilon_2 A_2}} \quad (2.96)$$

where

- q_{12} = radiative energy transfer rate from surface 1 to surface 2 (W)
- σ = Stefan-Boltzmann constant ($W/m^2 \cdot K^4$)
- T_1 = surface 1 temperature (K)
- T_2 = surface 2 temperature (K)
- ϵ_1 = surface 1 emissivity
- ϵ_2 = surface 2 emissivity
- A_1 = surface 1 area (m^2)
- A_2 = surface 2 area (m^2)
- F_{12} = view factor from surface 1 to surface 2

The emissivities may be computed by a default relation (from the COR package for oxidized steel surfaces) or may be computed by evaluation of user-specified real-valued control functions. A modification to account for the presence of a water film on either surface is applied and is the same as that described in Section 2.6.2.1 for radiative exchanges with the atmosphere. The areas used in the above equation correspond to the uncovered portions above the swollen liquid level of the adjacent CVH control volume. Radiative energy exchange between the surfaces of a pair is not calculated (i.e., q_{12} is set to 0.0) when:

- (1) either of the surfaces is covered by a pool,
- (2) either of the surface emissivities is determined to be zero, or
- (3) the input view factor is zero.

2.6.3 Pool Convection Heat Transfer

Natural, forced, or mixed convection heat transfer to the pool is determined at a surface by the following criteria:

Region	Criteria	Equation
Natural Convection	$Re^2 < 1.0Gr$	(2.97)
Forced Convection	$Re^2 > 10.0Gr$	(2.98)

HS Package Reference Manual

Mixed Convection	$1.0Gr \leq Re^2 \leq 10.0Gr$	(2.99)
------------------	-------------------------------	--------

where

Re = Reynolds number for pool

Gr = Grashof number for pool

Ra = Rayleigh number for pool

The constants in Equations (2.97) through (2.99) are implemented as sensitivity coefficient array C4080.

The pool natural convection heat transfer correlations have the following form:

$$Nu = C Ra^m + D \quad (2.100)$$

where

Nu = Nusselt number

Ra = Rayleigh number

C, m, D = constants dependent on flow condition and geometry

The constants C , m , and D in Equation (2.100) have been implemented as sensitivity coefficient arrays C4151 – C4162 and default values are presented in Table 2.3 for the various flow conditions and geometries.

The pool forced convection heat transfer correlations have the following form:

$$Nu = C Re^m Pr^n + D \quad (2.101)$$

where

Nu = Nusselt number

Re = Reynolds number

Pr = Prandtl number

C, m, n, D = constants dependent on flow condition and geometry

The constants C , m , n , and D in Equation (2.101) have been implemented as sensitivity coefficient arrays C4163 – C4174 and are presented in Table 2.3 for the various flow conditions and geometries.

The Nusselt number in the mixed convection regime is a linear interpolation between the Nusselt numbers for the natural and forced convection regimes, based on the ratio Re^2/Gr . This is the same method employed for atmosphere heat transfer, and an example is shown in Section 2.6.1. As with atmosphere heat transfer, the sensitivity coefficients defining the limits of natural and forced convection (sensitivity coefficient array C4080) may be chosen to eliminate the mixed convection regime for the pool in favor of use of the maximum of natural and forced convection heat transfer.

Laminar or turbulent natural convection heat transfer to the pool is determined at a surface by the following criteria:

Region	Criteria	Equation
Laminar Natural Convection	$Ra < 10^9$	(2.102)
Turbulent Natural Convection	$Ra > 10^{10}$	(2.103)
Transition between Laminar and Turbulent Natural Convection	$10^9 \leq Ra \leq 10^{10}$	(2.104)

The constants in Equations (2.102) through (2.104) are implemented as sensitivity coefficient arrays C4081 – C4083 for rectangular, cylindrical, and spherical (hemispherical) geometries.

Laminar or turbulent forced convection heat transfer to the pool is determined at a surface by the following criteria:

Region	Criteria	Equation
Laminar Forced Convection	$Re < 3 \times 10^5$ (rectangular)	(2.105a)
	$Re < 2 \times 10^3$ (cylindrical/spherical)	(2.105b)
Turbulent Forced Convection	$Re > 6 \times 10^5$ (rectangular)	(2.106a)
	$Re > 1 \times 10^4$ (cylindrical/spherical)	(2.106b)
Transition between Laminar and Turbulent Forced Convection	$3 \times 10^5 \leq Re \leq 6 \times 10^5$ (rectangular)	(2.107a)
	$2 \times 10^3 \leq Re \leq 1 \times 10^4$ (cylindrical/spherical)	(2.107b)

The constants in Equations (2.105) through (2.107) are implemented as sensitivity coefficient arrays C4084 – C4086 for rectangular, cylindrical, and spherical (hemispherical) geometries.

The Nusselt number in the transition region is a linear interpolation between the Nusselt numbers for the laminar and turbulent regimes. The interpolation is based on the Rayleigh number for natural convection and the Reynolds number for forced convection. This is the same method employed for atmosphere heat transfer, and an example is shown in Section 2.6.1. As with atmosphere heat transfer, the sensitivity coefficients defining the limits of laminar and turbulent convection (sensitivity coefficient arrays C408m) may be chosen to eliminate the transition regime for the pool in favor of use of the maximum of laminar and turbulent convection heat transfer.

2.6.4 Pool Boiling Heat Transfer

If a heat structure is submerged in a pool or a film is present and the heat structure surface temperature, T_{surf} , is greater than the saturation temperature, T_{sat} , at the total control volume pressure, pool boiling heat transfer from the heat structure is assumed. Using the heat structure surface temperature and various liquid properties, the logic for choosing the appropriate pool boiling regime is given by:

Nucleate boiling (Rohsenow) is calculated if

$$q''_{nb} \text{ (Rohsenow)} \leq q''_{chf} \text{ (Zuber)}$$

Film boiling (modified Bromley) is calculated if

$$q''_{film} \text{ (modified Bromley)} \geq q''_{mfilm} \text{ (Zuber)}$$

where

q''_{nb} = nucleate boiling heat flux given by Equation (2.108), W/m^2

q''_{chf} = critical heat flux given by Equation (2.110), W/m^2

q''_{film} = film boiling heat flux give by Equation (2.112), W/m^2

q''_{mfilm} = minimum film boiling heat flux given by Equation (2.111), W/m^2

If neither of these conditions is met, the surface is in transition boiling and a linear interpolation of the surface temperature is used to determine the heat flux at that temperature.

For all the above cases, once a heat flux has been determined, an effective heat transfer coefficient is evaluated as the ratio of heat flux over the difference between the surface

and pool temperatures. This heat transfer coefficient is used as the boundary heat transfer coefficient in the solution of the heat conduction equations.

2.6.4.1 Nucleate Boiling

The nucleate boiling heat flux is obtained through the Rohsenow relation [6]

$$\left[\frac{c_{pl}(T_{surf} - T_{sat})}{h_{fg}} \right] = C_{sf} \left[\frac{q_{nb}''}{\mu h_{fg}} \left(\frac{\sigma}{g(\rho_l - \rho_v)} \right)^{1/2} \right]^n Pr^m \quad (2.108)$$

where

- q_{nb}'' = nucleate boiling heat flux, W/m²
- c_{pl} = heat capacity of liquid at T_{sat} , J/kg•K
- T_{surf} = temperature of surface, K
- T_{sat} = saturation temperature in boundary volume, K
- C_{sf} = constant determined empirically for different surfaces and fluids (default = 0.013)
- μ = dynamic viscosity of liquid at T_{avg} , kg/m•s
- h_{fg} = latent heat in boundary volume of this surface, J/kg
- σ = surface tension at T_{avg} , N/m
- g = acceleration of gravity, m/s²
- ρ_l = density of liquid at T_{sat} , kg/m³
- ρ_v = density of vapor at T_{sat} , kg/m³
- n = constant (default = 0.33)
- Pr = Prandtl number of liquid in boundary volume
- m = constant (default = 1.0)
- T_{avg} = $(T_{surf} + T_{sat}) / 2$, K

HS Package Reference Manual

The constants C_{sf} , m , and n in Equation (2.108) have been implemented as sensitivity coefficient array C4180.

The surface tension of water is given as a function of temperature by

$$\sigma = 0.2358(1 - 0.625 T_R) T_R^{1.256} + c \quad (2.109)$$

where

- σ = surface tension, N/m
- T = temperature, K
- T_R = $1 - T / 647.3$
- c = constant (default = 0.0)

The constants in Equation (2.109), including c , have been implemented as sensitivity coefficient array C4000.

2.6.4.2 Critical Heat Flux

The critical heat flux is given by

$$q_{chr}'' = 0.18 \rho_v h_{fg} [\sigma (\rho_l - \rho_v) g / \rho_v^2]^{1/4} [\rho_l / (\rho_l + \rho_v)]^{1/2} \quad (2.110)$$

where

- q_c'' = critical heat flux, W/m²
- ρ_v = density of vapor at T_{sat} , kg/m³
- ρ_l = density of liquid at T_{sat} , kg/m³
- h_{fg} = latent heat in boundary volume, J/kg
- g = acceleration of gravity, m/s²
- σ = surface tension at T_{avg} , N/m
- T_{avg} = $(T_{surf} + T_{sat}) / 2$, K

T_{sat} = saturation temperature in boundary volume, K

T_{surf} = temperature of this surface, K

The constants in Equation (2.110) have been implemented as sensitivity coefficient array C4181. Zuber gives a leading coefficient of 0.131, while 0.18 is the value suggested by Rohsenow, see Reference [5].

2.6.4.3 Minimum Film Boiling Heat Flux

The minimum film boiling heat flux is given by Zuber [5] as

$$q''_{mfilm} = 0.09 \rho_v h_{fg} [\sigma (\rho_l - \rho_v) g / \rho_l^2]^{1/4} [\rho_l / (\rho_l + \rho_v)]^{1/2} \quad (2.111)$$

where

q''_{mfilm} = minimum film boiling heat flux, W/m²

The constants in Equation (2.111) have been implemented as sensitivity coefficient array C4182.

2.6.4.4 Stable Film Boiling

The film boiling heat flux is given by Bromley [5] as

$$q''_{film} = 0.943 [\rho_v (\rho_l - \rho_v) g k_v^3 (h_{fg} + (1/2) c_{pv} \Delta T) / \mu_v L_c]^{1/4} \Delta T^{0.75} \quad (2.112)$$

where

q''_{film} = film boiling heat flux, W/m²

L_c = characteristic length of this surface, m

ΔT = $T_{surf} - T_{sat}$, K

T_{surf} = temperature of this surface, K

T_{sat} = saturation temperature in boundary volume, K

g = acceleration due to gravity, m/s²

HS Package Reference Manual

- h_{fg} = latent heat in boundary volume, J/kg
- ρ_l = density of liquid at T_{sat} , kg/m³
- ρ_v = density of vapor at T_{sat} , kg/m³
- c_{pv} = heat capacity of vapor at T_{sat} , J/kg•K
- T_{avg} = $(T_{surf} + T_{sat}) / 2$, K
- μ_v = dynamic viscosity of vapor at T_{avg} , kg/m•s
- k_v = thermal conductivity of vapor at T_{avg} , W/m•K

The constants in Equation (2.112) have been implemented as sensitivity coefficient array C4183.

2.6.4.5 Transition Boiling

If transition boiling occurs at a surface, the heat flux is calculated as follows. First the surface temperatures at critical heat flux and minimum film boiling are calculated from

$$T_c = T_{sat} + (q_c'' \Delta T^3 / q_{NB}'')^{1/3} \quad (2.113)$$

$$T_{mfilm} = T_{sat} + [q_{mfilm}'' \Delta T^{0.75} / (q_{film}'' + q_{rad}'')]^{4/3} \quad (2.114)$$

where

- T_{sat} = saturation temperature in boundary volume, K
- ΔT = $T_{surf} - T_{sat}$, K
- q_c'' = critical heat flux given by Equation (2.110), W/m²
- q_{NB}'' = nucleate boiling heat flux given by Equation (2.108), W/m²
- q_{mfilm}'' = minimum film boiling heat flux given by Equation (2.111), W/m²
- q_{film}'' = film boiling heat flux given by Equation (2.112), W/m²
- q_{rad}'' = radiation to pool heat flux given by Equation (2.116), W/m²

The constants in Equations (2.113) and (2.114) are sensitivity coefficients 4180(4) and 4183(3), respectively.

With these temperatures known, the transition boiling heat flux is then obtained by logarithmic interpolation between the critical heat flux and the minimum film boiling heat flux based on $(T - T_{sat})$ values and includes the radiation heat flux. Therefore, after simplification, the transition boiling heat flux is given by

$$q''_{tran} = \exp\left(\frac{\ln(q''_c)(\ln \Delta T_{surf} - \ln \Delta T_{mfilm}) + \ln(q''_{mfilm})(\ln \Delta T_c - \ln \Delta T_{surf})}{\ln \Delta T_c - \ln \Delta T_{mfilm}}\right) + q''_{rad} \quad (2.115)$$

where

q''_{tran} = transition boiling heat flux, W/m²

T_c = critical temperature, K

ΔT_{surf} = $T_{surf} - T_{sat}$, K

ΔT_{mfilm} = $T_{mfilm} - T_{sat}$, K

ΔT_c = $T_c - T_{sat}$, K

q''_{rad} = radiation heat flux calculated by Equation (2.116), W/m²

2.6.4.6 Radiation During Boiling

Radiation heat transfer between a surface and the boundary volume pool is calculated during stable film and transition boiling. The radiation to pool heat flux is given by

$$q''_{rad} = C \sigma (T_{surf}^4 - T_{pool}^4) \quad (2.116)$$

where

q''_{rad} = radiation to pool heat flux, W/m²

T_{surf} = temperature of surface, K

T_{pool} = temperature of pool in boundary volume, K

σ = Stefan-Boltzmann constant, 5.669×10^{-8} W/m²•K⁴

HS Package Reference Manual

The constant C in Equation (2.116) defaults to 1.0 and has been implemented as sensitivity coefficient array C4184.

2.6.5 Energy Transfer to Control Volumes

The energy that is transferred from a heat structure surface to the boundary volume pool is:

$$\Delta Q_{pool}^m = q_{pool}^{*m} x_{pool} A \Delta t_m \quad (2.117)$$

Likewise, the energy that is transferred from a heat structure surface to the boundary volume atmosphere is:

$$\Delta Q_{atm}^m = q_{atm}^{*m} (1 - x_{pool}) A \Delta t_m \quad (2.118)$$

where

ΔQ_{pool}^m = energy transferred between heat structure surface and pool between times t_{m-1} and t_m , J

ΔQ_{atm}^m = energy transferred between heat structure surface and atmosphere between times t_{m-1} and t_m , J

q_{pool}^{*m} = heat flux to pool at time t_m , W/m²

q_{atm}^{*m} = heat flux to atmosphere at time t_m , W/m²

A = heat structure boundary surface area, m²

x_{pool} = fraction of boundary surface in pool of boundary volume

Δt_m = timestep size ($t_m - t_{m-1}$), s

These time-surface integrals are evaluated at each boundary surface to determine the total energy transferred between each heat structure and its respective boundary volume atmosphere and pool. These integrals are used to update the energy communication arrays for the CVH package.

2.7 Mass Transfer

Condensation occurs on a structure surface if its temperature is below the dew point of the associated atmosphere, and mass transfer from that surface has been enabled through user input (see the description for record HSCCCCC400 in the HS Users' Guide). The dew point is the saturation temperature corresponding to the partial pressure of steam in the bulk atmosphere of the boundary volume (obtained from the CVH data base). Evaporation from an existing film on a heat structure surface occurs if the surface temperature of the film exceeds the dew point. (A model to treat film flashing at the structure/film interface, when the temperature exceeds the boiling temperature, has not been activated because it has been unnecessary.)

In nearly pure steam environments, the rate of condensation is limited only by heat transfer through the structure, i.e. by the ability of the structure to dissipate the latent heat of vaporization that is released by condensation. Hence, in nearly pure steam environments, the rates of condensation and evaporation will self-adjust to whatever values are required to maintain the saturation temperature at the film/atmosphere interface.

As noncondensibles are introduced into the condensing steam, their accumulation near the film surface from local steam depletion tends to inhibit the flow of fresh steam to the film surface and restricts the rate of condensation. Consequently, when the ratio of the steam partial pressure to the total pressure in the boundary volume (obtained from the CVH data base) falls below a user-prescribed threshold, VPFRAC (also sensitivity coefficient 4200 with a default value of 0.9995), a mass transfer rate limitation is imposed on the rate of condensation. Experimental evidence indicates that the value of VPFRAC (below which diffusion rate limitations to condensation mass transfer become significant) can depend on the degree of turbulence. As the turbulence decreases, the value of VPFRAC should be increased to account for the inhibiting effect of even very small amounts of noncondensibles in a stagnant environment. Conversely, in a well-mixed system, the value of VPFRAC may have to be reduced to avoid artificially limiting the condensation rate. It is suggested that the user vary the value of VPFRAC in sensitivity studies, if uncertainty in the rate of condensation is of much concern.

The mass transfer rate limitation is a function of the diffusion mass transfer coefficient, which is calculated at a heat structure boundary surface whenever the surface is exposed to the atmosphere of its boundary volume. This coefficient is related to the atmosphere Nusselt number through a heat transfer analogy and is calculated by a Sherwood number correlation involving the Nusselt, Prandtl, and Schmidt numbers. This correlation is presented in Section 2.7.1.

The mass transfer rate-limited expression for condensation or evaporation at a surface exposed to a noncondensable-bearing atmosphere is formulated using a mechanistic approach which models the diffusion of a condensable vapor through a gas layer that contains noncondensable gases. Section 2.7.2 discusses this expression. If the surface temperature is greater than the critical temperature, 647.2°K, diffusion mass transfer is

HS Package Reference Manual

not calculated. However, the diffusion mass transfer coefficient is still calculated using Equation (2.124) since the radionuclide package requires this quantity.

2.7.1 Sherwood Number for Diffusion Mass Transfer

The mass transfer coefficient is related to the atmosphere Nusselt number by a heat and mass transfer analogy. In addition to the use of the Nusselt, Reynolds, and Prandtl numbers, the HS package uses the following dimensionless variables for its mass transfer calculations:

$$\text{Schmidt number } (Sc) = \mu/(\rho D)$$

$$\text{Sherwood number } (Sh) = h_D L_c/D$$

where

μ = dynamic viscosity of atmosphere at average of surface and atmosphere temperatures, kg/m•s

ρ = density of atmosphere, kg/m³

D = diffusivity, m²/s

h_D = mass transfer coefficient, m/s

L_c = characteristic length or dimension of surface, m

A Sherwood number correlation is used to calculate a diffusion mass transfer coefficient. The correlation is

$$Sh = C Nu^a Sc^b Pr^d \quad (2.119)$$

where

Nu = Nusselt number

Pr = Prandtl number

The constants C , a , b , and d have been implemented as sensitivity coefficient array C4201. The default values are:

C = 1.0

$$a = 1.0$$

$$b = 1/3$$

$$d = -1/3$$

The mass transfer coefficient is then obtained by

$$h_D = F_m Sh D / L_c \quad (2.120)$$

where F_m is an arbitrary, nonnegative scaling factor (with a default value of 1.0) that may be specified by the user at any surface. Refer to Section 2.6 for further discussion of this scaling factor and a caution concerning its use.

2.7.2 Condensation and Evaporation with Noncondensibles

The principal expression for condensation or evaporation mass flux at a surface exposed to an atmosphere with a significant partial pressure of noncondensable gases (i.e., $P_{stm} < VPFRAC \times P_{tot}$) is formulated using a mechanistic approach which models the diffusion of a condensable vapor through a gas layer that contains noncondensable gases [5]. The condensation mass flux is given by:

$$\dot{m}_c = h_D \rho_v \ln(\Delta P_{srf} / \Delta P_{atm}) \quad (2.121)$$

where

\dot{m}_c = mass flux at this surface, $\text{kg}/\text{m}^2 \cdot \text{s}$

h_D = mass transfer coefficient, m/s

ρ_v = density of vapor at $T_{sat}(P_{tot})$, kg/m^3

ΔP_{srf} = $P_{tot} - P_{srf}$, Pa

ΔP_{atm} = $P_{tot} - P_{stm}$, Pa

P_{tot} = total control volume pressure, Pa

P_{srf} = saturation pressure of steam at the surface temperature, Pa

P_{stm} = steam partial pressure in the control volume, Pa

Because Equation (2.121) is singular when the P_{srf} reaches P_{tot} it is necessary to bound the rate of evaporation as the surface temperature reaches $T_{sat}(P_{tot})$. This is done by using a flashing heat transfer coefficient to limit the rate of evaporation as follows:

$$\dot{m}_e = h_e \min(0, T_{dew} - T_{srf}) / h_{fg} \quad (2.122)$$

$$\dot{m} = \max(\dot{m}_c, \dot{m}_e) \quad (2.123)$$

where

h_e = flashing heat transfer coefficient, $W/m^2 \cdot K$

h_{fg} = latent heat of vaporization for steam, J/kg

T_{dew} = control volume dew point temperature, K

T_{srf} = surface temperature, K

and h_e has been implemented as sensitivity coefficient 4202, with a default value of $5 \times 10^5 W/m^2 \cdot K$.

2.7.3 Mass-Energy Transfer to Control Volumes

The mass which is transferred between the surface of a heat structure and the atmosphere of its boundary volume between times t_{m-1} and t_m is the value of the integral from t_{m-1} to t_m of the product of the mass flux and the area of the surface which is exposed to the atmosphere:

$$\Delta m^m = \dot{m} A (1 - x_{pool}) \Delta t_m \quad (2.124)$$

where

Δm^m = mass transferred between heat structure surface and atmosphere between times t_{m-1} and t_m , kg

\dot{m} = mass flux at heat structure surface, $kg/m^2 \cdot s$

A = heat structure boundary surface area, m^2

x_{pool} = fraction of boundary surface in pool of boundary volume

Δt_m = system timestep size ($t_m - t_{m-1}$), s

Mass transfer is not considered if the pool fraction is greater than the critical pool fraction CPFAL for the structure as defined in Section 2.4.

The time-surface integral of the mass flux is evaluated during each computational cycle for each surface to determine the total mass of the liquid on each heat structure boundary surface. Its value is constrained so that no more steam is condensed than is present in its boundary volume and no more liquid is evaporated or flashed than is present on the surface.

If more than a user-specified fraction (sensitivity coefficient 4203(2), with a default value of 90%) of the steam in a control volume is condensed during a computational cycle, then remedial action is taken. If the current timestep size is greater than a user-specified value (sensitivity coefficient 4203(1), with a default value of -1. s), then the HS package requests that the computational cycle be repeated with a smaller timestep size to eliminate the excessive condensation. The requested timestep size is equal to the current value times the ratio of the maximum amount of steam that may condense divided by the actual, excessive amount that would have condensed without the requested fallback. If the current timestep size is less than the value prescribed by sensitivity coefficient 4203(1), then the condensation flux (mass transfer rate) on each surface associated with this boundary volume is reduced by the same factor that would have been applied to the timestep size with the fallback option. The HS (not the entire MELCOR cycle) calculation is then repeated with the modified mass transfer rates. The fallback option is the default and recommended option because it does not alter the mechanistically calculated condensation rates. The scaling option may falsify the solution and should be avoided, if possible. Excessive condensation is a result of violating a timestep size constraint imposed by the explicit coupling between the HS and CVH packages (and is akin to the material Courant timestep limit). In some situations, it may be possible to avoid excessive condensation by re-nodalizing the problem to reduce the ratio of the surface area for condensation to the volume of steam available for condensation.

The liquid mass which is transferred to a heat structure surface by other packages is obtained from an array in the HS package data base whose elements are updated using an interface routine that can be called by any package.

For each heat structure surface, the mass and energy transfer is calculated for the steam which was condensed from or added to its boundary volume atmosphere and the liquid deposited in the boundary volume pool. The results of these calculations are used to update the mass and energy communication arrays for the CVH package. If the heat structure surface is part of a film tracking network, then the film thickness will be determined dynamically as a function of the film flow rate and the drainage from the surface will be partitioned between the boundary volume pool, the boundary volume fog

and the surfaces of other heat structures in the user-specified network. The film tracking model is discussed in Section 2.8.2.

2.8 Liquid Film Modeling

The mass, thickness, and specific enthalpy of a liquid film on a heat structure boundary surface are first determined during the initialization procedure in MELGEN execution. Calculation of these properties is also carried out during MELCOR execution. The models that are used to determine liquid film properties are described in Section 2.8.1. Section 2.8.2 describes the film tracking model, which is based on the model in CONTAIN [4] and is user-activated to track film drainage over a user-specified network of connected structure surfaces.

2.8.1 Film Models

During MELGEN and MELCOR execution, the mass of a liquid film on a heat structure boundary surface is determined from

- (1) calculation of the mass which is transferred between this surface and its boundary volume by condensation, evaporation or draining,
- (2) the liquid mass which is transferred to this surface by other packages, and
- (3) the liquid mass which is transferred to this surface by external sources (tabular function or control function) or film drainage from other heat structure surfaces, if the surface is part of a user-defined film tracking network.

The mass of the liquid film and the film surface and structure surface temperatures enable its thickness and specific enthalpy to be determined. The film equations are nodalized so that half of the film mass is associated with the film/structure interfacial node and the other half is associated with the atmosphere/film interfacial node. Therefore, the average specific enthalpy of the film is given by $0.5 \cdot [h_f(T_{s,srf}) + h_f(T_{f,srf})]$, where $h_f(T)$ is the specific enthalpy of the film at temperature T , $T_{s,srf}$ is the film/structure interfacial temperature and $T_{f,srf}$ is the atmosphere/film interfacial temperature.

For structures which are not part of a film tracking network, the condensate and deposited liquid is permitted to accumulate on a surface until the film thickness reaches a maximum. If the liquid mass is sufficiently large that the film thickness exceeds this maximum, then the excess liquid is deposited in the pool of the boundary volume of the surface. The maximum thickness of a liquid film on a surface is determined in one of two ways:

- (1) for geometries for which the convective heat transfer coefficient through the film (see Section 2.6.1.1) is obtained from a correlation as a function of the Reynolds number of the film flow, the Reynolds number is also used to obtain the film

thickness from the correlations used by the film tracking model (see Section 2.8.2 below) or

- (2) for all other geometries the maximum film thickness is obtained from a user-adjustable value. The user-adjustable value, δ_{max} , has been implemented as sensitivity coefficient 4251(2) with a default value of 5×10^{-4} m.

2.8.2 Film Tracking Model

For structures which are part of a film tracking network, the film thickness on a surface is determined iteratively as a function of the Reynolds number of the film flow rate as follows. First, the Reynolds number of the film flow is given by

$$Re_f = 2(\dot{m}_{in} + \dot{m}_{out}) / (w \mu_f) \quad (2.125)$$

where \dot{m}_{in} is the mass inflow rate (kg/s) from film drainage to the surface from other surfaces in the network and water deposited on the surface by other MELCOR packages, \dot{m}_{out} is the mass outflow rate (kg/s) from film drainage from this surface (which is to be determined iteratively), w is the width of this surface and μ_f is the bulk viscosity of the film. As an initial guess \dot{m}_{out} is set equal to zero. The film thickness as a function of Re_f is given by the following correlation

$$\delta_f = C_{f,l} \cdot \delta^* \cdot Re_f^{ef,l}, \text{ if } Re_f < Re_{LAM} \quad (2.126)$$

$$= C_{f,t} \cdot \delta^* \cdot Re_f^{ef,t}, \text{ if } Re_f > Re_{TURB}$$

=determined by interpolation between limits at Re_{LAM} and Re_{TURB} , otherwise

$$\delta^* = [(\mu_f / \rho_f)^2 / (g \cdot \sin \theta)]^{1/3}$$

where the constants $C_{f,x}$, exponents ef,x and limits Re_x (where x represents laminar or turbulent) in Equation (2.126) have been implemented as sensitivity coefficients 4253, and ρ_f and θ are the film density and angle of inclination of the surface from horizontal, respectively. The film thickness can also be determined from the conservation of film mass as

$$\delta_f = [m_{f,0} + (\dot{m}_{in} + \dot{m}_c - \dot{m}_{out}) \cdot \Delta t] / (\rho_f A_{surf}) \quad (2.127)$$

where $m_{f,0}$ is the film mass at the start of the timestep Δt , \dot{m}_c is the condensation rate (a negative value indicates evaporation) and A_{srf} is the surface area. Equation (2.127) has been presented for the case of rectangular geometry; the equations for cylindrical and spherical geometry are different because the film thickness is related to film volume differently.

For given values of $m_{f,0}$, \dot{m}_{in} , and \dot{m}_c , Equations (2.126) and (2.127) can be solved simultaneously by iterating on the value of \dot{m}_{out} to determine consistent values of δ_f and \dot{m}_{out} . Note, however, that if the value of δ_f given by Equation (2.126) with $\dot{m}_{out} = 0$ exceeds the value of δ_f given by Equation (2.127) with $\dot{m}_{out} = 0$, then the film thickness cannot possibly achieve the steady-state value consistent with Equation (2.126) during the given timestep. When a steady-state value consistent with Equation (2.126) is impossible for a timestep, \dot{m}_{out} is set equal to zero and Equation (2.127) is used to determine δ_f .

A user-specified minimum film thickness, δ_{min} , has been implemented as sensitivity coefficient 4251(1) to prevent film flow when the film thickness is less than the specified value (default value is 10^{-9} m). This can be used to inhibit film flow on rough surfaces until a reasonably thick film is established. Hence, when the solution to Equations (2.126) and (2.127) is less than δ_{min} , then δ_f in Equation (2.127) is set equal to δ_{min} to determine the value of \dot{m}_{out} , if a positive value is possible; otherwise, δ_f is equal to the value obtained from Equation (2.127) with \dot{m}_{out} set equal to zero.

The outflow (drainage) from the film tracking solution, \dot{m}_{out} , is partitioned between the CVH pool associated with the surface, "rain" passed to the SPR package via the TP package and the other drainage surfaces associated with the given surface through the user-specified film tracking network.

2.9 Stored Energy of a Heat Structure

The total stored energy of each heat structure, including surface films, is initialized during MELGEN execution. The stored energy of the structure itself is obtained by integrating the product of the volumetric heat capacity weight and the absolute temperature over the volume of the heat structure. The energy of the films is added to that total to arrive at a total structure energy storage. Therefore, the initial stored energy is

$$E^0 = f \sum_{i=1}^N G_i^m T_i^0 + m_{film,L}^0 h_{film,L}^0 + m_{film,R}^0 h_{film,R}^0 \quad (2.128)$$

where

- E^0 = initial stored energy of heat structure, J
- f = geometry factor with the following values for different geometries,
 = surface area of heat structure for rectangular geometries, m^2
 = axial length of heat structure for cylindrical geometries, m
 = 1.0 for spherical and hemispherical geometries.
- G_i^0 = volumetric heat capacity weight
 = $C_{p,j}^0 HVR$ for $i = 1$
 = $C_{p,j-1}^0 HVL_i + C_{p,j}^0 HVR_i$ for $i = 2, \dots, N - 1$
 = $C_{p,j-1}^0 HVL_i$ for $i = N$
- $C_{p,j}^0$ = initial volumetric heat capacity of mesh interval i , $J/m^3 \cdot K$
- HVL_i = left (inside) volume weight for mesh interval i , defined in Sections 2.1.1 and 2.2.1
- HVR_i = right (outside) volume weight for mesh interval i , defined in Sections 2.1.1 and 2.2.1
- T_i^0 = initial temperature of node i , K
- T_{i-1}^0 = initial temperature of node $i - 1$, K
- $m_{film,L}^0$ = initial mass of film on left boundary surface, kg
- $h_{film,L}^0$ = initial specific enthalpy of film on left boundary surface, J/kg
- $m_{film,R}^0$ = initial mass of film on right boundary surface, kg
- $h_{film,R}^0$ = initial specific enthalpy of film on right boundary surface, J/kg

During MELCOR execution, the change in the stored energy of each heat structure is calculated every cycle. This is obtained by integrating the product of the volumetric heat capacity weight and the change in temperature between times t_{m-1} and t_m over the volume of the heat structure, and including the energy change of the surface films. Therefore,

$$\Delta E^m = f \sum_{i=1}^N G_i^m (T_i^m - T_i^{m-1}) + m_{film,L}^m h_{film,L}^m - m_{film,L}^{m-1} h_{film,L}^{m-1} + m_{film,R}^m h_{film,R}^m - m_{film,R}^{m-1} h_{film,R}^{m-1} \quad (2.129)$$

where

ΔE^m = change in stored energy of heat structure between times t_{m-1} and $t_{m,j}$

G_i^m = volumetric heat capacity weight

= $C_{\rho,i}^m HVR_i$ for $i = 1$

= $C_{\rho,i-1}^m HVL_i + C_{\rho,i}^m HVR_i$ for $i = 2, \dots, N - 1$

= $C_{\rho,i-1}^m HVL_i$ for $i = N$

$C_{\rho,i}^m$ = volumetric heat capacity of mesh interval i at time t_m , $J/m^3 \cdot K$

T_i^m = temperature of node i at time t_m , K

T_i^{m-1} = temperature of node i at time t_{m-1} , K

$m_{film,L}$ = mass of film on left boundary surface, kg

$h_{film,L}$ = specific enthalpy of film on left boundary surface, kg

$m_{film,R}$ = mass of film on right boundary surface, kg

$h_{film,R}$ = specific enthalpy of film on right boundary surface, kg

m = denotes quantity of time t_m

$m+1$ = denotes quantity at time $t_m + \Delta t_m$

2.10 Degassing Model

The HS package degassing model assumes that the gas release occurs uniformly over the degassing temperature range. The contribution to the degassing rate for each mesh interval whose temperature exceeds the previously attained maximum is the product of the

source density, volume of the mesh interval, and the fraction of the degassing temperature range that the present maximum represents. Therefore,

$$g_k^m = \sum f \rho_{gas} (HVL + HVR) \frac{(T_2 - T_1)}{(T_{DGmax} - T_{DGmin})} / \Delta t_m \quad (2.130)$$

where

- g_k^m = degassing rate for k -th source at time t_m , kg/s
- \sum = sum over all heat structure nodes containing gas sources
- f = geometry factor
 - = surface area of heat structure for rectangular geometries, m^2
 - = axial length of heat structure for cylindrical geometries, m
 - = 1.0 for spherical or hemispherical geometries
- ρ_{gas} = source density, kg/m^3
- HVL = volume weight for left surface (Table 2.1 and Table 2.2)
- HVR = volume weight for right surface (Table 2.1 and Table 2.2)
- T_2 = $\min (T_{nmax}^m, T_{DGmax})$, K
- T_1 = $\min (T_{nmax}^{m-1}, T_{DGmax})$, K
- T_{nmax}^m = maximum temperature in mesh interval n at time t_m , K
- T_{nmax}^{m-1} = maximum temperature in mesh interval n at time t_{m-1} , K
- T_{DGmax} = upper temperature in degassing temperature range, K
- T_{DGmin} = lower temperature in degassing temperature range, K
- Δt_m = system timestep size ($t_m - t_{m-1}$), s

The HS package calculates the mass and internal energy of the gas (at the boundary volume temperature) which is released by each source through the present computational

cycle. These data are then used to update the mass and energy transfer communication arrays for the CVH package.

2.11 Ice Condenser Model

The ice condenser model allows the description of certain features found in Westinghouse PWR ice condenser containments. This model is a specially modified application of the heat structure degassing model described in Section 2.10. The user activates the ice condenser logic by including a prescribed keyword in the input for multiple solid, vertical cylindrical structures. A special gas source is defined to release liquid water into the pool of the outer associated CVH volume. The degassing temperature range should have a lower temperature of 274 K to avoid problems associated with limits of the thermodynamic and material properties routines. The upper temperature of the degassing range should be the saturation temperature to account for the sensible heating of the melt water. The heat of reaction of the gas source should include sensible heating of the ice from its actual subcooled temperature to the melting point, the latent heat of fusion, and the sensible heat addition to the melt water from melt to the upper value of the specified degassing temperature range. A special ice condenser Nusselt number multiplier has been added to the gas source input to account for effects not explicitly modeled that may affect the rate of heat transfer to the ice cylinder. Similarly, an ice condenser radionuclide deposition surface area enhancement factor has been added to account for unmodeled effects that will enhance the rate of radionuclide deposition on the ice condenser. Finally, a parameter has been added that can be adjusted by user input to vary the rate of decrease of the ice surface area as the ice melts. The ice surface area will vary as

$$(V/V_o)^{EXPICE}$$

where

V = current ice volume

V_o = initial ice volume

EXPICE = user-specified exponent

The total surface area for heat transfer to the ice condenser (ice and baskets) is the initial surface area of the cylindrical ice columns, A_o, multiplied by the factor

$$[RNDICE + (1 - RNDICE) \cdot (V/V_o)^{EXPICE}]$$

to provide a smooth transition to the minimum surface area of the ice baskets, $RNDICE \times A_o$, where $RNDICE$ is user defined. The total surface area for RN deposition is equal to the ice surface area plus the surface area of the ice baskets. The “gas” source density is that of liquid water.

MELCOR will automatically account for the volume change associated with the reduction in ice mass as melting proceeds. The user should define tabular input to specify properties for the metal baskets that hold the granular ice. The appropriate density is the value of the metal mass divided by the total volume occupied by the baskets. The thermal conductivity should exceed the value associated with ice to account for steam penetration into the granular matrix and conduction in the metal. The specified heat capacity is that of the metal.

2.12 Steel Melt Model

To allow for core boundary structure heating and subsequent melting, an option has been included in the degassing model to allow the user to input stainless steel as a degassing source. This option has been included only for use when the COR package is being used and is ignored otherwise. The implementation of the stainless steel degassing source is very similar to that used for ice as part of the ice condenser model (described above) except the heat of reaction of the stainless steel gas source should only include the latent heat of fusion. Because stainless steel is not a hydrodynamic material included in the CVH package, the volume of the melting stainless steel is associated with the COR package materials. As such, these materials are represented by the CVH package as “virtual volume” and, as with the ice condenser model, the volume changes due to melting are explicitly represented.

To prevent potential problems of adding a large amount of heat to a stainless steel degassing structure with an insignificant residual mass, a sensitivity coefficient, 4205, has been provided as a lower limit such that if the remaining unmelted structure mass falls below this limit, then the structure is assumed to have completely melted. When the structure is calculated to have completely melted, it is deactivated and HS processing for this structure is discontinued.

2.13 Communication with Other Packages

After completing the calculations discussed in Sections 2.1 through 2.12, the HS package communicates various changes to other packages using well-defined communication interfaces. The HS package communicates to the CVH package any mass, energy, and virtual volume changes in each control volume due to the following mechanisms:

- (1) heat transfer between each heat structure and the pool and atmosphere of its boundary volumes

HS Package Reference Manual

- (2) condensation of steam onto each heat structure from the atmosphere of its boundary volumes
- (3) evaporation or flashing of liquid (water) from each heat structure boundary surface into the atmosphere of its boundary volumes
- (4) deposition of liquid (water) from each heat structure into the pool of its boundary volumes
- (5) degassing of materials within each heat structure

The virtual volume with which the HS package is concerned is the volume occupied by all water films, ice condenser ice and meltable (degassible) steel associated with the core boundary structure melting model. Initial values of virtual volume are calculated during MELGEN execution and changes in virtual volume are calculated each computational cycle during MELCOR execution.

Prior to communication of control volume mass and energy changes to the CVH package, the HS package determines if these changes will lead to a negative mass of some material. If a negative mass is detected, the HS package requests that the present computational cycle be repeated with a timestep reduction and the changes not be communicated to the CVH package.

During MELCOR execution, the HS package calculates and communicates to the RadioNuclide (RN) package the fraction of liquid (water) mass on each heat structure boundary surface deposited during each computational cycle in the pool of its boundary volume. These fractions are used to calculate the relocation of radionuclides from deposition surfaces to the pools of their boundary volumes.

3. Solution Methods

The finite-difference approximation to the heat conduction equation with boundary conditions utilized by the HS package results in a tridiagonal system of N equations ($N+1$ or $N+2$ if there is a liquid film on one or both surfaces) for a heat structure with N ($N+1$ or $N+2$) temperature nodes. In order to reduce roundoff problems, the temperature of the heat structure relative to the minimum value of that heat structure is used to set up and solve the equations. The solution procedure is usually more complex than the standard solution for a tridiagonal system of equations. The boundary conditions often include energy input due to mass transfer and may include the deposition of energy from other sources such as decay-heat of radionuclides. Furthermore, the temperature nodes near the surface of a heat structure may be too closely spaced to accurately calculate the temperature at the surface, or the computational timestep may be large. This section discusses some of the special solution procedures that are used to obtain the steady-state and transient temperature distribution of a heat structure.

3.1 Iteration Strategy

By default an iterative procedure is employed to determine the temperature profile in each heat structure. This procedure repeats the following calculations until either convergence is attained or a maximum number of iterations is performed:

- (1) thermal properties
- (2) heat transfer coefficients
- (3) mass transfer
- (4) boundary condition coefficients
- (5) temperature distribution

Convergence is determined by testing the relative error in several dependent variables calculated during the temperature iteration:

- (1) the temperature at each node in the structure (including the film interfacial temperature[s]),
- (2) the mass of the film(s) (if the film thickness exceeds 10^{-5} m), and
- (3) the boiling heat transfer coefficient(s).

The relative error for dependent variable X is defined as

$$ERR_x = (X^m / X^{m-1}) - 1 \quad (3.1)$$

where

X^{m-1} = value of X at iteration $m-1$

X^m = value of X at iteration m

If the relative error in the temperature profile falls below a threshold value (ERR_{pp} in Section 3.3 below) during an iteration, then material properties are generally not recalculated for that iteration step. Values from the previous iteration step are used until the relative error again becomes higher than ERR_{pp} or until convergence is achieved. However, during degassing, properties must be updated after every iteration to ensure sufficient accuracy of the degassing rate.

Relaxation of the pool boiling heat transfer coefficient may be required in some situations, since it is extremely sensitive to changes in the surface temperature. Because relaxation

HS Package Reference Manual

effectively falsifies the value of the heat transfer coefficient until the relaxed value stabilizes, it is necessary to check the relative difference (error) between the unrelaxed value (which is determined by the latest surface temperature iterate) and the relaxed value. When pool boiling occurs, the pool heat transfer coefficient h_{pool}^m is relaxed between temperature iterations to be:

$$W_B h_{pool}^m + (1 - W_B) h_{pool}^{m-1}$$

where

h_{pool}^{m-1} = pool heat transfer coefficient at iteration $m-1$, $W/m^2 \cdot K$

h_{pool}^m = pool heat transfer coefficient at iteration m , $W/m^2 \cdot K$

and W_B is the modified relaxation parameter, which is set to an initial value that depends on whether it is a steady-state or transient iteration (RLX_B in Sections 3.2 and 3.3 below), and which is then decreased by a factor of 0.95 for each iteration during which the relative error in the boiling surface temperature is greater than -0.5 (i.e., the boiling surface temperature is not oscillating excessively so that relaxation may be reduced).

The system of equations describing the transient temperatures within a structure can become ill-conditioned if the timestep becomes too large. A precision limit (P_{imat} in Section 3.3) is imposed in the routine that performs the direct inversion of the tridiagonal coefficient matrix. If the relative difference between terms used in evaluating a nonzero difference in the algorithm is less than this limit, then there are too few significant figures in the difference to achieve the requested degree of precision. During MELGEN execution this condition is fatal but may be corrected by reducing the value of Δt_o , discussed in Section 3.2 below. During MELCOR execution the cycle will be repeated with a smaller timestep in an attempt to alleviate the problem.

There are three levels of convergence criteria used: the desired convergence criteria, a more stringent override convergence criterion, and the less stringent acceptance convergence criteria. The desired and acceptance criteria may be assigned different values for MELGEN and MELCOR execution, as discussed in Sections 3.2 and 3.3, respectively.

The desired convergence criteria are normally stringent enough to ensure reasonable accuracy in the overall results in the absence of phenomena that demand very high temperature resolution. During the occurrence of phenomena such as degassing or mass transfer (condensation/evaporation), however, very small errors in temperature can cause quite large errors in degassing and mass transfer rates. Therefore, during the occurrence of degassing or mass transfer, the desired temperature convergence criteria are overridden

by the override temperature convergence criterion (as long as it is more stringent). The override temperature convergence criterion is contained in sensitivity coefficient array 4055 and discussed in Section 3.3 below.

The iteration procedure for a heat structure will continue until either the desired criteria (or the override criterion during degassing or mass transfer) have been met or the iteration count reaches a prescribed maximum. During override, convergence is declared after the maximum number of iterations if the desired criteria have been met, even though the more stringent criterion has not been satisfied. If the acceptance criteria have not been satisfied for all tested variables on a heat structure after the maximum number of permitted iterations is performed, failure is declared for that heat structure. If the acceptance criteria have been met but the desired criteria have not been met, then success is declared but a message is issued to warn the user that the desired criteria were not met.

3.2 Steady-State Convergence Criteria

During MELGEN execution, an initial temperature distribution is calculated for a given heat structure if specified by user input. The following constants are the iteration parameters used for steady-state heat conduction calculations. They are implemented as sensitivity coefficient array C4051.

- ITR_{ss} = maximum number of permitted steady-state iterations (default = 400)
- ERR_{ss} = desired relative error tolerance for temperatures during steady-state calculations (default = 10^{-5})
- Δt_o = initial steady-state timestep (default = 10^5 s)
- ERF_{ss} = desired relative error tolerance for film mass for steady-state calculations (default = 10^{-2})
- DIE_{ss} = acceptable relative error tolerance for temperature during steady-state calculations (default = 10^{-2})

There is no acceptance criterion for film mass; the iteration procedure will continue for ITR_{ss} iterations in an attempt to satisfy the desired criterion, ERF_{ss} , but after ITR_{ss} iterations the film mass value is declared acceptable no matter what. The following coefficients are the iteration relaxation parameters used for steady-state heat conduction calculations to mitigate temperature oscillations. They are implemented as sensitivity coefficient array C4052.

- RLX_B = steady-state boiling heat transfer coefficient relaxation parameter (default = 0.0)

HS Package Reference Manual

ERR_B = desired steady-state boiling heat transfer coefficient error tolerance (default = 0.05)

The boiling heat transfer coefficient relative error acceptance criterion is 100%, that is it may double or vanish.

If any heat structure fails to meet the acceptance criteria, a restart file is not written and MELCOR execution may not begin.

3.3 Transient Convergence Criteria

During MELCOR execution, an iterative procedure is invoked if specified by user input (highly recommended). The following constants are the iteration parameters used for transient heat conduction calculations. They are implemented as sensitivity coefficient array C4055.

ITR_{tm} = maximum number of transient iterations (default = 30.)

ERR_{tm} = desired relative error tolerance for temperature during transient conduction calculations (default = 0.0005)

ITR_{cut} = minimum number of transient iterations required to prevent increase of the timestep size (default = 31.)

ERR_{prp} = minimum relative error tolerance for material property determination (default = 0.01)

P_{illmat} = tridiagonal matrix solver precision requirement (default = 1.0×10^{-10})

ERR_{ovr} = error tolerance override during degassing/mass transfer (default = 5.0×10^{-6})

ERF_{tm} = maximum relative error tolerance for film mass during transient conduction calculations (default = 0.01)

DIE_{tm} = maximum relative error tolerance for transient temperature during conduction calculations (default = 0.005)

There is no acceptance criterion for film mass; the iteration procedure will continue for ITR_{tm} in an attempt to satisfy the desired criterion, ERF_{tm} , but after ITR_{tm} iterations the film mass value is declared acceptable no matter what. The boiling heat transfer coefficient relative error acceptance criterion is 100%, that is, it may double or vanish.

Although inactive by default, the value of ITR_{cut} can be adjusted downward (below ITR_{tm}) to prevent the MELCOR system timestep from increasing if the HS package is taking too

many iterations per timestep. Judicious use of this feature requires comparing total CPU usage for various strategies.

The following constants are the relaxation parameters used for transient calculations. These parameters are implemented as sensitivity coefficient array C4056:

RLX_B = transient boiling heat transfer coefficient relaxation parameters (default = 0.9)

ERR_T = transient boiling heat transfer coefficient error tolerance (default = 0.05)

If the temperature solution fails for any structure during a calculation cycle, the HS package will immediately request that the cycle be repeated with the timestep reduced by a factor of one half. Failure may occur for several reasons, including excessive error in the temperatures, excessive error in the boiling heat transfer coefficient, numerical problems associated with finite precision or the generation of an out-of-range temperature (less than 273 K or greater than 4990 K), either legitimately or from divergence of the iterative algorithm.

4. Timestep Control

Timestep control is exercised by the Heat Structure package in cases (a) and (b) below by the HS package requesting that the current timestep be repeated with a smaller timestep size to correct the problem.

- (a) condensation is causing excessive steam depletion in the CVH package as discussed in Section 2.7.3 or,
- (b) the temperature solution for a heat structure fails to converge within the prescribed maximum number of iterations as discussed in Section 3.3. (a timestep reduction request to one-half the current timestep will also be made if a physically unreasonable value is detected during the iterative solution).

In these cases, the HS package will request that the current timestep be repeated with a smaller timestep size to attempt to correct the problem.

APPENDIX A: Sensitivity Coefficients

This appendix provides the sensitivity coefficients associated with various correlations and modeling parameters used in the HS package and described in this reference manual.

Equation or Section	Coefficient	Value	Units
(2.109)	C4000(1)	0.2358	N/m
	C4000(2)	1.0	
	C4000(3)	-0.625	K ⁻¹
	C4000(4)	1.256	
	C4000(5)	0.	N/m
	C4000(6)	1.0	
	C4000(7)	647.3	K
Section 3.2	C4051(1)	400.	
	C4051(2)	10 ⁻⁵	
	C4051(3)	10 ⁵	s
	C4051(4)	0.01	
	C4051(5)	0.01	
Section 3.2	C4052(1)	0.0	
	C4052(2)	0.05	
Section 3.3	C4055(1)	30.	
	C4055(2)	0.0005	
	C4055(3)	31.	
	C4055(4)	0.01	
	C4055(5)	10 ⁻¹⁰	
	C4055(6)	5.x10 ⁻⁶	
	C4055(7)	0.01	
	C4055(8)	0.005	
Section 3.3	C4056(1)	0.9	
	C4056(2)	0.05	
(2.79) - (2.81)	C4060(1)	1.0	
	C4060(2)	10.0	
(2.85) - (2.87)	C4061(1)	10 ⁹	
	C4061(2)	10 ¹⁰	
	C4062(1)	10 ⁹	
	C4062(2)	10 ¹⁰	
	C4063(1)	10 ⁹	
	C4063(2)	10 ¹⁰	
(2.88a)-(2.90b)	C4064(1)	3.0x10 ⁵	
	C4064(2)	6.0x10 ⁵	
	C4065(1)	2.0x10 ³	

HS Package Reference Manual

Equation or Section	Coefficient	Value	Units
	C4065(2)	10^4	
	C4066(1)	2.0×10^3	
	C4066(2)	10^4	
(2.4)	C4071(1)	0.02	
	C4071(2)	0.98	
(2.97) - (2.99)	C4080(1)	1.0	
	C4080(2)	10.0	
(2.102) - (2.104)	C4081(1)	10^9	
	C4081(2)	10^{10}	
	C4082(1)	10^9	
	C4082(2)	10^{10}	
	C4083(1)	10^9	
	C4083(2)	10^{10}	
(2.105) - (2.107)	C4084(1)	3.0×10^5	
	C4084(2)	6.0×10^5	
	C4085(1)	2.0×10^3	
	C4085(2)	10^4	
	C4086(1)	2.0×10^3	
	C4086(2)	10^4	
(2.82)	C4101(1)	0.046	
	C4101(2)	1/3	
	C4101(3)	0.	
(2.82)	C4102(1)	0.046	
	C4102(2)	1/3	
	C4102(3)	0.	
(2.82)	C4103(1)	0.228	
	C4103(2)	0.226	
	C4103(3)	0.	
(2.82)	C4104(1)	0.046	
	C4104(2)	1/3	
	C4104(3)	0.	
(2.82)	C4105(1)	0.046	
	C4105(2)	1/3	
	C4105(3)	0.	
(2.82)	C4106(1)	0.228	
	C4106(2)	0.226	
	C4106(3)	0.	
(2.82)	C4107(1)	0.59	
	C4107(2)	0.25	
	C4107(3)	0.	

HS Package Reference Manual

Equation or Section	Coefficient	Value	Units
(2.82)	C4108(1)	0.59	
	C4108(2)	0.25	
	C4108(3)	0.	
(2.82)	C4109(1)	0.43	
	C4109(2)	0.25	
	C4109(3)	12.0	
(2.82)	C4110(1)	0.10	
	C4110(2)	1/3	
	C4110(3)	0.	
(2.82)	C4111(1)	0.10	
	C4111(2)	1/3	
	C4111(3)	0.	
(2.82)	C4112(1)	0.43	
	C4112(2)	0.25	
	C4112(3)	2.0	
(2.83)	C4113(1)	8.235	
	C4113(2)	0.	
	C4113(3)	0.	
	C4113(4)	0.	
(2.83)	C4114(1)	48/11	
	C4114(2)	0.	
	C4114(3)	0.	
	C4114(4)	0.	
(2.83)	C4115(1)	48/11	
	C4115(2)	0.	
	C4115(3)	0.	
	C4115(4)	0.	
(2.83)	C4116(1)	0.023	
	C4116(2)	0.8	
	C4116(3)	1/3	
	C4116(4)	0.	
(2.83)	C4117(1)	0.023	
	C4117(2)	0.8	
	C4117(3)	1/3	
	C4117(4)	0.	
(2.83)	C4118(1)	0.023	
	C4118(2)	0.8	
	C4118(3)	1/3	
	C4118(4)	0.	
(2.83)	C4119(1)	0.664	

HS Package Reference Manual

Equation or Section	Coefficient	Value	Units
	C4119(2)	0.5	
	C4119(3)	1/3	
	C4119(4)	0.	
(2.83)	C4120(1)	0.664	
	C4120(2)	0.5	
	C4120(3)	1/3	
	C4120(4)	0	
(2.83)	C4121(1)	0.60	
	C4121(2)	0.5	
	C4121(3)	1/3	
	C4121(4)	2.0	
(2.83)	C4122(1)	0.037	
	C4122(2)	0.8	
	C4122(3)	1/3	
	C4122(4)	0.	
(2.83)	C4123(1)	0.037	
	C4123(2)	0.8	
	C4123(3)	1/3	
	C4123(4)	0.	
(2.83)	C4124(1)	0.60	
	C4124(2)	0.5	
	C4124(3)	1/3	
	C4124(4)	2.0	
(2.100)	C4151(1)	0.046	
	C4151(2)	1/3	
	C4151(3)	0.	
(2.100)	C4152(1)	0.046	
	C4152(2)	1/3	
	C4152(3)	0.	
(2.100)	C4153(1)	0.228	
	C4153(2)	0.226	
	C4153(3)	0.	
(2.100)	C4154(1)	0.046	
	C4154(2)	1/3	
	C4154(3)	0.	
(2.100)	C4155(1)	0.046	
	C4155(2)	1/3	
	C4155(3)	0.	
(2.100)	C4156(1)	0.228	
	C4156(2)	0.226	

HS Package Reference Manual

Equation or Section	Coefficient	Value	Units
	C4156(3)	0.	
(2.100)	C4157(1)	0.59	
	C4157(2)	0.25	
	C4157(3)	0.	
(2.100)	C4158(1)	0.59	
	C4158(2)	0.25	
	C4158(3)	0.	
(2.100)	C4159(1)	0.43	
	C4159(2)	0.25	
	C4159(3)	2.0	
(2.100)	C4160(1)	0.10	
	C4160(2)	1/3	
	C4160(3)	0.	
(2.100)	C4161(1)	0.10	
	C4161(2)	1/3	
	C4161(3)	0.	
(2.100)	C4162(1)	0.43	
	C4162(2)	0.25	
	C4162(3)	2.0	
(2.101)	C4163(1)	8.235	
	C4163(2)	0.	
	C4163(3)	0.	
	C4163(4)	0.	
(2.101)	C4164(1)	48/11	
	C4164(2)	0.	
	C4164(3)	0.	
	C4164(4)	0.	
(2.101)	C4165(1)	48/11	
	C4165(2)	0.	
	C4165(3)	0.	
	C4165(4)	0.	
(2.101)	C4166(1)	0.023	
	C4166(2)	0.8	
	C4166(3)	1/3	
	C4166(4)	0.	
(2.101)	C4167(1)	0.023	
	C4167(2)	0.8	
	C4167(3)	1/3	
	C4167(4)	0.	
(2.101)	C4168(1)	0.023	

HS Package Reference Manual

Equation or Section	Coefficient	Value	Units
	C4168(2)	0.8	
	C4168(3)	1/3	
	C4168(4)	0.	
(2.101)	C4169(1)	0.664	
	C4169(2)	0.5	
	C4169(3)	1/3	
	C4169(4)	0.	
(2.101)	C4170(1)	0.664	
	C4170(2)	0.5	
	C4170(3)	1/3	
	C4170(4)	0.	
(2.101)	C4171(1)	0.60	
	C4171(2)	0.5	
	C4171(3)	1/3	
	C4171(4)	2.0	
(2.101)	C4172(1)	0.037	
	C4172(2)	0.8	
	C4172(3)	1/3	
	C4172(4)	0.	
(2.101)	C4173(1)	0.037	
	C4173(2)	0.8	
	C4173(3)	1/3	
	C4173(4)	0.	
(2.101)	C4174(1)	0.60	
	C4174(2)	0.5	
	C4174(3)	1/3	
	C4174(4)	2.0	
(2.108)	C4180(1)	0.013	
	C4180(2)	0.5	
	C4180(3)	1.0	
	C4180(4)	0.33	
(2.110)	C4181(1)	0.18	
	C4181(2)	0.25	
	C4181(3)	0.5	
(2.111)	C4182(1)	0.09	
	C4182(2)	0.25	
	C4182(3)	0.5	
(2.112)	C4183(1)	0.943	
	C4183(2)	0.25	
	C4183(3)	0.75	

HS Package Reference Manual

Equation or Section	Coefficient	Value	Units
(2.116)	C4184(1)	0.943	
Section 2.7	C4200(1)	0.9995	
(2.119)	C4201(1)	1.0	
	C4201(2)	1.0	
	C4201(3)	1/3	
	C4201(4)	-1/3	
(2.122)	C4202(1)	5×10^5	W/m ² -K
Section 2.7.3	C4203(1)	-1.0	
	C4203(2)	0.9	
Section 2.12	C4205(1)	10.	kg
Section 2.6.1.1	C4210(1)	30.	
	C4210(2)	100.	
	C4210(3)	(not used)	
	C4210(4)	0.1686289	
Section 2.6.1.1	C4211(1)	0.943	
	C4211(2)	0.25	
Section 2.6.1.1	C4212(1)	0.3333333	
	C4212(2)	-0.44	
	C4212(3)	5.82×10^{-6}	
	C4212(4)	0.8	
	C4212(5)	0.3333333	
	C4212(6)	0.5	
Section 2.6.1.1	C4213(1)	10^6	
	C4213(2)	10^8	
	C4213(3)	10^{10}	
Section 2.6.1.1	C4214(1)	0.6	
	C4214(2)	0.2	
Section 2.6.1.1	C4215(1)	0.72	
	C4215(2)	0.19	
Section 2.6.1.1	C4220(1)	30.	
	C4220(2)	100.	
	C4220(4)	0.9715642	
Section 2.6.1.1	C4221(1)	0.729	
	C4221(2)	0.25	
Section 2.6.1.1	C4222(1)	0.3333333	
	C4222(2)	-0.44	
	C4222(3)	5.82×10^{-6}	
	C4222(4)	0.8	
	C4222(5)	0.3333333	
	C4222(6)	0.5	

HS Package Reference Manual

Equation or Section	Coefficient	Value	Units
Section 2.6.1.1	C4230(1)	30.	
	C4230(2)	100.	
Section 2.6.1.1	C4231(1)	0.815	
	C4231(2)	0.25	
Section 2.6.1.1	C4232(1)	0.3333333	
	C4232(2)	-0.44	
	C4232(3)	5.82×10^{-6}	
Section 2.6.1.1	C4232(4)	0.8	
	C4232(5)	.3333333	
	C4232(6)	0.5	
Section 2.8.1	C4251(1)	10^{-9}	
Section 2.8.2	C4251(2)	0.0005	
Sections 2.6.1.2 & 2.8.2	C4253(1)	0.909	
	C4253(2)	0.3333333	
	C4253(3)	0.115	
	C4253(4)	0.6	
	C4253(5)	1000.	
	C4253(6)	3000.	
	C4253(7)	-0.44	
	C4253(8)	5.82×10^{-6}	
	C4253(9)	0.8	
	C4253(10)	0.3333333	
	C4253(11)	0.5	

References

1. V. H. Ransom et al., RELAP5/MOD1 Code Manual Volume 1: System Models and Numerical Methods, NUREG/CR-1826, EGG-2070, R2, September 1981.
2. C. O. Bennett and J. E. Myers, Momentum, Heat, and Mass Transfer, 3rd ed., McGraw-Hill, New York, 1982, p. 341.
3. D. K. Edwards, On the Use of Total Radiation Properties of Gases, ANL/RAS 75-12, April 1975.
4. D. K. Edwards and R. Matavosian, "Scaling Rules for Total Absorptivity and Emissivity of Gases," Trans. ASME, JHT, Vol. 106, pp. 684-689, November 1984.
5. K. K. Murata, et al., "Code Manual for CONTAIN 2.0: A Computer Code for Nuclear Reactor Containment Analysis," NUREG/CR-6533, SAND97-1735, 1997.
6. J. G. Collier, Convective Boiling and Condensation, 2nd ed., McGraw-Hill, New York, 1981.

Material Properties (MP) Package Reference Manual

The MELCOR Material Properties package models many of the properties needed by the various physics packages. This is done by using analytical laws, correlations, or linear tables. New materials and their properties may be defined through user input, and properties for default materials may be redefined by user input.

This document identifies the default material property values and functions used in the MELCOR MP package. References for the data are provided. Detailed descriptions of input requirements are provided in the MP Package Users' Guide.

The thermodynamic properties of water vapor and liquid water are contained in the H₂O package and cannot be modified through user input. Properties of noncondensable gases are calculated by the NCG package. A description of the default values and available user input options is provided in the MELCOR NonCondensable Gas (NCG) Package Users' Guide.

CORCON and VANESA properties are included in the Cavity (CAV) and RadioNuclide (RN) packages, respectively. See the reference manuals and users' guides for those packages.

Contents

1.	Default Material Properties.....	7
2.	Specific Enthalpy as a Function of Temperature	9
2.1	Zircaloy	10
2.2	Zirconium Oxide	11
2.3	Uranium Dioxide.....	11
2.4	Stainless Steel.....	12
2.5	Stainless Steel Oxide	13
2.6	Boron Carbide	13
2.7	Silver-Indium-Cadmium	14
2.8	Uranium Metal	14
2.9	Graphite	14
2.10	Aluminum	15
2.11	Aluminum Oxide	16
2.12	Cadmium.....	16
2.13	Stainless Steel 304.....	16
2.14	Lithium Aluminum.....	17
2.15	Uranium Aluminum.....	18
2.16	Carbon Steel	19
3.	Temperature as a Function of Special Enthalpy	19
4.	Specific Heat Capacity as a Function of Temperature	20
4.1	Zircaloy	21
4.2	Zirconium Oxide	21
4.3	Uranium Dioxide.....	21
4.4	Stainless Steel.....	22
4.5	Stainless Steel Oxide	23
4.6	Boron Carbide	23
4.7	Silver-Indium-Cadmium	23
4.8	Uranium Metal	24
4.9	Graphite	24
4.10	Concrete.....	25
4.11	Aluminum	25
4.12	Aluminum Oxide	26
4.13	Cadmium.....	26
4.14	Stainless Steel 304.....	27
4.15	Lithium Aluminum.....	27
4.16	Uranium Aluminum.....	28
4.17	Carbon Steel	29
5.	Thermal Conductivity as a Function of Temperature	30

MP Package Reference Manual

5.1	Tabular	30
5.1.1	Water	30
5.1.2	Steam	31
5.1.3	Air	33
5.1.4	Zircaloy	34
5.1.5	Zirconium Oxide.....	35
5.1.6	Uranium Dioxide	35
5.1.7	Stainless Steel (SS).....	35
5.1.8	Stainless Steel Oxide.....	36
5.1.9	Boron Carbide.....	36
5.1.10	Silver-Indium-Cadmium	36
5.1.11	Uranium Metal.....	37
5.1.12	Graphite	37
5.1.13	Concrete	38
5.1.14	Aluminum.....	38
5.1.15	Aluminum Oxide.....	38
5.1.16	Cadmium	39
5.1.17	Stainless Steel 304	40
5.1.18	Lithium Aluminum	41
5.1.19	Uranium Aluminum	42
5.1.20	Carbon Steel.....	42
5.2	Eucken Correlation for a Single, Pure Gas	43
5.3	Wassijewa Equation for a Combination of Low-Pressure Gases	43
6.	Dynamic Viscosity as a Function of Temperature	45
6.1	Tabular	45
6.1.1	Water	45
6.1.2	Steam	46
6.1.3	Air	47
6.1.4	Hydrogen	47
6.1.5	Deuterium	48
6.2	Chapman-Enskog Equation for a Single, Pure Gas	49
6.3	Chapman-Enskog Equation for a Combination of Low-Pressure Gases..	51
7.	Binary Mass Diffusion Coefficient	52
7.1	Binary Mass Diffusion Coefficient as a Function of Temperature and Pressure.....	52
7.2	Chapman-Enskog Equation for a Pair of Low-Pressure Gases	53
7.3	Chapman-Enskog Equation for a Combination of Low-Pressure Gases..	55
8.	Density.....	55
8.1	Constant Density.....	55
8.2	Tabular as a Function of Temperature.....	56
8.2.1	Zircaloy	57

8.2.2	Zirconium Oxide.....	57
8.2.3	Uranium Dioxide	57
8.2.4	Stainless Steel	57
8.2.5	Stainless Steel Oxide.....	57
8.2.6	Boron Carbide.....	58
8.2.7	Silver-Indium-Cadmium	58
8.2.8	Uranium Metal.....	58
8.2.9	Graphite	59
8.2.10	Concrete	59
8.2.11	Aluminum.....	59
8.2.12	Aluminum Oxide.....	59
8.2.13	Cadmium	60
8.2.14	Stainless Steel 304	61
8.2.15	Lithium Aluminum	62
8.2.16	Uranium Aluminum	62
8.2.17	Carbon Steel.....	63
8.3	Calculated as a Function of Temperature and Pressure.....	63
8.3.1	Air	63
8.3.2	Steam	64
9.	Constant Melting Temperature.....	72
10.	Constant Latent Heat of Fusion	72
11.	References.....	73

List of Figures

Figure 8.1.	Methods for Computing the Compressibility from Table 8.1 Data.	71
-------------	---	----

List of Tables

Table 2.1	Default material properties, property mnemonics, and user input capabilities.9	
Table 6.1.	Collision Integral, Ω_v , as a Function of the Dimensionless Temperature, T^* [17].....	50
Table 7.1.	Collision Integral, Ω_D , as a Function of Dimensionless Temperature, T_{AB}^* [17].....	54
Table 8.1.	Compressibility of Steam as a Function of Temperature (K) and Pressure (MPa) (Ref. 9).....	68

1. Default Material Properties

The MELCOR Material Properties (MP) package models many common properties needed by the various phenomenological packages through the use of analytical laws, correlations, and tabulated values. These properties include thermodynamic state and transport properties needed for structural materials, as well as transport properties for water and noncondensable gases. (Thermodynamic state properties for these fluids are provided separately by the H2O and NCG packages; see the NCG/H2O Reference Manual.)

In a few cases, stand-alone codes that have been wholly integrated into MELCOR still use properties defined within those codes; a notable example is CORCON, which has been integrated into the Cavity (CAV) package. Also, properties unique to a package, such as those for trace species used in the RadioNuclide (RN) package, are generally modeled within that package. The Core (COR), Fuel Dispersal Interactions (FDI), and Heat Structures (HS) packages use principally the structural materials properties, while the Control Volume Hydrodynamics (CVH), Engineered Safety Features (ESF), Containment Sprays (SPR), and RN packages use principally the fluid transport properties.

The following 34 materials, listed with their mnemonic identifiers, are defined in the Material Properties package:

- | | |
|-----------------------------------|---------------------------------|
| 1. Water (WATER) | 19. Carbon Dioxide (CO2) |
| 2. Steam (STEAM) | 20. Carbon Monoxide (CO) |
| 3. Air (AIR) | 21. Nitrogen (N2) |
| 4. Hydrogen (H2) | 22. Nitric Oxide (NO) |
| 5. Helium (HE) | 23. Nitrous Oxide (N2O) |
| 6. Argon (AR) | 24. Ammonia (NH3) |
| 7. Deuterium (D2) | 25. Acetylene (C2H2) |
| 8. Zircaloy (ZR) | 26. Methane (CH4) |
| 9. Zirconium Oxide (ZRO2) | 27. Ethylene (C2H4) |
| 10. Uranium Dioxide (UO2) | 28. Uranium Hexafluoride (UF6) |
| 11. Stainless Steel (SS) | 29. Aluminum (ALUM) |
| 12. Stainless Steel Oxide (SSOX) | 30. Aluminum Oxide (AL2O3) |
| 13. Boron Carbide (B4C) | 31. Cadmium (CADM) |
| 14. Silver-Indium-Cadmium (AGINC) | 32. Stainless Steel 304 (SS304) |
| 15. Uranium Metal (UMETL) | 33. Lithium Aluminum (LIAL) |
| 16. Graphite (GRAPH) | 34. Uranium Aluminum (UAL) |
| 17. Concrete (CON) | 35. Carbon Steel (CS) |
| 18. Oxygen (O2) | |

Material 11, Stainless Steel (SS), is a type 347 stainless steel and is typically used in the Core package, whereas material 32 (SS304) is a type 304 stainless steel.

The following properties are defined in the package:

MP Package Reference Manual

	Type	Units
1. Enthalpy as a function of temperature	Tabular	J/kg
2. Temperature as a function of enthalpy	Tabular	K
3. Specific Heat Capacity as a function of temperature	Tabular	J/kg-K
4. Thermal Conductivity as a function of temperature		
a. From tables	Tabular	W/m-K
b. From Eucken correlation and Wassijewa equation	Calculated	W/m-K
5. Dynamic Viscosity as a function of temperature		
a. From tables	Tabular	kg/m-s
b. From Chapman-Enskog equations and Lennard-Jones potential parameters	Calculated	kg/m-s
6. Binary Diffusion Coefficient		
a. Function of temperature and pressure	Calculated	m ² /s
b. From Chapman-Enskog equations and Lennard-Jones potential parameters	Calculated	m ² /s
7. Density		
a. Constant	Constant	kg/m ³
b. Function of temperature	Tabular	kg/m ³
c. Function of temperature and pressure	Calculated	kg/m ³
8. Melting Temperature	Constant	K
9. Latent Heat of Fusion	Constant	J/kg

Default values are provided for some, but not all, combinations of materials and physical properties. Table 2.1 summarizes the default values available. A 'T' indicates that the default function can be changed through user-defined tabular functions and an MPMATnnnmm input record. A 'C' indicates that the default function can be changed through user-defined constant values input on an MPMATnnnmm record. An 'X' indicates that the default function cannot be changed through user input. A blank space indicates that no default is provided, but may be supplied by the user, although in some cases that property for that material may not be used by MELCOR.

Also shown is the mnemonic(s) used to add new values or alter the default values through user input for those properties which can be changed.

Sections 1 through 10 identify the default values for those combinations defined in MELCOR. User definition of the materials properties is also discussed in each section.

2. Specific Enthalpy as a Function of Temperature

The specific enthalpy may be computed from either a user-specified tabular function or a MELCOR default table.

The user-specified tabular function to define a new material or to override the default table for an existing material is invoked by using a standard tabular function (see the TF Package Users' Guide) to input the enthalpy (J/kg) as a function of temperature (K). Negative enthalpies are permitted. Currently, there are no checks made on the consistency of user-input values for enthalpy, specific heat capacity, melting temperature, and latent heat of fusion; this could be rectified in future code versions.

The following materials have default tables for enthalpy:

Zircaloy	Graphite
Zirconium Oxide	Aluminum
Uranium Dioxide	Aluminum Oxide
Stainless Steel	Cadmium
Stainless Steel Oxide	Stainless Steel 304
Boron Carbide	Lithium Aluminum
Silver-Indium-Cadmium	Uranium Aluminum
Uranium Metal	Carbon Steel

Table 2.1 Default material properties, property mnemonics, and user input capabilities.

Property*:	1	2	3	4a	4b	5a	5b	6a	6b	7a	7b	7c	8	9
Mnemonic:	ENH	TMP	CPS	THC	SIG EPS	VIS	SIG EPS	n/a	SIG EPS	DEN	RHO	n/a	MLT	LHF
WATER				T			T							
STEAM				T	C	T	C		C			X		
AIR				T	C	T	C		C			X		
H2					C	T	C		C					
HE					C		C		C					
AR					C		C		C					
D2					C	T	C		C					
ZR	T	T	T	T						C	T		C	C
ZRO2	T	T	T	T						C	T		C	C
UO2	T	T	T	T						C	T		C	C
SS	T	T	T	T						C	T		C	C
SSOX	T	T	T	T						C	T		C	C
B4C	T	T	T	T						C	T		C	C
AGINC	T	T	T	T						C	T		C	C

MP Package Reference Manual

Property*:	1	2	3	4a	4b	5a	5b	6a	6b	7a	7b	7c	8	9
Mnemonic:	ENH	TMP	CPS	THC	SIG EPS	·VIS	SIG EPS	n/a	SIG EPS	DEN	RHO	n/a	MLT	LHF
UMETL	T	T	T	T						C	T		C	C
GRAPH	T	T	T	T						C	T		C	
CON			T	T							T			
O2					C		C		C					
CO2					C		C		C					
CO					C		C		C					
N2					C		C		C					
NO					C		C		C					
N2O					C		C		C					
NH3					C		C		C					
C2H2					C		C		C					
CH4					C		C		C					
C2H4					C		C		C					
UF6					C		C		C					
STEAM + AIR								X						
STEAM + H2								X						
ALUM	T	T	T	T						C	T		C	C
AL2O3	T	T	T	T						C	T		C	C
CADM	T	T	T	T						C	T		C	C
SS304	T	T	T	T						C	T		C	C
LIAl	T	T	T	T						C	T		C	C
UAL	T	T	T	T						C	T		C	C
CS	T	T	T	T						C	T		C	C

T - The default function can be changed using tabular functions and an MPMATnnnmm input record.

C - The default function can be changed using constant values input on an MPMATnnnmm record.

X - The default function cannot be changed through user input.

Note: A blank space indicates that no default is provided, but may be supplied by the user, although in some cases the property may not be used.

* See Section 1 for a full description of these properties.

The default specific enthalpy values are computed by linear interpolation of the tabulated values listed below. The tabular values were computed by integrating the tables of specific heat capacities from Section 4. The latent heat of fusion from Section 10 was added at the melting point given in Section 9 over a range of 0.01 K.

2.1 Zircaloy

The default tabular values of specific enthalpy as a function of temperature for Zircaloy are listed below. Linear extrapolation is allowed from both ends of the tabulated range.

Zircaloy

Temperature	Specific Enthalpy (J/kg)
300.0	0.0
400.0	21915.0
640.0	105110.0
1090.0	263960.0
1093.0	265275.5
1113.0	276195.5
1133.0	288245.5
1153.0	301585.5
1173.0	316935.5
1193.0	332795.5
1213.0	346685.5
1233.0	357565.5
1248.0	363753.0
2098.0	666353.0
2098.01	891353.0
3598.0	1425353.0

2.2 Zirconium Oxide

The default tabular values of specific enthalpy as a function of temperature for zirconium oxide are listed below. Linear extrapolation is allowed from both ends of the tabulated range.

Zirconium Oxide

Temperature (K)	Specific Enthalpy (J/kg)
300.0	0.0
2990.0	1464167.0
2990.01	2171167.0
3500.0	2448760.0

2.3 Uranium Dioxide

The default tabular values of specific enthalpy as a function of temperature for uranium dioxide are listed below. Linear extrapolation is allowed from both ends of the tabulated range.

Uranium Dioxide

Temperature (K)	Specific Enthalpy (J/kg)
300.0	33143.0
400.0	58419.0
500.0	85883.0
600.0	114638.0

MP Package Reference Manual

Uranium Dioxide

Temperature (K)	Specific Enthalpy (J/kg)
700.0	144257.0
800.0	174517.0
900.0	205288.0
1000.0	236492.0
1100.0	268080.0
1200.0	300023.0
1300.0	332309.0
1400.0	364947.0
1500.0	397973.0
1600.0	431455.0
1700.0	465502.0
1800.0	500266.0
1900.0	535945.0
2000.0	572782.0
2100.0	611064.0
2200.0	651111.0
2300.0	693275.0
2400.0	737927.0
2500.0	785450.0
2600.0	836232.0
2700.0	890656.0
2800.0	949096.0
2900.0	1011906.0
3000.0	1079422.0
3113.0	1161764.0
3113.01	1435764.0
3513.0	1636964.0

2.4 Stainless Steel

The default tabular values of specific enthalpy as a function of temperature for stainless steel are listed below. Linear extrapolation is allowed from both ends of the tabulated range.

Stainless Steel

Temperature (K)	Specific Enthalpy (J/kg)
300.0	0.0
400.0	48926.0
500.0	99624.0
600.0	152092.0
700.0	206332.0
800.0	262343.0

Stainless Steel

Temperature (K)	Specific Enthalpy (J/kg)
900.0	320125.0
1000.0	379679.0
1100.0	441003.0
1200.0	504099.0
1300.0	568966.0
1400.0	635604.0
1500.0	704014.0
1600.0	774194.0
1700.0	846146.0
1700.01	1114146.0
1800.0	1186986.0
3800.0	2643786.0

2.5 Stainless Steel Oxide

The default tabular values of specific enthalpy as a function of temperature for stainless steel oxide are listed below. Linear extrapolation is allowed from both ends of the tabulated range.

Stainless Steel Oxide

Temperature (K)	Specific Enthalpy (J/kg)
300.0	0.0
1870.0	785000.0
1870.01	1383000.0
3500.0	2198000.0

2.6 Boron Carbide

The default tabular values of specific enthalpy as a function of temperature for boron carbide are listed below. Linear extrapolation is allowed from both ends of the tabulated range.

Boron Carbide

Temperature (K)	Specific Enthalpy (J/kg)
300.0	0.0
2620.0	1160000.0
2620.01	1660000.0
3500.0	2100000.0

2.7 Silver-Indium-Cadmium

The default tabular values of specific enthalpy as a function of temperature for silver-indium-cadmium are listed below. Linear extrapolation is allowed from both ends of the tabulated range.

Silver-Indium-Cadmium

Temperature (K)	Specific Enthalpy (J/kg)
300.0	0.0
400.0	21759.0
500.0	44031.0
600.0	66801.0
700.0	90091.0
800.0	113890.0
900.0	138200.0
1000.0	163010.0
1075.0	211000.0
1075.01	309000.0
1100.0	315350.0
5000.0	1306600.0

2.8 Uranium Metal

The default tabular values of specific enthalpy as a function of temperature for uranium metal are listed below. Linear extrapolation is allowed from the lower end of the tabulated range. No extrapolation is allowed from the upper end of the tabulated range.

Uranium Metal

Temperature (K)	Specific Enthalpy (J/kg)
300.0	0.0
400.0	12050.0
600.0	39150.0
800.0	71350.0
1000.0	106950.0
1200.0	141050.0
1406.0	172259.0
1406.01	222499.0
5000.0	732847.0

2.9 Graphite

The default tabular values of specific enthalpy as a function of temperature for Graphite are listed below. Linear extrapolation is allowed from the lower end of the tabulated range. No extrapolation is allowed from the upper end of the tabulated range.

Graphite

Temperature (K)	Specific Enthalpy (J/kg)
300.0	0.0
773.0	547910.0
1273.0	1414010.0
1773.0	2381110.0
2273.0	3405060.0
2773.0	4464560.0
3866.0	6879871.0
5000.0	9456545.0

2.10 Aluminum

The default tabular values of specific enthalpy as a function of temperature for aluminum are listed below. Linear extrapolation is allowed from both ends of the tabulated range.

Aluminum

Temperature (K)	Specific Enthalpy (J/kg)
273.15	0.00
313.15	36056.00
353.15	72822.00
393.15	110304.00
433.15	148506.00
473.15	187432.00
513.15	227088.00
553.15	267464.00
593.15	308580.00
633.15	350458.00
673.15	393086.00
713.15	436470.00
753.15	480616.00
793.15	525528.00
833.15	571210.00
873.15	617668.00
913.15	664908.00
933.00	688643.00
933.01	1086443.00
1000.00	1165269.00
1500.00	1753519.00
2000.00	2341769.00

2.11 Aluminum Oxide

The default tabular values of specific enthalpy as a function of temperature for aluminum oxide are listed below. Linear extrapolation is allowed from both ends of the tabular range.

Aluminum Oxide

Temperature (K)	Specific Enthalpy (J/kg)
273.15	0.0
298.0	19243.0
350.0	62146.0
400.0	107619.0
500.0	206437.0
600.0	312785.0
800.0	540165.0
1000.0	780637.0
1500.0	1410855.0
2327.0	2518696.0
2327.01	3588710.0
5000.0	7386414.0

2.12 Cadmium

The default tabular values of specific enthalpy as a function of temperature for cadmium are listed below. Linear extrapolation is allowed from both ends of the tabulated range.

Cadmium

Temperature (K)	Specific Enthalpy (J/kg)
298.15	0.00
400.00	24093.00
500.00	48813.00
594.00	73079.00
594.01	128347.00
600.00	129933.00
700.00	156373.00
800.00	182813.00
900.00	209253.00
1000.00	235693.00
1040.00	246269.00

2.13 Stainless Steel 304

The default tabular values of specific enthalpy as a function of temperature for stainless steel 304 are listed below. Linear extrapolation is allowed from both ends of the tabulated range.

Stainless Steel 304

Temperature (K)	Specific Enthalpy (J/kg)
300.00	0.00
400.00	52005.00
500.00	105370.00
600.00	160085.00
700.00	216155.00
800.00	273585.00
900.00	332375.00
1000.00	392520.00
1100.00	454020.00
1200.00	516880.00
1300.00	581095.00
1400.00	646665.00
1500.00	713630.00
1600.00	781950.00
1700.00	851590.00
1700.01	1120790.00
1800.00	1200800.00
1900.00	1280810.00
2000.00	1360820.00
2500.00	1760870.00
3000.00	2160920.00

2.14 Lithium Aluminum

The default tabular values of specific enthalpy as a function of temperature for lithium aluminum are listed below. Linear extrapolation is allowed from both ends of the tabulated range.

Lithium Aluminum

Temperature (K)	Specific Enthalpy (J/kg)
298.15	0.00
313.15	14357.00
353.15	53199.00
393.15	92877.00
433.15	133411.00
473.15	174815.00
513.15	217007.00
533.15	259879.00
593.15	303449.00
633.15	347739.00
673.15	392737.00
713.15	438455.00

MP Package Reference Manual

Lithium Aluminum

Temperature (K)	Specific Enthalpy (J/kg)
753.15	484913.00
793.15	532121.00
833.15	580081.00
873.15	628799.00
917.00	683118.00
917.01	1081568.00
1000.00	1183866.00
1100.00	1307111.00
1200.00	1430341.00

2.15 Uranium Aluminum

The default tabular values of specific enthalpy as a function of temperature for uranium aluminum are listed below. Linear extrapolation is allowed from both ends of the tabulated range.

Uranium Aluminum

Temperature (K)	Specific Enthalpy (J/kg)
293.15	0.00
333.15	26818.00
373.15	54172.00
413.15	82068.00
453.15	110512.00
493.15	139512.00
533.15	169072.00
573.15	199198.00
613.15	229900.00
653.15	261184.00
693.15	293056.00
733.15	325524.00
773.15	358596.00
813.15	392278.00
853.15	426578.00
893.15	461506.00
919.00	484411.00
919.01	484421.00
962.00	522131.00
1039.00	589676.00
1123.00	663125.00
1128.50	667919.00
1128.51	957919.00
1223.00	1040285.00

Uranium Aluminum

Temperature (K)	Specific Enthalpy (J/kg)
1305.00	1111757.00
1338.00	1140519.00
1500.00	1281719.00
2000.00	1717519.00

2.16 Carbon Steel

The default tabular values of specific enthalpy as a function of temperature for carbon steel are listed below. Linear extrapolation is allowed from both ends of the tabulated range.

Carbon Steel

Temperature (K)	Specific Enthalpy (J/kg)
273.15	0.0
373.15	45667.0
473.15	95490.8
573.15	149471.4
673.15	207608.3
773.15	271000.8
873.15	341966.8
923.15	381218.1
973.15	424656.3
1023.15	475944.8
1033.15	488295.9
1073.15	531838.7
1123.15	571090.0
1223.15	642265.5
1349.82	729771.6
1373.15	745920.6
1473.15	815868.4
1573.15	886996.6
1673.15	959305.2
1773.15	1032794.1
1810.90	1060843.1
1810.91	1332803.1
5000.00	3709472.4

3. Temperature as a Function of Special Enthalpy

The temperature as a function of specific enthalpy may be computed from either a user-specified tabular function or a MELCOR default table.

MP Package Reference Manual

The user-specified tabular function to define a new material or to override the default table for an existing material is invoked by using a standard tabular function (see the TF Package Users' Guide) to input the temperature (K) as a function of enthalpy (J/kg). Currently, there are no checks made on the consistency of user-input values for enthalpy, specific heat capacity, melting temperature, and latent heat of fusion; this could be rectified in future code versions.

The following materials have default tables for temperature as a function of enthalpy:

Zircaloy	Boron Carbide	Aluminum Oxide
Zirconium Oxide	Silver-Indium-Cadmium	Cadmium
Uranium Dioxide	Uranium Metal	Stainless Steel 304
Stainless Steel	Graphite	Lithium Aluminum
Stainless Steel Oxide	Aluminum	Uranium Aluminum
Carbon Steel		

The default specific enthalpy values are calculated by linear interpolation of tabulated values computed by inverting the tables of specific enthalpy as a function of temperature from Section 2. Extrapolation rules are the same as those listed in Section 2.

4. Specific Heat Capacity as a Function of Temperature

The specific heat capacity at constant pressure may be computed from either a user-specified tabular function or a MELCOR default table defined in subroutine MPDFVL.

The user-specified tabular function to define a new material or to override the default table for an existing material is invoked by using a standard tabular function (see the TF Package Users' Guide) to input the specific heat capacity (J/kg-K) as a function of temperature (K). There are no checks made on the consistency of user-input values for enthalpy, specific heat capacity, melting temperature, and latent heat of fusion.

The following materials have default tables for specific heat capacity:

Zircaloy	Concrete
Zirconium Oxide	Aluminum
Uranium Dioxide	Aluminum Oxide
Stainless Steel	Cadmium
Stainless Steel Oxide	Stainless Steel 304
Boron Carbide	Lithium Aluminum
Silver-Indium-Cadmium	Uranium Aluminum
Uranium Metal	Carbon Steel
Graphite	

The default specific heat capacity values are computed by linear interpolation of the tabulated values listed below. Data sources are given with each table.

4.1 Zircaloy

The default tabular values of specific heat capacity as a function of temperature for Zircaloy are listed below. No extrapolation is allowed.

Zircaloy

Temp(K)	Specific Heat Capacity (J/kg-K)	Data Source
273.1	275.0	Ref. [1], extrapolated
400.0	302.0	Ref. [1]
640.0	331.0	Ref. [1]
1090.0	375.0	Ref. [1]
1093.0	502.0	Ref. [1]
1113.0	590.0	Ref. [1]
1133.0	615.0	Ref. [1]
1153.0	719.0	Ref. [1]
1173.0	816.0	Ref. [1]
1193.0	770.0	Ref. [1]
1213.0	619.0	Ref. [1]
1233.0	469.0	Ref. [1]
1248.0	356.0	Ref. [1]
2098.0	356.0	Ref. [1]
5000.0	356.0	Ref. [1], extrapolated

4.2 Zirconium Oxide

The default tabular values of specific heat capacity as a function of temperature for zirconium oxide are listed below. No extrapolation is allowed.

Zirconium Oxide

Temp (K)	Specific Heat Capacity (J/kg-K)	Data Source
273.15	544.3	Ref. [1]
5000.0	544.3	Ref. [1]

4.3 Uranium Dioxide

The default tabular values of specific heat capacity as a function of temperature for uranium dioxide are listed below. No extrapolation is allowed.

Uranium Dioxide

Temp (K)	Specific Heat Capacity (J/kg-K)	Data Source
273.15	230.22	Ref. [1], extrapolated

MP Package Reference Manual

Uranium Dioxide

Temp (K)	Specific Heat Capacity (J/kg-K)	Data Source
400.0	265.84	Ref. [1]
500.0	282.07	Ref. [1]
600.0	292.36	Ref. [1]
700.0	299.67	Ref. [1]
800.0	305.31	Ref. [1]
900.0	309.98	Ref. [1]
1000.0	314.03	Ref. [1]
1100.0	317.69	Ref. [1]
1200.0	321.15	Ref. [1]
1300.0	324.59	Ref. [1]
1400.0	328.24	Ref. [1]
1500.0	332.40	Ref. [1]
1600.0	337.43	Ref. [1]
1700.0	343.76	Ref. [1]
1800.0	351.84	Ref. [1]
1900.0	362.14	Ref. [1]
2000.0	375.09	Ref. [1]
2100.0	391.08	Ref. [1]
2200.0	410.45	Ref. [1]
2300.0	433.45	Ref. [1]
2400.0	460.23	Ref. [1]
2500.0	490.88	Ref. [1]
2600.0	525.40	Ref. [1]
2700.0	563.71	Ref. [1]
2800.0	605.67	Ref. [1]
2900.0	651.09	Ref. [1]
3000.0	699.73	Ref. [1]
3113.0	758.23	Ref. [1]
3113.01	503.0	Ref. [1]
5000.0	503.0	Ref. [1], extrapolated

4.4 Stainless Steel

The default tabular values of specific heat capacity as a function of temperature for 347 stainless steel are listed below. No extrapolation is allowed.

Stainless Steel

Temp (K)	Specific Heat Capacity (J/kg-K)	Data Source
273.15	475.6	Ref. [1], extrapolated
400.0	498.1	Ref. [1]
500.0	515.8	Ref. [1]
600.0	533.5	Ref. [1]

Stainless Steel

Temp (K)	Specific Heat Capacity (J/kg-K)	Data Source
700.0	551.3	Ref. [1]
800.0	569.0	Ref. [1]
900.0	586.7	Ref. [1]
1000.0	604.4	Ref. [1]
1100.0	622.1	Ref. [1]
1200.0	639.8	Ref. [1]
1300.0	657.5	Ref. [1]
1400.0	675.2	Ref. [1]
1500.0	693.0	Ref. [1]
1600.0	710.7	Ref. [1]
1700.0	728.4	Ref. [1]
1700.01	728.4	Ref. [1]
1800.0	728.4	Ref. [1]
5000.0	728.4	Ref. [1], extrapolated

4.5 Stainless Steel Oxide

The default tabular values of specific heat capacity as a function of temperature for stainless steel oxide are listed below. No extrapolation is allowed.

Stainless Steel Oxide

Temp (K)	Specific Heat Capacity (J/kg-K)	Data Source
273.15	500.0	Estimated
5000.0	500.0	Estimated

4.6 Boron Carbide

The default tabular values of specific heat capacity as a function of temperature for boron carbide are listed below. No extrapolation is allowed.

Boron Carbide

Temp (K)	Specific Heat Capacity (J/kg-K)	Data Source
273.15	500.0	Estimated
5000.0	500.0	Estimated

4.7 Silver-Indium-Cadmium

The default tabular values of specific heat capacity as a function of temperature for silver-indium-cadmium are listed below. Linear extrapolation below 300 K is permitted.

Silver-Indium-Cadmium

Temp (K)	Specific Heat Capacity (J/kg-K)	Data Source
300.0	215.04	Ref. [2]

MP Package Reference Manual

Silver-Indium-Cadmium

Temp (K)	Specific Heat Capacity (J/kg-K)	Data Source
400.0	220.14	Ref. [2]
500.0	225.23	Ref. [2]
600.0	230.33	Ref. [2]
700.0	235.42	Ref. [2]
800.0	240.52	Ref. [2]
900.0	245.61	Ref. [2]
1000.0	250.71	Ref. [2]
1075.0	254.15	Ref. [2]
5000.0	254.15	Ref. [2]

4.8 Uranium Metal

The default tabular values of specific heat capacity as a function of temperature for uranium metal are listed below. No extrapolation is allowed.

Uranium Metal

Temp (K)	Specific Heat Capacity (J/kg-K)	Data Source
273.15	113.6	Ref. [3], p. 758, extrapolated
300.0	116.0	Ref. [3], p. 758
400.0	125.0	Ref. [3], p. 758
600.0	146.0	Ref. [3], p. 758
800.0	176.0	Ref. [3], p. 758
1000.0	180.0	Ref. [3], p. 758
1200.0	161.0	Ref. [3], p. 758
1406.0	142.0	Ref. [3], p. 758, extrapolated
5000.0	142.0	Constant from melting point of 1406 K

4.9 Graphite

The default tabular values of specific heat capacity as a function of temperature for graphite are listed below. No extrapolation is allowed.

Graphite

Temp (K)	Specific Heat Capacity (J/kg-K)	Data Source
273.15	665.16	Ref. [4], p. 180, generic graphite, extrapolated
298.0	711.7	Ref. [4], p. 180, generic graphite
773.0	1601.3	Ref. [4], p. 180, generic graphite
1273.0	1863.0	Ref. [4], p. 180, generic graphite
1773.0	2005.3	Ref. [4], p. 180, generic graphite
2273.0	2090.6	Ref. [4], p. 180, generic graphite
2773.0	2147.5	Ref. [4], p. 180, generic graphite

Graphite

Temp (K)	Specific Heat Capacity (J/kg-K)	Data Source
3866.0	2272.0	Ref. [4], p. 180, generic graphite, extrapolated
5000.0	2272.0	Constant from melting point of 3866 K

4.10 Concrete

The default tabular values of specific heat capacity as a function of temperature for concrete are listed below. No extrapolation is allowed.

Concrete

Temp (K)	Specific Heat Capacity (J/kg-K)	Data Source
273.15	837.3	Ref. [5], p. 635, stone concrete @ 294 K
5000.0	837.3	Ref. [5], p. 635, stone concrete @ 294 K

4.11 Aluminum

The default tabular values of specific heat capacity as a function of temperature for aluminum are listed below. Constant extrapolation is allowed from both ends of the tabulated range.

Aluminum

Temp (K)	Specific Heat Capacity (J/kg-K)	Data Source
273.15	892.60	Ref. [6]
313.15	910.20	Ref. [6]
353.15	928.10	Ref. [6]
393.15	946.00	Ref. [6]
433.15	964.10	Ref. [6]
473.15	982.20	Ref. [6]
513.15	1000.60	Ref. [6]
553.15	1018.20	Ref. [6]
593.15	1037.60	Ref. [6]
633.15	1056.30	Ref. [6]
673.15	1075.10	Ref. [6]
713.15	1094.10	Ref. [6]
753.15	1113.20	Ref. [6]
793.15	1132.40	Ref. [6]
833.15	1151.70	Ref. [6]
873.15	1171.20	Ref. [6]
913.15	1190.80	Ref. [6]
933.00	1200.60	Ref. [6]
933.01	1176.50	Ref. [6]

MP Package Reference Manual

Aluminum

Temp (K)	Specific Heat Capacity (J/kg-K)	Data Source
1000.00	1176.50	Ref. [6]
1500.00	1176.50	Ref. [6]
2000.00	1176.50	Ref. [6]

4.12 Aluminum Oxide

The default tabular values of specific heat capacity as a function of temperature for aluminum oxide are listed below. Constant extrapolation is allowed from both ends of the tabulated range.

Aluminum Oxide

Temp (K)	Specific Heat Capacity (J/kg-K)	Data Source
273.15	774.38	Ref. [7]
298.0	774.38	Ref. [7]
350.0	875.73	Ref. [7]
400.0	943.20	Ref. [7]
500.0	1033.16	Ref. [7]
600.0	1093.80	Ref. [7]
800.0	1180.00	Ref. [7]
1000.0	1224.72	Ref. [7]
1500.0	1296.15	Ref. [7]
2327.0	1383.03	Ref. [7]
2327.01	1420.77	Ref. [7]
5000.0	1420.77	Ref. [7]

4.13 Cadmium

The default tabular values of specific heat capacity as a function of temperature for cadmium are listed below. Constant extrapolation is allowed from both ends of the tabulated range.

Cadmium

Temp (K)	Specific Heat Capacity (J/kg-K)	Data Source
298.15	231.30	Ref. [6]
400.00	241.80	Ref. [6]
500.00	252.60	Ref. [6]
594.00	263.70	Ref. [6]
594.01	264.40	Ref. [6]
600.00	264.40	Ref. [6]
1040.00	264.40	Ref. [6]

4.14 Stainless Steel 304

The default tabular values of specific heat capacity as a function of temperature for stainless steel 304 are listed below. Constant extrapolation is allowed from both ends of the tabulated range.

Stainless Steel 304

Temp (K)	Specific Heat Capacity (J/kg-K)	Data Source
300.00	513.20	Ref. [6]
400.00	526.90	Ref. [6]
500.00	540.40	Ref. [6]
600.00	553.90	Ref. [6]
700.00	567.50	Ref. [6]
800.00	581.10	Ref. [6]
900.00	594.70	Ref. [6]
1000.00	608.20	Ref. [6]
1100.00	621.80	Ref. [6]
1200.00	635.40	Ref. [6]
1300.00	648.90	Ref. [6]
1400.00	662.50	Ref. [6]
1500.00	676.80	Ref. [6]
1600.00	689.60	Ref. [6]
1700.00	703.20	Ref. [6]
1700.01	800.10	Ref. [6]
1800.00	800.10	Ref. [6]
3000.00	800.10	Ref. [6]

4.15 Lithium Aluminum

The default tabular values of specific heat capacity as a function of temperature for lithium aluminum are listed below. Constant extrapolation is allowed from both ends of the tabulated range.

Lithium Aluminum

Temp (K)	Specific Heat Capacity (J/kg-K)	Data Source
298.15	953.50	Ref. [6]
313.15	960.80	Ref. [6]
353.15	981.30	Ref. [6]
393.15	1002.60	Ref. [6]
433.15	1024.10	Ref. [6]
473.15	1046.10	Ref. [6]
513.10*	1063.50	Ref. [6]
553.15	1080.10	Ref. [6]
593.15	1098.40	Ref. [6]

MP Package Reference Manual

Lithium Aluminum

Temp (K)	Specific Heat Capacity (J/kg-K)	Data Source
633.15	1116.10	Ref. [6]
673.15	1133.80	Ref. [6]
713.15	1152.10	Ref. [6]
753.15	1170.80	Ref. [6]
793.15	1189.60	Ref. [6]
833.15	1208.40	Ref. [6]
873.15	1227.50	Ref. [6]
917.00	1250.00	Ref. [6]
917.01	1232.50	Ref. [6]
1000.00	1232.50	Ref. [6]
1100.00	1232.40	Ref. [6]
1200.00	1232.20	Ref. [6]

* Value differs slightly from reference. MELCOR/SR-Mod3 Fortran value is used.

4.16 Uranium Aluminum

The default tabular values of specific heat capacity as a function of temperature for uranium aluminum are listed below. Constant extrapolation is allowed from both ends of the tabulated range.

Uranium Aluminum

Temp (K)	Specific Heat Capacity (J/kg-K)	Data Source
293.15	663.80	Ref. [6]
333.15	677.10	Ref. [6]
373.15	690.60	Ref. [6]
413.15	704.20	Ref. [6]
453.15	718.00	Ref. [6]
493.15	732.00	Ref. [6]
533.15	746.00	Ref. [6]
573.15	760.30	Ref. [6]
613.15	774.80	Ref. [6]
653.15	789.40	Ref. [6]
693.15	804.20	Ref. [6]
733.15	819.20	Ref. [6]
773.15	834.40	Ref. [6]
813.15	849.70	Ref. [6]
853.15	865.30	Ref. [6]
893.15	881.10	Ref. [6]
919.00	891.10	Ref. [6]
919.01	877.20	Ref. [6]
962.00	877.20	Ref. [6]

Uranium Aluminum

Temp (K)	Specific Heat Capacity (J/kg-K)	Data Source
1039.00	877.20	Ref. [6]
1123.00	871.60	Ref. [6]
1223.00	871.60	Ref. [6]
1305.00	871.60	Ref. [6]
1338.00	871.60	Ref. [6]
1500.00	871.60	Ref. [6]

4.17 Carbon Steel

The default tabular values of specific heat capacity as a function of temperature for carbon steel are listed below. Constant extrapolation is allowed from both ends of the tabulated range.

Carbon Steel

Temp (K)	Specific Heat Capacity (J/kg-K)	Data Source
273.15	435.89	Ref. [8]
373.15	477.45	Ref. [8]
473.15	519.02	Ref. [8]
573.15	560.59	Ref. [8]
673.15	602.15	Ref. [8]
773.15	665.70	Ref. [8]
873.15	753.62	Ref. [8]
923.15	816.43	Ref. [8]
973.15	921.10	Ref. [8]
1023.15	1130.44	Ref. [8]
1033.15	1339.78	Ref. [8]
1073.15	837.36	Ref. [8]
1123.15	732.69	Ref. [8]
1223.15	690.82	Ref. [8]
1349.82	690.82	Ref. [8]
1373.15	693.58	Ref. [8]
1473.15	705.38	Ref. [8]
1573.15	717.18	Ref. [8]
1673.15	728.99	Ref. [8]
1773.15	740.79	Ref. [8]
1810.90	745.25	Ref. [8]
1810.91	745.25	Ref. [8]
5000.00	745.25	Ref. [8]

5. Thermal Conductivity as a Function of Temperature

The thermal conductivity may be computed from two different methods. One method, used for structural materials in the COR and HS packages, utilizes tabular data which may be either a user-specified tabular function or a MELCOR default table. The other method, used for noncondensable gases and optionally for steam and air, utilizes the Eucken correlation for single, low-pressure gases and the Wassijewa equation for a combination of gases.

5.1 Tabular

The user-specified tabular function to define a new material or to override the default table for an existing material is invoked by using a standard tabular function to input the thermal conductivity (W/m-K) as a function of temperature (K).

The following materials have default tables for thermal conductivity:

Water	Uranium Dioxide	Uranium Metal	Cadmium
Steam	Stainless Steel	Graphite	Stainless Steel 304
Air	Stainless Steel Oxide	Concrete	Lithium Aluminum
Zircaloy	Boron Carbide	Aluminum	Uranium Aluminum
Zirconium Oxide	Silver-Indium-Cadmium	Aluminum Oxide	Carbon Steel

The default thermal conductivity values are computed by linear interpolation of the tabulated values listed below. Data sources are given with each table.

5.1.1 Water

The default tabular values of thermal conductivity as a function of temperature for liquid water are listed below. No extrapolation is allowed.

Water

Temp (K)	Thermal Conductivity (W/m-K)	Data Source
255.37	0.551	Ref. [9]
273.15	0.569	Ref. [9]
283.15	0.586	Ref. [9]
293.15	0.602	Ref. [9]
303.15	0.617	Ref. [9]
313.15	0.630	Ref. [9]
323.15	0.643	Ref. [9]
333.15	0.653	Ref. [9]
343.15	0.662	Ref. [9]
353.15	0.669	Ref. [9]

Water

Temp (K)	Thermal Conductivity (W/m-K)	Data Source
363.15	0.675	Ref. [9]
373.15	0.680	Ref. [9]
383.15	0.683	Ref. [9]
393.15	0.685	Ref. [9]
403.15	0.687	Ref. [9]
413.15	0.687	Ref. [9]
423.15	0.686	Ref. [9]
433.15	0.684	Ref. [9]
443.15	0.681	Ref. [9]
453.15	0.676	Ref. [9]
463.15	0.671	Ref. [9]
473.15	0.664	Ref. [9]
483.15	0.657	Ref. [9]
493.15	0.648	Ref. [9]
503.15	0.639	Ref. [9]
513.15	0.629	Ref. [9]
523.15	0.617	Ref. [9]
533.15	0.604	Ref. [9]
543.15	0.589	Ref. [9]
553.15	0.573	Ref. [9]
563.15	0.557	Ref. [9]
573.15	0.540	Ref. [9]
583.15	0.522	Ref. [9]
593.15	0.503	Ref. [9]
603.15	0.482	Ref. [9]
613.15	0.460	Ref. [9]
623.15	0.435	Ref. [9]
633.15	0.401	Ref. [9]
647.245	0.318	Ref. [9], extrapolated to critical point

5.1.2 Steam

The default tabular values of thermal conductivity as a function of temperature for steam are listed below. Constant extrapolation is allowed from the upper end of the tabulated range. No extrapolation is allowed from the lower end of the tabulated range.

Steam

Temp (K)	Thermal Conductivity (W/m-K)	Data Source
255.37	0.0144	Ref. [9]
273.15	0.0176	Ref. [9]
293.15	0.0188	Ref. [9]
313.15	0.0201	Ref. [9]

MP Package Reference Manual

Steam

Temp (K)	Thermal Conductivity (W/m-K)	Data Source
333.15	0.0216	Ref. [9]
353.15	0.0231	Ref. [9]
373.15	0.0245	Ref. [9]
393.15	0.0260	Ref. [9]
413.15	0.0277	Ref. [9]
433.15	0.0295	Ref. [9]
453.15	0.0313	Ref. [9]
473.15	0.0331	Ref. [9]
493.15	0.0351	Ref. [9]
513.15	0.0371	Ref. [9]
533.15	0.0391	Ref. [9]
553.15	0.0412	Ref. [9]
573.15	0.0433	Ref. [9]
593.15	0.0455	Ref. [9]
613.15	0.0478	Ref. [9]
633.15	0.0501	Ref. [9]
653.15	0.0525	Ref. [9]
673.15	0.0548	Ref. [9]
693.15	0.0573	Ref. [9]
713.15	0.0597	Ref. [9]
733.15	0.0622	Ref. [9]
753.15	0.0648	Ref. [9]
773.15	0.0673	Ref. [9]
793.15	0.0699	Ref. [9]
813.15	0.0725	Ref. [9]
833.15	0.0752	Ref. [9]
853.15	0.0778	Ref. [9]
873.15	0.0805	Ref. [9]
893.15	0.0832	Ref. [9]
913.15	0.0859	Ref. [9]
933.15	0.0887	Ref. [9]
953.15	0.0914	Ref. [9]
973.15	0.0942	Ref. [9]
993.15	0.0970	Ref. [9]
1013.15	0.0998	Ref. [9]
1033.15	0.1026	Ref. [9]
1053.15	0.1054	Ref. [9]
1073.15	0.1081	Ref. [9]
1200.00	0.130	Ref. [9]
1400.00	0.187	Ref. [9]
1600.00	0.219	Ref. [9]

Steam

Temp (K)	Thermal Conductivity (W/m-K)	Data Source
1800.00	0.263	Ref. [9]
2000.00	0.333	Ref. [9]
2200.00	0.459	Ref. [9]
2400.00	0.690	Ref. [9]
2600.00	1.110	Ref. [9]
2800.00	1.820	Ref. [9]
3000.00	2.940	Ref. [9]
3200.00	4.495	Ref. [9]
3400.00	6.625	Ref. [9]
3600.00	7.610	Ref. [9]
3800.00	7.765	Ref. [9]
4000.00	7.280	Ref. [9]

5.1.3 Air

The default tabular values of thermal conductivity as a function of temperature for air are listed below. Linear extrapolation is allowed from the upper end of the tabulated range. No extrapolation is allowed from the lower end of the tabulated range.

Air

Temp (K)	Thermal Conductivity (W/m-K)	Data Source
255.370	0.0227081	Ref. [10]
310.926	0.0270005	Ref. [10]
366.482	0.0311544	Ref. [10]
422.038	0.0360006	Ref. [10]
477.594	0.0399815	Ref. [10]
533.150	0.0425777	Ref. [10]
588.706	0.0458662	Ref. [10]
644.262	0.0491547	Ref. [10]
699.818	0.0524432	Ref. [10]
755.374	0.0553856	Ref. [10]
810.930	0.0583280	Ref. [10]
866.486	0.0610972	Ref. [10]
922.042	0.0638665	Ref. [10]
977.598	0.0664627	Ref. [10]
1033.154	0.0690589	Ref. [10]
1088.710	0.0718282	Ref. [10]
1144.266	0.0740782	Ref. [10]
1199.822	0.0763283	Ref. [10]
1255.378	0.0785783	Ref. [10]
1310.934	0.0808284	Ref. [10]
1366.490	0.0830784	Ref. [10]

MP Package Reference Manual

Air

Temp (K)	Thermal Conductivity (W/m-K)	Data Source
1422.046	0.0853284	Ref. [10]
1477.602	0.0874054	Ref. [10]
1533.158	0.0896554	Ref. [10]
1588.714	0.0920786	Ref. [10]
1644.270	0.0941555	Ref. [10]
1699.826	0.0960594	Ref. [10]
1755.382	0.0979633	Ref. [10]
1810.938	0.0998672	Ref. [10]
1866.494	0.101425	Ref. [10]
1922.050	0.103156	Ref. [10]
1977.606	0.105060	Ref. [10]
2033.162	0.107137	Ref. [10]
2088.718	0.209040	Ref. [10]
2144.274	0.110425	Ref. [10]
2199.830	0.111810	Ref. [10]
2255.386	0.113367	Ref. [10]
2310.942	0.115098	Ref. [10]
2366.498	0.116829	Ref. [10]
2422.054	0.113367	Ref. [10]
2477.610	0.120118	Ref. [10]
2533.166	0.121675	Ref. [10]

5.1.4 Zircaloy

The default tabular values of thermal conductivity as a function of temperature for Zircaloy are listed below. No extrapolation is allowed.

Zircaloy

Temp (K)	Thermal Conductivity (W/m-K)	Data Source
273.15	12.1	Ref. [1], p. 218, formula
293.2	12.6	Ref. [1], p. 221, Zircaloy-2
473.2	14.5	Ref. [1], p. 221, Zircaloy-2
673.2	17.0	Ref. [1], p. 221, Zircaloy-2
873.2	19.9	Ref. [1], p. 221, Zircaloy-2
1073.2	23.1	Ref. [1], p. 221, Zircaloy-2
1269.2	26.2	Ref. [1], p. 219, Zircaloy-4
1508.2	31.7	Ref. [1], p. 219, Zircaloy-4
1624.2	36.3	Ref. [1], p. 219, Zircaloy-4
1771.2	41.8	Ref. [1], p. 219, Zircaloy-4
2098.2	58.4	Ref. [1], p. 218, formula
5000.0	58.4	Constant beyond melting point of 2098 K

5.1.5 Zirconium Oxide

The default tabular values of thermal conductivity as a function of temperature for zirconium oxide are listed below. No extrapolation is allowed.

Zirconium Oxide

Temp (K)	Thermal Conductivity (W/m-K)	Data Source
273.15	1.94	Ref. [1], p. 224, formula
500.0	1.98	Ref. [1], p. 224, formula
750.0	2.06	Ref. [1], p. 224, formula
1000.0	2.17	Ref. [1], p. 224, formula
1250.0	2.28	Ref. [1], p. 224, formula
1500.0	2.39	Ref. [1], p. 224, formula
2000.0	2.49	Ref. [1], p. 224, formula
5000.0	2.49	Constant beyond 2000 K

5.1.6 Uranium Dioxide

The default tabular values of thermal conductivity as a function of temperature for uranium dioxide are listed below. No extrapolation is allowed.

Uranium Dioxide

Temp (K)	Thermal Conductivity (W/m-K)	Data Source
273.15	9.24	Ref. [11], p. 104, extrapolated
366.3	7.79	Ref. [11], p. 104
539.0	6.53	Ref. [1], p. 30
757.0	4.92	Ref. [1], p. 30
995.0	3.87	Ref. [1], p. 30
1182.0	3.20	Ref. [1], p. 30
1490.0	2.53	Ref. [1], p. 30
1779.0	2.19	Ref. [1], p. 30
1975.0	2.17	Ref. [1], p. 30
2181.0	2.25	Ref. [1], p. 30
2373.0	2.56	Ref. [1], p. 30
2577.0	2.80	Ref. [1], p. 35
2773.0	3.15	Ref. [1], p. 35
3026.0	3.75	Ref. [1], p. 35
3113.0	3.96	Ref. [1], p. 35, extrapolated
5000.0	3.96	Constant beyond melting point of 3113 K

5.1.7 Stainless Steel (SS)

The default tabular values of thermal conductivity as a function of temperature for stainless steel (SS), type 347, are listed below. No extrapolation is allowed.

MP Package Reference Manual

Stainless Steel (SS)

Temp (K)	Thermal Conductivity (W/m-K)	Data Source
273.15	13.8	Ref. [3], p. 757, extrapolated
400.0	15.8	Ref. [3], p. 757
600.0	18.9	Ref. [3], p. 757
800.0	21.9	Ref. [3], p. 757
1000.0	24.7	Ref. [3], p. 757
1700.0	34.5	Ref. [3], p. 757, extrapolated
5000.0	34.5	Constant beyond melting point of 1700 K

5.1.8 Stainless Steel Oxide

The default tabular values of thermal conductivity as a function of temperature for stainless steel oxide are listed below.

Stainless Steel Oxide

Temp (K)	Thermal Conductivity (W/m-K)	Data Source
273.15	20.0	Estimated
5000.0	20.0	Estimated

5.1.9 Boron Carbide

The default tabular values of thermal conductivity as a function of temperature for boron carbide are listed below. No extrapolation is allowed.

Boron Carbide

Temp (K)	Thermal Conductivity (W/m-K)	Data Source
273.15	2.0	Estimated
5000.0	2.0	Estimated

5.1.10 Silver-Indium-Cadmium

The default tabular values of thermal conductivity as a function of temperature for silver-indium-cadmium are listed below. No extrapolation is allowed.

Silver-Indium-Cadmium

Temp (K)	Thermal Conductivity (W/m-K)	Data Source
300.0	57.088	Ref. [2]
400.0	64.992	Ref. [2]
500.0	72.010	Ref. [2]
600.0	78.140	Ref. [2]
700.0	83.384	Ref. [2]
800.0	87.740	Ref. [2]
900.0	91.208	Ref. [2]
1000.0	93.790	Ref. [2]

Silver-Indium-Cadmium

Temp (K)	Thermal Conductivity (W/m-K)	Data Source
1050.0	94.748	Ref. [2]
1075.0	48.000	Ref. [2]
5000.0	48.000	Ref. [2]

5.1.11 Uranium Metal

The default tabular values of thermal conductivity as a function of temperature for uranium metal are listed below. No extrapolation is allowed.

Uranium Metal

Temp (K)	Thermal Conductivity (W/m-K)	Data Source
273.15	24.31	Ref. [11], p. 104, extrapolated
298.0	25.12	Ref. [11], p. 104
366.3	27.34	Ref. [11], p. 104
421.9	28.38	Ref. [11], p. 104
477.4	29.34	Ref. [11], p. 104
533.0	30.28	Ref. [11], p. 104
588.6	31.32	Ref. [11], p. 104
644.1	32.22	Ref. [11], p. 104
699.7	33.22	Ref. [11], p. 104
755.2	34.09	Ref. [11], p. 104
810.8	35.04	Ref. [11], p. 104
866.3	35.90	Ref. [11], p. 104
921.9	36.68	Ref. [11], p. 104
977.4	37.37	Ref. [11], p. 104
1033.0	38.07	Ref. [11], p. 104
1406.0	42.77	Ref. [11], p. 104, extrapolated
5000.0	42.77	Constant beyond melting point of 1406

5.1.12 Graphite

The default tabular values of thermal conductivity as a function of temperature for graphite are listed below. No extrapolation is allowed.

Graphite

Temp (K)	Thermal Conductivity (W/m-K)	Data Source
273.15	35.55	Ref. [12], irradiated graphite
5000.0	35.55	Ref. [12], irradiated graphite

5.1.13 Concrete

The default tabular values of thermal conductivity as a function of temperature for concrete are listed below. No extrapolation is allowed.

Concrete

Temp (K)	Thermal Conductivity (W/m-K)	Data Source
273.15	0.9344	Ref. [5], p. 635, stone concrete @ 294 K
5000.0	0.9344	Ref. [5], p. 635, stone concrete @ 294 K

5.1.14 Aluminum

The default tabular values of thermal conductivity as a function of temperature for aluminum are listed below. Constant extrapolation is allowed from both ends of the tabulated range.

Aluminum

Temp (K)	Thermal Conductivity (W/m-K)	Data Source
273.15	236.00	Ref. [6]
300.00	237.00	Ref. [6]
350.00	240.00	Ref. [6]
400.00	240.00	Ref. [6]
500.00	237.00	Ref. [6]
600.00	232.00	Ref. [6]
700.00	226.00	Ref. [6]
800.00	220.00	Ref. [6]
900.00	213.00	Ref. [6]
933.00	211.00	Ref. [6]
933.01	90.70	Ref. [6]
1000.00	93.00	Ref. [6]
1100.00	96.40	Ref. [6]
1200.00	99.40	Ref. [6]
1300.00	102.00	Ref. [6]

5.1.15 Aluminum Oxide

The default tabular values of thermal conductivity as a function of temperature for aluminum oxide are listed below. Constant extrapolation is allowed from both ends of the tabular range.

Aluminum Oxide

Temp (K)	Thermal Conductivity (W/m-K)	Data Source
273.15	18.73	Ref. [7]
300.0	17.27	Ref. [7]
350.0	15.12	Ref. [7]

Aluminum Oxide

Temp (K)	Thermal Conductivity (W/m-K)	Data Source
400.0	13.47	Ref. [7]
500.0	11.11	Ref. [7]
600.0	9.49	Ref. [7]
700.0	8.31	Ref. [7]
800.0	7.41	Ref. [7]
900.0	6.69	Ref. [7]
1000.0	6.11	Ref. [7]
1200.0	5.22	Ref. [7]
1400.0	4.57	Ref. [7]
1600.0	4.07	Ref. [7]
1800.0	3.68	Ref. [7]
2000.0	3.36	Ref. [7]
2400.0	2.87	Ref. [7]
2800.0	2.51	Ref. [7]
3400.0	2.12	Ref. [7]
4200.0	1.77	Ref. [7]
5000.0	1.42	Ref. [7]

5.1.16 Cadmium

The default tabular values of thermal conductivity as a function of temperature for cadmium are listed below. Constant extrapolation is allowed from both ends of the tabulated range.

Cadmium

Temp (K)	Thermal Conductivity (W/m-K)	Data Source
273.15	97.50	Ref. [6]
283.15	97.30	Ref. [6]
293.15	97.00	Ref. [6]
303.15	96.80	Ref. [6]
313.15	96.60	Ref. [6]
323.15	96.40	Ref. [6]
333.15	96.20	Ref. [6]
343.15	96.00	Ref. [6]
353.15	95.70	Ref. [6]
363.15	95.50	Ref. [6]
373.15	95.30	Ref. [6]
383.15	95.10	Ref. [6]
393.15	94.90	Ref. [6]
403.15	94.70	Ref. [6]
413.15	94.40	Ref. [6]
423.15	94.20	Ref. [6]
433.15	94.00	Ref. [6]

MP Package Reference Manual

Cadmium

Temp (K)	Thermal Conductivity (W/m-K)	Data Source
443.15	93.70	Ref. [6]
453.15	93.50	Ref. [6]
463.15	93.20	Ref. [6]
473.15	92.90	Ref. [6]
483.15	92.60	Ref. [6]
493.15	92.30	Ref. [6]
503.15	91.90	Ref. [6]
513.15	91.60	Ref. [6]
523.15	91.20	Ref. [6]
533.15	90.80	Ref. [6]
543.15	90.40	Ref. [6]
553.15	89.90	Ref. [6]
563.15	89.40	Ref. [6]
573.15	88.90	Ref. [6]
583.15	88.40	Ref. [6]
594.00	87.90	Ref. [6]
594.01	41.60	Ref. [6]
600.00	42.00	Ref. [6]
700.00	49.00	Ref. [6]
800.00	55.90	Ref. [6]
1040.00	72.50	Ref. [6]

5.1.17 Stainless Steel 304

The default tabular values of thermal conductivity as a function of temperature for stainless steel 304 are listed below. Constant extrapolation is allowed from the lower end of the tabulated range. Linear extrapolation is allowed from the upper end of the tabulated range.

Stainless Steel 304

Temp (K)	Thermal Conductivity (W/m-K)	Data Source
300.00	13.00	Ref. [6]
400.00	14.60	Ref. [6]
500.00	16.20	Ref. [6]
600.00	17.80	Ref. [6]
700.00	19.40	Ref. [6]
800.00	21.10	Ref. [6]
900.00	22.70	Ref. [6]
1000.00	24.30	Ref. [6]
1100.00	25.90	Ref. [6]
1200.00	27.50	Ref. [6]
1300.00	29.10	Ref. [6]
1400.00	30.80	Ref. [6]

Stainless Steel 304

Temp (K)	Thermal Conductivity (W/m-K)	Data Source
1500.00	32.40	Ref. [6]
1600.00	34.00	Ref. [6]
1700.00	35.60	Ref. [6]
1700.01	17.80	Ref. [6]
1800.00	18.10	Ref. [6]
1900.00	18.50	Ref. [6]
2000.00	18.80	Ref. [6]
2100.00	19.10	Ref. [6]
2200.00	19.40	Ref. [6]
2300.00	19.80	Ref. [6]
2400.00	20.10	Ref. [6]
2500.00	20.40	Ref. [6]
2600.00	20.70	Ref. [6]
2700.00	21.10	Ref. [6]
2800.00	21.40	Ref. [6]
2900.00	21.70	Ref. [6]
3000.00	22.00	Ref. [6]

5.1.18 Lithium Aluminum

The default tabular values of thermal conductivity as a function of temperature for lithium aluminum are listed below. Constant extrapolation is allowed from both ends of the tabulated range.

Lithium Aluminum

Temp (K)	Thermal Conductivity (W/m-K)	Data Source
273.15	236.00	Ref. [6], Aluminum value
300.00	237.00	Ref. [6], Aluminum value
350.00	240.00	Ref. [6], Aluminum value
400.00	240.00	Ref. [6], Aluminum value
500.00	237.00	Ref. [6], Aluminum value
600.00	232.00	Ref. [6], Aluminum value
700.00	226.00	Ref. [6], Aluminum value
800.00	220.00	Ref. [6], Aluminum value
900.00	213.00	Ref. [6], Aluminum value
933.00	211.00	Ref. [6], Aluminum value
933.01	90.70	Ref. [6], Aluminum value
1000.00	93.00	Ref. [6], Aluminum value
1100.00	96.40	Ref. [6], Aluminum value
1200.00	99.40	Ref. [6], Aluminum value
1300.00	102.00	Ref. [6], Aluminum value

MP Package Reference Manual

5.1.19 Uranium Aluminum

The default tabular values of thermal conductivity as a function of temperature for uranium aluminum are listed below. Constant extrapolation is allowed from both ends of the tabulated range.

Uranium Aluminum

Temp (K)	Thermal Conductivity (W/m-K)	Data Source
293.15	142.60	Ref. [6]
333.15	144.90	Ref. [6]
373.15	146.80	Ref. [6]
413.15	148.20	Ref. [6]
453.15	149.20	Ref. [6]
493.15	149.70	Ref. [6]
533.15	149.80	Ref. [6]
573.15	149.50	Ref. [6]
613.15	148.80	Ref. [6]
653.15	147.50	Ref. [6]
693.15	145.90	Ref. [6]
733.15	143.80	Ref. [6]
773.15	141.30	Ref. [6]
813.15	138.30	Ref. [6]
853.15	134.90	Ref. [6]
893.15	131.10	Ref. [6]
919.00	128.40	Ref. [6]
919.01	96.60	Ref. [6]
962.00	96.60	Ref. [6]
1039.00	97.00	Ref. [6]
1123.00	98.60	Ref. [6]
1223.00	99.60	Ref. [6]
1305.00	100.00	Ref. [6]
1338.00	100.00	Ref. [6]
1500.00	100.00	Ref. [6]

5.1.20 Carbon Steel

The default tabular values of thermal conductivity as a function of temperature for carbon steel are listed below. No extrapolation is allowed.

Carbon Steel

Temp (K)	Thermal Conductivity (W/m-K)	Data Source
273.15	45.437	Ref. [8]
373.15	44.229	Ref. [8]
473.15	42.681	Ref. [8]

Carbon Steel

Temp (K)	Thermal Conductivity (W/m-K)	Data Source
573.15	40.794	Ref. [8]
673.15	38.568	Ref. [8]
773.15	36.002	Ref. [8]
873.15	33.098	Ref. [8]
973.15	29.854	Ref. [8]
1076.80	26.135	Ref. [8]
1173.15	27.100	Ref. [8]
1273.15	28.100	Ref. [8]
1373.15	29.100	Ref. [8]
1473.15	30.100	Ref. [8]
1573.15	31.100	Ref. [8]
1673.15	32.100	Ref. [8]
1773.15	33.100	Ref. [8]
1810.90	33.477	Ref. [8]
5000.00	33.477	Ref. [8]

5.2 Eucken Correlation for a Single, Pure Gas

The thermal conductivity, λ_i , of a single low-pressure gas may be computed using the Eucken correlation [13]:

$$\lambda_i = \left(C_{vi} + \frac{9R}{4M_i} \right) \mu_i \quad (W / m - K) \quad (5.2.1)$$

where,

C_{vi} = heat capacity at constant volume (J/kg-K), calculated by the NCG package (see the NCG/H2O Package Reference Manual)

R = universal gas constant, 8.31441 J/mol-K

μ_i = viscosity (kg/m-s), calculated by the MP package (see Section 6)

M_i = molecular weight (kg/mol), set by the NCG package

5.3 Wassijewa Equation for a Combination of Low-Pressure Gases

The thermal conductivity, λ_{mix} , of a combination of gases may be computed using the Wassijewa equation with the Mason and Saxena modification for the A_{ij} term [13]:

MP Package Reference Manual

$$\lambda_{mix} = \sum_{i=1}^n \frac{\lambda_i y_i}{\sum_{j=1}^n y_j A_{ij}} \quad (5.3.1)$$

where,

y_i = mole fraction of gas i

λ_i = thermal conductivity of pure gas i (see Section 5.2)

$$A_{ij} = \frac{[1 + (\mu_i / \mu_j)^{1/2} (M_j / M_i)^{1/4}]^2}{[8(1 + M_i / M_j)]^{1/2}}$$

$$= \frac{1}{\sqrt{8}} \left(\frac{M_j}{M_i} \right) \left(\frac{M_i}{M_j + M_i} \right)^{1/2} \left[\left(\frac{M_i}{M_j} \right)^{1/4} + \left(\frac{\mu_i}{\mu_j} \right)^{1/2} \right]^2$$

μ_i = viscosity of pure gas i (kg/m-s), (see Section 6)

M_i = molecular weight of gas i (kg/mol), set by the NCG package

The mole fractions, y_i , may be expressed in terms of the gas masses, m_i , using,

$$y_i = \frac{m_i / M_i}{\sum_{j=1}^n m_j / M_j} \quad (5.3.2)$$

yielding,

$$\lambda_{mix} = \sum_{i=1}^n \frac{m_i \lambda_i}{\sum_{j=1}^n m_j \left(\frac{M_i}{M_j} \right) A_{ij}} \quad (5.3.3)$$

or

$$\lambda_{mix} = \sqrt{8} \sum_{i=1}^n \frac{m_i \lambda_i}{\sum_{j=1}^n m_j \left(\frac{M_i}{M_j + M_i} \right)^{1/2} \left[\left(\frac{M_i}{M_j} \right)^{1/4} + \left(\frac{\mu_i}{\mu_j} \right)^{1/2} \right]^2} \quad (5.3.4)$$

6. Dynamic Viscosity as a Function of Temperature

The dynamic viscosity may be computed from two different methods. One method, used for structural materials in the COR and HS packages, utilizes tabular data which may be either a user-specified tabular function or a MELCOR default table. The other method, used for noncondensable gases and optionally for steam and air, utilizes the Chapman-Enskog equations for low-pressure gases based on constant Lennard-Jones potential parameters, σ and ε/k , which may be either user-specified or MELCOR default values.

6.1 Tabular

The user-specified tabular function to define a new material or to override the default table for an existing material is invoked by using a standard tabular function (see the TF Package Users' Guide) to input the viscosity (kg/m-s) as a function of temperature (K).

The following materials have default tables for viscosity:

- Water
- Steam
- Air
- Hydrogen
- Deuterium

The default viscosity values are computed by linear interpolation of the tabulated values listed below. Data sources are given with each table.

6.1.1 Water

The default tabular values of dynamic viscosity as a function of temperature for liquid water are listed below. No extrapolation is allowed.

Water		
Temp (K)	Dynamic Viscosity (kg/m-s)	Data Source
255.370	0.00264402	Ref. [11]
283.148	0.00130962	Ref. [11]
310.926	0.000681596	Ref. [11]
338.704	0.000434554	Ref. [11]
366.482	0.000305081	Ref. [11]
394.260	0.000235136	Ref. [11]
422.038	0.000186025	Ref. [11]
449.816	0.000156261	Ref. [11]
477.594	0.000135426	Ref. [11]
499.850	0.000117267	Ref. [11]

MP Package Reference Manual

Water

Temp (K)	Dynamic Viscosity (kg/m-s)	Data Source
522.050	0.000106999	Ref. [11]
544.250	0.0000985165	Ref. [11]
566.450	0.0000915221	Ref. [11]
588.750	0.0000833372	Ref. [11]
610.950	0.0000723248	Ref. [11]
633.150	0.0000581872	Ref. [11]
647.245	0.0000492111	Ref. [14], p. 103

6.1.2 Steam

The default tabular values of dynamic viscosity as a function of temperature for steam are listed below. Linear extrapolation is allowed from the upper end of the tabulated range. No extrapolation is allowed from the lower end of the tabulated range.

Steam

Temp (K)	Dynamic Viscosity (kg/m-s)	Data Source
255.15	0.00000724	Ref. [9]
273.15	0.00000804	Ref. [9]
313.15	0.00000966	Ref. [9]
353.15	0.0000113	Ref. [9]
393.15	0.0000129	Ref. [9]
433.15	0.0000146	Ref. [9]
473.15	0.0000162	Ref. [9]
513.15	0.0000178	Ref. [9]
553.15	0.0000194	Ref. [9]
593.15	0.0000211	Ref. [9]
633.15	0.0000227	Ref. [9]
673.15	0.0000243	Ref. [9]
713.15	0.0000260	Ref. [9]
753.15	0.0000276	Ref. [9]
793.15	0.0000292	Ref. [9]
833.15	0.0000308	Ref. [9]
873.15	0.0000325	Ref. [9]
913.15	0.0000341	Ref. [9]
953.15	0.0000357	Ref. [9]
993.15	0.0000375	Ref. [9]
1033.15	0.0000391	Ref. [9]
1073.15	0.0000406	Ref. [9]
1200.00	0.0000454	Ref. [9]
1400.00	0.0000512	Ref. [9]
1600.00	0.0000563	Ref. [9]
1800.00	0.0000612	Ref. [9]

Steam

Temp (K)	Dynamic Viscosity (kg/m-s)	Data Source
2000.00	0.0000659	Ref. [9]
2200.00	0.0000703	Ref. [9]
2400.00	0.0000742	Ref. [9]
2600.00	0.0000775	Ref. [9]
2800.00	0.0000798	Ref. [9]
3000.00	0.0000810	Ref. [9]
3200.00	0.0000814	Ref. [9]
3400.00	0.0000816	Ref. [9]
3600.00	0.0000825	Ref. [9]
3800.00	0.0000851	Ref. [9]
4000.00	0.0000895	Ref. [9]

6.1.3 Air

The default tabular values of dynamic viscosity as a function of temperature for air are listed below. Linear extrapolation is allowed from the upper end of the tabulated range. No extrapolation is allowed from the lower end of the tabulated range.

Air

Temp (K)	Dynamic Viscosity (kg/m-s)	Data Source
99.820	0.00000852739	Ref. [9]
299.820	0.0000184686	Ref. [9]
499.820	0.0000267132	Ref. [9]
699.820	0.0000333208	Ref. [9]
899.820	0.0000389908	Ref. [9]
1099.820	0.0000439763	Ref. [9]
1299.820	0.0000484856	Ref. [9]
1499.820	0.0000525781	Ref. [9]
1699.820	0.0000564325	Ref. [9]
1899.820	0.0000599596	Ref. [9]
2099.820	0.0000640075	Ref. [9]
2299.820	0.0000671625	Ref. [9]
2499.820	0.0000698561	Ref. [9]
2699.820	0.0000723414	Ref. [9]

6.1.4 Hydrogen

The default tabular values of dynamic viscosity as a function of temperature for hydrogen are listed below. Linear extrapolation is allowed from the upper end of the tabulated range. No extrapolation is allowed from the lower end of the tabulated range.

MP Package Reference Manual

Hydrogen

Temp (K)	Dynamic Viscosity (kg/m-s)	Data Source
100.0	0.0000042105	Ref. [15], p.284
200.0	0.0000068129	Ref. [15], p.284
250.0	0.0000079232	Ref. [15], p.284
280.0	0.0000085523	Ref. [15], p.284
300.0	0.0000089594	Ref. [15], p.284
400.0	0.000010867	Ref. [15], p.284
500.0	0.000012642	Ref. [15], p.284
600.0	0.000014290	Ref. [15], p.284
700.0	0.000015846	Ref. [15], p.284
800.0	0.000017335	Ref. [15], p.284
900.0	0.000018756	Ref. [15], p.284
1000.0	0.000020128	Ref. [15], p.284
1100.0	0.000021440	Ref. [15], p.284
1200.0	0.000022754	Ref. [16]
1300.0	0.000024078	Ref. [16]
4000.0	0.000059839	Ref. [16], extrapolated

6.1.5 Deuterium

The default tabular values of dynamic viscosity as a function of temperature for deuterium are listed below. No extrapolation is allowed from the lower end of the tabulated range. Linear extrapolation is allowed from the upper end of the tabulated range.

Deuterium

Temp (K)	Dynamic Viscosity (kg/m-s)	Data Source
100.0	0.00000579	Ref. [6]
120.0	0.00000662	Ref. [6]
140.0	0.00000739	Ref. [6]
160.0	0.00000814	Ref. [6]
180.0	0.00000885	Ref. [6]
200.0	0.00000955	Ref. [6]
220.0	0.00001022	Ref. [6]
240.0	0.00001087	Ref. [6]
260.0	0.00001151	Ref. [6]
280.0	0.00001214	Ref. [6]
300.0	0.00001274	Ref. [6]
320.0	0.00001332	Ref. [6]
340.0	0.00001388	Ref. [6]
360.0	0.00001445	Ref. [6]
380.0	0.00001501	Ref. [6]
400.0	0.00001554	Ref. [6]
420.0	0.00001606	Ref. [6]

Deuterium

Temp (K)	Dynamic Viscosity (kg/m-s)	Data Source
440.0	0.00001658	Ref. [6]
460.0	0.00001709	Ref. [6]
480.0	0.00001758	Ref. [6]
500.0	0.00001805	Ref. [6]

6.2 Chapman-Enskog Equation for a Single, Pure Gas

$$\mu_i = 2.6693 \times 10^{-6} \frac{\sqrt{1000 M T}}{\sigma^2 \Omega_v} \quad \text{kg/m-s} \quad (6.2.1)$$

The viscosity, μ_i , of a single, low-pressure gas may be computed using the Chapman-Enskog viscosity equation [17]:

where,

M = molecular weight (kg/mol)

T = gas temperature (K)

σ = collision diameter ($\text{\AA} \equiv 10^{-10} \text{m}$)

Ω_v = collision integral

$$= 2.785 \left(\frac{T^*}{0.3} \right)^{-0.4} \quad T^* < 0.3 \text{ (extrapolated)}$$

$$= f(T^*) \text{ from Table 6.1 below} \quad 0.3 \leq T^* < 100$$

$$= 0.5882 \left(\frac{T^*}{100} \right)^{-0.145} \quad T^* \geq 100$$

$$T^* = \frac{k T}{\varepsilon}$$

ε/k = characteristic energy/Boltzmann's constant (K)

The following materials have default tables for the Lennard-Jones potential parameters, σ and ε/k [13, 18]:

σ (\AA) ε/k (K)

MP Package Reference Manual

	σ (Å)	ϵ/k (K)
Steam	2.641	809.1
Air	3.711	78.6
Hydrogen	2.827	59.7
Helium	2.551	10.22
Argon	3.542	93.3
Deuterium	2.948	39.3
Oxygen	3.467	106.7
Carbon Dioxide	3.941	195.2
Carbon Monoxide	3.690	91.7
Nitrogen	3.798	71.4
Nitric Oxide	3.492	116.7
Nitrous Oxide	3.828	232.4
Ammonia	2.900	558.3
Acetylene	4.033	231.8
Methane	3.758	148.6
Ethylene	4.163	224.7
Uranium Hexafluoride	5.967	236.8

The default values for σ and ϵ/k may be changed using the mnemonics SIG and EPS as described in the MP Users' Guide.

Table 6.1. Collision Integral, Ω_v , as a Function of the Dimensionless Temperature, T^* [17].

T^*	Ω_v	T^*	Ω_v	T^*	Ω_v
0.30	2.785	1.65	1.264	4.00	0.9700
0.35	2.628	1.70	1.248	4.10	0.9649
0.40	2.492	1.75	1.234	4.20	0.9600
0.45	2.368	1.80	1.221	4.30	0.9553
0.50	2.257	1.85	1.209	4.40	0.9507
0.55	2.156	1.90	1.197	4.50	0.9464
0.60	2.065	1.95	1.186	4.60	0.9422
0.65	1.982	2.00	1.175	4.70	0.9382
0.70	1.908	2.10	1.156	4.80	0.9343
0.75	1.841	2.20	1.138	4.90	0.9305
0.80	1.780	2.30	1.122	5.00	0.9269
0.85	1.725	2.40	1.107	6.00	0.8963
0.90	1.675	2.50	1.093	7.00	0.8727
0.95	1.629	2.60	1.081	8.00	0.8538

T^*	Ω_v	T^*	Ω_v	T^*	Ω_v
1.00	1.587	2.70	1.069	9.00	0.8379
1.05	1.549	2.80	1.058	10.00	0.8242
1.10	1.514	2.90	1.048	20.00	0.7432
1.15	1.482	3.00	1.039	30.00	0.7005
1.20	1.452	3.10	1.030	40.00	0.6718
1.25	1.424	3.20	1.022	50.00	0.6504
1.30	1.399	3.30	1.014	60.00	0.6335
1.35	1.375	3.40	1.007	70.00	0.6194
1.40	1.353	3.50	0.9999	80.00	0.6076
1.45	1.333	3.60	0.9932	90.00	0.5973
1.50	1.314	3.70	0.9870	100.00	0.5882
1.55	1.296	3.80	0.9811		
1.60	1.279	3.90	0.9755		

6.3 Chapman-Enskog Equation for a Combination of Low-Pressure Gases

The viscosity of a mixture of gases can be computed by combining the individual viscosities of the pure substances using the following equation with the Wilke's approximation for the term, ϕ_{ij} [13]

$$\mu_{mix} = \frac{\sum_{i=1}^n y_i \mu_i}{\sum_{j=1}^n y_j \phi_{ij}} \quad (6.3.1)$$

where,

y_i = mole fraction of gas i

μ_i = viscosity of pure gas i (see Section 6.2)

$$\begin{aligned} \phi_{ij} &= \frac{\left[1 + (\mu_i / \mu_j)^{1/2} (M_j / M_i)^{1/4}\right]^2}{\left[8(1 + M_i / M_j)\right]^{1/2}} \\ &= \frac{1}{\sqrt{8}} \left(\frac{M_j}{M_i}\right) \left(\frac{M_i}{M_j + M_i}\right)^{1/2} \left[\left(\frac{M_i}{M_j}\right)^{1/4} + \left(\frac{\mu_i}{\mu_j}\right)^{1/2}\right]^2 \end{aligned}$$

MP Package Reference Manual

M_i = molecular weight of gas i (kg/mol), set by the NCG package

The mole fractions, y_i , may be expressed in terms of the gas masses, m_i , using,

$$y_i = \frac{m_i / M_i}{\sum_{k=1}^n m_k / M_k} \quad (6.3.2)$$

yielding,

$$\mu_{mix} = \sum_{i=1}^n \frac{m_i \mu_i}{\sum_{j=1}^n m_j \left(\frac{M_i}{M_j} \right) \phi_{ij}} \quad (6.3.3)$$

or

$$\mu_{mix} = \sqrt{8} \sum_{i=1}^n \frac{m_i \mu_i}{\sum_{j=1}^n m_j \left(\frac{M_j}{M_j + M_i} \right)^{1/2} \left[\left(\frac{M_i}{M_j} \right)^{1/4} + \left(\frac{\mu_i}{\mu_j} \right)^{1/2} \right]^2} \quad (6.3.4)$$

7. Binary Mass Diffusion Coefficient

The binary diffusion coefficients are computed using two different methods depending on which MELCOR package requires the information. The diffusion coefficients required for COR, CVH, and HS packages are computed by the MP package using the equations given in Section 7.1, below. RN1 utilizes the MP package noncondensable gas Lennard-Jones parameters for the calculation of fission product vapor binary diffusion coefficients as described in Section 7.2.

7.1 Binary Mass Diffusion Coefficient as a Function of Temperature and Pressure

The diffusion coefficient is computed from different correlations for each pair of materials. The diffusion coefficient (m^2/s) is defined as a function of temperature (K) and pressure (Pa) for two pairs of materials.

For steam and air, the following correlation is used (origin unknown):

$$D = 4.7931 \times 10^{-5} \left(\frac{T^{1.9}}{P} \right) \quad (7.1.1)$$

For steam and hydrogen, the correlation is taken from Reference [19]:

$$D = 6.60639 \times 10^{-4} \left(\frac{T^{1.68}}{P} \right) \quad (7.1.2)$$

An error message is printed if the input temperature or pressure is less than zero. There is currently no means by which the user can change these correlations.

7.2 Chapman-Enskog Equation for a Pair of Low-Pressure Gases

The binary diffusion coefficient, D_{AB} , for a pair of low-pressure gases may be computed using the Chapman-Enskog equation [17]:

$$D_{AB} = 1.88292 \times 10^{-2} \frac{\sqrt{T^3 \left(\frac{0.001}{M_A} + \frac{0.001}{M_B} \right)}}{P \sigma_{AB}^2 \Omega_{D,AB}} \quad m^2 / s \quad (7.2.1)$$

where,

M_A = molecular weight of gas A (kg/mol)

M_B = molecular weight of gas B (kg/mol)

T = gas temperature (K)

P = gas pressure (Pa)

σ_A = collision diameter of gas A ($\text{\AA} \cong 10^{-10} \text{m}$)

σ_B = collision diameter of gas B ($\text{\AA} \cong 10^{-10} \text{m}$)

σ_{AB} = effective collision diameter of gas A and B ($\text{\AA} \cong 10^{-10} \text{m}$)

$$= 1/2(\sigma_A + \sigma_B)$$

$\Omega_{D,AB}$ = collision integral

$$= 2.662 \left(T_{AB}^* / 0.3 \right)^{-0.5} \quad T_{AB}^* < 0.3 \text{ (extrapolated)}$$

MP Package Reference Manual

$$= f(T_{AB}^*) \text{ from Table 7.1 below } 0.3 \leq T_{AB}^* < 100$$

$$= 0.5170(T_{AB}^*/100)^{-0.155} \quad T_{AB}^* \geq 100 \text{ (extrapolated)}$$

$$T_{AB}^* = (k T / \varepsilon_{AB})$$

$$\varepsilon_{AB}/k = \text{effective characteristic energy/Boltzmann's constant for gas A and B (K)}$$

$$= 1/k(\varepsilon_A \varepsilon_B)^{1/2}$$

$$\varepsilon_A/k = \text{effective characteristic energy/Boltzmann's constant for gas A (K)}$$

$$\varepsilon_B/k = \text{effective characteristic energy/Boltzmann's constant for gas B (K)}$$

The table of Lennard-Jones potential parameters, σ and ε/k , is given in Section 6.2. The default values for σ and ε/k may be changed using the mnemonics SIG and EPS as described in the MP Users' Guide.

Table 7.1. Collision Integral, Ω_D , as a Function of Dimensionless Temperature, T_{AB}^* [17].

T_{AB}^*	Ω_D	T_{AB}^*	Ω_D	T_{AB}^*	Ω_D
0.30	2.662	1.65	1.153	4.00	0.8836
0.35	2.476	1.70	1.140	4.10	0.8788
0.40	2.318	1.75	1.128	4.20	0.8740
0.45	2.184	1.80	1.116	4.30	0.8694
0.50	2.066	1.85	1.105	4.40	0.8652
0.55	1.966	1.90	1.094	4.50	0.8610
0.60	1.877	1.95	1.084	4.60	0.8568
0.65	1.798	2.00	1.075	4.70	0.8530
0.70	1.729	2.10	1.057	4.80	0.8492
0.75	1.667	2.20	1.041	4.90	0.8456
0.80	1.612	2.30	1.026	5.00	0.8422
0.85	1.562	2.40	1.012	6.00	0.8124
0.90	1.517	2.50	0.9996	7.00	0.7896
0.95	1.476	2.60	0.9878	8.00	0.7712
1.00	1.439	2.70	0.9770	9.00	0.7556
1.05	1.406	2.80	0.9672	10.00	0.7424

T_{AB}	Ω_D	T_{AB}	Ω_D	T_{AB}	Ω_D
1.10	1.375	2.90	0.9576	20.00	0.6640
1.15	1.346	3.00	0.9490	30.00	0.6232
1.20	1.320	3.10	0.9406	40.00	0.5960
1.25	1.296	3.20	0.9328	50.00	0.5756
1.30	1.273	3.30	0.9256	60.00	0.5596
1.35	1.253	3.40	0.9186	70.00	0.5464
1.40	1.233	3.50	0.9120	80.00	0.5352
1.45	1.215	3.60	0.9058	90.00	0.5256
1.50	1.198	3.70	0.8998	100.00	0.5170
1.55	1.182	3.80	0.8942		
1.60	1.167	3.90	0.8888		

7.3 Chapman-Enskog Equation for a Combination of Low-Pressure Gases

The effective binary diffusion coefficient, D_{im} , for gas i in a mixture of m low-pressure gases can be computed as [17]:

$$\frac{1-y_i}{D_{im}} = \sum_{j=1, \neq i}^m \left(\frac{y_j}{D_{ij}} \right) \quad (7.3.1)$$

where,

y_i = mole fraction of gas i , and

D_{ij} = binary diffusion coefficient for gas pair ij (m^2/s).

8. Density

The density of most materials may be computed as a constant value, a user-specified tabular function or a MELCOR default table. The default function for the densities of air and steam, however, are fixed by the code and cannot be changed through user input.

8.1 Constant Density

The constant density may be input by the user or read from a MELCOR default table. There are no checks made on the consistency of user-input values for enthalpy, specific heat capacity, melting temperature, and latent heat of fusion.

MP Package Reference Manual

The following materials have default values for the constant density:

Material	Density (kg/m ³)	Data Source
Zircaloy	6500.0	Ref. [20]
Zirconium Oxide	5600.0	Ref. [20]
Uranium Dioxide	10960.0	Ref. [20]
Stainless Steel	7930.0	Ref. [20]
Stainless Steel Oxide	5180.0	Ref. [20]
Boron Carbide	2520.0	Ref. [20]
Silver-Indium-Cadmium	9689.4	Ref. [2], @ 1000 K
Uranium Metal	18210.0	Ref. [11], p. 78
Graphite	1730.0	Ref. [4], p. 436
Carbon Steel	7752.9	Ref. [8]

8.2 Tabular as a Function of Temperature

The user-specified tabular function to define a new material or to override the default table for an existing material is invoked by using a standard tabular function (see the TF Package Users' Guide) to input the density (kg/m³) as a function of temperature (K). The densities used by the COR and FDI packages (see the users' guides for these packages) for user-defined tabular functions will be determined by evaluating the respective tabular functions at 1000 K. If the input tabular function does not allow an evaluation to be made at 1000 K, an input error occurs. Currently, only constant functions should be user-input, since temperature dependent values are not addressed by the HS package.

The following materials have default tables for density which may be altered through user input tabular functions:

- Zircaloy
- Zirconium Oxide
- Uranium Dioxide
- Stainless Steel
- Stainless Steel Oxide
- Boron Carbide
- Silver-Indium-Cadmium
- Uranium Metal
- Graphite
- Concrete

The default density values for the above materials are computed by linear interpolation of the tabulated values listed in Sections 8.2.1 through 8.2.11, below. Data sources are given with each table.

8.2.1 Zircaloy

The default tabular values of density as a function of temperature for Zircaloy are listed below. No extrapolation is allowed.

Zircaloy		
Temp (K)	Density (kg/m ³)	Data Source
273.15	6500.0	Ref. [20]
5000.0	6500.0	Ref. [20]

8.2.2 Zirconium Oxide

The default tabular values of density as a function of temperature for zirconium oxide are listed below. No extrapolation is allowed.

Zirconium Oxide		
Temp (K)	Density (kg/m ³)	Data Source
273.15	5600.0	Ref. [20]
5000.0	5600.0	Ref. [20]

8.2.3 Uranium Dioxide

The default tabular values of density as a function of temperature for uranium dioxide are listed below. No extrapolation is allowed.

Uranium Dioxide		
Temp (K)	Density (kg/m ³)	Data Source
273.15	10960.0	Ref. [20]
5000.0	10960.0	Ref. [20]

8.2.4 Stainless Steel

The default tabular values of density as a function of temperature for stainless steel are listed below. No extrapolation is allowed.

Stainless Steel		
Temp (K)	Density (kg/m ³)	Data Source
273.15	7930.0	Ref. [20]
5000.0	7930.0	Ref. [20]

8.2.5 Stainless Steel Oxide

The default tabular values of density as a function of temperature for stainless steel oxide are listed below. No extrapolation is allowed.

Stainless Steel Oxide

Temp (K)	Density (kg/m ³)	Data Source
273.15	5180.0	Ref. [20]
5000.0	5180.0	Ref. [20]

8.2.6 Boron Carbide

The default tabular values of density as a function of temperature for boron carbide are listed below. No extrapolation is allowed.

Boron Carbide

Temp (K)	Density (kg/m ³)	Data Source
273.15	2520.0	Ref. [20]
5000.0	2520.0	Ref. [20]

8.2.7 Silver-Indium-Cadmium

The default tabular values of density as a function of temperature for silver-indium-cadmium are listed below. No extrapolation is allowed.

Silver-Indium-Cadmium

Temp (K)	Density (kg/m ³)	Data Source
273.15	9689.4	Ref. [2], @ 1000 K
5000.0	9689.4	Ref. [2], @ 1000 K

8.2.8 Uranium Metal

The default tabular values of density as a function of temperature for uranium metal are listed below. No extrapolation is allowed.

Uranium Metal

Temp (K)	Density (kg/m ³)	Data Source
273.15	19080.0	Ref. [11] p. 78, extrapolated
298.0	19050.0	Ref. [11] p. 78
366.3	18970.0	Ref. [11] p. 78
477.4	18870.0	Ref. [11] p. 78
588.6	18760.0	Ref. [11] p. 78
699.7	18640.0	Ref. [11] p. 78
810.8	18500.0	Ref. [11] p. 78
921.9	18330.0	Ref. [11] p. 78
1406.0	17580.0	Ref. [11], p. 78, extrapolated
5000.0	17580.0	Constant beyond melting point of 1406 K

8.2.9 Graphite

The default tabular values of density as a function of temperature for graphite are listed below. No extrapolation is allowed.

Graphite

Temp (K)	Density (kg/m ³)	Data Source
273.15	1730.0	Ref. [4], p. 436, nuclear graphite, grade A
5000.0	1730.0	Ref. [4] p. 436, nuclear graphite, grade A

8.2.10 Concrete

The default tabular values of density as a function of temperature for concrete are listed below. No extrapolation is allowed.

Concrete

Temp (K)	Density (kg/m ³)	Data Source
273.15	2306.7	Ref. [5], p. 635, stone concrete @ 294 K
5000.0	2306.7	Ref. [5], p. 635, stone concrete @ 294 K

8.2.11 Aluminum

The default tabular values of density as a function of temperature for aluminum are listed below. Constant extrapolation is allowed from the lower end of the tabulated range. Linear extrapolation is allowed from the upper end of the tabulated range.

Aluminum

Temp (K)	Density (kg/m ³)	Data Source
273.15	2705.00	Ref. [6]
300.00	2701.00	Ref. [6]
400.00	2681.00	Ref. [6]
500.00	2661.00	Ref. [6]
600.00	2639.00	Ref. [6]
800.00	2591.00	Ref. [6]
933.00	2559.00	Ref. [6]
933.01	2385.00	Ref. [6]
1000.00	2365.00	Ref. [6]
1200.00	2305.00	Ref. [6]
1400.00	2255.00	Ref. [6]

8.2.12 Aluminum Oxide

The default tabular values of density as a function of temperature for aluminum oxide are listed below. Linear extrapolation is allowed from the upper end of the tabulated range.

MP Package Reference Manual

Aluminum Oxide

Temp (K)	Density (kg/m ³)	Data Source
273.15	4000.0	Ref. [7]
5000.0	4000.0	Ref. [7]

8.2.13 Cadmium

The default tabular values of density as a function of temperature for cadmium are listed below. Constant extrapolation is allowed from both ends of the tabulated range.

Cadmium

Temp (K)	Density (kg/m ³)	Data Source
273.15	8670.0	Ref. [6]
283.15	8660.0	Ref. [6]
293.15	8650.0	Ref. [6]
303.15	8640.0	Ref. [6]
313.15	8630.0	Ref. [6]
323.15	8620.0	Ref. [6]
333.15	8610.0	Ref. [6]
343.15	8600.0	Ref. [6]
353.15	8590.0	Ref. [6]
363.15	8580.0	Ref. [6]
373.15	8570.0	Ref. [6]
383.15	8561.0	Ref. [6]
393.15	8551.0	Ref. [6]
403.15	8541.0	Ref. [6]
413.15	8531.0	Ref. [6]
423.15	8521.0	Ref. [6]
433.15	8511.0	Ref. [6]
443.15	8501.0	Ref. [6]
453.15	8491.0	Ref. [6]
463.15	8481.0	Ref. [6]
473.15	8470.0	Ref. [6]
483.15	8460.0	Ref. [6]
493.15	8450.0	Ref. [6]
503.15	8439.0	Ref. [6]
513.15	8428.0	Ref. [6]
523.15	8417.0	Ref. [6]
533.15	8406.0	Ref. [6]
543.15	8395.0	Ref. [6]
553.15	8384.0	Ref. [6]
563.15	8372.0	Ref. [6]
573.15	8360.0	Ref. [6]
583.15	8348.0	Ref. [6]

Cadmium

Temp (K)	Density (kg/m ³)	Data Source
594.00	8336.0	Ref. [6]
594.01	8016.0	Ref. [6]
600.00	8010.0	Ref. [6]
800.00	7805.0	Ref. [6]
1000.00	7590.0	Ref. [6]
1040.00	7547.0	Ref. [6]

8.2.14 Stainless Steel 304

The default tabular values of density as a function of temperature for stainless steel 304 are listed below. Constant extrapolation is allowed from both ends of the tabulated range.

Stainless Steel 304

Temp (K)	Density (kg/m ³)	Data Source
273.15	8025.00	Ref. [6]
323.15	8003.00	Ref. [6]
373.15	7981.00	Ref. [6]
423.15	7958.00	Ref. [6]
473.15	7936.00	Ref. [6]
523.15	7914.00	Ref. [6]
573.15	7891.00	Ref. [6]
623.15	7869.00	Ref. [6]
673.15	7847.00	Ref. [6]
723.15	7824.00	Ref. [6]
773.15	7802.00	Ref. [6]
823.15	7780.00	Ref. [6]
873.15	7757.00	Ref. [6]
923.15	7735.00	Ref. [6]
973.15	7713.00	Ref. [6]
1023.15	7690.00	Ref. [6]
1073.15	7668.00	Ref. [6]
1123.15	7646.00	Ref. [6]
1173.15	7623.00	Ref. [6]
1223.15	7601.00	Ref. [6]
1273.15	7579.00	Ref. [6]
1373.15	7534.00	Ref. [6]
1473.15	7489.00	Ref. [6]
1573.15	7445.00	Ref. [6]
1673.15	7400.00	Ref. [6]
1700.00	7388.00	Ref. [6]
1700.01	6926.00	Ref. [6]
1800.00	6862.00	Ref. [6]

MP Package Reference Manual

Stainless Steel 304

Temp (K)	Density (kg/m ³)	Data Source
1900.00	6785.00	Ref. [6]
2000.00	6725.00	Ref. [6]
2100.00	6652.00	Ref. [6]
2200.00	6576.00	Ref. [6]
2300.00	6498.00	Ref. [6]
2400.00	6416.00	Ref. [6]
2500.00	6331.00	Ref. [6]
2600.00	6243.00	Ref. [6]
2700.00	6152.00	Ref. [6]
2800.00	6058.00	Ref. [6]
2900.00	5961.00	Ref. [6]
3000.00	5861.00	Ref. [6]

8.2.15 Lithium Aluminum

The default tabular values of density as a function of temperature for lithium aluminum are listed below. Constant extrapolation is allowed from the lower end of the tabulated range. Linear extrapolation is allowed from the upper end of the tabulated range.

Lithium Aluminum

Temp (K)	Density (kg/m ³)	Data Source
273.15	2664.00	Ref. [6]
300.00	2660.00	Ref. [6]
400.00	2640.00	Ref. [6]
500.00	2620.00	Ref. [6]
600.00	2600.00	Ref. [6]
800.00	2551.00	Ref. [6]
917.00	2524.00	Ref. [6]
917.01	2348.00	Ref. [6]
1000.00	2328.00	Ref. [6]
1200.00	2269.00	Ref. [6]
1400.00	2120.00*	Ref. [6]*

* Value differs slightly from reference. MELCOR/SR-Mod3 Fortran value is used.

8.2.16 Uranium Aluminum

The default tabular values of density as a function of temperature for uranium aluminum are listed below. Constant extrapolation is allowed from both ends of the tabulated range.

Uranium Aluminum

Temp (K)	Density (kg/m ³)	Data Source
----------	------------------------------	-------------

Uranium Aluminum

Temp (K)	Density (kg/m ³)	Data Source
400.00	3507.00*	Ref. [6]*
500.00	3469.00	Ref. [6]
600.00	3448.00	Ref. [6]
700.00	3425.00	Ref. [6]
800.00	3402.00	Ref. [6]
919.00	3371.00	Ref. [6]
919.01	3202.00	Ref. [6]
962.00	3196.00	Ref. [6]
1005.00	3180.00	Ref. [6]
1005.01	3260.00	Ref. [6]
1039.00	3197.00	Ref. [6]
1123.00	3159.00	Ref. [6]
1223.00	3117.00	Ref. [6]
1323.00	3076.00	Ref. [6]
1338.00	3071.00	Ref. [6]
1400.00	3051.00	Ref. [6]

* Value differs slightly from reference. MELCOR/SR-Mod3 Fortran value is used.

8.2.17 Carbon Steel

The default tabular values of density as a function of temperature for carbon steel are listed below. No extrapolation is allowed.

Carbon Steel

Temp (K)	Density (kg/m ³)	Data Source
273.15	7752.9	Ref. [8]
5000.00	7752.9	Ref. [8]

8.3 Calculated as a Function of Temperature and Pressure

The default density functions for air and steam are described in Sections 8.3.1 and 8.3.2, below. These default functions may not be altered through user input.

8.3.1 Air

The density (kg/m³) of air is computed from the gas law:

$$\rho = MW \times Pres / (R \times T \times CPRS) \quad (8.3.1)$$

where,

MP Package Reference Manual

- MW* = Molecular weight, 0.028966 kg/mol
- Pres* = Pressure (Pa)
- R* = Universal gas constant, 8.31441 J/(mol-K)
- T* = Temperature (K)
- CPRS* = Compressibility, 1.0

8.3.2 Steam

The density (kg/m³) of steam is computed from the gas law:

$$\rho = MW \times Pres / (R \times T \times CPRS) \quad (8.3.2)$$

where,

- MW* = Molecular Weight, 0.018016 kg/mol
- Pres* = Pressure (Pa)
- R* = Universal gas constant, 8.31441 J/(mol-K)
- T* = Temperature (K)
- CPRS* = Given

in

MP Package Reference Manual

Table 8.1 The value of CPRS is determined by standard interpolation on T and P for those points bounded by values from

MP Package Reference Manual

Table 8.1. For those points which lie outside the bounds of the table, various methods are used for determining CPRS. Figure 8.1 is a graphic illustration of the values shown on

Table 8.1. The figure is divided into 10 regions, each of which has its own method for computing the compressibility.

- Region 1: Points in this region are assigned a compressibility of 0.9978. This corresponds to the value of CPRS at (0.0068884 MPa, 311.72 K).
- Region 2: CPRS for points in this region are computed by linear interpolation on temperature of the values for the pressure, $P = 0.0068884$ MPa.
- Region 3: Points in this region are assigned a compressibility of 1.0000. This corresponds to the value of CPRS at (0.0068884 MPa, 1033.0 K).
- Region 4: CPRS for points in this region are computed by linear interpolation on pressure of the smallest values for the pressures on the left and right sides of (P,T).
- Region 5: CPRS for points in this region are computed by linear interpolation, first on temperature , then on pressure, of the bounding values on the left side and the value corresponding to the minimum temperatures on the right side.
- Region 6: CPRS for points in this region are computed by linear interpolation, first on temperature , then on pressure, of the bounding values.
- Region 7: Points in this region are assigned the maximum value for compressibility, 1.0000.
- Region 8: Points in this region are assigned a compressibility of 0.9134. This corresponds to the value of CPRS at (1.3786 MPa, 467.37 K).
- Region 9: CPRS for points in this region are computed by linear interpolation on temperature of the values for the pressure, $P = 1.3786$ MPa.
- Region 10: Points in this region are assigned a compressibility of 0.9995. This corresponds to the value at (1.3786 MPa, 1366.33 K).

MP Package Reference Manual

Table 8.1. Compressibility of Steam as a Function of Temperature (K) and Pressure (MPa) (Ref. 9).

Pressure (MPa)	0.0068884	0.034462	0.068953	0.10130	0.13786	0.27572	0.41358
Temp (K)							
311.72	0.9978						
345.34		0.9927					
362.55			0.9881				
366.33	0.9991	0.9946	0.9889				
372.99				0.9846			
381.87					0.9811		
388.55	0.9993	0.9959	0.9916				
388.56				0.9875	0.9825		
403.70						0.9702	
410.77	0.9995	0.9969	0.9936				
410.78				0.9905	0.9866	0.9726	
417.85							0.9610
428.59							
433.00	0.9997	0.9976	0.9950	0.9925	0.9898	0.9786	0.9672
437.37							
444.83							
451.38							
455.22	0.9998	0.9981	0.9960	0.9941	0.9919	0.9830	0.9739
457.22							
462.52							
467.37							
477.44	0.9999	0.9985	0.9967	0.9952	0.9934	0.9862	0.9789
499.67	1.0000	0.9988	0.9974	0.9959	0.9944	0.9886	0.9826
505.22							
533.00	1.0000	0.9991	0.9980	0.9969	0.9959	0.9913	0.9867
560.78							
588.56	1.0000	0.9995	0.9987	0.9981	0.9973	0.9941	0.9911
644.11	1.0000	0.9996	0.9992	0.9986	0.9982	0.9959	0.9938
699.67	1.0000	0.9998		0.9991	0.9987	0.9971	0.9956
755.22							
810.78	1.0000	1.0000	0.9998	0.9996	0.9994	0.9985	0.9976
921.89	1.0000	1.0000	1.0000	0.9999	0.9998	0.9992	0.9987
1033.00	1.0000	1.0000	1.0000	1.0000	0.9999	0.9997	0.9992
1144.11				1.0000	1.0000	0.9998	0.9998
1255.22						1.0000	1.0000
1366.33							1.0000
1477.44							

**This front page
intentionally left blank**

MP Package Reference Manual

Table 8.1 Compressibility of Steam as a Function of Temperature (K) and Pressure (MPa) (Ref. 9) (Cont)

Pressure (MPa)	0.55145	0.68931	0.82717	0.96502	1.1029	1.2407	1.3786
Temp (K)							
311.72							
345.34							
362.55							
366.33							
372.99							
381.87							
388.55							
388.56							
403.70							
410.77							
410.78							
417.85							
428.59	0.9528						
433.00	0.9552						
437.37		0.9432					
444.83			0.9383				
451.38				0.9316			
455.22	0.9646	0.9550	0.9449	0.9347			
457.22					0.9255		
462.52						0.9193	
467.37							0.9134
477.44	0.9714	0.9637	0.9561	0.9478	0.9397	0.9310	0.9223
499.67	0.9766	0.9703					
505.22			0.9657	0.9595	0.9533	0.9469	0.9406
533.00	0.9822	0.9775	0.9727	0.9681	0.9630	0.9580	0.9532
560.78			0.9779	0.9741	0.9701	0.9663	0.9622
588.56	0.9880	0.9850	0.9819	0.9787	0.9756	0.9723	0.9691
644.11	0.9916	0.9895	0.9872	0.9852	0.9830	0.9807	0.9785
699.67	0.9940	0.9924	0.9909	0.9893	0.9877	0.9861	0.9845
755.22						0.9899	0.9887
810.78	0.9967	0.9958	0.9950	0.9941	0.9933	0.9924	0.9916
921.89	0.9982	0.9976	0.9971	0.9966	0.9962	0.9956	0.9951
1033.00	0.9990	0.9986	0.9983	0.9980	0.9977	0.9974	0.9970
1144.11	0.9994	0.9992	0.9990	0.9989	0.9986	0.9984	0.9983
1255.22	0.9998	0.9996	0.9995	0.9994	0.9993	0.9991	0.9990
1366.33	1.0000	0.9999	0.9998	0.9998	0.9997	0.9996	0.9995
1477.44		1.0000			1.0000		

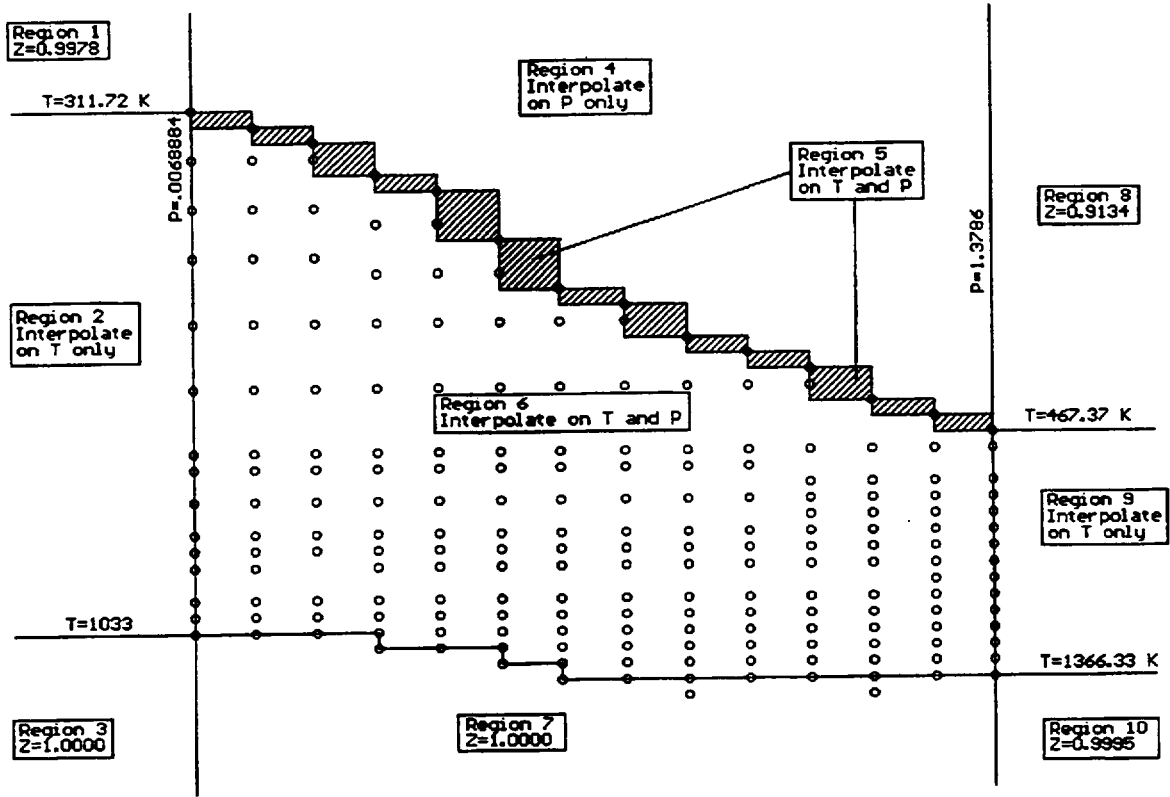


Figure 8.1. Methods for Computing the Compressibility from

Table 8.1 Data.

9. Constant Melting Temperature

The melting temperature may be input by the user or read from a MELCOR default table. There are no checks made on the consistency of user-input values for enthalpy, specific heat capacity, melting temperature, and latent heat of fusion.

The following materials have default tables for the melting temperature:

Material	Melt Temperature (K)	Data Source
Zircaloy	2098.0	Ref. [1]
Zirconium Oxide	2990.0	Ref [20]
Uranium Dioxide	3113.0	Ref. [1]
Stainless Steel	1700.0	Estimated
Stainless Steel Oxide	1870.0	Ref. [20], Fe ₃ O ₄
Boron Carbide	2620.0	Ref. [20]
Silver-Indium-Cadmium	1075.0	Ref. [2]
Uranium Metal	1406.0	Ref. [20]
Graphite	3866.0	Ref. [4]
Aluminum	933.0	Ref. [6]
Aluminum Oxide	2327.0	Ref. [7]
Cadmium	594.0	Ref. [6]
Stainless Steel 304	1700.0	Ref. [6]
Lithium Aluminum	917.0	Ref. [6]
Uranium Aluminum	1128.5	Ref. [6], average of solidus and liquidus points
Carbon Steel	1810.9	Ref. [8]

10. Constant Latent Heat of Fusion

The latent heat of fusion may be input by the user or read from a MELCOR default table. There are no checks made on the consistency of user-input values for enthalpy, specific heat capacity, melting temperature, and latent heat of fusion.

The following materials have default tables for the latent heat of fusion:

Material	Heat of Fusion (J/kg)	Data Source
Zircaloy	2.25E5	Ref. [1]
Zirconium Oxide	7.07E5	Ref [20]
Uranium Dioxide	2.74E5	Ref [1]
Stainless Steel	2.68E5	Estimated

Material	Heat of Fusion (J/kg)	Data Source
Stainless Steel Oxide	5.98E5	Ref. [20], Fe ₃ O ₄
Boron Carbide	5.00E5	Estimated
Silver-Indium-Cadmium	9.80E4	Ref. [2]
Uranium Metal	5.025E4	Ref. [4]
Aluminum Oxide	1.07E6	Ref. [21]
Aluminum	3.978E5	Ref. [6]
Cadmium	5.500E4	Ref. [6]
Stainless Steel 304	2.692E5	Ref. [6]
Lithium Aluminum	3.9845E5	Ref. [6]
Uranium Aluminum	2.900E5	Ref. [6]
Carbon Steel	2.71960E5	Ref. [8]

11. References

1. D. L. Hagrman, G. A. Reymann, and R. E. Mason, MATPRO VERSION 11 (Revision 1) A Handbook of Materials Properties for Use in the Analysis of Light Water Reactor Fuel Rod Behavior, NUREG/CR-0497 and TREE-1280 Rev. 1, EG&G Idaho, Inc., Idaho Falls, ID (February 1980).
2. D. L. Hagrman, Materials Properties for Severe Core Damage Analysis, EGG-CDD-5801, EG&G, Idaho Falls, ID (May 1982).
3. F. P. Incropera and D. P. Dewitt, Fundamentals of Heat Transfer, John Wiley and Sons, New York (1981).
4. CRC Handbook of Tables for Applied Engineering Science, 2nd ed., Ed. by R. E. Bolz and G. L. Tuve, CRC Press, Boca Raton FL (1973).
5. F. Kreith, Principles of Heat Transfer, 3rd ed., Intext Educational Publishers, New York (1973).
6. R. C. Nause and M. T. Leonard, Thermophysical Property Assessment Report for Savannah River Site Production Reactor Materials, Science Applications International Corporation, SAIC Report No. 89/6507, Rev. 1 (May 1990).
7. Thermodynamic and Transport Properties for the CONTAIN Code, Sandia National Laboratories, NUREG/CR-5173 (December 1988).
8. Data for carbon steel duplicate those defined and used in the Bottom Head (BH) package. Values were obtained from various subroutines included in that package. References cited in the coding are: (1) Y. S. Touloukian, Thermophysical Properties

MP Package Reference Manual

- of High Temperature Solid Materials, and (2) the ASTM Metals Handbook (pages 1-63, 64) for low-alloy steels (particularly, SA508 steel).
9. N. B. Vargaftik, Handbook of Physical Properties of Liquids and Gases: Pure Substances and Mixtures, 2nd ed., Springer-Verlag (1975).
 10. E. R. G. Eckert and R. M. Drake, Jr., Heat and Mass Transfer, McGraw-Hill, New York (1959).
 11. M. M. Wakil, Nuclear Heat Transport, International Textbook Co., New York (1971).
 12. Heard, et al., N-Reactor Safety Enhancement Report HEDL-TC 2977, Westinghouse Hanford Company, September 1987.
 13. R. Reid, et al., The Properties of Gases and Liquids, McGraw-Hill, New York (1970).
 14. 1967 Steam Tables, Electrical Research Association, St. Martin's Press, New York (1967).
 15. J. Hilsenrath, et al., Tables of Thermodynamic and Transport Properties, Pergamon Press, New York (1960).
 16. D. R. Pitts and L. E. Sissom, Schaum's Outline of Theory and Problems of Heat Transfer, McGraw-Hill, New York (1977).
 17. R. Bird, et al., Transport Phenomena, John Wiley and Sons, New York (1960).
 18. J. K. Fink, R. Simms and B. A. Brock, Material Properties for HWR-NPR Severe Accident Studies, Argonne National Laboratory, ANL/NPR-90/005 (March 1990).
 19. L. Baker and C. Just, Studies of Metal-Water Reactions at High temperatures; III. Experimental and Theoretical Studies of the Zirconium-Water Reaction, ANL-6548, Argonne National Laboratory, Chicago (May 1962).
 20. CRC Handbook of Chemistry and Physics, 63rd ed., CRC Press, Boca Raton, FL (1982).
 21. CRC Handbook of Chemistry and Physics, 71st ed., CRC Press, Boca Raton, FL (1990).

Noncondensable Gas (NCG) and Water (H2O) Packages Reference Manual

Noncondensable gases in the Control Volume Hydrodynamics (CVH) package are modeled as ideal gases. The constant volume heat capacity is approximated as an analytic function of temperature. The equation of state for water is based on the analytic expression for the Helmholtz function used to generate the familiar Keenan and Keyes Steam Tables. [1] This document describes the constitutive relations used for the water and noncondensable gases equations of state, and it lists the default values of the associated constants for the gases provided in the NCG library.

User input requirements for the NCG package are described in the NCG Users' Guide. There is no input allowed for the H2O package.

Contents

1. NCG Equation of State5
1.1 Integration Constants in the Energy Function6

2. H2O Equation of State7
2.1 Single-Phase Properties.....8
2.2 Mixed-Phase Properties8

3. NCG Library8

References 16

1. NCG Equation of State

Noncondensable gases in the Control Volume Hydrodynamics (CVH) package are modeled as ideal gases. The specific internal energy and enthalpy of an ideal gas is a function only of its temperature, T , the natural state (reference) temperature, T_n , its energy of formation, e_{form} , its enthalpy of formation, h_{form} , the universal gas constant, R , and its molecular weight, w .

$$e(T) = \int_{T_n}^T c_v(T') dT' + e_{form} \quad (1.1)$$

$$h(T) = \int_{T_n}^T \left(c_v(T') + \frac{R}{W} \right) dT' + h_{form} \quad (1.2)$$

The pressure, P , is a function of the mass density, ρ , the temperature, T , the universal gas constant, R , and the molecular weight, w ,

$$P = \frac{\rho R T}{w} \quad (1.3)$$

The noncondensable gases in MELCOR are characterized by the temperature dependent constant volume specific heat, $c_v(T)$, the natural state (reference) temperature, T_n , the energy of formation, e_{form} , the entropy at the reference temperature, s_0 (this quantity is not currently used in the calculation but is included for completeness), and the molecular weight of the material, w .

The specific heat for each noncondensable gas calculated from an analytic fit in the general form

$$c_v(T) = c_{v0} + c_{v1}T + c_{v2}T^2 + c_{v3}T^3 + \frac{c_{vsqrt}}{\sqrt{T}} + \frac{c_{vm1}}{T} + \frac{c_{vm2}}{T^2} \quad (1.4)$$

for the temperature range $T_{low} \leq T \leq T_{up}$, where T_{low} and T_{up} may be different for each gas. The value at T_{low} is used for $T < T_{low}$, and the value at T_{up} is used for $T > T_{up}$.

Using this constitutive relation for the specific heat, the internal energy is given by

NCG/H2O Packages Reference Manual

$$e(T) = e_0 + c_{v0}T + \frac{1}{2}c_{v1}T^2 + \frac{1}{3}c_{v2}T^3 + \frac{1}{4}c_{v3}T^4 + 2c_{vsqrt}\sqrt{T} + c_{vm1}\ln(T) - \frac{c_{vm2}}{T} \quad (1.5)$$

for $T_{low} \leq T \leq T_{up}$, and is extrapolated outside that range using the constant limiting specific heat at T_{low} or T_{up} are used. Here

$$e_0 = e_{form} - c_{v0}T_n - \frac{1}{2}c_{v1}T_n^2 - \frac{1}{3}c_{v2}T_n^3 - \frac{1}{4}c_{v3}T_n^4 - 2c_{vsqrt}\sqrt{T_n} - c_{vm1}\ln(T_n) + \frac{c_{vm2}}{T_n} \quad (1.6)$$

Each of the coefficients can be specified via user input, as described in the NCG Users' Guide. Appropriate default coefficients for gases of interest from JANAF [2] and other sources are included in the noncondensable gas equation of state library, as described in Section 2. The default natural temperature used is 298.15 K; this may be changed with sensitivity coefficient 2090.

The reader may note that the definition of e_0 is actually inconsistent unless T_n lies in the range $T_{low} \leq T_n \leq T_{hi}$. For a number of gases (N_2 , O_2 , CH_4 , CO and CO_2), T_{low} is 300 K while T_n is 298.15. In these cases, the discrepancy is less than 10 J/kg and is totally insignificant compared to heats of reaction (several MJ/kg). Although the discrepancy for D_2 ($T_{low} = 600$ K) is significantly greater, this gas is not used in light water reactor simulations.

1.1 Integration Constants in the Energy Function

A modified thermochemical reference point is used in the NCG package. That is, all heats of formation of compounds are included in the enthalpy functions, as in JANAF tables. The advantage is that all heats of reaction are implicitly contained in the enthalpy functions. For example, in a reaction



taking place at constant temperature and pressure, total enthalpy is conserved. The heat released is the difference between the enthalpy of the reactants and that of the products. This is simply the chemists' definition of the heat of reaction,

$$Q_R(T) = h_A(P, T) + h_B(P, T) - h_{AB}(P, T) \quad (1.8)$$

Therefore, chemical reactions (such as gas combustion simulated by the Burn package) can be treated simply as changes in the masses of various materials; the associated heat effects are accounted for automatically through the equations of state.

Since only differences in enthalpy are significant, one integration constant may be chosen for each element represented in the collection of gases in the database. Conventional practice is to choose these integration constants such that the enthalpy of each element is zero in its standard state (25°C, 1 atm, with the material in its most stable state). However, water properties in MELCOR are defined (in the H2O package) consistent with Keenan and Keyes Steam Tables [1], as discussed in Section 2. Because water is formed from hydrogen and oxygen, the integration constants for hydrogen, oxygen, and water may *not* be chosen independently. The conventional integration constant is used for hydrogen in the NCG package, but the integration constant for oxygen has therefore been chosen such that the reference point for water vapor is consistent with that used by Keenan and Keyes. This results in a shift in the integration constant for *every* oxygen-containing gas in the NCG package compared to its conventional JANAF value. For all other gases, the integration constants are consistent with conventional practice.

In actuality, the reference point used will be significant only if a gas is chemically active. For current MELCOR models, the only such gases are H₂, D₂, O₂, CO, CO₂, and CH₄. (CH₄ is active *only* if the B₄C reaction in the COR package is enabled, in which case the heat of reaction data used there are not fully compatible with NCG data.) Thus, the user need not worry much about the reference points for other (in particular, user-defined) gases. If chemically active gases are modified, the reference point energy must not be arbitrarily redefined.

2. H2O Equation of State

The equation of state for water is based on the analytic expression for the Helmholtz function, $\psi(\rho, T)$, that was used to generate the familiar Keenan and Keyes Steam Tables [1]. The expression, involving a double power series with log and exponential terms, may be found in the Appendix to the 1969 tables. It contains approximately 50 constant coefficients. These cannot be changed in MELCOR.

NCG/H2O Packages Reference Manual

The Keenan and Keyes formulation is augmented by JANAF data [2] for temperatures greater than 1589 K (2400 °F). The resulting equation of state is valid for temperatures greater than 273.15 K and for pressures less than 100 MPa.

2.1 Single-Phase Properties

The H2O package determines all single-phase thermodynamic properties of water as functions of density and temperature from the equation for ψ . For example, pressure and internal energy may be expressed in terms of the first derivatives of ψ as

$$P = \rho^2 (\partial \psi / \partial \rho)_T \quad (2.1)$$

$$e = \psi + T s = \psi - T (\partial \psi / \partial T)_\rho \quad (2.2)$$

where s is entropy. These are evaluated from the equation for ψ and those for its analytic term-by-term derivatives. The quantities $(\partial P / \partial T)_\rho$, $(\partial P / \partial \rho)_T$, and $c_v = (\partial e / \partial T)_\rho$, which involve the three independent second derivatives of ψ , are evaluated similarly.

2.2 Mixed-Phase Properties

The coexistence curve (the saturation line) is defined by points where P , T , and the Gibbs function $g = \psi + P / \rho$ are equal for two different values of ρ . This curve was determined by a calculation external to MELCOR. All properties of each phase were tabulated at 1 K intervals and are included as data in the H2O package. The properties of two-phase states are evaluated from these tables, using the lever rule.

3. NCG Library

A library of data for gases of interest is available for use. Any of the numbers may be changed via user input. The available gases and the associated constants are defined below. Ten user-defined gases called GAS k , where k is any letter from A to J, can also be used, but the user must defined all the values for the associated constants. Units for the parameters are given in the NCG Users Guide.

NCG/H2O Packages Reference Manual

Hydrogen (H₂)	
	MELCOR Name: H2
	Molecular Weight: 0.0020162
<i>C_{v0}</i> :	-17849.
<i>C_{v1}</i> :	11.28298
<i>C_{v2}</i> :	-2.1081958E-3
<i>C_{v3}</i> :	1.5635602E-7
<i>C_{vsqrt}</i> :	865616.
<i>C_{vm1}</i> :	-8188058.3
<i>C_{vm2}</i> :	1.925734E8
<i>T_{low}</i> :	100.
<i>T_{up}</i> :	6000.
<i>e_f</i> :	0.
<i>S₀</i> :	0.

Deuterium (D₂)	
	MELCOR Name: D2
	Molecular Weight: 0.00400
<i>C_{v0}</i> :	5508.8
<i>C_{v1}</i> :	-2.0277
<i>C_{v2}</i> :	3.3827E-3
<i>C_{v3}</i> :	-1.0842E-6
<i>C_{vsqrt}</i> :	0.
<i>C_{vm1}</i> :	0.
<i>C_{vm2}</i> :	0.
<i>T_{low}</i> :	600.
<i>T_{up}</i> :	1500.
<i>e_f</i> :	0.
<i>S₀</i> :	0.

Helium (He)	
	MELCOR Name: HE
	Molecular Weight: 0.004003
<i>C_{v0}</i> :	5231.0
<i>C_{v1}</i> :	0.
<i>C_{v2}</i> :	0.
<i>C_{v3}</i> :	0.
<i>C_{vsqrt}</i> :	0.
<i>C_{vm1}</i> :	0.
<i>C_{vm2}</i> :	0.

NCG/H2O Packages Reference Manual

T_{low} :	1.
T_{up} :	10000.
e_f :	0.
s_0 :	0.

Nitrogen (N₂)

MELCOR Name: N2	
Molecular Weight: 0.02801	
C_{v0} :	1.117E3
C_{v1} :	0.
C_{v2} :	0.
C_{v3} :	0.
C_{vsqrt} :	0.
C_{vm1} :	-2.880E5
C_{vm2} :	5.348E7
T_{low} :	300.
T_{up} :	5000.
e_f :	0.
s_0 :	0.

Oxygen (O₂)

MELCOR Name: O2	
Molecular Weight: 0.032	
C_{v0} :	1245.
C_{v1} :	0.
C_{v2} :	0.
C_{v3} :	0.
C_{vsqrt} :	-16763.
C_{vm1} :	1.111E5
C_{vm2} :	0.
T_{low} :	300.
T_{up} :	2778.
e_f :	1.7828E7
s_0 :	0.

NCG/H2O Packages Reference Manual

Argon (Ar)	
	MELCOR Name: AR
	Molecular Weight: 0.03994
C_{v0} :	525.26
C_{v1} :	0.
C_{v2} :	0.
C_{v3} :	0.
C_{vsqrt} :	0.
C_{vm1} :	0.
C_{vm2} :	0.
T_{low} :	1.
T_{up} :	10000.
e_f :	0.
S_0 :	0.

Methane (CH₄)	
	MELCOR Name: CH4
	Molecular Weight: 0.0160324
C_{v0} :	660.6
C_{v1} :	3.462
C_{v2} :	0.
C_{v3} :	0.
C_{vsqrt} :	0.
C_{vm1} :	0.
C_{vm2} :	0.
T_{low} :	300.
T_{up} :	833.
e_f :	-4.5153E6
S_0 :	0.

NCG/H2O Packages Reference Manual

Carbon Monoxide (CO)	
	MELCOR Name: CO
	Molecular Weight: 0.028
C_{v0} :	1.116E3
C_{v1} :	0.
C_{v2} :	0.
C_{v3} :	0.
C_{vsqrt} :	0.
C_{vm1} :	-2.7312E5
C_{vm2} :	4.9348E7
T_{low} :	300.
T_{up} :	5000.
e_f :	6.3286E6
S_0 :	0.

Carbon Dioxide (CO₂)	
	MELCOR Name: CO2
	Molecular Weight: 0.044
C_{v0} :	1351.35
C_{v1} :	0.
C_{v2} :	0.
C_{v3} :	0.
C_{vsqrt} :	0.
C_{vm1} :	-3.4497E5
C_{vm2} :	4.138E7
T_{low} :	300.
T_{up} :	3500.
e_f :	4.0785E6
S_0 :	0.

NCG/H2O Packages Reference Manual

Acetylene (C₂H₂)	
	MELCOR Name: C2H2
	Molecular Weight: 0.026016
<i>C_{v0}</i> :	1.1457E3
<i>C_{v1}</i> :	0.
<i>C_{v2}</i> :	0.
<i>C_{v3}</i> :	0.
<i>C_vsqrt</i> :	0.
<i>C_{vm1}</i> :	0.
<i>C_{vm2}</i> :	0.
<i>T_{low}</i> :	1.
<i>T_{up}</i> :	10000.
<i>e_f</i> :	8.8104E6
<i>s₀</i> :	0.

Ethylene (C₂ H₄)	
	MELCOR Name: C2H4
	Molecular Weight: 0.028032
<i>C_{v0}</i> :	334.51
<i>C_{v1}</i> :	1.7568
<i>C_{v2}</i> :	0.
<i>C_{v3}</i> :	0.
<i>C_vsqrt</i> :	0.
<i>C_{vm1}</i> :	0.
<i>C_{vm2}</i> :	0.
<i>T_{low}</i> :	194.
<i>T_{up}</i> :	611.1
<i>e_f</i> :	1.9536E6
<i>s₀</i> :	0.

NCG/H2O Packages Reference Manual

Ammonia (NH₃)	
	MELCOR Name: NH3
	Molecular Weight: 0.017029
<i>C_{v0}</i> :	1.7012E3
<i>C_{v1}</i> :	0.
<i>C_{v2}</i> :	0.
<i>C_{v3}</i> :	0.
<i>C_{vsqrt}</i> :	0.
<i>C_{vm1}</i> :	0.
<i>C_{vm2}</i> :	0.
<i>T_{low}</i> :	1.
<i>T_{up}</i> :	10000.
<i>e_f</i> :	-2.557E6
<i>S₀</i> :	0.

Nitrogen Monoxide (NO)	
	MELCOR Name: NO
	Molecular Weight: 0.03005
<i>C_{v0}</i> :	6.8985E2
<i>C_{v1}</i> :	0.
<i>C_{v2}</i> :	0.
<i>C_{v3}</i> :	0.
<i>C_{vsqrt}</i> :	0.
<i>C_{vm1}</i> :	0.
<i>C_{vm2}</i> :	0.
<i>T_{low}</i> :	1.
<i>T_{up}</i> :	10000.
<i>e_f</i> :	6.561E6
<i>S₀</i> :	0.

NCG/H2O Packages Reference Manual

Nitrous Oxide (N₂O)	
	MELCOR Name: N2O
	Molecular Weight: 0.04401
<i>C_{v0}</i> :	736.32
<i>C_{v1}</i> :	0.
<i>C_{v2}</i> :	0.
<i>C_{v3}</i> :	0.
<i>C_{vsqrt}</i> :	0.
<i>C_{vm1}</i> :	0.
<i>C_{vm2}</i> :	0.
<i>T_{low}</i> :	1.
<i>T_{up}</i> :	10000.
<i>e_f</i> :	4.6699E6
<i>S₀</i> :	0.

User Defined Gases (-)	
	MELCOR Name: GAS _k , k = A, B, ... , J
	Molecular Weight: -1.
<i>C_{v0}</i> :	-1.
<i>C_{v1}</i> :	-1.
<i>C_{v2}</i> :	-1.
<i>C_{v3}</i> :	-1.
<i>C_{vsqrt}</i> :	-1.
<i>C_{vm1}</i> :	-1.
<i>C_{vm2}</i> :	-1.
<i>T_{low}</i> :	-1.
<i>T_{up}</i> :	-1.
<i>e_f</i> :	-1.
<i>S₀</i> :	-1.

References

1. J. H. Keenan, et al., Steam Tables: Thermodynamic Properties of Water, Including Vapor, Liquid, and Solid Phases (SI Units), John Wiley & Sons, Inc., New York (1978).
2. JANAF Thermochemical Tables, Dow Chemical Company, Thermal Research Laboratory, Midland, MI (1965).

Passive Autocatalytic Recombiner (PAR) Package Reference Manual

The MELCOR ESF package models the physics for the various engineered safety features (ESFs) in a nuclear power plant. The Passive Autocatalytic Recombiner (PAR) package constitutes a subpackage within the ESF package, and calculates the hydrogen removal rate from the operation of hydrogen recombiners. This reference manual gives a description of the physical models and numerical solutions implemented in the PAR package.

User input for running MELGEN and MELCOR with the PAR package activated is described separately in the Passive Autocatalytic Recombiner section of the Users' Guide.

Contents

- 1. Introduction5
- 2. Model Description6
- 3. Discussion and Development Plans.....10
- 4. References.....11

1. Introduction

The MELCOR ESF package models the thermal-hydraulic behavior of various engineered safety features (ESFs) in nuclear power plants. One ESF is designed to react hydrogen in a reactor containment in a continuous manner with the goal of preventing hydrogen concentrations from increasing to levels that could produce large scale hydrogen deflagration or even detonations. There are a number of methods for achieving hydrogen removal. The most common method is the use of igniters, which provide local ignition sources that will precipitate hydrogen burns near the lower burn limits. However, these systems depend on the availability of a power source, which in certain accident sequences may be lost. In addition these systems will not operate under certain steam inerted conditions which can lead the igniter system to precipitate a large burn when inerted conditions are removed. The passive autocatalytic systems, however, do not require a power source and are not strongly affected by inerted conditions. The benefits derived from this type of hydrogen control system are obvious and are under study for possible backfitting to existing power plants.

The Passive Autocatalytic Recombiner (PAR) package constitutes a subpackage within the ESF package and calculates the rate of hydrogen removal generated by PAR type hydrogen removal systems. The default MELCOR model is based on the Fischer model [1], which is a parametric model developed for a particular type of PAR unit. The user input provides correlation coefficients for the general mathematical form of the model. These coefficients are used by the code to calculate the total gas flow rate through a PAR unit. From the PAR gas flow rate together with user provided PAR efficiencies, transient relaxation times, delay times, and the internally calculated hydrogen mole fractions, a per-PAR-unit hydrogen reaction rate is calculated. This rate is then multiplied by the current timestep and the user provided number of active PAR units to determine the change in hydrogen, oxygen, and steam masses. These differential masses are then passed to CVH as sources/sinks.

It is noted that one particular PAR design has been developed, studied, tested, and reported on in the technical literature. This type of PAR was developed by the NIS Company in Hanau, Germany. The design consists of parallel plate cartridges containing palladium-coated aluminum micropellets. It has been tested in a series of experiments as described in References [1], [2] and [3]. The Reference [3] tests are of particular interest because these tests of the NIS PAR were performed at the Sandia National Laboratories/NM *for the NRC*.

The type of PAR used as the default model in the MELCOR model is the NIS type of PAR. This type of PAR was chosen as the default model because of the literature available and because this was the type studied by the NRC; see Reference [3]. It should be noted that other PAR designs are available. However, it is likely that many other specific designs can be modeled within the parametric framework described here. In the event that it is desired

PAR Package Reference Manual

to study a design concept sufficiently different from the type described here, it was necessary to provide a more general input option. This provides the user with the option to specify a control function with which the PAR flow rate can be calculated as a function of one or more system variables. In addition, an option is provided that allows the user to specify the PAR efficiency through the use of a control function. A more detailed description of the model is provided in the next section

2. Model Description

The chemical recombination of hydrogen and oxygen to produce steam and release energy is described by the equation



The hydrogen reaction rate for a single PAR unit may be expressed in terms of the total volumetric flow rate passing through the unit as follows:

$$R_H = \eta \rho_H Q f(t) \quad (2.2)$$

where

R_H = hydrogen reaction rate (kg/sec)

ρ_H = hydrogen density of entering gas (kg/m³)

η = hydrogen reaction efficiency (~0.85)

Q = total gas-phase volumetric flow rate through the unit (m³/sec)

$f(t) = \left[1 - e^{-\left[\frac{t-t_0}{\tau}\right]} \right]$ = relaxation time function during the initial PAR heat-up

τ = characteristic heat-up time (~1800 sec)

t_0 = time of PAR initiation (s)

t = time after PAR initiation (s)

The relaxation time function is intended to account for the observed transient interval before the PAR attains steady-state operation. It is thought that the primary transient effect

is due to the time required for the catalytic elements to come up to operating temperature. For the configuration tested in Reference [1], the relaxation time, τ , was determined to be on the order of half an hour.

The total volumetric flow rate through a PAR unit may, in the general case, be provided by the user through control functions. However, an expression for NIS type PAR units [1,4] has been found to accurately describe the flow rate, and is given by:

$$Q = a C_H^b \quad (2.3)$$

where

- C_H = hydrogen concentration (mole fraction)
- a = constant that depends on PAR unit design parameters (~0.67 kg/sec)
- b = exponent that depends on PAR unit design parameters (~0.307)

Some of the parameters in Equations (2.2) and (2.3) will be provided by the CVH package in the MELCOR code. For the NIS model, other than the current time, the hydrogen density and mole fraction are the only two required parameters. Depending on the specifics of the model, however, user-defined PAR flow rates may depend on other CVH parameters such as temperature or pressure.

For typical containment volumes, a number of PAR units will be required to control the H_2 concentration. The total hydrogen depletion rate is then found simply by summing the rates from the individual units in a particular control volume. The user may specify more than one type of PAR and specify the number of units of each PAR type in a single control volume or distributed in a number of control volumes.

The transient effects described by the term $f(t)$ in Equation (2.2) derives from the solution for a single step function in hydrogen concentration with the initial concentration being zero, and the hydrogen concentration in a control volume remaining constant.

In general, however, the hydrogen concentration will not remain constant and may in fact involve multiple 'bursts' of hydrogen injection into a containment volume combined with continued releases from the vessel or from ex-vessel fuel/metal, fuel/concrete interactions. It is assumed here that if there is an increase in H_2 concentration, which implies an eventual increase in volumetric flow through the PAR (Equation (2.3)), then the time dependence of the change in flow will follow the same relaxation behavior implied by Equation (2.4). Based on this assumption, a more general approach to the transient effects is employed in the MELCOR model. The transient effects are described by the differential equation:

PAR Package Reference Manual

$$\frac{dQ}{dt} = \frac{1}{\tau} [Q_{ss} - Q] \quad (2.4)$$

where Q is the volumetric flow rate, and Q_{ss} is the steady-state flow rate implied by the hydrogen concentration found from Equation (2.3). Integrating Equation (2.4) over timestep, Δt , in which the flow rate changes from Q_{old} to Q_{new} , gives the following result:

$$Q_{new} = Q_{ss} \left[1 - e^{-\Delta t/\tau} \right] + Q_{old} e^{-\Delta t/\tau} \quad (2.5)$$

Equation (2.5) will provide for transient effects, but requires that the hydrogen reaction rate be carried as a dynamic variable with the old and new values stored in the main variable array. Note that the transient term $f(t)$ is now implicit in the flow rate equation. It should also be noted that Equation (2.5) is applied on a timestep-by-timestep basis so that the flow rates and H_2 burn rates will respond in a continuous manner to transient conditions such as increases or decreases in the hydrogen concentration. It is thus, not necessary to track the thermal response of the PAR catalytic elements. The temperature of the PAR catalytic elements is implicit in the correlations used in the Fischer model, but is not explicitly available as an output parameter.

As described by Equation (2.1), the recombination of hydrogen results in an oxygen depletion rate and a steam mass increase rate. Since the reaction is exothermic, there is an associated change in gas temperature. These rates are given as follows for the control volume in which the PAR unit is located:

$$\frac{dm(H_2)}{dt} = -R_H, \text{ kg/s} \quad (2.6)$$

$$\frac{dm(O_2)}{dt} = -\frac{M_{O_2}}{2M_{H_2}} * R_H, \text{ kg/s} \quad (2.7)$$

$$\frac{dm(H_2O)}{dt} = \frac{M_{O_2}}{2M_{H_2}} * R_H, \text{ kg/s} \quad (2.8)$$

$$\frac{dH}{dt} = \sum_{i=1}^N w_{i,in} h_{i,in} - \sum_{i=1}^N w_{i,out} h_{i,out}, \text{ W} \quad (2.9)$$

Note that in Equations (2.6) through (2.8), M refers to the molecular weight of the species. The indices on the sums in Equation (2.9), for the change in total enthalpy H , refer to the

specific gas constituents (H_2 , O_2 , H_2O , CO , CO_2 , etc.), while w and h refer to the mass flow rate and specific enthalpy of each constituent. Also, because MELCOR uses a consistent reference point (JANIF Convention) for all gas-phase thermodynamic properties, the heating rate given by Equation (2.9) is not needed as a source in the CVH package. JANAF refers to a set of thermochemical tables [5]. The JANAF convention implicitly includes all heats of formation in the enthalpy functions for each material. In so doing, the heat of reaction, for example in the burning of hydrogen and oxygen, is included in the enthalpy of the reaction product (steam in this example). The advantage is that all chemical reactions, such as those generated in this PAR Package, can be treated simply as changes in the masses of the reactants and products, and the heat effects are accounted for automatically through the equations of state.

The mass rates computed by the PAR Package in Equations (2.6) through (2.8) will be multiplied by the current timestep and the differential masses passed to the CVH package.

The PAR testing discussed in Reference [3] did not identify any problem regarding "remaining capacity" in terms of possible degradation of the catalytic elements.

In addition, it is important to note that the literature [2] does address the investigations into possible decrease of the PAR performance because of catalyst inhibitors and poisons. The investigations performed indicate that the effects of catalyst inhibitors and poisons are negligible. However, if further studies provide evidence that catalytic elements can be degraded, an option is provided that allows the user to specify the PAR efficiency, η , by a control function that can be a function of time, aerosol concentration, etc.

The change of gas temperature as it passes through the PAR can be estimated by noting that, since no mass or energy has been added from external sources to the gas stream (with the exception noted later), the enthalpy flow rates in and out of the PAR unit must be equal. Thus, from Equation (2.10), the following relationship between the inlet and outlet conditions must exist,

$$\sum_{i=1}^N w_{i,in} h_{i,in} = \sum_{i=1}^N w_{i,out} h_{i,out} \quad (2.10)$$

$w_{i,out}$ = the mass flow rate of the i th gas-phase species exiting the PAR (kg/s),

$w_{i,in}$ = the mass flow rate of the i th gas-phase species entering the PAR (kg/s),

$h_{i,out}$ = the specific enthalpy of the i th gas-phase species exiting the PAR (J/kg),
and

$h_{i,in}$ = the specific enthalpy of the i th gas-phase species entering the PAR (J/kg).

PAR Package Reference Manual

The outlet temperature is then evaluated by a Newton's method iteration in which the inlet enthalpy flow (the left side of Equation (2.10)) is evaluated and successive estimates of the outlet temperature are calculated until the difference between the inlet enthalpy rate and the outlet enthalpy rate are effectively zero to within a specified limit.

It should be noted that the estimate of outlet temperature will not be accurate during rapid transient situations. During periods in which the PAR elements are heating up or cooling down some fraction of the energy is transferred to or from the PAR elements. In the former case the outlet temperature is over-predicted and in the latter under-predicted. Because the outlet temperature is only an output variable and does not affect any other calculations in the model or in the code, this is not a serious deficiency.

3. Discussion and Development Plans

Although the proposed model is rather simple and was developed in the form of a correlation for a specific design configuration, it is thought that it will provide the capability to accurately model the operation of the NIS type PAR unit in particular. It should also provide the capability to treat a wide variety of similar catalytic reactors given the required performance characteristics. In addition, the options that provide for a user-specified flow rate and efficiency through the use of Control Functions will provide the required additional flexibility and utility to model any type of PAR unit.

For lack of sufficient data regarding other catalytically induced reactions, the current model does not provide for the reaction of CO or other combustible species. Future improvements to the PAR models may consider these reactions.

4. References

1. K. Fischer, "Qualification of Passive Catalytic Module for Hydrogen Mitigation," Nuclear Technology, Vol. 112, p. 58 (October 1995).
2. EPRI report, "Qualification of Passive Autocatalytic Recombiners for Combustion Gas Control in ALWR Containments," EPRI Electric Power Research Institute, Palo Alto CA (April 8, 1993).
3. T. K. Blanchat and A. C. Malliakos (NRC/RES), "Passive Autocatalytic Recombiner (PAR) Tests at the SNL," CSARP Meeting (May 1998).
4. R. Sher, J. Li, and D. E. Leaver, "Models for Evaluating the Performance of Passive Autocatalytic Recombiners (PARs)," 1995 National Heat Transfer Conference, Portland OR, ANS Proceedings, HTC-Vol. 8 (August 5 – 9, 1995).
5. JANAF Thermochemical Tables, DOW Chemical Company, Thermal Research Laboratory, Midland, MI (1965.)

RadioNuclide (RN) Package Reference Manual

The RadioNuclide (RN) package models the behavior of fission product aerosols and vapors and other trace species, including release from fuel and debris, aerosol dynamics with vapor condensation and revaporization, deposition on structure surfaces, transport through flow paths, and removal by engineered safety features. The package also allows for simplified chemistry controlled by the user.

Boundary conditions for the various models are obtained from other MELCOR packages: fluid conditions are obtained from the Control Volume Hydrodynamics (CVH) package, fuel and debris temperatures are obtained from the Core (COR) and Cavity (CAV) packages, and structure surface temperatures are obtained from the Heat Structures (HS) package. The COR and CAV packages also provide information regarding bulk debris relocation, allowing the RN package to perform relocation of unreleased fission products in parallel. Likewise, advection of radionuclides between control volumes is done using CVH flows, and wash-off of radionuclides deposited on heat structures is determined from drainage of water films calculated by the HS package. The RN package determines decay heat power for current radionuclide inventories from the Decay Heat (DCH) package when requested by each of these packages.

This document describes in detail the various models incorporated in the RN package in MELCOR. Details on input to the RN package can be found in the RN Users' Guide.

Contents

1.	Introduction	6
2.	Detailed Models	9
2.1	General Framework.....	9
2.2	Initial Radionuclide Inventories.....	12
2.3	Release of Radionuclides.....	15
2.3.1	Core Release.....	15
2.3.2	Fuel-Cladding Gap.....	21
2.3.3	Cavity Release.....	21
2.4	Aerosol Dynamics	22
2.4.1	Aerosol Mass and Size Distributions.....	24
2.4.2	MAEROS Equations	26
2.4.3	Sources.....	42
2.4.4	Resuspension	43
2.5	Condensation/Evaporation	43
2.5.1	Water.....	43
2.5.2	Fission Product Vapors.....	48
2.6	Decay Heat Distribution.....	52
2.7	ESF Models.....	53
2.7.1	Pool Scrubbing.....	53
2.7.2	Filters	56
2.7.3	Sprays.....	57
2.8	Fission Product Chemistry	62
2.8.1	Class Reactions	62
2.8.2	Class Transfers.....	63
2.8.3	Example.....	64
2.9	Chemisorption on Surfaces.....	65
2.9.1	Implementation	65
2.9.2	Comparison to Exact Solution.....	66
2.9.3	Implementation Restrictions.....	68
2.10	Hygroscopic Aerosols.....	68
2.10.1	The Mason Equation for Particle Growth	69
2.10.2	Transition Regime Corrections to the Mason Equation.....	71
2.10.3	MELCOR Solution to the Mason Equation.....	72
2.10.4	User Suggestions Concerning Use of the Hygroscopic Model....	73
2.11	Iodine Pool Model.....	74
2.11.1	Introduction	74
2.11.2	Features of Iodine Pool Model.....	75
2.11.3	Criteria for Application of the Model.....	76
2.11.4	Detailed Description of the Model.....	76
2.11.5	Interaction with MELCOR	77

RN Package Reference Manual

2.11.6	Order of Calculation of Model	80
2.11.7	Submodels in the Iodine Pool Model	83
2.11.8	Data Base Supporting Model Validation	106
3.	Discussion and Development Plans.....	107
3.1	RCS Deposition.....	107
3.2	Chemical Reactions with Surfaces.....	107
3.3	Aqueous Chemistry.....	108
Appendix A:	RN Package Sensitivity Coefficients	110
Appendix B:	Agglomeration Kernels	125
Appendix C:	Aerosol Surface Area	129
Appendix D:	Pool Scrubbing Vent Exit Region Modeling.....	131
D.1	Globule Formation.....	131
D.2	Vent Exit Region Scrubbing Models	132
D.2.1	Steam Condensation	132
D.2.2	Inertial Impaction	133
D.2.3	Centrifugal, Diffusional and Gravitational Deposition.....	134
Appendix E:	Pool Scrubbing Swarm Rise Region Modeling.....	137
E.1	Bubble Characteristics.....	137
E.2	Bubble Heat and Mass Transfer.....	138
E.3	Particle Scrubbing in the Bubbles.....	140
Appendix F:	Iodine Vapor Scrubbing in the Swarm Rise Region.....	145
References	151

List of Figures

Figure 2.1	MAEROS Aerosol Model	23
Figure 2.2	Schematic Representation of the Iodine Transformations Considered	77
Figure 2.3	Interface between MELCOR and Iodine Pool Model	79
Figure 2.4	Calculation Flow of MELCOR Iodine Pool Model	81

List of Tables

Table 2.1	RN Class Compositions.....	10
Table 2.2	COR Material to RN Class Mapping	11
Table 2.3	RN Class to VANESA Species Mapping.....	11
Table 2.4	VANESA Species to RN Class Mapping.....	11

RN Package Reference Manual

Table 2.5 Representative Species in Iodine Pool Model	79
Table 2.6 Kinetic Equations for Water Radiolysis.....	92
Table 2.7 Reactions of Iodine	93
Table 2.8 Reactions of Ferrous and Ferric Ions	97
Table 2.9 Organic Reactions	98
Table 2.10 Variable Rates	99
Table 2.11 Acid Dissociation Constants	100
Table 2.12 Primary Products of Water Radiolysis	101

1. Introduction

Since MELCOR is intended as a tool for probabilistic risk assessment (PRA), it must account for the release and transport of radioactive fission products that upon release to the environment become the *source term*, which is one major product of the overall accident calculation in MELCOR. Source terms are then used to calculate consequences as the end product of the PRA. Such processes as thermal-hydraulics and core degradation are calculated in MELCOR to support calculation of the source term.

The RadioNuclide (RN) package in MELCOR calculates the release and transport behavior of fission product vapors and aerosols. Most of the models and concepts included in the RN package are discussed in detail in the fission product phenomena assessment report prepared at the beginning of MELCOR development [1]. Only a brief overview of the concepts and models is included in this section; Section 2 contains detailed descriptions of the models used in the RN package.

As a source term code, MELCOR is especially concerned with those fission products (and daughters) released during an accident, which are particularly important for determining consequences and risks. However, to model the transport of these important fission products properly, it is necessary to model the transport of other mass that affects the transport of radionuclide mass. For example, radiocesium will exist as CsOH, so the mass of the hydroxide must be modeled, and if the CsOH aerosol interacts with concrete or water aerosols, the transport and thus the mass of the latter must also be modeled. Accordingly, MELCOR treats the molecular forms of all important fission products and also models the transport of all nonradioactive masses (water and concrete or other structural aerosols) with which fission products may interact. Therefore, in this manual the term *radionuclide* is generally taken to mean all masses, both radioactive and nonradioactive masses, that affect fission product transport.

Rather than tracking all fission product isotopes, the masses of all the isotopes of an element are modeled as a sum; that is, the total element mass, not its individual isotopes, is modeled. Furthermore, elements are combined into material *classes*, groups of elements with similar chemical behavior. Fifteen material classes are typically used, thirteen containing fission products, plus water, and concrete oxides. Combination of classes to form new classes upon release, such as Cs + I to CsI, is permitted. The decay heat power per unit initial mass for each class is determined by the Decay Heat (DCH) package based on the class compositions.

Initial radionuclide inventories for each class are generally based on whole-core inventories calculated using the ORIGEN code [2, 3], and distributions may be specified for the fuel in the core, the fuel-cladding gap, any initial cavity debris, and the atmosphere and pool of any control volume. Until released as vapors or aerosols, fission products within the fuel are transported with the fuel as it relocates from core cell to core cell or is ejected to the reactor cavity. The decay heat power from radionuclides contained in a control volume,

both those that are gas borne and those deposited on heat structure surfaces or contained in water pools, can be apportioned among the atmosphere, surfaces, and pools according to specifications supplied by the user, thus allowing the different penetrating powers of α , β , and γ radiation to be modeled appropriately. Radiation is allocated to various surfaces in the control volume on the basis of area.

Release of radionuclides can occur from the fuel-cladding gap by exceeding a failure temperature criterion or losing intact geometry, from material in the core using the various CORSOR empirical release correlations [4,5] based on fuel temperatures, and during core-concrete interactions in the reactor cavity using the VANESA [6] release model. After release to a control volume, masses may exist as aerosols and/or vapors, depending on the vapor pressure of the radionuclide class and the volume temperature.

Aerosol dynamic processes and the condensation and evaporation of fission product vapors after release from fuel are considered within each MELCOR control volume. The aerosol dynamics models are based on MAEROS [7], a multisection, multicomponent aerosol dynamics code, but without calculation of condensation. Aerosols can deposit directly on surfaces such as heat structures and water pools, or can agglomerate and eventually fall out once they exceed the largest size specified by the user for the aerosol size distribution. Aerosols deposited on surfaces cannot currently be resuspended.

The condensation and evaporation of radionuclide vapors at the aerosol surfaces, pool surfaces, and heat structure surfaces are decoupled from MAEROS. These processes are evaluated by the rate equations from the TRAP-MELT2 code [8], which are based on the surface area, mass transfer coefficients, and the difference between the present surface concentration and the saturation surface concentration.

The steam condensation/evaporation is also decoupled from the MAEROS solution for agglomeration and deposition in order to reduce the stiffness of the differential equation set. The amount of steam condensed or aerosol water evaporated is calculated by thermodynamics routines called by the Control Volume Hydrodynamics (CVH) package.

Water droplets are transported as *fog* by the CVH package and treated as water-class aerosol by the RN package. (Water in pools or condensed on surfaces is not treated by the RN package.) Other radionuclide aerosols and vapors are transported between control volumes by bulk fluid flow of the atmosphere and the pool, assuming zero slip between the radionuclides and the host medium (steam, water, etc.). In addition, in the absence of bulk flow, aerosols may move by Brownian motion or by gravitational settling through openings between control volumes.

The difference between CVH fog and RN water-class masses in a control volume at the end of the CVH advancement represents net condensation of water onto or evaporation from the aerosols in that volume. The net change in water mass is imposed on the water-class inventory in the RN package, which then uses the Mason equation [9] to distribute the mass change over the aerosol size distribution in the control volume.

RN Package Reference Manual

Models are available for the removal of radionuclides by pool scrubbing, filter trapping, and containment spray scrubbing. The pool scrubbing model is based on the SPARC code [10], and treats both spherical and elliptical bubbles. The model includes condensation at the pool entrance, Brownian diffusion, gravitational setting, inertial impaction, and evaporative forces for the rising bubble. Currently, only aerosols are removed by pool scrubbing in the RN package. Water condensation and evaporation are calculated within the CVH package using its own implementation of SPARC modeling (see the CVH Reference Manual). The filter model can remove aerosols and fission product vapors with a specified maximum mass loading. The containment spray model is based on the model in HECTR 1.5 [11] and removes both vapors and aerosols from the atmosphere.

Chemistry effects can be simulated in MELCOR through the *class reaction* and *class transfer* models, which are controlled entirely by user-specified parameters. The class reaction process uses a first-order reaction equation to simulate reversible chemical reactions. The class transfer process, which can instantly change the material class or location of a radionuclide mass, can be used to simulate fast, irreversible chemical reactions. With these two processes, phenomena including adsorption, chemisorption and other important chemical reactions can be simulated. Only fission product vapors are currently treated with these mechanisms. In addition, chemisorption of radionuclides on surfaces can be simulated with the chemisorption model.

Most intravolume processes involving radionuclides are calculated first in the RN package, including fission product release, aerosol agglomeration and deposition, fission product condensation and evaporation, distribution of decay heat, and chemical interactions. The effects of these processes are included in the hydrodynamic transport and thermodynamic calculations performed in the CVH package, executed subsequently.

The transport of fission products is inferred from the transport of hydrodynamic materials, but the CVH package may subcycle during a MELCOR timestep. Since radionuclide advection must also abide by the Courant limit, the transport calculations are performed by RN package utility routines called from within the CVH subcycle loop. Part of this transport process includes removal of fission product aerosols and vapors, for example, by filters.

After CVH has advanced through the full MELCOR system timestep, the additional intervolumetric process of pool scrubbing is calculated. While water condensation/evaporation is an intravolumetric process, it also is calculated after the CVH package thermodynamics calculations have been performed so that the mass of water condensed in a control volume during the timestep is known.

2. Detailed Models

2.1 General Framework

The RN package operates on the principle of material classes, which are groups of elements that have similar chemical properties. The number of classes is specified on the RN1001 input record, with a default of 15 classes. Classes are generally referred to by their class name or representative element. Combination of masses in these classes upon release to form compounds in other classes, such as Cs + I to CsI, is permitted subject to stoichiometric constraints (e.g., excess Cs is retained in the Cs class). For the RN package, the classes must be in numerical order without any gaps. A maximum of 30 classes can presently be employed.

Each class is described by the following set of properties for use in various models:

1	release rates in core	(see Section 2.3)
2	molecular weights	(see Section 2.3)
3	vapor pressure	(see Section 2.5)
4	vapor diffusivity	(see Section 2.5)
5	decay heat power	(see DCH Package Users' Guide)

Two molecular weight values are used for each class, the *elemental* molecular weight (i.e., the element's atomic weight) and the *compound* molecular weight, which are specified in sensitivity coefficient array 7120 (see Appendix A). The elemental molecular weight is used to determine the number of moles of *radioactive* material that are released and available for combination with other RN classes. The compound molecular weight is used to increase the released mass due to combination upon release with *nonradioactive* materials if that is expected to occur (e.g., Cs with H₂O to form CsOH). *Total* class masses after release therefore include both radioactive and nonradioactive masses. In addition, nonradioactive masses from bulk materials in the Core or Cavity package (e.g., cladding Zircaloy, structural steel, control poison, or concrete) may be released as vapors or aerosols and added to the total class masses but not to the radioactive masses of the class to which the materials are assigned.

Some models in the RN package use groupings of elements different from the groupings defined in Table 2.1. Transfers of masses between various models must therefore use *mapping* strategies.

For the transfer of bulk, nonradioactive, Core package structural masses released by the CORSOR models to the RN classes (see Section 2.3), the default mapping defined in Table 2.2 is employed. This mapping may be changed with input records RNCRCLXX, but this practice is discouraged. Note from Table 2.2 that B₄C control poison in BWRs is

RN Package Reference Manual

mapped totally into the boron class, whereas Ag-In-Cd control poison in PWRs is split between the Cd and Sn classes using the percentages shown.

The VANESA model for radionuclide releases from debris in the cavity (see Section 2.3) recognizes 25 different species groups (for most, several different compounds of one element), and mapping must be used both to transfer RN class masses in the debris (as initially specified and as transferred from the COR and/or Fuel Dispersal Interactions [FDI] packages) to the VANESA groups and also to transfer them back again into the RN classes as VANESA calculates releases. The default mappings for to-VANESA and from-VANESA transfers are defined in Table 2.3 and Table 2.4, respectively. These mappings may be changed with input records RNCLVNXX and RNVNCLXX.

Table 2.1 RN Class Compositions

Class Name	Representative	Member Elements
1. Noble Gases	Xe	He, Ne, Ar, Kr, Xe, Rn, H, N
2. Alkali Metals	Cs	Li, Na, K, Rb, Cs, Fr, Cu
3. Alkaline Earths	Ba	Be, Mg, Ca, Sr, Ba, Ra, Es, Fm
4. Halogens	I	F, Cl, Br, I, At
5. Chalcogens	Te	O, S, Se, Te, Po
6. Platinoids	Ru	Ru, Rh, Pd, Re, Os, Ir, Pt, Au, Ni
7. Early Transition Elements	Mo	V, Cr, Fe, Co, Mn, Nb, Mo, Tc, Ta, W
8. Tetravalent	Ce	Ti, Zr, Hf, Ce, Th, Pa, Np, Pu, C
9. Trivalent	La	Al, Sc, Y, La, Ac, Pr, Nd, Pm, Sm, Eu, Gd, Tb, Dy, Ho, Er, Tm, Yb, Lu, Am, Cm, Bk, Cf
10. Uranium	U	U
11. More Volatile Main Group	Cd	Cd, Hg, Zn, As, Sb, Pb, Tl, Bi
12. Less Volatile Main Group	Sn	Ga, Ge, In, Sn, Ag
13. Boron	B	B, Si, P
14. Water	H ₂ O	H ₂ O
15. Concrete	--	--

In addition to the 25 VANESA groups, two additional groups can be transferred to VANESA but are changed before VANESA uses them. They are I (VANESA group 26), which is combined automatically with Cs, and Xe (VANESA group 27), which VANESA releases immediately. VANESA assumes that Cs is in excess so that no elemental I remains as debris is added to the cavity. Also, aerosol products from concrete ablation (VANESA groups 12 through 16) are automatically transferred to the RN concrete class, and bulk gases (VANESA group 1) are transferred directly to the CVH package. The user should not specify mapping values for any of these VANESA groups.

Table 2.2 COR Material to RN Class Mapping

COR Material		RN Class (Rep. Element)		
1	UO2	10	U	
2	Zr	8	Ce	
3	ZrO2	8	Ce	
4	Steel	7	Mo	
5	Steel Oxide	7	Mo	
6	Control Rod Poison	13	B	100% BWR / 0% PWR
		11	Cd	0% BWR / 5% PWR
		12	Sn	0% BWR / 95% PWR

Table 2.3 RN Class to VANESA Species Mapping

RN Class		VANESA Species	
1	Xe	27	Xe (released instantaneously)
2	Cs	19	Cs
3	Ba	20	Ba
4	I	26	I (immediately forms CsI)
5	Te	9	Te
6	Ru	6	Ru
7	Mo	5	Mo
8	Ce	23	Ce
9	La	22	La
10	U	17	U
11	Cd	8	Sb
12	Sn	7	Sn
13	B	0	(RN class not present in fuel)
14	H2O	0	(RN class not present in fuel)
15	Concrete	0	(RN class not present in fuel)

Warning: If a class is redefined from the default values, or if a new class is added, all of the properties, including mappings, should be evaluated and possibly redefined through the RN sensitivity coefficients. Default values for these properties are defined based on the elements in each class. Whether default values are appropriate when classes are modified must be determined by the user. Note that the DCH package might also have to be redefined in a consistent manner.

Table 2.4 VANESA Species to RN Class Mapping

VANESA Species		RN Class	
1	bulk gases (from CORCON)	(released by CAV pkg to CVH)	
2	Fe	7	Mo

RN Package Reference Manual

VANESA Species		RN Class	
3	Cr	7	Mo
4	Ni	6	Ru
5	Mo	7	Mo
6	Ru	6	Ru
7	Sn	12	Sn
8	Sb	11	Cd
9	Te	5	Te
10	Ag	12	Sn
11	Mn	7	Mo
12	Ca (from concrete ablation)	15	Concrete
13	Al (from concrete ablation)	15	Concrete
14	Na (from concrete ablation)	15	Concrete
15	K (from concrete ablation)	15	Concrete
16	Si (from concrete ablation)	15	Concrete
17	U	10	U
18	Zr	8	Ce
19	Cs	2	Cs
20	Ba	3	Ba
21	Sr	3	Ba
22	La	9	La
23	Ce	8	Ce
24	Nb	7	Mo
25	Csl	2	Cs and 4 I
26	I	(combined with Cs by VANESA)	
27	Xe	(released by VANESA)	

2.2 Initial Radionuclide Inventories

Initial inventories and distributions of radionuclides must be specified for the core, for the cavity, and for control volume pools and atmospheres. (Inventories for some locations may be zero initially.) Masses can be distributed among core cells according to radial and axial decay heat power profiles in the core. In addition, a fraction of the radionuclides in a core cell can be designated as residing in the fuel-cladding gap.

Total radioactive class masses are normally determined by the DCH package from the operating power of the reactor and the mass of each element in the class per unit of operating power (see the DCH Package Reference Manual and Users' Guide). RN package input generally defines only the initial distribution of these masses in the core and cavity through reference values and multipliers specified on the RNFPNijjXX input records. However, options are provided to use these records to specify the class masses directly. These options are useful for analysis of experiments.

The total mass inventories for all RN classes in a particular core cell or in a cavity are normally calculated from user-specified multipliers r_1 and r_2 as

$$M_x = r_1 r_2 M_{x,ref} \quad (2.1)$$

where $M_{x,ref}$ is a reference value for class x that may be taken as the total class mass defined by the DCH package or as the inventory in some other core cell or cavity location, depending on the option chosen. For core cells, r_1 and r_2 typically represent axial and radial multipliers to specify the decay heat power profile in the core, while for cavities they are arbitrary. If the DCH package option is chosen, however, the mass of the uranium class (default class 10) is calculated by decrementing the total uranium mass in the Core package, $M_{U,COR}$ by the sum of the masses in the remaining classes, i.e.,

$$M_{U,RN} = M_{U,COR} - \sum_{i \neq U} M_i \text{ (Uranium class only)} \quad (2.2)$$

Optionally, as specified on the RNFPNijjXX records, the mass for a specified class in a particular core cell or cavity location may be input directly as

$$M_x = r_1 r_2 \quad (2.3)$$

where r_1 is typically chosen as the total mass, with r_2 defined as the fraction of that mass in the core cell or cavity location. The various options are additive and may be combined as convenient. Note that masses can also be reduced if a negative multiplier is used.

The masses given by Equations (2.1) through (2.3) determine the total radioactive mass of radionuclides in a particular core cell, including the fuel-cladding gap. The fraction of radioactive mass that resides in the gap is determined by the parameter r_1 input on the RNGAPijjXX input record series (different from r_1 input on RNFPNijjXX). Depending on the input option chosen, the gap fraction F_x may be specified directly for each class as

$$F_x = r_1 \quad (2.4)$$

or it may be calculated as a proportion of the gap fraction $F_{x,ref}$ at some other location,

$$F_x = r_1 F_{x,ref} \quad (2.5)$$

For a core cell, the radioactive masses residing in the fuel and gap, $M_{x,fuel}$ and $M_{x,gap,R}$, respectively, are thus given by

RN Package Reference Manual

$$M_{x,fuel} = (1 - F_x) M_x \quad (2.6)$$

$$M_{x,gap,R} = F_x M_x \quad (2.7)$$

The total masses residing in the gap must be calculated to account for the addition of nonradioactive material from presumed chemical reactions following release from the fuel. (See the discussion of total vs. radioactive masses in Section 2.1.) If the gap fraction has been specified directly from Equation (2.4), the total gap mass $M_{x,gap,T}$ is given by

$$M_{x,gap,T} = r_2 M_{x,gap,R} \quad (2.8)$$

where r_2 is the ratio of total mass to radioactive mass (usually the ratio of compound to elemental molecular weights, matching the values in sensitivity coefficient array 7120; see Appendix A), whereas if the gap fraction has been specified as a proportion r_1 of the gap fraction at some other location with Equation (2.6), the total gap mass is that same fraction of the total gap mass $M_{x,gap,T,ref}$ at the other location,

$$M_{x,gap,T} = r_1 M_{x,gap,T,ref} \quad (2.9)$$

in which case no value is needed for r_2 since it is already reflected in $M_{x,gap,T,ref}$ (any value input for r_2 is ignored).

The distribution of radionuclide masses between fuel and gap in a core cell will change with time due to release and the relocation of fuel. When fuel is relocated by the COR package, the radionuclides still residing in the fuel are transported with it. Relocation of the gap radionuclide mass is not necessary since cladding failure and gap release will always occur before fuel relocates (see Section 2.3.2).

In addition to the radioactive masses initially residing in the fuel or fuel-cladding gap, nonradioactive bulk masses in other packages, such as Zircaloy fuel rod cladding, may be released as vapors or aerosols by the RN package release models. Initial inventories for these bulk masses are already available in the appropriate package database and no additional input is needed for the RN package. Release of core or cavity masses by the RN package does not change the mass values in the other packages. For example, the mass of Zircaloy in the COR package is not modified by release of Zircaloy aerosols in the RN package. The errors introduced by this assumption should be very small since the fractions of core and cavity materials that are released as vapors and aerosols are very small. Nevertheless, the user should be aware that mass is not explicitly conserved in this modeling.

The user may also directly specify the initial radionuclide aerosol and/or vapor inventory for any class in any control volume by using the RNAGXXX, RNALXXX, RNVGXXX, and RNVLXXX input record series.

2.3 Release of Radionuclides

Release of radionuclides can occur from the core fuel (with nonradioactive releases from other core structures), from the fuel-cladding gap, and from material in the cavity. At present, no material can be released from the reactions treated in the FDI package. The release models used in each of these areas are discussed below.

2.3.1 Core Release

Radioactive and nonradioactive material may be released from the core. As described in Sections 2.1 and 2.2, the radionuclides residing in the COR package fuel are assumed to be in elemental form and therefore to have only radioactive mass (no associated molecular mass). Upon release from fuel, the total class masses are converted to compound form with a corresponding increase in mass from the added nonradioactive material (e.g., the hydroxide mass in CsOH). By default the release models are used to calculate the release of radioactive radionuclides from core fuel material (i.e. UO₂) only, which exists in the intact fuel component, in refrozen fuel material on other components and in particulate debris.

In order to apply the release models to core materials other than fuel, such as the fuel rod cladding, the user must change the default values of the core material release multipliers contained in sensitivity coefficient array 7100. For these other core materials, the mapping scheme described in Section 2.1 (with defaults in Table 2.2) determines the apportioning of the core masses among the RN classes, and the entire masses are considered nonradioactive. Hence, by changing the release multiplier for Zr from 0.0 to 0.5, for example, the user will obtain half the fractional release rates calculated by the release correlations for Zr in the cladding, canisters and particulate debris. However, because the mass of structural Zr in the cladding component is enormous compared to the mass of Zr class fission products in the fuel component, the actual release rate (fractional rate times the available mass) from the cladding may be quite large. Because the core release models were developed for fuel releases, their use to calculate the release of structural materials in other components is questionable.

Before cladding failure has occurred, radionuclides released from the fuel in the core are transferred to the gap inventory and are released to the surrounding atmosphere of control volume only upon cladding failure. (However, they are reported by RN output as "released.") After cladding failure, radionuclides released from the core are transferred to the atmosphere of control volumes as specified in the Core package input, which defines channel and bypass control volumes for each core cell. These volumes are used by the RN package as follows:

RN Package Reference Manual

Core Component	RN Release Volume
Intact:	
Fuel	Channel
Cladding	Channel
Control Rods	Bypass
Canisters	Split Equally Between Channel and Bypass
Conglomerate Debris:	
Refrozen on Cladding	Channel
Refrozen on Control Rods	Bypass
Refrozen on Canisters	Channel
Particulate Debris:	
All	Channel

In addition to releases in the core calculated by the RN package, the reaction modeled in the Core package of B_4C in control rods with steam can release B_2O_3 to the RN package. The class specified on the RN1001 input record for B_2O_3 receives this mass in the bypass control volume defined for that core cell.

Three options are currently available for the release of radionuclides from the core fuel component; the CORSOR, CORSOR-M [4] or CORSOR-Booth [5] model may be specified on Input Record RNFP000. The CORSOR-BOOTH model contains low and high burn-up options. In addition, the CORSOR and CORSOR-M release rates can be modified to be a function of the component surface-to-volume ratio as compared to a base value, derived from the experimental data on which CORSOR is based. The surface areas, volumes, and temperatures of the components used in the calculation are obtained from the COR package database. Because none of these radionuclide release models can be considered truly general or universally applicable, it is recommended that concerned users refer to the release model references [4, 5] for a more complete description of modeling assumptions and limitations.

The reduction in release rate of the tellurium class by the presence of unoxidized zirconium can be modeled if desired. The parameters affecting this option are controlled by sensitivity coefficient array 7105 for CORSOR and CORSOR-M and within array 7107 for CORSOR-Booth (see Appendix A). The release rate of Te is reduced by a release rate multiplier (with a default value of $1/40 = 0.025$) until the mass of unoxidized intact metal cladding falls below a cut-off fraction (default value of 0.7) of the total mass of intact cladding (including the oxide mass). The default values are based on discussion in Reference [12].

Note that for each core component, the same correlation is used to calculate the release rate for a given class using the individual temperature of that component. That is, the calculation of release of radionuclides from fuel, cladding, canisters, control rods, and particulate debris differs only in the temperature used. Separate correlations for these

components are not employed since their form is not compatible with the MELCOR structure.

2.3.1.1 *CORSOR*

The original CORSOR model correlates the fractional release rate in exponential form,

$$\dot{f} = A \exp(BT) \quad \text{for } T \geq T_i \quad (2.10)$$

where \dot{f} is the release rate (fraction per minute), A and B are empirical coefficients based on experimental data, and T is the core cell component temperature in degrees Kelvin. Different values for A and B are specified for three separate temperature ranges. The lower temperature limit T_i for each temperature range and the A and B values for that range are defined for each class in sensitivity coefficient array 7101 (see Appendix A). If the cell temperature is below the lowest temperature limit specified, no release is calculated.

2.3.1.2 *CORSOR-M*

The CORSOR-M model correlates the same release data used for the CORSOR model using an Arrhenius form,

$$\dot{f} = k_o \exp(-Q/RT) \quad (2.11)$$

The values of k_o , Q , and T are in units of min^{-1} , kcal/mole, and K , respectively. The value of R is 1.987×10^{-3} in $(\text{kcal/mole})K^{-1}$. The values of k_o and Q for each class are implemented in sensitivity coefficient array 7102 (see Appendix A).

2.3.1.3 *CORSOR-Booth*

The CORSOR-Booth model considers mass transport limitations to radionuclide releases and uses the Booth model for diffusion with empirical diffusion coefficients for cesium releases. Release fractions for other classes are calculated relative to that for cesium. The classical or effective diffusion coefficient for cesium in the fuel matrix is given by

$$D = D_o \exp(-Q/RT) \quad (2.12)$$

RN Package Reference Manual

where R is the universal gas constant, T is the temperature, Q is the activation energy, and the pre-exponential factor D_0 is a function of the fuel burn-up. For fuel with burn-up in excess of 30,000 MWD/MTU the model uses a value for D_0 five times larger than the value it uses for fuels with lower burn-up. The two default values for D_0 , the transition burn-up value, and the activation energy Q , based on experimental data for the release of fission gases from fuel test samples [13], are all given in sensitivity coefficient array 7106 (see Appendix A).

The cesium release fraction at time t is calculated from an approximate solution of Fick's law for fuel grains of spherical geometry [14],

$$f = 6 \sqrt{\frac{D' t}{\pi}} - 3 D' t \quad \text{for } D' t < 1/\pi^2 \quad (2.13)$$

$$f = 1 - \frac{6}{\pi^2} \exp(-\pi^2 D' t) \quad \text{for } D' t > 1/\pi^2 \quad (2.14)$$

where

$$D' t = Dt/a^2 \quad (\text{dimensionless})$$

$$a = \text{equivalent sphere radius for the fuel grain}$$

The release rate of Cs during a time interval t to $t + \Delta t$ from the fuel grain is calculated as

$$\text{Release rate}_{\text{Cs}} = \frac{[f(\sum D' \Delta t)_{t+\Delta t} - f(\sum D' \Delta t)_t] V \rho}{F \Delta t} \quad (2.15)$$

where ρ is the molar density in the fuel, V is the fuel volume, F is the fraction of the Cs inventory remaining in the fuel grain, and the summations are done over the timesteps up to time $(t + \Delta t)$ and t , respectively.

The release rate formulation in the CORSOR-Booth model is also limited by mass transfer through the gas-phase. The gas-phase mass transport release rate from the fuel rod for species k , \dot{m}_k , is calculated using an analogy from heat transfer as

$$\frac{1}{\dot{m}_k} = \frac{D_{\text{fuel}} RT}{A_{\text{fuel}} Nu D_{k,\text{gas}} P_{k,\text{eq}}} \quad (2.16)$$

where

D_{fuel} = diameter of fuel pellet

A_{fuel} = fuel rod flow contact area

$D_{k,gas}$ = diffusivity of class k in the gas mixture

Nu = Nusselt number

$P_{k,eq}$ = equilibrium vapor pressure of class k at temperature T

The effective release rate for Cs given by Equation (2.16) is a combination of the rates given by diffusion and by gas-phase mass transport. Therefore, the contribution from diffusion only is taken as

$$DIFF_{Cs} = \left[\frac{1}{\text{Release rate}_{Cs}} - \frac{1}{\dot{m}_{Cs}} \right]^{-1} \quad (2.17)$$

The diffusion release rate for species other than cesium is given by multiplying the cesium release rate by an appropriate scaling factor S_k for each RN class k :

$$DIFF_k = DIFF_{Cs} S_k \quad (2.18)$$

Nominal values for S_k are given in sensitivity coefficient array 7103. For certain conditions of cladding oxidation and temperature, the scaling factors must be modified for some classes. When the oxide mass fraction exceeds a critical value F_{k1} and the temperature exceeds a critical value T_{k1} , the class scaling factor is given by

$$S_k = S_{k1} \exp(C_k T) \quad (2.19)$$

where T is not allowed to exceed a maximum value T_{max} . When the oxide mass fraction is below a minimum value F_{k2} , the class scaling factor is given by

$$S_k = S_{k2} \quad (2.20)$$

Values for F_{k1} , T_{k1} , S_{k1} , C_k , T_{max} , F_{k2} , and S_{k2} are all contained within sensitivity coefficient array 7107.

The combined mass transport and diffusion release rate $\dot{m}_{tot,k}$ for class k is then

$$\dot{m}_{tot,k} = \frac{1}{DIFF_k^{-1} + \dot{m}_k^{-1}} \quad (2.21)$$

The fractional release rate for the inventory of class k is calculated as

$$\dot{f}_k \text{ (fraction/s)} = \frac{\dot{m}_{tot,k}}{\rho V} \left[F - \frac{P_{k,bulk}}{P_{k,eq}} \right] \quad (2.22)$$

2.3.1.4 Surface-to-Volume Ratio

In the CORSOR and CORSOR-M release expressions, the effect on the release rate of the surface-to-volume ratio of the material from which release occurs is not treated. An option has been added to include the effect of this ratio as follows:

$$\dot{f} = \dot{f}_{CORSOR(-M)} (S/V)_{structure} / (S/V)_{base} \quad (2.23)$$

where the $(S/V)_{base}$ value has been derived from the original CORSOR data with a value of 422.5 m^{-1} that is stored in sensitivity coefficient array 7104 (see Appendix A). Values for $(S/V)_{structure}$ are calculated from component surfaces and volumes in the Core package (see Section 3 of the COR Package Reference Manual) and thus reflect the effects of core degradation on the surface-to-volume ratios of core components.

2.3.1.5 Class Combination at Release

The release model also can provide for the combination of different donor classes into a new class based on the elemental molecular weights. An example is the combination upon release of Cs and I atoms to form CsI molecules, which is modeled by moving stoichiometric amounts of Cs and I mass from the Cs and I classes into a new CsI class. The number of moles of each class that combine is defined by RNCLSNNXX input data. This combination occurs instantaneously upon release and is only limited by the availability of the released mass during that timestep. If there is an excess of any donor class during the timestep, that excess material stays in the original class. Chemical reactions that take place once release has been completed can be approximated using the models discussed in Section 2.8.

Note: The class combination model is only used for release from the fuel in the core and not for tabular or control function input sources defined using the RNASXXX or RNVSXXX records.

2.3.2 Fuel-Cladding Gap

Release of the radionuclides in the fuel-cladding gap (initial inventory plus masses from fuel release) occurs on cladding failure. Cladding failure is assumed to occur if either a temperature criterion is exceeded or if the intact cladding geometry has been lost due to candling or oxidation. It is assumed that the gaps in each radial ring can communicate axially between core cells, so when cladding in one axial level in a radial ring fails, the gap inventory for that entire ring is released. The cladding failure temperature for each core cell is specified on the RNgapij00 input record, with a default value of 1173 K (900° C) [15]. The control volume that receives the gap release is the channel control volume associated with the core cell where failure occurs, as defined by the CORijj01 input records (see the COR Package Users' Guide).

2.3.3 Cavity Release

For release of radionuclides from the cavity due to core-concrete interactions, the VANESA model [6] has been implemented in MELCOR and is coupled to CORCON [16] during every timestep. The control volume for cavity releases is specified in the Cavity package input. If a water pool is present, pool scrubbing calculations are performed to apportion the released mass between the pool and the atmosphere.

A number of changes have been made to the stand-alone VANESA program to allow it to function within the MELCOR framework. The major changes are:

- (1) The concrete composition used in VANESA is converted from CORCON input using the following mapping, rather than input independently:

CORCON Mass Fraction	VANESA Mass Fraction
CaO + MgO	CaO
Al ₂ O ₃	Al ₂ O ₃
Na ₂ O	Na ₂ O
K ₂ O	K ₂ O
SiO ₂	SiO ₂
Fe ₂ O ₃ (converted to FeO) + MnO	FeO
Ti ₂ O	Ti ₂ O
Cr ₂ O ₃	Cr ₂ O ₃
Rebar	Fe

- (2) To ensure conservation of mass in the calculations, the rate of addition of concrete decomposition products (gases and condensed-phase oxides) is now derived from CORCON results by forward differences, rather than the central difference scheme originally in VANESA.

RN Package Reference Manual

- (3) Core debris masses (and associated radionuclides) may be added as a function of time throughout the transient.
- (4) Both radioactive and total masses are tracked. The fraction of the radioactive mass released is assumed to be the same as the fraction of total mass released.
- (5) The radioactive inventory is used (by default) to calculate the decay heat in the Cavity package. It is partitioned between the metallic and oxidic phases according to the assumed chemical state of the VANESA class. This partitioning accounts for the difference between elemental mass (e.g., Ba) and compound mass (e.g., BaO) and the mapping of released structural materials (e.g., Fe) into the nonradioactive portions of RN inventories.
- (6) Pool scrubbing calculations are done by the RN package rather than the model in stand-alone VANESA.

2.4 Aerosol Dynamics

This section describes the models used in the RN package to predict the behavior of aerosols during an accident in a LWR. Fission products may be aerosolized as they are released from fuel early in a LWR accident and later expelled from the reactor coolant system. Other events and processes that occur late in the accident, such as core-concrete interactions, pool boiling, direct containment heating, and deflagrations, may also generate (or resuspend) aerosols. High structural temperatures may also result in aerosolization of nonradioactive materials.

The principal aerosol quantities of interest are the mass and composition of aerosol particles and their distribution throughout the reactor coolant system and containment. The calculation of aerosol agglomeration and deposition processes is based on the MAEROS [7] computer code, but without direct inclusion of condensation or evaporation within the MAEROS solution framework. Vapor condensation on and evaporation from aerosol particles are handled separately to reduce the stiffness of the differential equation set and to ensure consistency with the calculation of these processes by other models and packages, as described later.

MAEROS is a multisectional, multicomponent aerosol dynamics code that evaluates the size distribution of each type of aerosol mass, or *component*, as a function of time. This size distribution is described by the mass in each size bin, or *section*. Each section may have a different chemical composition as described by the masses of various components for that section. In other words, a section is an aerosol size group and a component is a particular type of aerosol material. Since MELCOR operates on a radionuclide class structure, as discussed earlier, a mapping between RN classes and MAEROS aerosol components must be specified by the user.

Figure 2.1 illustrates the sectional representation of a two-component aerosol with 5 sections. The mass concentrations of component 1 in the five sections are given by the stair-stepped line that bounds the lower crosshatched region. The total aerosol mass concentrations in the five sections are given by the uppermost stair-stepped line. Therefore, the mass concentrations of component 2 in the five sections are given by the upper shaded region.

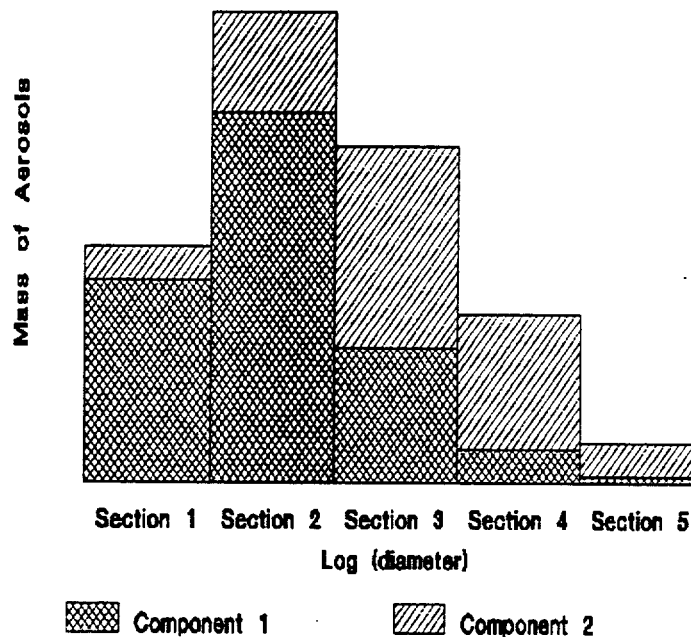


Figure 2.1 MAEROS Aerosol Model

One powerful feature of MELCOR is that water condensation on and evaporation from aerosols is modeled in a manner consistent with the thermal/hydraulic calculations in the CVH and HS packages. That is, the latent heat associated with the coolant mass transfer between the atmosphere and aerosol surfaces is incorporated in the total internal energy transfer to and from the atmosphere. In addition, condensation and evaporation of fission product vapors on aerosols is calculated in parallel with condensation on and evaporation from heat structure surfaces, but without consideration of the latent heat of condensation of the vapor, since it is negligible compared to the energy of the atmosphere and the heat structure.

The MELCOR calculation of changes in aerosol distribution and location within a plant considers the following general processes:

- (1) aerosol phenomenological sources from other packages, such as release from fuel rods or during core-concrete interactions, and/or arbitrary user-specified sources;

RN Package Reference Manual

- (2) condensation and evaporation of water and fission products to and from aerosol particles;
- (3) particle agglomeration (or coagulation), whereby two particles collide and form one larger particle;
- (4) particle deposition onto surfaces or settling through flow paths into lower control volumes;
- (5) advection of aerosols between control volumes by bulk fluid flows; and
- (6) removal of aerosol particles by engineered safety features (ESFs), such as filter trapping, pool scrubbing, and spray washout.

The RN package includes models to simulate each of these processes, but only user-defined aerosol sources and agglomeration and deposition processes are formally coupled in the MAEROS integrated solution framework. Aerosol sources from other phenomenological packages in MELCOR and condensation on and evaporation from aerosols are decoupled and treated outside the MAEROS solution. This section describes principally the details of the implementation of MAEROS within MELCOR. Section 2.4.1 describes in more detail how the component/class mapping scheme works and how the particle size distribution is represented in MELCOR. The general MAEROS equations and the specific models for aerosol agglomeration and deposition are described in Section 2.4.2. Section 2.4.3 provides information on how various aerosol sources are treated, and Section 2.4.4 discusses the MELCOR aerosol resuspension model (not yet implemented).

Condensation and evaporation processes for both aerosols and heat structure surfaces are described later in Section 2.5, and Section 2.6 describes the modeling for advection of aerosols between control volumes. Section 2.7 describes the removal of aerosols by ESFs.

2.4.1 Aerosol Mass and Size Distributions

In MELCOR, one or more RN classes can be assigned to a component, as specified on the RNCCXXX input records, but a particular class cannot be assigned to more than one component. For each control volume, the fractions within a particular component of each class assigned to that component are determined before the aerosol dynamics calculation is performed to determine the new size distribution. These fractions necessarily sum to unity. After the aerosol dynamics calculation, the masses for each aerosol size, the deposited masses, and the fallout masses for each class are determined by multiplying the appropriate component mass values by the previously calculated class mass fraction. In effect, all classes assigned to the same component are assumed to have the same size distribution.

The aerosol particle size distribution is discretized into particle size bins called *sections*. The distribution of aerosol mass within a section is treated as constant with respect to the logarithm of particle mass. The user may input any arbitrary initial aerosol size distribution for any fission product class by specifying the mass in each size section at the initial time (see the RNAGXXX and RNALXXX input records). The initial aerosol water mass (fog) is determined from the CVH package input data only and is put in the smallest aerosol section; an error message is generated if an attempt is made to initialize water aerosol mass through RN input.

The number of sections and components to be used in the aerosol calculations, as well as the minimum and maximum aerosol diameters, are specified by the user (see input records RN1001 and RN1100). Individual section boundaries are calculated from these values so that the ratio of the upper and lower bound diameter of each section is the same. A check is also made that the ratio of the upper to lower mass boundary for each section is greater than or equal to two to assure that the calculations will conform to the assumptions made in the derivation of the MAEROS equations. If this constraint is not met, an error message is generated and the calculation terminates.

Although the aerosol component distributions from the MAEROS calculation are not stored permanently, the class distributions are used to calculate the mass median diameter and geometric standard deviation for the wet, dry and component distributions in each control volume for editing. The wet distribution is the sum over all classes including water; the dry distribution, which is commonly determined experimentally, is the sum over all classes excluding water; and the component distribution is the sum over all classes assigned to the particular component. The mass median diameter is defined to be the diameter above and below which half the total mass (wet, dry or component mass) in the distribution occurs,

$$0.5 \times \int_0^{\infty} f_m(D) dD = \int_0^{D'} f_m(D) dD \quad (2.24)$$

where D' is the mass median diameter and $f_m(D) dD$ is the mass in the distribution between diameter D and $D + dD$. The geometric standard deviation, σ_G , is defined as

$$(\ln \sigma_G)^2 = \frac{\int_0^{\infty} \ln^2(D/\bar{D}) f_m(D) dD}{\int_0^{\infty} f_m(D) dD} \quad (2.25)$$

where \bar{D} is the logarithmic mass mean diameter defined by

$$\ln(\bar{D}) = \frac{\int_0^{\infty} \ln(D) f_m(D) dD}{\int_0^{\infty} f_m(D) dD} \quad (2.26)$$

In MELCOR, any aerosol particles that are calculated to grow larger (by agglomeration or condensation) than the maximum size section, are assumed to *fall out* onto either floor-type heat structures or into adjacent lower control volumes. Aerosols that fall out into a lower control volume are put in the largest size section of the aerosol distribution in that control volume and thus should quickly deposit or fall out onto floor structures. This is described in more detail in Section 2.4.2.2.

2.4.2 MAEROS Equations

The aerosol agglomeration and deposition models from MAEROS are used to calculate the changing aerosol size distributions as these processes affect the aerosol in each control volume at each timestep. Particle agglomeration, deposition onto heat structure surfaces, fallout onto floors or into lower control volumes, and the effects of user-defined aerosol sources are all integrated in the MAEROS calculation.

The modeling of the aerosol size distribution is governed by a complex integro-differential equation. MAEROS was developed as a method of discretizing this equation into a form that can be solved numerically. In their method (and using their notation), the full range of aerosol masses is divided into m contiguous arbitrarily sized sections, and Q_ℓ is defined as the total mass of aerosol per unit volume of fluid in section ℓ at time t . Thus,

$$Q_\ell(t) = \sum_{k=1}^s Q_{\ell,k}(t) \quad (2.27)$$

where $Q_{\ell,k}(t)$ is the mass of component k in section ℓ , and s is the total number of components. The upper bound of section $\ell - 1$ is equal to the lower bound of section ℓ for $\ell = 2, 3, \dots, m$. These equations can be written

$$\begin{aligned}
 \frac{dQ_{\ell,k}}{dt} = & \frac{1}{2} \sum_{j=1}^{\ell-1} \sum_{i=1}^{\ell-1} \left[{}^{1a}\bar{\beta}_{i,j,\ell} Q_{j,k} Q_i + {}^{1b}\bar{\beta}_{i,j,\ell} Q_{i,k} Q_j \right] \\
 & - \sum_{i=1}^{\ell-1} \left[{}^{2a}\bar{\beta}_{i,\ell} Q_i Q_{\ell,k} - {}^{2b}\bar{\beta}_{i,\ell} Q_{\ell} Q_{i,k} \right] \\
 & - \frac{1}{2} {}^3\bar{\beta}_{\ell,\ell} Q_{\ell} Q_{\ell,k} - Q_{\ell,k} \sum_{i=\ell+1}^m {}^4\bar{\beta}_{i,\ell} Q_i + {}^1\bar{G}_{\ell,k} Q_{\ell} \\
 & - \sum_{i=1}^{N_a} \left[{}^2\bar{G}_{\ell,k} Q_{\ell,k} - {}^2\bar{G}_{\ell\pm 1,j} Q_{\ell\pm 1,k} \right] + {}^3\bar{G}_{\ell\pm 1,k} Q_{\ell\pm 1} + \bar{S}_{\ell,k} - \bar{R}_{\ell,k}
 \end{aligned} \tag{2.28}$$

where

$dQ_{\ell,k}(t)/dt$ = time rate of change of aerosol mass of component k (per unit volume) in section ℓ at time t

k = aerosol component (for example, water or a specific FP) = 1, 2, ..., N_a

ℓ = discretized section (or physical size range) of the aerosol = 1, 2, 3, ..., m

$\ell \pm 1$ = $\ell - 1$ for condensation, or $\ell + 1$ for evaporation

Each term in Equation (2.28) represents a distinct mechanism for changes in mass concentration of component k in a particular section. Time integration of Equation (2.28) requires that the coefficients used in each term be known on a sectional basis. These sectional coefficients correspond to the following mechanisms:

$\bar{\beta}$ = agglomeration (or coagulation), $m^3/s\text{-kg}$

\bar{G} = gas-to-particle conversion (condensation/evaporation), s^{-1}

\bar{S} = sources, $kg/m^3\text{-s}$

\bar{R} = removal (deposition) $kg/m^3\text{-s}$

The $\bar{\beta}$'s are called sectional coagulation coefficients, and they can be evaluated by using a variety of formulas that incorporate the effects of the different physical processes. These processes include gravitational agglomeration (a larger particle overtakes a smaller one as they both fall) and agglomeration through diffusion (either Brownian or turbulent), and are described in more detail in Section 2.4.2.1. The six agglomeration terms in the Gelbard-Seinfeld approach refer respectively to the following processes:

RN Package Reference Manual

${}^{1a}\bar{\beta}_{i,j,\ell}$	addition of component k in section ℓ , by removal of component k in section j when a particle in section j coagulates with a particle in section i to form a particle in section ℓ .
${}^{1b}\bar{\beta}_{i,j,\ell}$	addition of component k in section ℓ , by removal of component k in section i when a particle in section i coagulates with a particle in section j to form a particle in section ℓ .
${}^{2a}\bar{\beta}_{i,\ell}$	removal of component k in section ℓ , resulting from a particle in section i coagulating with a particle in section ℓ .
${}^{2b}\bar{\beta}_{i,\ell}$	addition of component k in section ℓ , resulting from a particle in section i coagulating with a particle in section ℓ , with the resulting particle remaining in section ℓ .
${}^3\bar{\beta}_{\ell,\ell}$	removal of component k in section ℓ , by two particles in section ℓ coagulating and the resulting particle is in a section higher than ℓ .
${}^4\bar{\beta}_{i,\ell}$	removal of component k in section ℓ , by a particle in section ℓ coagulating with a particle in section i , where $i > \ell$.

The four condensation terms represented by the \bar{G} coefficients correspond to the following processes:

${}^1\bar{G}_{\ell,k}$	addition (removal) of component k within section ℓ by condensation (evaporation) of component k onto (from) particles in that section;
${}^2\bar{G}_{\ell,j}$	transfer of existing component k from section ℓ to section $\ell + 1$ ($\ell - 1$) by condensation (evaporation) of component i onto (from) particles in section ℓ ;
${}^2\bar{G}_{\ell\pm 1,j}$	transfer of existing component k from section $\ell - 1$ ($\ell + 1$) to section ℓ by condensation (evaporation) of component i onto (from) particles in section $\ell - 1$ ($\ell + 1$); and
${}^3\bar{G}_{\ell\pm 1,k}$	transfer of changed mass of component k from section $\ell - 1$ ($\ell + 1$) to section ℓ by condensation (evaporation) of component k onto (from) particles in section $\ell - 1$ ($\ell + 1$). This term vanishes in the limit that aerosol masses are large compared to molecular masses.

Water condensation on and evaporation from aerosol particles are the principal couplings between thermal-hydraulics and aerosol behavior. However, these terms are not used directly in the MELCOR implementation of MAEROS. As described in Section 2.5.1, water condensation and evaporation are treated separately (but still using the MAEROS-calculated coefficients for water, as discussed in Section 2.5.1) for consistency with the water thermodynamics calculated in the CVH package.

Furthermore, fission product condensation onto and evaporation from aerosols are also integrated with the calculation of fission product condensation and evaporation on heat structure surfaces by the TRAP-MELT model, as described in Section 2.5.2, and are thus treated outside the MAEROS framework as well.

In Equation (2.28), particle removal (or deposition) is addressed by the $\bar{\mathfrak{R}}$ term. Deposition occurs through a number of processes, including gravitational settling, diffusion to surfaces, thermophoresis (a Brownian process causing migration of particles toward lower temperatures), and diffusio-phoresis (deposition induced by condensation of water vapor onto structural surfaces). The sectional deposition coefficients are described in more detail in Section 2.4.2.2.

Aerosol sources are included by the \bar{S} term in Equation (2.28). Currently, only sources defined by the user as tabular functions of time are directly included in the MAEROS equations. Sources from phenomenological models are added directly to the aerosol sectional distributions as described later in Section 2.4.3.

Intraparticle chemical reactions can occur between constituents of the aerosol. The modeling of aerosol size/composition changes resulting from chemical reactions is not currently implemented in MELCOR, but this phenomenon could easily be included in the sectional model.

Simplifications in the coefficients and in Equation (2.28) occur if the geometric constraint

$$m_{i+1}/m_i > 2 \quad (2.29)$$

is satisfied, where m_i is the particle mass at the lower boundary of section i . The geometric constraint ensures that the agglomeration of two particles results in a new particle that will fit into either the section that contains the larger of the two original particles or the section just above it. This constraint thus reduces the number of sectional agglomeration coefficients. As stated earlier in Section 2.4.1, input specifying the section boundaries is checked to verify that this constraint is met.

Equation (2.28) is used in MELCOR to describe the evolution of the aerosol size and composition distributions within each control volume. Each control volume has its own particle size and chemical composition distributions, and the aerosols are carried from one control volume to another by gas flow and may be removed by ESFs, as described in Section 2.7.

2.4.2.1 Agglomeration

When two aerosol particles collide, they can combine to form a larger particle. This process is known as agglomeration or coagulation. The sectional method used in MAEROS treats four agglomeration processes: Brownian diffusion, differential gravitational settling, and turbulent agglomeration by shear and inertial forces. A basic assumption about these processes is that simultaneous agglomeration of three or more particles is negligible.

RN Package Reference Manual

The full dependence of the agglomeration coefficients β (m^3/s) upon the aerosol and atmosphere properties as implemented in MELCOR is given in the equations in Appendix B. The dependence on atmosphere properties is not considered to be a major source of uncertainty in the aerosol calculations. The dependence on particle diameter and key modeling parameters can be summarized as follows:

Brownian:	$\beta_B \propto \gamma \chi^{-1} f(d_i, d_j)$
Gravitational:	$\beta_{grav} \propto \varepsilon_g \gamma^2 \chi^{-1} (d_i + d_j)^2 (d_i^2 - d_j^2)$
Turbulent, Shear:	$\beta_T \propto \gamma^3 \varepsilon^{1/2} (d_i + d_j)^3$
Turbulent, Inertial:	$\beta_{T2} \propto \gamma^2 \chi^{-1} \varepsilon^{3/4} (d_i + d_j)^2 (d_i^2 - d_j^2)$

In these proportionalities, γ and χ are the agglomeration and dynamic shape factors, respectively, and ε is the turbulent energy dissipation density, all of which are specified on user Input Record RNMS000. Variables d_i and d_j are the diameters of the two interacting particles, with $d_i > d_j$. The collision efficiency for gravitational agglomeration is represented by ε_g , with a specific value (discussed below) calculated in the code. The magnitude of the Brownian kernel increases with increasing values of the size ratio d_i/d_j . The role of the various parameters appearing in the kernels is also discussed below.

Except when they include significant amounts of liquid, aerosol particles are not usually assumed to be spherical, and the effective aerosol densities may be significantly less than the bulk density of the materials of which the aerosols are composed. In aerosol codes, these effects may be taken into account by using a formalism based on fully dense spherical aerosols modified through the use of the agglomeration shape factor γ and the dynamic shape factor χ . The shape factors γ and χ are input by the user to represent the effect of nonspherical shape upon aerosol collision cross sections and aerosol-atmosphere drag forces, respectively. Unit values of the shape factors correspond to dense aerosol of spherical shape, while porous spherical agglomerates lead, in theory, to values somewhat greater than unity. Highly irregular aerosols and agglomerates can have shape factors substantially greater than unity, often with γ and χ being quite unequal.

Given experimental data for aerosol shapes and densities applicable to LWR accidents, shape factors could, in principle, be derived theoretically. Because this is not practical, empirical values are obtained by fitting code calculations to the results of aerosol experiments. The values obtained may be sensitive to aerosol composition and to atmospheric conditions, especially to relative humidity. Humid conditions tend to produce more nearly spherical aerosols due to condensation of water on aerosol agglomerates. Only limited information is available concerning the dependence of shape factors upon the relevant parameters (for example, particle characteristics and atmospheric conditions), and these parameters are themselves quite uncertain under accident conditions. Default values of unity are set for both factors in MELCOR.

Agglomeration rates can be enhanced by turbulence in the atmosphere. In the past, very little attention has been given to estimating values of turbulent energy dissipation density ε appropriate for accident conditions, and uncertainty in its value may contribute to uncertainty in the aerosol agglomeration rates. In MELCOR, the user can input the value of ε or use the default value of $0.001 \text{ m}^2/\text{s}^3$.

The gravitational collision efficiency ε_g of unity corresponds to the assumption that collision cross sections are equal to the geometric cross sections. It is well known that hydrodynamic interactions between particles (i.e., the tendency of a particle to follow streamlines in flow around another particle) can yield collision efficiencies much less than unity, especially for particles that are unequal in size. The problem of collisions between falling (spherical) aerosols has been the object of much detailed theoretical and experimental study, and may be more complex than can be represented by the simple expressions normally used in aerosol codes. In MELCOR, the value of ε_g is given by

$$\varepsilon_g = 1.5d_j^2 / (d_i + d_j)^2 \quad (2.30)$$

where d_j is the smaller of the two aerosol particle diameters. It has been argued [17, 18] that using 0.5 instead of 1.5 as the coefficient in Equation (2.30) gives a better representation and that other corrections are needed when the size ratio d_i/d_j is less than about 2 and/or d_i is greater than about $20 \mu\text{m}$. However, more recent experimental measurements of collision efficiencies by Gelbard et al. [19] do not support these proposed revisions and, instead, gave collision efficiencies in reasonable agreement with Equation (2.30). These measurements involved studying the collisions of spheres at higher Reynolds numbers than those typical of aerosols and the results therefore may not be totally conclusive; however, arguments for modifying Equation (2.30) are not judged to be any more convincing.

The agglomeration model used in MELCOR receives temperature, pressure, and mass flow rate information from the CVH package. The turbulent agglomeration kernels are combined as

$$\beta_{TT} = c_s (\beta_{T1} + \beta_{T2})^{1/2} \quad (2.31)$$

where c_s is a particle sticking coefficient (default value of unity), which may be specified on Input Record RNMS000. (This sticking coefficient also appears in the other Brownian and gravitational agglomeration kernels.) The total turbulent kernel is added to the Brownian and gravitational kernels to obtain a total agglomeration kernel β_T which is then integrated over sections for use in Equation (2.28):

$$\beta_T = \beta_B + \beta_{grav} + \beta_{TT} \quad (2.32)$$

Examination of the relations for the agglomeration kernels in the proportionalities given above shows that the effects of gravitational collision efficiency, aerosol shape factors, and turbulence are coupled together in a highly nonlinear fashion. The dependence upon the various parameters differs among the different agglomeration mechanisms, and the net effects are strongly size-dependent. Hence, it is possible to give only a few generalizations.

All the agglomeration processes are enhanced by large values of the agglomeration shape factor γ , with the effect being largest for turbulent shear agglomeration and smallest for Brownian agglomeration. Large values of the dynamic shape factor reduce all the kernels (calculational coefficients) except the turbulent shear kernel, which is unaffected. Hence, large values of the shape factors enhance the relative importance of turbulence, especially for the turbulent shear effect. Reference [18] includes sensitivity studies examining the implications of uncertainties in these shape factors as well as in the turbulent energy dissipation density ε .

2.4.2.2 Deposition, Settling, and Fallout

Aerosols can directly deposit onto heat structure and water pool surfaces through four processes calculated within MAEROS. All heat structure surfaces are automatically designated as deposition surfaces for aerosols using information from the HS package, unless made inactive through user input. The parameters obtained from the HS package are:

- (1) Geometric orientation
- (2) Surface area in the atmosphere
- (3) Surface heat flux
- (4) Mass transfer coefficient
- (5) Water condensation mass flux

Each surface of a MELCOR heat structure must be designated as a ceiling, a floor, or a wall, since MAEROS only calculates deposition kernels for these orientations. The default treatment is:

The upper surface of a rectangular heat structure with an angle of inclination less than 45 degrees is considered to be a floor, and the lower surface a ceiling. The heat structure orientation parameter ALPHA on HS Input Record HSCCCCC002

determines both the inclination and whether the "left" surface is the upper or the lower surface.

Both surfaces of a rectangular heat structure with an angle of inclination greater than 45 degrees, and both surfaces of cylinders and spheres are treated as walls.

The inner (left) surface of a bottom-half hemisphere is treated as a floor and the outer (right) surface as a ceiling. For a top-half hemisphere, the treatment is reversed.

The user can override these default orientations or deactivate a surface for aerosol deposition through the RNDSXXX input records. However, if the surface of a structure is deactivated for the purposes of deposition, it is also removed from consideration in the calculation of condensation and evaporation of fission product vapors, as discussed in Section 2.5. (Note that the orientation of a structure does not otherwise affect the rate of condensation or evaporation.)

If a control volume contains a water pool, the pool surface is treated as a floor for the purposes of deposition. The area of the water pool is extracted from the CVH database.

Aerosols can also *settle* from one control volume to another through *flowthrough areas* (i.e., the gravitational settling and Brownian diffusion kernels in MAEROS described below are applied to flowthrough areas in addition to HS and pool surfaces). Such areas will ordinarily correspond to open flow paths between the control volumes, through which aerosols and radionuclide vapors are also advected. The appropriate flow areas, path elevations, etc., are specified in the RNSETXXX input records. Aerosols are not transported through these areas if the flow path is blocked by a water pool.

Finally, aerosols can agglomerate and become larger than the user-specified maximum diameter. These aerosols are assumed to immediately deposit onto water pools or horizontal heat structure surfaces or to settle from one control volume to another through *flowthrough areas* defined as part of RN input. The term *fallout* in MELCOR is used exclusively for this immediate deposition or settling of aerosols larger than the maximum user-specified diameter. All control volumes must have at least one upward-facing deposition surface (floor) or flowthrough area defined to receive fallout aerosols generated by this mechanism. During MELGEN a check is made for the existence of at least one such area; if none is present, an error message is generated and no restart file is written.

The MAEROS deposition kernel for each type of surface is made up of four contributions: gravitational deposition, Brownian diffusion to surfaces, thermophoresis, and diffusiophoresis. Of these natural depletion processes, gravitational deposition is often the dominant mechanism for large control volumes such as those typically used to simulate the containment, although phoretic effects may be significant in some cases (e.g., diffusiophoresis during water condensation). Particle diffusion is generally considered to be a relatively unimportant deposition process. The contribution of each of these

RN Package Reference Manual

processes to the deposition kernel for each type of heat structure surface and for pools and flowthrough areas in MELCOR is summarized below:

Surface	Deposition Kernel ¹			
	grav	BD	therm	diffus
Heat Structure				
Floor	+	+	+	+
Wall	0	+	+	+
Ceiling	-	+	+	+
Pool	+	+	+ ²	+ ²
Flowthrough Area	+	+	0	0

¹ The symbols +, 0, and - mean a positive contribution, no contribution, and a negative contribution, respectively. Of course, the total deposition kernel for any surface can not be less than zero.

² Included in the general formulation but currently zeroed out internally.

The velocities calculated for each of these deposition processes are defined below.

Gravitational Deposition

Gravitational deposition is effective only for upward-facing surfaces (i.e., floors and water pools) and flowthroughs to lower control volumes; for downward-facing surfaces (i.e., ceilings), this mechanism works to oppose other deposition processes. The gravitational deposition velocity is given by

$$v_{grav} = \frac{d_p^2 \rho_p g C_m}{18 \mu \chi} \quad (2.33)$$

where

v_{grav} = the downward terminal velocity (m/s)

d_p = the particle diameter (m)

ρ_p = the particle density (kg/m³)

g = acceleration of gravity = 9.8 m/s²

C_m = the particle mobility, or Cunningham slip correction factor, which reduces the Stokes drag force to account for noncontinuum effects

The particle mobility, or Cunningham slip correction factor, in the equation above is expressed as

$$C_m = 1 + \frac{2\lambda}{d_p} [F_{slip} + 0.4 \exp(-1.1d_p / 2\lambda)] \quad (2.34)$$

where

- λ = mean free path of air at 298 K ($\sim 0.069 \cdot 10^{-6}$ m)
- F_{slip} = slip factor specified on Input Record RNMS000 (default value of 1.257)
- μ = viscosity of air at 298 K [$\sim 1.8 \cdot 10^{-5}$ (N \cdot s/m²)]
- χ = dynamic shape factor

This model assumes that the aerosol particle Reynolds number Re , based on particle diameter and net deposition velocity, is much less than 1. This physically means that inertial effects of the flow may be neglected. This Reynolds number is not to be confused with the bulk mass flow (air, steam, aerosol particles) Reynolds number based on the dimensions and velocities calculated by the CVH package, which is typically much greater than 1.

Brownian Diffusion

Deposition can also result from diffusion of aerosols in a concentration gradient from a higher to a lower concentration region. The diffusive deposition velocity is given by

$$V_{diff} = \frac{\sigma T C_m}{3\pi \mu \chi d_p \Delta} \quad (2.35)$$

where

- V_{diff} = diffusion deposition velocity (m/s)
- σ = Boltzmann constant = $1.38 \cdot 10^{-23}$ (J/s \cdot m²K⁴)
- T = atmosphere temperature (K)
- μ = viscosity (N \cdot s/m²)
- χ = dynamic shape factor
- Δ = user-specified diffusion boundary layer thickness specified on Input Record RNMS000 (default value of 10^{-5} m)

RN Package Reference Manual

under the assumption that there is no gas velocity perpendicular to the deposition surface. This impaction mechanism is most effective for larger aerosol particle sizes.

Thermophoresis

This aerosol deposition mechanism results from the force exerted on aerosol particles by temperature gradients in the bulk gas. The thermophoretic deposition velocity v_{therm} is given by

$$v_{therm} = \frac{3 \mu C_m (c_t Kn + k_{gas}/k_p)}{2 \chi \rho_{gas} T (1 + 3 F_{slip} Kn) (1 + 2 c_t Kn + k_{gas}/k_p)} \nabla T \quad (2.36)$$

where

Kn = $2\lambda / d_p$ (Knudsen number)

k_{gas}/k_p = ratio of thermal conductivity of gas over that for aerosol particle k_p , and is user-specified (on Input Record RNMS000)

∇T = structure surface temperature gradient (K/m)

ρ_{gas} = gas density (kg/m³)

T = wall temperature (K)

F_{slip} = slip factor

c_t = constant associated with the thermal accommodation coefficients (specified on Input Record RNMS000 with default value of 2.25)

The coefficient of ∇T in Equation (2.36) is calculated for each of the four aerosol coefficient sets at minimum/maximum temperature and pressure and stored as described in Section 2.4.2.3. The actual temperature gradient at each heat structure surface, calculated from the heat flux q'' obtained from the HS package as

$$\nabla T = -q''/k_{air} \quad (2.37)$$

is used with an interpolated coefficient (see Section 2.4.2.3) to calculate the actual diffusion velocity. The thermal conductivity of air, k_{air} , is evaluated at the surface temperature of the heat structure using the properties of air for consistency with the evaluation of the aerosol coefficients with air properties.

Diffusiophoresis

When water condenses on (evaporates from) a structure surface, composition gradients will exist in the adjacent gas which will affect aerosol deposition on the surface. Two related mechanisms produce these gradients. First, a net molar flux of gas toward (away from) the condensing (evaporating) surface will exist, and this net flux, commonly called the Stefan flow [20], will tend to move aerosol particles with it. Second, differences in the momentum transferred by molecular impacts on opposite sides of the particle will tend to drive the particle in the direction of decreasing concentration of the heavier constituent. By some definitions, only this second component constitutes diffusiophoresis; however, in this discussion the term "diffusiophoresis" will be used to represent the net result of both effects and the equations given include both effects. Note that when the noncondensable gas is heavier than steam, as in air-steam mixtures, the differential molecular impact effect opposes the Stefan flow (which dominates the net result); the effects are in the same direction if the noncondensable gas is lighter than steam.

The treatment in MELCOR is valid for particle sizes large compared with molecular mean free paths, a condition which will generally apply for accident analyses. A diffusiophoretic deposition velocity (including the Stefan flow) $V_{diffusio}$ is calculated from

$$V_{diffusio} = \left(\frac{\sqrt{M_s}}{X_s \sqrt{M_s} + X_{NC} \sqrt{M_{NC}}} \right) \left(\frac{W_{cond}}{\rho_b} \right) \text{ if } W_{cond} \geq 0 \text{ (condensation)} \quad (2.38)$$

$$V_{diffusio} = W_{cond} / \rho_s \quad \text{if } W_{cond} < 0 \text{ (evaporation)} \quad (2.39)$$

where

- M_s = molecular weight of water (kg/mole)
- M_{NC} = molecular weight of noncondensable gases (air)
- W_{cond} = condensation mass flux to the surface (kg/s-m²)
- ρ_b = density of bulk gas (kg/m³)
- ρ_s = saturation density of water vapor (kg/m³)
- X_s = mole fraction of water vapor in the bulk gas
- X_{NC} = mole fraction of noncondensable gases in the bulk gas

The condensation mass flux is obtained from the HS package. Note that the differential molecular impact effect is ignored in MELCOR for evaporation ($W_{cond} < 0$). The velocity

RN Package Reference Manual

calculated is toward the surface for condensation and away from the surface for evaporation.

MELCOR calculates these four velocities, representing deposition by gravity, diffusion, thermophoresis, and diffusiophoresis, for each surface. The sum gives the aerosol removal rate term $\overline{\mathcal{R}}_{\ell,k}$ ($\text{kg}/\text{m}^3 \cdot \text{s}$) in Equation (2.28) in the form

$$\overline{\mathcal{R}}_{\ell,k} = \sum_{j=1}^{N_{str}} K_{j,\ell} K_{\ell,k} \quad (2.40)$$

where

N_{str} = total number of heat structure surfaces and/or pool surfaces for aerosol deposition in the control volume

$K_{j,\ell}$ = deposition rate for the heat structure j for aerosol section ℓ (s^{-1})

$Q_{\ell,k}$ = aerosol density for section ℓ of component k (kg/m^3)

$K_{j,\ell}$ in Equation (2.41) is defined as

$$K_{j,\ell} = \frac{A_j}{V} (v_{grav} + v_{diff} + v_{therm} + v_{diffusio}) \quad (2.41)$$

where

A_j = area of heat structure surface j (m^2)

V = control volume atmosphere volume (m^3)

The total component mass that deposits on all surfaces from each section is calculated by MAEROS. The fraction $Fr_{j,\ell}$ of the mass in each section that deposits on surface j in the control volume is given by the simple expression

$$Fr_{j,\ell} = \frac{A_j K_{j,\ell}}{\sum_j^{N_{str}} A_j K_{j,\ell}} \quad (2.42)$$

For fallout aerosols the procedure is similar except that the areas are summed for the floor heat structures, pool, and flowthrough areas; no kernels are involved since any kernel would be common to all surfaces involved. The total fallout mass calculated by agglomeration in MAEROS is then distributed over the floor heat structures, pools, and passes through flowthrough areas proportional to the area of each as follows:

$$Fr_i = A_i / \sum_i^{N_{sur}} A_i \quad (2.43)$$

where N_{sur} is the total number of surfaces and flowthrough areas.

If part or all of a water film drains from a surface of a heat structure to the pool in the associated control volume, any fission products deposited on that surface or in the water film are normally relocated with the water, in proportion to the fraction of the film that is drained. However, the user may change this for any class by resetting the corresponding value in sensitivity coefficient array 7136 to the fraction of the class assumed to be dissolved in, and therefore to relocate with, the film.

When a phase (pool or atmosphere) in a control volume ceases to exist, the aerosols it contains must be relocated. If the pool in a volume completely evaporates, any aerosols in the pool are distributed between the floor heat structures and the flowthrough areas according to Equation (2.43). If the atmosphere in a control volume that is almost completely filled with water completely condenses, all the suspended aerosol mass is added to the aerosol mass in the pool because it is assumed that the pool will then completely fill the control volume.

2.4.2.3 Numerical Implementation

In stand-alone MAEROS, the full aerosol dynamics equations are integrated using a conventional Runge-Kutta integration routine [21]. Because the integration is stopped and restarted only at times when an edit is desired, this approach is both accurate and efficient. However, in MELCOR the integration must be stopped at the end of each system timestep and restarted at the beginning of the next to account for the continuous coupling with other MELCOR models, most of which must be exercised outside the MAEROS framework. These include aerosol release from fuel in the Core package, aerosol generation during core-concrete interactions by the MELCOR implementation of VANESA, fog condensation or evaporation calculated by CVH package thermodynamics, simultaneous condensation or evaporation of fission product vapors on heat structure and aerosol particle surfaces, and advection of aerosols between control volumes as controlled by CVH flow rates. Because of this, the Runge-Kutta solver can be very inefficient (the startup costs become excessive) and, for very short steps, there is little or no increase in accuracy over an explicit (forward Euler) integration.

RN Package Reference Manual

Therefore, in MELCOR appropriate rates of change are evaluated at the beginning of each system timestep and, if an explicit step will produce only small changes in the sectional densities, the distribution is updated using this explicit Euler step. Otherwise, the Runge-Kutta solver is used to advance the equations. The criteria for "small change in the sectional densities" and the error tolerances for the Runge-Kutta solution are controlled by the sensitivity coefficients in array 7000 (see Appendix A). If the Runge-Kutta solver does not converge within the requested tolerances, the RN package will reduce the timestep to one-half the current value and write a message to the output and diagnostic files informing the user.

Whether the new aerosol distribution is calculated by an explicit step or by the Runge-Kutta solver, a check is performed to ensure that component masses are conserved within a suitable tolerance (given by a sensitivity coefficient in array 7000; see Appendix A). If this check fails, the RN package will reduce the timestep to one-half the current value and write a message to the output and diagnostic file informing the user.

The calculation of the MAEROS coefficients is somewhat costly; a full calculation for 20 sections requires about 10 s processing time on a CRAY 1S computer. Therefore, the coefficients are calculated on the first call to the aerosol model for use throughout the entire problem. Input records describing these coefficients (the RNCFXXX series) are written to a file automatically and may be read in from this file on a subsequent restart if called for on the RNACOEf record, but this practice is not recommended because of the possibility of user file handling errors. Sensitivity coefficient array 7001 contains error tolerances for numerical integration of the MAEROS coefficients.

Using a constant set of coefficients imposes some modeling constraints however, because various parameters embedded in the coefficients, such as material properties for the CVH atmosphere, are also effectively held fixed despite the fact that they should vary with changing conditions during the problem. Several of the terms in Equation (2.28) also contain driving forces. The coefficients of these forces are calculated and stored.

The following constraints pertain to the current coefficient set:

a	The aerosol material density is assumed to be the same for all components (specified by the user on Input Record RN1100).
b	The aerosol shape, as modeled by the dynamic and agglomeration shape factors (specified by the user on Input Record RNMS000), is independent of aerosol composition.
c	The medium in which the aerosol processes are assumed to occur has fixed properties, taken as those for air.
d	The degree of turbulent agglomeration is fixed throughout the problem, specified by the user on Input Record RNMS000.

e	Other parameters that control deposition rates do not depend on particle composition. For example, the ratio of the thermal conductivity of air to that of the aerosol material is fixed.
---	---

The pressure and temperature of the atmosphere are embedded in these coefficients and are fixed for a single set of coefficients. However, the aerosol module actually calculates four sets of coefficients at points given by combinations of two temperatures (T_{min} and T_{max}) and two pressures (P_{min} and P_{max}), all of which may be specified by the user. The effects of changing thermal-hydraulic conditions during the problem are approximated by interpolating between these sets of coefficients. The T_{min} , T_{max} , P_{min} , and P_{max} parameters are chosen to bound the temperatures and pressures expected in the calculation, and are specified on user Input Record RNPT000.

The interpolated sectional coefficients CF_i for agglomeration or deposition mechanism i are given by

$$CF_i = (1 - F_T) \left[(1 - F_p) AC_{11,i} + F_p AC_{12,i} \right] + F_T \left[(1 - F_p) AC_{21,i} + F_p AC_{22,i} \right] \quad (2.44)$$

where

$AC_{11,i}$ = the aerosol coefficient for mechanism i for the lower atmospheric temperature (T_{min}) and pressure (P_{min})

$AC_{12,i}$ = the aerosol coefficient for mechanism i for the lower atmospheric temperature (T_{min}) and higher pressure (P_{max})

$AC_{21,i}$ = the aerosol coefficient for mechanism i for the higher atmospheric temperature (T_{max}) and lower pressure (P_{min})

$AC_{22,i}$ = the aerosol coefficient for mechanism i for the higher atmospheric temperature (T_{max}) and pressure (P_{max})

and F_T and F_p in Equation (2.45) are defined as

$$F_T = \left(\frac{T_{gas} - T_{min}}{T_{max} - T_{min}} \right) \quad (2.45)$$

and

$$F_p = \left(\frac{P_{gas} - P_{min}}{P_{max} - P_{min}} \right) \quad (2.46)$$

where

T_{gas} = cell temperature (K), and

P_{gas} = cell pressure (Pa).

At the expense of larger sets of coefficients, some of the constraints above could be removed by interpolating to accommodate other changing parameters or by separating the coefficients so that a relevant parameter is not embedded, but this is not currently allowed through user input.

2.4.3 Sources

In stand-alone MAEROS, sources of aerosols are included in the differential equation solution at a constant source rate over that timestep. In MELCOR, however, only user-defined sources are treated in this way; sources generated by models in other packages are currently added as a single increment because of the explicit coupling of these packages. Since masses that are added to the aerosol scheme could be from the previous timestep or the present timestep, depending on the calling sequence of the various packages, all masses to be added from other models are lumped together and added to the aerosol size distribution at the start of the timestep.

Sources of aerosols are calculated in-vessel by the fuel-cladding gap release model and the CORSOR release models, as described in Section 2.3.1. Aerosols generated by these models are put into the smallest aerosol section, consistent with the production of small particles by gas-to-particle conversion. Sources of aerosols are also calculated ex-vessel by the VANESA model, as described in Section 2.3.2. The size distribution for these aerosols is assumed to be log-normal, with median diameter and standard deviation given by VANESA.

A number of time-dependent aerosol sources (specified on record RN1001) can also be specified for a control volume by the user (see the RNASXXX input record series). The aerosols can be put in either the control volume pool or atmosphere, with the time rate of the source specified by a tabular function. The mass added is determined by multiplying the mass addition rate (an input constant times the value of the tabular function at the midpoint of the current timestep) by the timestep, or

$$M_{added} = \left[\frac{dM}{dt} \right] \Delta t = [C \times TF(t + \Delta t / 2)] \Delta t \quad (2.47)$$

where C is the mass addition constant XM on the RNASXXX input records, TF is the tabular function value, and t and Δt are the time and timestep, respectively. The size distribution of the source can be uniform, log-normal with respect to log diameter, or user specified, and is constant with time.

2.4.4 Resuspension

The resuspension model in MELCOR depends on other packages for activation. A package can call for an arbitrary fraction of deposited aerosols in a control volume to be resuspended at any time. However, no package at present has a model to calculate the fraction of deposited mass to be resuspended. User input is not available to activate resuspension. **Therefore, resuspension is currently not calculated.** When implemented, however, the user will be allowed to specify the size distribution of resuspended mass on the RNARXXX input records.

2.5 Condensation/Evaporation

Fission products and water can condense onto or evaporate from aerosols, heat structure surfaces, and water pools. Aerosol water is identified with "fog" in the CVH package. The change in fog mass is determined by thermodynamics calculated within the CVH package and is distributed over aerosol sections by the RN package as described below in Section 2.5.1. Water condensation and evaporation for heat structure and water pool surfaces are treated solely in the HS and CVH packages, respectively. The calculation of fission product vapor condensation and evaporation in the RN package is described in Section 2.5.2.

2.5.1 Water

The stand-alone version of MAEROS includes terms, given in Equation (2.28), for particle growth resulting from condensation of water onto (and shrinkage from evaporation of water from) aerosols. In MELCOR, these terms are not included with the MAEROS numerical solution for agglomeration and deposition. The reason is that inclusion of these terms makes the MAEROS equations "stiff" and therefore computationally difficult to solve, because the characteristic time for mass transfer is small compared to other characteristic times in the problem.

There are two approaches available in MELCOR to deal with condensation and evaporation of aerosol water. The original model, which neglects hygroscopic, surface

RN Package Reference Manual

tension, and molecular free path effects, is described in this section. The user has the option to specify (as part of RN package input) the use of a more detailed model that includes these effects, as described in Section 2.10. The original model is used by default.

In addition to neglect of hygroscopic and surface tension effects, the original MELCOR model assumes that both the temperature difference between gas and aerosols and the characteristic time for mass transfer to and from aerosols may also be neglected. Under these assumptions, the atmosphere can never become significantly supersaturated, and can be significantly subsaturated only if there is no water available to evaporate from the aerosols. In short, the system of atmosphere plus aerosol water must be in thermodynamic equilibrium.

This makes the aerosol assumptions consistent with the equation of state as described in the Control Volume Thermodynamics (CVT) Package Reference Manual, and avoids the need to estimate the disequilibrium between liquid and vapor within a basically equilibrium formulation of thermodynamics or to reconcile calculations including rate effects in the RN package with calculations based on equilibrium thermodynamics within the CVT package. It also allows the water on aerosols to be identified with "fog" in the CVT package.

This reduces the task of the RN package to one of distributing the total change in fog mass, as calculated by equilibrium thermodynamics in the CVT package, among the aerosol sections. In general, this is done with changes in sectional water masses proportional to the appropriate relative rates, which are all proportional to the same super- or sub-saturation driving force, and the actual driving force need not be calculated. However, in a few cases (e.g., a sudden decompression in a volume with little or no initial aerosol content) the condensation rate necessary to maintain equilibrium may exceed that possible on existing aerosols. In such cases, a very rough estimate of the limiting condensation rate is made (as described below), and the excess water is assumed to form new aerosols in the smallest aerosol section by spontaneous nucleation.

The MAEROS equations do not account for the distribution of *composition* of particles within a single section. This major simplification of the general equations resulted from approximating all material densities as equal, rendering the agglomeration and deposition coefficients independent of composition. Thus the evolution of particle composition and size distribution is independent of composition for these two processes. The composition distribution can be important in cases of water condensation or evaporation, where a change in water mass can carry a wet aerosol particle from one size section to another. A full treatment would require both the tracking of a more general size-and-composition distribution, and the inclusion of models to account for the differing rates of condensation of water on particles of differing composition.

In MELCOR, two assumptions are permitted for condensation/evaporation of water. The first is equivalent to assuming that all particles within a section have the same composition, and allows changes in water mass to freely carry particles of other materials from one size section to another. If water condenses on and then evaporates from a dry aerosol, the

final distribution calculated using this treatment will not match the initial one—even in the absence of agglomeration or deposition—and may contain particles smaller than any initially present. The alternative assumption is that condensation and evaporation of water are ineffective in moving other materials from section to section. This is sometimes described as “allowing water to condense only on water.” The errors in this treatment are different from—but no less serious than—those in the first treatment. The two options, while not necessarily representing limiting cases, allow a user to investigate the potential importance of the effects modeled.

Condensation within a section is evaluated explicitly. The total change in water mass is taken as proportional to the sum over sections of the ${}^1\overline{G}$ term in Equation (2.28) for water, using start-of-step aerosol masses (the ${}^2\overline{G}$ growth terms cancel when summed over all sections, while the ${}^3\overline{G}$ terms are infinitesimal contributors in the differential limit and are ignored). Since the new total water mass on aerosols is equal to the new fog mass calculated by the CVH package, the normalization constant, A , can therefore be determined from the equation

$$\Delta m_w = A \Delta t \sum_{\ell} {}^1\overline{G}_{\ell,w} Q_{\ell} \quad (2.48)$$

where Δm_w is the total mass of water which must be condensed, as required by the CVH package.

The rate of growth of an individual aerosol particle as a result of condensation is given by the Mason equation [9] as

$$\begin{aligned} \frac{dm}{dt} &= \rho_1 4 \pi r \left(r \frac{dr}{dt} \right) \\ &= \frac{4 \pi r (S - 1)}{a + b} \end{aligned} \quad (2.49)$$

where a and b are heat flux and vapor diffusion terms, respectively,

$$a = \frac{M_w i_{fg}^2}{k_v R T^2} \quad (2.50)$$

$$b = \frac{R T}{P_{sat} D M_w} \quad (2.51)$$

RN Package Reference Manual

and where

m	= particle mass
ρ_1	= particle density
S	= ambient saturation ratio
r	= mean aerosol particle radius of section i
M_w	= molecular weight of water
i_{fg}	= latent heat of water
k_v	= vapor thermal conductivity
R	= gas constant
T	= ambient temperature
P_{sat}	= saturation pressure at T
D	= diffusivity of water vapor in air

Equations (2.48) through (2.51) can be combined to relate the normalization constant A and the $\overline{G}_{\ell,w}$ term to the Mason equation:

$$\begin{aligned} \frac{dm_w}{dt} &= \sum_{\ell} N_{\ell} \left\langle \frac{dm}{dt} \right\rangle = \sum_{\ell} Q_{\ell} \left\langle \frac{1}{m} \frac{dm}{dt} \right\rangle = \sum_{\ell} Q_{\ell} \left\langle \frac{4\pi r}{m} \right\rangle \frac{(S-1)}{a+b} \\ &= \sum_{\ell} Q_{\ell} \overline{G}_{\ell,w} A \end{aligned} \quad (2.52)$$

where N_{ℓ} is the number of particles in section ℓ and the angle brackets denote an appropriate sectional average. Therefore, the MAEROS coefficient $\overline{G}_{\ell,w}$ can be evaluated as an appropriate sectional average of $4\pi r/m$ and A can be taken as the term $(S-1)/(a+b)$, which is independent of size. Equations (2.49) and (2.52) are consistent if an effective value of the saturation ratio S , which varies through the timestep, is chosen appropriately. A limiting rate on condensation can be estimated from Equation (2.52), using an upper bound on the saturation ratio based on the assumption that all vapor destined to condense exists in the vapor phase at the start of the step. That is,

$$S_{\max} = 1 + \Delta m_w / m_{v,sat} \quad (2.53)$$

where Δm_w is again the mass of water to be condensed and $m_{v,sat}$ is the mass of water vapor at saturation in the atmosphere. If the required condensation exceeds this limiting rate, A in Equation (2.48) is set to the limiting value, $(S_{max} - 1)/(a + b)$, and the excess water is simply put into the smallest aerosol section, consistent with the assumption that excess water that cannot condense on existing aerosol, structures, or pools condenses by homogeneous nucleation, forming small fog droplets.

Transfer from section to section by growth of aerosols is evaluated implicitly; that is, the ${}^2\overline{G}_{1,w}$ terms are evaluated using end-of-step masses. For condensation, aerosols can only grow, and by definition there can be no growth into the smallest section. This allows the new masses to be evaluated in a single pass from the smallest section to the largest by forward substitution,

$$Q_{1,k}^n = \frac{Q_{1,k}^{o+}}{1 + A \Delta t {}^2\overline{G}_{1,w}} \quad (2.54)$$

$$Q_{\ell,k}^n = \frac{Q_{\ell,k}^{o+} + A \Delta t {}^2\overline{G}_{\ell-1,w} Q_{\ell-1,k}^n}{1 + A \Delta t {}^2\overline{G}_{\ell,w}} \quad (2.55)$$

where $Q_{\ell,k}^{o+}$ is the start-of-step mass for all classes but water, in which case it includes the explicitly calculated condensation. Note that, from a strictly numerical standpoint, no negative masses can be predicted by this equation if there were none at the start of the step.

The treatment of evaporation is very similar to that for condensation. Evaporation within a section is calculated explicitly, and the total is normalized to the change in water mass required by the CVH package, but no rate limit is considered. If one or more explicitly calculated water masses would be negative, they are set to zero and the remaining (positive) masses renormalized to the correct total.

As in condensation, the section-to-section transfers are evaluated implicitly in a single pass, this time from the largest to the smallest. Experience has shown that one further modification is necessary. If the limit and renormalize procedure just mentioned is used, the value of A used for section-to-section transfers out of each section must be made to agree with the effective value of A used for evaporation from that section. This is easily done by defining

$$A_s \Delta t = \frac{Q_{\ell,w}^{o+} - Q_{\ell,w}^o}{{}^1G_{\ell,w} Q_{\ell}} \quad (2.56)$$

where A_s is simply the normalization constant A in cases where no dryout occurred.

2.5.2 Fission Product Vapors

The condensation and evaporation of fission product vapors to and from heat structures, pool surfaces, and aerosols is evaluated by the same equations as in the TRAP-MELT2 code [8]. The fission product vapor masses in the control volume atmosphere and condensed on the aerosol and heat structure surfaces are determined by rate equations based on the surface areas, mass transfer coefficients, atmosphere concentration, and the saturation concentrations corresponding to the temperatures of the surfaces:

$$\frac{dM_a}{dt} + \sum_i \frac{dM_i}{dt} = 0 \quad (2.57)$$

$$\frac{dM_i}{dt} = A_i k_i (C_a - C_i^s) \quad (2.58)$$

where

C_a = M_a / V = concentration of vapor in atmosphere

C_i^s = saturation concentration of vapor in atmosphere at temperature of surface i

M_i = condensed mass of vapor on surface i

V = volume of atmosphere

A_i = area of surface i

k_i = mass transfer coefficient for surface i

and subscript i denotes any heat structure surface, pool surface, or aerosol section.

These differential equations can be solved as in TRAP-MELT2 to yield the following algebraic equations:

$$C_a = M_a / V = \frac{\beta}{\alpha} - \left(\frac{\beta}{\alpha} - C_{a0} \right) e^{-\alpha \Delta t} \quad (2.59)$$

$$M_i = M_{i,0} + A_i k_i \left(\frac{\beta}{\alpha} - C_i^s \right) \Delta t - A_i k_i \left(\frac{\beta}{\alpha} - C_{a0} \right) \left(\frac{1 - e^{-\alpha \Delta t}}{\alpha} \right) \quad (2.60)$$

where

$$\alpha = \sum_i A_i k_i / V \quad (2.61)$$

$$\frac{\beta}{\alpha} = \frac{\sum_i A_i k_i C_i^s}{\sum_i A_i k_i} \quad (2.62)$$

and subscript 0 denotes the value at start of the timestep, Δt .

Total sectional areas A_p for aerosols are calculated from the average particle in each section, as derived in Appendix C:

$$A_p = 12\pi \left(\frac{3}{4\pi} \right)^{2/3} \frac{M}{\ln(m_2/m_1)} (m_1^{-1/3} - m_2^{-1/3}) \quad (2.63)$$

The mass transfer coefficient k_p for aerosols is based on zero slip flow, or Sherwood number = 2.0.

All HS package heat structures are automatically included for condensation and evaporation of fission product vapors unless made inactive through user input on RNDXXXX records. The area of the heat structure in the atmosphere A_w is used to define the net area for fission product vapor interactions. This area is the total heat structure area times the fraction of the heat structure in the atmosphere as determined by the HS package.

Although fission products may condense on pool surfaces, evaporation of fission products residing in control volume pools is not permitted. The fission product vapor location within a phase in a control volume (pool or atmosphere) may change when one phase is no longer present. Any vapor mass associated with a disappearing phase is added to the remaining phase in that control volume.

The mass transfer coefficient for condensation of fission product vapors onto heat structure surfaces, k_w , is calculated based on the mass transfer coefficient, k_{HS} , for water condensation onto a heat structure surface calculated by the HS package, which uses the steam-air diffusivity, $D_{st,a}$:

RN Package Reference Manual

$$k_w = k_{HS} D_{k,g} / D_{st,a} \quad (2.64)$$

The vapor diffusivity for the fission product vapors in the bulk gas, $D_{k,g}$, is calculated from the following equation as presented in Welty, Wicks, and Wilson [22]:

$$D_{k,g} = \frac{1 - y_k}{\sum_n (y_n / D_{k,n})} \quad (2.65)$$

where

- y_k = mole fraction of trace vapor k
- y_n = mole fraction of bulk gas n
- $D_{k,n}$ = binary diffusivity of vapor k in gas n

The binary diffusivities are evaluated from the following expression from Bird, Stewart, and Lightfoot [23]:

$$D_{A,B} = 0.0018583 \frac{[T^3 (M_A^{-1} + M_B^{-1})]^{1/2}}{P \sigma_{AB}^2 \Omega_{D,AB}} \quad (2.66)$$

with

- $D_{A,B}$ = binary diffusivity in cm^2/s
- T = temperature in K
- P = pressure in atmospheres
- M_i = molecular weight in kg/kg-mole
- σ_{AB} = collision diameter in Angstroms = $0.5 (\sigma_A + \sigma_B)$
- $\Omega_{D,AB}$ = collision integral = function of kT/ε (see Table B-2 of Reference [23])

The actual calculation of D_{AB} is performed by a model in the Material Properties (MP) package, using data for the collision integral contained in the MP database. Values for the Lennard-Jones potential parameters σ and ε/k for the bulk gases are obtained from the MP database, while values for some of the fission product vapors, obtained from

Reference [23], are stored in RN sensitivity coefficient array 7111 (see Appendix A). Actual values are used for Xe and I₂; other classes are defaulted to values for air due to a lack of information. (The values for the bulk gases are the same ones used for calculation of viscosity in the absence of tabular data; they may be changed through MP input if desired.)

In addition to being used to determine the amount of each material class present as aerosol and as fission product vapor, the vapor pressure is used in the model for condensation and evaporation to determine the saturation concentrations, C_i^s , calculated from the perfect gas law,

$$C_i^s = \frac{P(T_i)M_w}{RT_i} \quad (2.67)$$

The expression for the vapor pressure is

$$\log_{10}(P) = -A/T + B + C \log_{10}(T) \quad (2.68)$$

with P and T in units of mm of Hg and K, respectively. The coefficients A , B , and C for each class are stored in sensitivity coefficient array 7110 for different temperature ranges (see Appendix A). Classes for which there are no data are assumed to have a default vapor pressure curve characteristic of a nonvolatile ceramic (zero vapor pressure below 3000 K and the vapor pressure of UO₂ above 3000 K); nondefault vapor pressure coefficients are defined for classes 2 (Cs), 3 (Ba), 4 (I), 5 (Te), 6 (Ru), 7 (Mo), 8 (Ce), 9 (La), 10 (UO₂), 11 (Ag), 12 (Sn), 13 (B₂O₃), and 16 (normally CsI), and class 1 (Xe) is always a vapor. (See the RN Package Users' Guide for details on defining temperature ranges and forcing classes to always be an aerosol or always a vapor.)

For temperatures above a maximum temperature value, T_{max} , the correlation is extrapolated. However, direct use of the correlation outside its range of applicability can return a pressure that decreases with increasing temperature, because C is negative and $C \log_{10}(T)$ can dominate $-A/T$. Therefore, the extrapolation uses

$$\log_{10}(P) = -A'/T + B' \quad (2.69)$$

The coefficients A' and B' are derived from the last range coefficient values A , B , and C by demanding that P and dP/dT be continuous at the matching temperature T_{max} . This requires

$$A' = A + C \log_{10}(e)T_{max} \quad (2.70)$$

$$B' = B + C [\log_{10}(e) + \log_{10}(T_{max})] \tag{2.71}$$

2.6 Decay Heat Distribution

All decay heat released by radionuclides in a control volume pool is assumed to be absorbed by that pool. None of this decay heat is added directly to any heat structure surface or to the atmosphere of the control volume.

The decay heat released by radionuclides in the control volume atmosphere and from those deposited on the various heat structure surfaces can be apportioned according to user specifications among the volume atmosphere, the surfaces of heat structures in that volume, and the pool surface (if a pool is present). Fractions may also be specified as going to the atmosphere and surfaces of other volumes to simulate decay radiation transmitted through flow paths. Defaults are provided, as discussed below.

Approximately one half of decay heat is generated as gamma radiation and one half as beta radiation. Because typical gaseous atmospheres are nearly transparent to typical gammas and fairly opaque to typical betas, deposition of decay heat in a volume atmosphere results primarily from absorption of beta radiation. (The split and the characteristic energies are not explicitly modeled by MELCOR.) These observations and solid angle considerations led to the default splits suggested by Reference [3]:

Decay Heat from Radionuclides in the Atmosphere	
Atmosphere of current CV	50%
Surfaces of current CV	50%
Atmosphere of other CVs	0%
Surfaces of other CVs	0%
Decay Heat from Radionuclides on Heat Structure Surfaces	
Current Heat Structure	50%
Atmosphere of current CV	25%
Other surfaces of current CV	25%
Atmosphere of other CVs	0%
Surfaces of other CVs	0%

All fractions are independent of the RN class. Those for airborne radionuclides can be changed on a volume-by-volume basis using the RNDHVXXX and RNDHVSXXX input record series. Those for radionuclides on surfaces can be modified similarly, on a surface-by-surface basis, using the RNDHSXXX and RNDHSSXXX input record series.

Decay heat from airborne or deposited radionuclides that is absorbed by surfaces in the same control volume is allocated among the surfaces in proportion to their areas. (Note that for deposited radionuclides the bearing surface is not included.) The areas considered are the portions of heat structure surfaces exposed to the atmosphere, and the surface of

the pool (if a pool is present). If there are no such surfaces, the fraction of decay heat allocated to the surfaces of a control volume is deposited instead in the atmosphere of that control volume.

The fractions specified as going to the local control volume atmosphere (by default or user input) are interpreted as the values appropriate for complete absorption of beta radiation. They must be reduced for small volumes or low densities, where the thickness of the atmosphere is insufficient to permit complete absorption of beta rays. This reduction is by a factor

$$\min(\rho_A D_{CV}/R_\beta, 1.0)$$

where ρ_A is the atmosphere density, D_{CV} is the characteristic dimension for absorption in the control volume, and R_β is the range of a typical beta particle (given in sensitivity coefficient array 7002, with a default value of 1.2 kg/m²; see Appendix A). D_{CV} has a default value given by the minimum of the cube root of the volume and the square root of the flow area from the CVH database (so as to be reasonable for both tanks and pipes). It can be modified using the RNDHLENXXX input record series.

Any reduction in deposition to the local atmosphere is compensated by proportionate increase in energy distributed to other surfaces in the volume and to the atmosphere and surfaces of other control volumes. (The calculation is bypassed if the sum of these other split coefficients is zero.)

2.7 ESF Models

Models are currently available for the removal of radionuclides by pool scrubbing, filter trapping, and spray scrubbing. These models are described in the following subsections. The normal RN deposition and condensation models described in Sections 2.4 and 2.5 are applied to heat structures used to model ice condensers; see the HS Package Reference Manual for a detailed description of methods used to model ice condensers, including a surface area enhancement factor for radionuclide deposition.

2.7.1 Pool Scrubbing

The pool scrubbing model in the RN package is based on the SPARC-90 code [10]. (The thermal-hydraulic aspects of pool scrubbing are modeled in the CVH package.) Aerosols and iodine vapor are removed by pool scrubbing; the model will also treat organic iodine vapor (CH₃I) but currently it is not included in the MELCOR RN class structure. Decontamination is calculated for those flow paths activated on the FLnnn02 input record (see the FL Package Users' Guide) and for gases evolved from core-concrete interactions

RN Package Reference Manual

in cavities activated on the CAVnn00 input record (see the CAV Package Users' Guide). By default, the model treats these cases by using the horizontal vent scrubbing option from SPARC-90 along with the flow area provided by the FL package (FLARA on input record FLnnn01) or the flow area calculated by the CAV package. However, the user may override the default venting treatment by providing appropriate input on the RN2PLSXX records. For consistency with the CVH package, pool scrubbing is only calculated if the submerged depth of the flow path is greater than the zero efficiency bubble rise height given in CVH sensitivity coefficient array 4405. The gases evolved from the core-concrete interactions calculated by VANESA are supplemented by an inferred steam flux generated by boiling at the cavity/pool interface. This flux is evaluated by dividing the cavity/pool interfacial heat flux calculated by CORCON by the latent heat of vaporization for water in the pool.

The decontamination factor (DF) is defined as the ratio of the radionuclide mass entering the pool to that leaving, and has a value greater than or equal to unity. However, when the iodine concentration in the pool divided by the equilibrium partition coefficient (discussed in Appendix F) exceeds the concentration of iodine vapor in the gas entering the pool, then iodine vapor scrubbing cannot occur and the corresponding decontamination factor must be equal to unity. (Furthermore, MELCOR is not structured to calculate iodine stripping from the pool under these conditions, so iodine removal from the pool is not considered.) If the iodine concentration in the bubbles is significant (i.e., exceeds a threshold value implemented in sensitivity coefficient array 7159 with a default value of 10^{-6} moles/cm³), a message is issued once per calculation by the scrubbing routine to inform the user of this condition.

The gas flow through the pool is described in two overlapping regions. In the vent exit region, the injected gas forms large, unstable globules. The initial size of the globule depends on the vent type and the noncondensable gas flow rate. As the globules rise they begin to break up into swarms of smaller bubbles. It is assumed that break-up is complete by the time the globule rises a distance equal to twelve times its initial diameter. In the swarm rise region, bubbles continually coalesce and redisperse during their erratic ascent. On average, however, it is assumed that they can be represented by oblate spheroids of a constant, stable size with the flatness given by a correlation depending on bubble size. The rise velocity of individual bubbles in the swarm relative to the liquid is given by a correlation depending on bubble size, also, and remains constant since the size remains constant. The swarm rise velocity represents the volumetric average velocity on a cross section of the swarm. Bubbles in the center rise faster than swarm periphery bubbles, and the swarm rise velocity increases as the swarm ascends because the volumetric flow rate of the swarm increases as the gas expands under a decreasing static head. In the SPARC-90 model, however, the swarm rise velocity is assumed to remain constant with a value given by the average of the value at the vent exit depth and the value at the pool surface. The bubbles in the swarm multiply (i.e., the number density increases) as the expanding bubbles split to preserve their stable size. The viscous shear of the liquid in

relative motion past the bubble causes the bubble surface and interior to move in a top-to-bottom rotation.

It is assumed that the inlet gas comes into thermal equilibrium with the pool almost instantaneously in the vent exit region. When this results in steam condensation in the inlet gas, aerosol particles and iodine vapors are removed in proportion to the reduction in the volumetric flow rate. Particle capture also occurs when the injection velocity is large because inertia forces the particles into the front boundary of the rapidly decelerating globules. For multihole vents with small orifices, centrifugal, diffusional and gravitational deposition are evaluated during gas injection because they are significant at the large velocities achieved. Details of globule formation and vent exit region scrubbing are given in Appendix D.

Scrubbing in the swarm rise region is evaluated by numerically marching through the region in several discrete spatial steps. At the beginning of each step, the fraction of the inlet gas that is still contained in the initial globule is determined. The remainder is assumed to be contained in bubbles. During each step the thermal hydraulic conditions within the bubbles are updated and used to evaluate the incremental removal of particles and iodine vapors during the step. The particle removal mechanisms modeled in the bubble include centrifugal and diffusional deposition and gravitational sedimentation. These mechanisms generate a flux of particles toward the bubble surface, where they are removed by absorption into the pool. The particle flux may be hindered by a flux of water vapor into the bubble, if evaporation is occurring at the bubble surface. Conversely, condensation onto the particles within the bubble because of supersaturation from bubble expansion will enhance particle removal. The vapor removal mechanism is diffusion, which also may be hindered if there is an evaporative flux into the bubble. The removal factor for each particle size and iodine vapors during the step is given by:

$$DF_{SR,i} = \frac{1}{f_{gl} + (1 - f_{gl})/DF_{BB,i}} \quad (2.72)$$

where

$DF_{BB,i}$ = removal factor inside the bubble

f_{gl} = fraction of inlet gas still in the initial globule

The cumulative removal factors for each particle size and iodine vapors in the swarm rise region are given by the product of the incremental removal factors at each step. Details of transient bubble behavior and particle scrubbing in the bubbles are given in Appendix E. Details of iodine scrubbing in the bubbles are given in Appendix F.

RN Package Reference Manual

The overall removal factor for each particle size and iodine vapors in the vent exit and swarm rise regions is given by:

$$DF_{OV,j} = DF_{EC} \cdot DF_{II,j} \cdot DF_{ER,j} \cdot DF_{SR,j} \quad (2.73)$$

where

DF_{EC} = DF from steam condensation in the vent exit region

$DF_{II,i}$ = DF from inertial impaction (of particles only) in the vent exit region

$DF_{ER,i}$ = DF from centrifugal, diffusional and gravitational capture (of particles only) in the vent exit region

$DF_{SR,i}$ = cumulative DF in swarm rise region

The overall removal factor for all particle sizes is obtained by dividing the sum of the inlet mass rates over all sizes by the sum of the outlet mass rates (the inlet rates for each size divided by the overall removal factor for that size) over all sizes:

$$DF_{OV,part} = \frac{\sum_{i=1}^{NBINS} \dot{m}_{part,i}}{\sum_{i=1}^{NBINS} \left(\frac{\dot{m}_{part,i}}{DF_{OV,i}} \right)} \quad (2.74)$$

2.7.2 Filters

The MELCOR RN package contains a simple filter model. When aerosols and vapors are transported through flow paths with the bulk fluid flow of pool and/or atmosphere calculated by the CVH package, some fraction of the transported RN materials may be removed by the action of filters in the flow path. A single filter can remove either aerosols or fission product vapors, but not both. However, a flow path can contain more than one filter. The efficiency of each filter is defined by decontamination factors, specified by user input. By default, a single decontamination factor is applied to all RN classes *except* water, for which the default DF is 1.0. Additional user input may be used to modify the DF on a class-by-class basis, *including the water class*. The parameters for the filter characteristics are specified on the RN2FLTXXYY input record series.

A maximum loading may be specified for each filter; when this loading is reached, no further RN materials will be removed (i.e., the DF is set to unity).

The effect of filter loading on the flow resistance of the associated flow path may be modeled through user input. This requires construction of a control function to link the laminar loss coefficient for the flow path (SLAM, input on segment record FLnnnSk; see the FL Package Users' Guide) to the filter loading. The filter loading may be obtained from one or more of the RN2-AMFLT or RN2-VMFLT control function arguments described in Section 5 of the RN Package Users' Guide.

The decay heat energy from radionuclides deposited on filters is given to the downstream control volume according to the vapor flow direction.

2.7.3 Sprays

The containment spray model used in MELCOR is the same as that in the HECTR code. The MELCOR Containment Sprays (SPR) package, which calculates the thermal-hydraulic behavior associated with spray systems, is coupled to the RadioNuclide package for the calculation of aerosol washout and atmosphere decontamination by the sprays.

The SPR Package Reference Manual describes the thermal-hydraulic modeling of the spray systems. To summarize here, the spray droplets are assumed to be spherical and isothermal and to fall through containment at their terminal velocity without a horizontal velocity component. Droplet heatup and cooldown in a steam environment are modeled using a correlation for forced convection heat transfer coefficients. Similarly, evaporation and condensation are modeled using a correlation for mass transfer coefficients. A standard integrator is used to integrate these transfer rates over the fall height of the spray droplet to obtain the final droplet mass and temperature. By comparing the droplet mass and temperature at the bottom of the compartment to the inlet conditions, the heat and mass transfer to a given droplet is computed. Total heat and mass transfer rates are calculated by multiplying the rates for one droplet by the total number of droplets of that size and summing over all droplet sizes.

The SPR-RN interface may produce nonphysical results if the SPR package is required to make multiple passes (numerically) through the same control volume on a given timestep. Therefore, the user is strongly encouraged to avoid this situation by limiting the spray activity to a single drop size in each spray train. The user must also ensure that only one spray train passes through each control volume. These restrictions are necessary only when the SPR and RN packages are used at the same time.

The particulate removal by sprays is a mechanistic treatment of removal processes, closely coupled to the thermal-hydraulic behavior calculated by the spray package. The user is cautioned to use a single drop size and a single spray train per volume because of the method by which the RN removal calculation is "piggybacked" onto the Spray Package thermal-hydraulic calculations. Specifically, the thermal-hydraulic stepwise integration over the spray train height is made first, then the RN removal processes are calculated by a simple trapezoidal integration over the step, using the appropriate end-of-interval values.

RN Package Reference Manual

Because each droplet size is integrated over the full height of fall separately, there exists the possibility of competing radionuclide removal by differing drop sizes and competing removal by different spray trains.

The particulate removal from sprays is modeled as a first-order rate process,

$$\frac{dM_k}{dt} = -\lambda_{k,i} M_k \quad (2.75)$$

where

M_k = mass of class k

$\lambda_{k,i}$ = rate constant, class k , droplet size i

The actual physical removal processes for vapors and aerosols are different and therefore different rate constants, λ , are associated with each process.

Vapor removal by adsorption is calculated using a stagnant film model for the adsorption efficiency. The vapor removal is calculated as an injection spray removal rate; no recirculation of spray liquid is considered. The expression for the rate constant is [24, 25, 26]:

$$\lambda_{k,i} = \frac{F_i E_{k,i} H}{V} \quad (2.76)$$

where

F_i = volumetric flow rate for droplets of size i

$E_{k,i}$ = adsorption efficiency for vapor class k

H = partition coefficient for partition of the vapor between spray water and gas

V = volume of control volume

The vapor absorption efficiency is given by the expression [27]

$$E_{k,i} = 1 - \exp \left[-\frac{6 k_g t_e}{2 r_i (H + k_g / k_l)} \right] \quad (2.77)$$

where k_g , the gas boundary layer mass transfer coefficient, is calculated using the Ranz and Marshall approximation [28] to the Frossling equation [29],

$$k_g = \frac{D_{k, gas}}{2r_i} (2.0 + 0.060 \text{ Re}^{1/2} \text{ Sc}^{1/3}) \quad (2.78)$$

and k_ℓ , the liquid boundary layer mass transfer coefficient, is calculated using Griffith's approximation for diffusion in a rigid drop [30],

$$k_\ell = \frac{\pi^2 D_{k, H_2O}}{3r_i} \quad (2.79)$$

In these equations,

r_i = drop radius

t_e = drop exposure time

$D_{k, gas}$ = diffusivity of vapor k through bulk gas

D_{k, H_2O} = diffusion constant for vapor k in liquid water

Re = Reynolds number, $2 \rho_g v_d r_i / \mu_g$

Sc = Schmidt number, $\mu_g / \rho_g D_{k, gas}$

v_d = drop velocity

Under LWR accident conditions, iodine may exist as a vapor over relatively long time periods in containment pressure/temperature conditions. Other materials have low vapor pressures at accident conditions that preclude their extended existence as vapors; that is, they will condense to aerosol forms quickly. The RN input record series RN2SPRXX allows the user to specify a limit on iodine adsorption by spray droplets using a partition coefficient. The partition coefficient for iodine, defined as the equilibrium ratio of the iodine density in the liquid to its density in the gas,

$$H = \rho_{l, eq} / \rho_{g, eq} \quad (2.80)$$

RN Package Reference Manual

is specified by the user for sprays containing different additives, with various recommended values ranging from 500 to 100,000 [31] listed in the RN Package Users' Guide.

Aerosol removal is calculated primarily by inertial impaction and interception; diffusiophoresis and diffusion effects are also included. No droplet interactions are considered. Impaction and interception are the primary removal mechanisms as long as droplet radii are in the 10 – 100 micron size range. From 1 – 10 microns diffusiophoresis becomes an important contributor; diffusion only becomes important for droplets with radii < 0.1 micron. The expression for the rate constant is [31]

$$\lambda_{k,i} = \frac{3F_i h E_{i,j}}{4Vr_i} \quad (2.81)$$

where F_i , V , and r_i are as defined before, h is the fall height of the drops, and E_{ij} is the efficiency of collection of aerosol particles in size section j by drops of size i .

For viscous flow around a sphere, the collection efficiency for interception (denoted by subscript ln) is given by the expression [32]

$$\varepsilon_{ln,vis} = (1+l)^2 \left[1 - \frac{3}{2(1+l)} + \frac{1}{2(1+l)^3} \right] \quad (2.82)$$

where $l = r_p / r_d$ and r_p and r_d are the radii of the particle and the drop, respectively.

For potential flow around a sphere, the collection efficiency for interception is given by the expression [32]

$$\varepsilon_{ln,pot} = (1+l)^2 - (1+l) \quad (2.83)$$

For potential flow around a sphere, the collection efficiency for inertial impaction (denoted by subscript lm) is given by the expression [33]

$$\varepsilon_{lm,pot} = \left[\frac{Stk}{Stk + 0.5} \right]^2 \quad (2.84)$$

for $Stk \geq 0.2$, is zero for $Stk \leq 0.0834$, and is given by interpolation for $0.0834 < Stk < 0.2$. For viscous flow around a sphere, the collection efficiency for inertial impaction is given by the expression [32]

$$\varepsilon_{Im,Vis} = \left[1 + \frac{0.75 \log_e (2 Stk)}{Stk - 1.214} \right]^{-2} \quad (2.85)$$

for $Stk > 1.214$, and is zero otherwise. Stk is the Stokes number,

$$Stk = \frac{2 r_p^2 \rho_p (v_d - v_p)}{9 \mu r_d} \quad (2.86)$$

where v_d and v_p are the terminal settling velocities of the drop and particle, respectively, and μ is the bulk gas viscosity. An interpolation scheme from Reference [33] is used to combine the potential and viscous efficiencies for both interception and inertial impaction:

$$\varepsilon_x = \frac{\varepsilon_{x,Vis} + \varepsilon_{x,Pot} (Re/60)}{1 + (Re/60)} \quad (2.87)$$

where Re is the drop Reynolds number and subscript x is either ln (interception) or lm (inertial impaction).

The collection efficiency due to diffusion is given by the expression [25]

$$\varepsilon_{diff} = 3.02 Re^{1/6} Pe^{-2/3} + 1.14 (Re/Pe)^{1/3} I + 0.57 Re^{1/3} I^2 \quad (2.88)$$

where Pe is the Peclet number, $2r_d(v_d - v_p)/D$.

The collection efficiency due to diffusiophoresis is given by the expression

$$\varepsilon_{diffusio} = \frac{4 r_d}{3 F h} \left[\frac{M_s^{1/2}}{X_s M_s^{1/2} + X_g M_g^{1/2}} \right] \frac{W_s}{c M_s} \quad (2.89)$$

where W_s is the mass condensation rate of steam on drops, M is molecular weight, X is mole fraction, c is the molar concentration of bulk gases, and subscripts s and g refer to steam and noncondensable bulk gases, respectively.

Finally, the collection efficiencies for different processes are combined using the following expression

$$E_{i,j} = 1 - \prod_k (1 - \varepsilon_{ijk}) \tag{2.90}$$

where subscript *k* refers to the collection process.

2.8 Fission Product Chemistry

Chemistry effects can be simulated in MELCOR through the use of *class reactions* and *class transfers*. The class reaction process uses a first-order reaction equation with forward and reverse paths. The class transfer process, which can change the material class or location of a radionuclide mass, can be used to simulate fast chemical reactions. With these two processes, phenomena including adsorption, chemisorption, and chemical reactions can be simulated.

Note: Only fission product vapors are considered in the chemistry models.

2.8.1 Class Reactions

The reaction process model in MELCOR is a first-order reversible reaction for a class going from state *C* in the gas-phase to state *C₁* on a surface, or

$$\frac{dM_c}{dt} = - \left(\frac{k_m A / V}{k_m A / V + k_f} \right) (k_f M_c - k_r M_{C_1}) \tag{2.91}$$

where

- k_m* = mass transfer rate constant for the process, based on the mass transfer coefficient calculated by the HS Package, (m/s)
- k_f* = forward reaction rate constant from user input, (s⁻¹)
- k_r* = reverse reaction rate constant from user input, (s⁻¹)
- A / V* = surface-to-volume ratio, where the surface area is that for the reaction and the volume is that of the control volume (m⁻¹).

The mass transfer rate constant is calculated in the same manner as the vapor condensation/evaporation diffusivity given in Section 2.5.

The solution technique is the same as for vapor condensation/evaporation under the assumption that the mass of *C₁* does not change during the timestep. This assumption

avoids solving a differential equation and allows the use of the same algebraic solution given in Section 2.5.

Alternatively, if the user specifies the use of a deposition velocity instead of the forward and reverse reaction rate constants,

$$\frac{dM_c}{dt} = -V_d(A/V)C = -\frac{dM_{c1}}{dt} \quad (2.92)$$

where V_d is the user input reaction deposition velocity in m/sec.

The reaction only occurs in user-specified control volumes and depends on the availability of the various classes as determined by the user input reaction stoichiometry. The first "from" class in the reaction must be in the vapor phase, while all the other specified classes must be deposited on the surface when the reaction occurs. Surfaces that can undergo reactions include heat structures, the pool surface, and aerosol surfaces as specified by the user. A flag to specify whether the reaction still occurs when a water film is present is also available. At the present time, water mass should not be used in the class reaction model.

In addition to the masses, reaction energy can also be specified for both the forward and reverse directions. The energy is in terms of the mass of the first "from" reacting class. This energy is added to the atmosphere in the case of reaction with aerosols, to the pool for a pool reaction, and to the heat structure if a surface reaction occurs.

2.8.2 Class Transfers

Mass transfers between classes may be accomplished by the transfer mechanisms. The user may change the class and location of aerosols and/or vapors in an arbitrary fashion. Therefore, this feature must be carefully used.

A stoichiometric reaction is specified, and the permitted control volumes and "from" and "to" states are given. The permitted states are aerosols or condensed vapors on a given surface of a heat structure, or aerosols or vapors in either the atmosphere or pool. A flag to determine if the transfer will proceed with a water film present is also available. Water should not be used in the class transfer model.

The mass transfer rate is given by the user as is the energy transfer information. The masses are changed as follows:

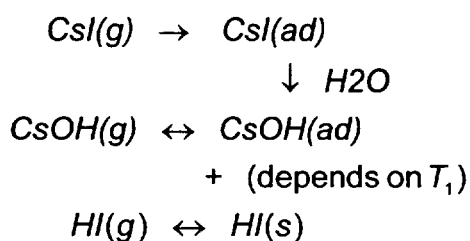
$$M_{from, t + \Delta t} = M_{from, t} - \frac{dM}{dt} \Delta t \quad (2.93)$$

$$M_{to, t+\Delta t} = M_{to, t} + \frac{dM}{dt} \Delta t \quad (2.94)$$

where dM/dt is the user-specified mass transfer rate. Thus, with this option, aerosols of Class A in the pool may be, for example, changed into condensed vapors of Class B on a heat structure. This model is used for fast reactions with the "from" and "to" state generally the same.

2.8.3 Example

As an example of both class reactions and class transfers, consider the adsorption of CsI on a surface with a known deposition velocity which is then transformed immediately to CsOH plus HI when adsorbed water is present. After the transformation, the revaporization of CsOH is delayed until the surface temperature reaches T_1 while the HI revaporization is simply mass transfer limited. In this case, CsI, CsOH, and HI are separate material classes, and the reaction diagram can be written as



where (g), (ad), and (s) are gaseous, adsorbed, and solid states, respectively.

This reaction can be simulated by the RN package by the following sequential class reactions and transfers:

$\text{CsI}(g) \rightarrow \text{CsI}(ad)$	rate constant for adsorption is supplied through input
$\text{CsI}(ad) \rightarrow \text{CsOH}(ad) + \text{HI}(s)$	instantaneous and complete transfer between classes when water is present. Note that the water mass is not included in the model; water mass is not explicitly conserved.
$\text{CsOH}(g) \rightarrow \text{CsOH}(ad)$	rate constant for adsorption supplied or condensation limited
$\text{CsOH}(ad) \rightarrow \text{CsOH}(g)$	reaction with zero rate constant below T_1 positive value or instantaneous above T_1
$\text{HI}(s) \leftrightarrow \text{HI}(g)$	controlled by condensation/evaporation

2.9 Chemisorption on Surfaces

The chemisorption model is implemented as a finite-difference version of the equations in [34]. The relevant radionuclide classes that are chemisorbed are removed from the vapor mass arrays and stored in chemisorption arrays. The chemisorption arrays correspond to six chemisorption classes. In accounting for radionuclide mass and decay power, the chemisorption classes are mapped back to the corresponding radionuclide class, so chemisorption output edits are ordered by the radionuclide class rather than by chemisorption class. Chemisorption shows up in the output edits as an additional column in the radionuclide mass edits.

2.9.1 Implementation

There are six chemisorption classes corresponding to the first six chemisorption equations in Table 1 of [34]. There is a mapping array that establishes the correspondence between the chemisorption classes and the radionuclide classes. The radionuclide classes are CsOH (2), I₂ (4), and the user-defined class used to model CsI (usually 16). There is no HI radionuclide class, and hence chemisorption class 5 is mapped to radionuclide class 4. There also is an array that establishes the type of surface material for the chemisorption class; at present, this only contains mapping for stainless steel and Zircaloy, although this could be extended by adding more materials to the database or by implementing a method of mapping between user-defined materials and the chemisorption classes.

The chemisorption rate equation is

$$\frac{dM_{ij}}{dt} = A_i k_{ij} C_j \quad (2.95)$$

M_{ij} = mass of species j chemisorbed on surface i (kg)

A_i = area of surface i (m²)

k_{ij} = chemisorption coefficient of species j on surface i (m/s)

C_j = concentration of species j in atmosphere (kg/m³)

The mass chemisorption coefficient k_{ij} is temperature dependent and is given as

$$k_{ij} = a_{ij} e^{-E_{ij}/RT_i} \quad (2.96)$$

where

a_{ij} = chemisorption coefficient for species j on surface type i (m/s)

RN Package Reference Manual

- E_{ij} = activation energy for species j on surface type i (J/kg)
 T_i = temperature of surface i (K)
 R = universal gas constant (8314 J/kg-K)

As implemented, a finite-difference equation of the form

$$M_{ij}^n = M_{ij}^0 + \Delta t A_i k_i(T_i) C_j \quad (2.97)$$

is used to advance the chemisorption equations in time. These equations are applied sequentially in each control volume, for each surface, for each chemisorption class. After all equations are applied in a given volume, the total chemisorbed for each vapor radionuclide class is checked to ensure that the total is not greater than the total vapor mass; the chemisorbed masses for the current timestep are reduced by the ratio of vapor mass to chemisorbed mass if this occurs. The chemisorbed masses are then subtracted from the corresponding radionuclide vapor mass to complete the timestep.

2.9.2 Comparison to Exact Solution

An exact solution to the chemisorption equations can be found over a timestep for comparison to the numerical solution given above. Briefly, noting that the change in mass of a given species chemisorbed on a given surface is the same as the negative change in the species in the vapor phase, that the vapor concentration is the vapor mass divided by the component volume, and that the sum of the changes over all surfaces is the total change in vapor mass, the chemisorption equations can be summed and written in terms of the vapor species mass as

$$\frac{dM_j}{dt} = -\frac{M_j}{V} \sum_i k_{ij} A_i \quad (2.98)$$

Defining an effective chemisorption rate for species j as

$$(kA)_j = \frac{1}{V} \sum_i k_{ij} A_i \quad (2.99)$$

The solution to the above equation is

$$M_j(t) = M_j^0 e^{-(kA)_j t} \quad (2.100)$$

where

M_j^0 = vapor mass at time zero (kg).

If we apply the exact equation over a timestep and expand in a Taylor series about the beginning of the timestep, we have

$$M_j = M_j^0 [1 - \Delta t (k A)_j + \dots] \quad (2.101)$$

after dropping higher powers of the timestep. This can be compared to the result of applying the finite-difference equations, which can be written as the sum also:

$$M_j = M_j^0 \left(1 - \Delta t \frac{1}{V} \sum_i k_{ij} A_i \right) = M_j^0 [1 - \Delta t (kA)_j] \quad (2.102)$$

Comparison of the two above equations shows that the finite-difference result is the same as the Taylor series expansion of the exact solution carried out through linear terms of the timestep. At this point, it might be asked, why not use the exact solution? This is not done because this is an exact solution for the change in the vapor mass, not the change in chemisorbed mass for each surface. The change in chemisorbed mass for each surface in the control volume cannot be backed out of the vapor solution.

An exact solution for each surface could be formed, given the assumption that the vapor mass remains constant over the timestep; these could then be summed, leading to an equation for vapor mass involving the sum of the exponents, rather than the exponential of the sum. When expanded in a Taylor series, this results in the same equation as the above equation.

The above expansion in Taylor series gives a criterion for the accuracy of the solution:

$$\frac{k_{ij} A_i}{V} \Delta t \ll 1 \quad (2.103)$$

The chemisorption coefficients are much less than 1, barring user input error (the largest coefficient, CsOH on stainless steel, is about 0.01 at 2500 K). The ratio A_j/V is less than 1 provided $V > 1 \text{ m}^3$; for typical MELCOR timesteps of 1 to 5 s, the lower limit on V for the above inequality to hold is about 1 cc, so it appears that the above will be true except for very small volumes.

2.9.3 Implementation Restrictions

As implemented, there is no provision for revaporization of chemisorbed species. Chemisorbed species will thus stay on the absorbing surface. The first six chemisorption equations listed in the design report, Table 1, are implemented as the default classes in the model, because the deposition coefficients for tellurium, rows 7 and 8 in Table 1, are zero. Also, the model is set up to use the materials in the MELCOR material properties database as surface materials. As presently coded, surfaces consisting of user-defined materials cannot be made active for chemisorption because there is no method to relate them to the chemisorption classes. Also, the database does not contain Inconel, which means that only chemisorption of CsI, CsOH, HI, and I₂ on stainless steel and Zircaloy can occur. The coding framework is set up to use Inconel if it is added to the database in the future.

As noted in [39], there was no trace of iodine when CsI was chemisorbed on stainless steel. This means that, realistically, the iodine mass from the CsI should be transferred to the HI or I₂ class when chemisorbing. In the present model, the iodine from the chemisorbed CsI is transferred to the condensed iodine class, so that it will be released on the next timestep. Because the CsI chemisorbed class is mapped to the CsI vapor class, and this class is treated separately in MELCOR from the Cs and iodine element classes, the chemisorbed Cs is transferred to the corresponding chemisorbed CsOH class (there currently are two each, for stainless steel and Inconel surfaces). This has two consequences: the CsI chemisorbed class is always zero, with the Cs showing up in the CsOH class, and the CsOH class must be active if the CsI class is active (this is the default).

2.10 Hygroscopic Aerosols

Aerosol particles that are soluble in water exhibit hygroscopic properties such that they can absorb moisture from an atmosphere with relative humidity less than 100%. This effect will lead to a growth of the particle size as water vapor condenses onto the soluble particle. An important consequence of this growth in size (and mass) is an increase in the gravitational settling rate, and the subsequent depletion of airborne fission product aerosols.

The hygroscopic model in MELCOR is based on the Mason equation describing the diffusion of water vapor molecules to the surface of an aerosol particle, and the conduction of the latent heat of vaporization away from the particle and to the bulk atmosphere. The model presented here includes the solubility (hygroscopic) effect. In addition, the Kelvin effect, (surface tension) as well as noncontinuum (free molecule) effects, both of which are important for very small particle sizes, are considered.

In MELCOR 1.8.5, some improvements to the earlier MELCOR 1.8.4 implementation of the hygroscopic effect are included. Principally these include an updated and generalized method for calculating the chemical activity of the soluble particle, and a means of

calculating a mean hygroscopic effect that considers the fact that not all aerosol materials are soluble and that multi-component aerosols can be comprised of varying proportions of soluble and non-soluble materials.

2.10.1 The Mason Equation for Particle Growth

The Mason equation [35] describes the rate of condensation or evaporation of water on an aerosol particle of radius r as:

$$\frac{dr}{dt} = \frac{1}{r} \frac{(S - S_r)}{a + b} \quad (2.104)$$

where,

$$S_r = A_r \cdot \exp\left(\frac{2M_w\sigma}{RT_\infty\rho_w r}\right). \quad (2.105)$$

In the Mason equation, S is the atmosphere saturation ratio, or relative humidity and S_r is the effective saturation ratio at the particle surface. (*Note to reader: a subscript "r" from here on indicates that the quantity is size or radius dependent.*) The term $(S - S_r)$ is the driving potential for condensation or evaporation. If the difference is positive, condensation will occur and if the difference is negative, evaporation takes place. The S_r term is a function of the chemical activity of the solution, A_r , which varies with the concentration of the solute (dissolved solid) within the solvent (water). The exponential term represents the Kelvin effect which resists condensation for small particles due to surface tension effects.

In Eq. (2.104), the terms a and b determine the time constant for the particle growth rate and are defined as:

$$a = \left(\frac{\Delta h_f^2 M_w \rho_w}{RT_\infty k_a}\right) \quad (2.106)$$

$$b = \left(\frac{RT_\infty \rho_w}{D_v^* M_v \rho_{sat}(T_\infty)}\right). \quad (2.107)$$

The term a accounts for the thermal conduction of the latent heat associated with condensation from the particle to the atmosphere, and the term b accounts for the diffusion of water vapor from the atmosphere to the particle surface. The other terms are defined in the following list of variables.

$$D_v^* = \text{effective vapor diffusion coefficient}$$

RN Package Reference Manual

k_a^*	=	effective thermal conductivity of atmosphere
M_w	=	molecular weight of water
T_∞	=	bulk atmosphere temperature
$P_{\text{sat}}(T_\infty)$	=	saturation pressure of bulk atmosphere gas
R	=	gas constant
r	=	particle radius
S	=	atmosphere saturation ratio (RH/100)
S_r	=	saturation ratio at particle surface
ρ_w	=	density of water
Δh_f	=	heat of vaporization of water
σ	=	water surface tension

The activity, A_r , is a function of the concentration of the solute and is the dominant term in the driving potential for condensation or evaporation, S_r . In the MELCOR 1.8.4 [36] implementation, the activity was estimated using the van't Hoff formula as follows:

$$A_r = \frac{1}{1 + \sum_i \frac{l_i n_i}{n_w}} \quad (2.108)$$

where n_i is the moles of solute i , n_w is moles of water, and l_i is the van't Hoff ionization constant for solute i . An important limitation in the 1.8.4 model was the fact that the sum in Eq. (2.108) in effect was "simplified" by assuming that all aerosols were soluble and all had the same ionization factor. Hence, the effective form for calculating activity in MELCOR 1.8.4 was:

$$A_r = \frac{1}{1 + \frac{l_s n_s}{n_w}} \quad (2.109)$$

where the subscript "s" refers to soluble aerosol (and all aerosols were considered soluble). In the present MELCOR 1.8.5 model, a generalized and more contemporary form for the activity is used as follows:

$$A_r = \exp \left[- \sum_i \frac{v_i n_i}{n_w} \right] \quad (2.110)$$

where,

n_s, n_i = moles of dissolved solute in wet particle (may be less than total)

- n_w = moles of water on wet particle
 v_i = ionization factor for solute molecule (usually 2).

Note that Eq. (2.108) constitutes a linear approximation of Eq. (2.110) for dilute solutions. The van't Hoff factors provided some correction to the linearization for concentrated solutions. In Eq. (2.110) the term v_i represents the number of ions formed when the solute becomes dissolved. This value is normally 2. The form for activity in Eq. (2.110) is more commonly encountered in chemistry texts describing the solute effect and is similar to that used in the CONTAIN [37] model for hygroscopic growth. Additionally, the present activity form estimates a *net* activity that is a mole weighted average of all aerosol materials within a given size range - soluble and insoluble. Finally, the value of n_i in the present model is limited by the saturation solubility of the aerosol component i . The importance of the revised activity formula is as follows. If the aerosol materials are insoluble or of low solubility, the aerosol will exhibit low hygroscopic behavior, and if the proportion of soluble materials in the aerosol composition is large, then a proportionally larger hygroscopic effect will result. This replaces the "all or none" treatment that was present in the MELCOR 1.8.4 model.

The activity term, A_r , is a function of the wet particle radius since, as the particle grows by condensation of water, the concentration of the solute decreases. When the soluble particle is virtually dry, any water on the drop acquires a concentration of dissolved solute that is limited to the maximum solubility of the solute (that is, the solution is saturated with solute). At this point the chemical activity is at its lowest value, and as a result, the driving potential, $S - S_r$, is at its highest value. Until sufficient water is acquired to completely dissolve the aerosol solid material, the activity remains at this minimum value. However, after this point the concentration of the solute begins to drop below the saturation value, resulting in an increase in the activity. When infinitely dilute, the activity approaches 1. In general, the value of S_r is dominated by the activity. As the particle acquires more water, the value of S_r increases thereby increasing the atmospheric humidity necessary to drive further condensation.

2.10.2 Transition Regime Corrections to the Mason Equation

The particle growth rate equations (2.104) - (2.107), make use of *effective* values for the air thermal conductivity and the diffusion coefficient for water vapor molecules in moist air. These effective values approach the nominal conductivity and diffusion coefficient values when the aerosol particle radius is large in comparison to the mean free path of the water vapor molecules. However, when the aerosol particle radius is on the order of the vapor molecule mean free path, these factors introduce correction terms to the otherwise continuum regime Mason model. Based on the derivation presented in Prupracher and Klett [35], the effective values of thermal conductivity and diffusion coefficient are determined by:

$$\dot{k}_a = \frac{k_a}{\left(\frac{r}{r + \Delta_T}\right) + \left(\frac{k_a}{r \alpha_T \rho_a c_{p,a}} \left(\frac{2\pi M_a}{RT_a}\right)^{1/2}\right)} \quad (2.111)$$

$$\dot{D}_v = \frac{D_v}{\left(\frac{r}{r + \Delta_v}\right) + \frac{D_v}{r \alpha_c} \left(\frac{2\pi M_a}{RT_a}\right)^{1/2}} \quad (2.112)$$

where

- α_c = 0.036, the condensation coefficient,
- α_T = 0.7, thermal accommodation coefficient,
- $c_{p,a}$ = atmosphere constant pressure specific heat,
- λ = vapor molecular mean free path,
- Δ_v = vapor jump distance $\approx 1.32\lambda$,
- Δ_T = thermal jump distance $\approx \lambda$, and
- M_a = atmosphere molecular weight.

2.10.3 MELCOR Solution to the Mason Equation

In the MELCOR implementation of the Mason expression, Eq.(2.104) is rewritten as

$$\frac{dr^2}{dt} = \frac{2 \cdot (S - S_r)}{a + b} \quad (2.113)$$

which, when expressed in an implicit backwards difference form becomes:

$$\left(r_{new}^2 - r_{old}^2 \right) = \frac{2 \cdot (S - S_r)}{a + b} \cdot (t_{new} - t_{old}) \quad (2.114)$$

where all of the right hand side terms are evaluated at the end of time step conditions. A zero-finder routine is used to solve for the new value of r^2 that results in a value for S_r satisfying Eq. (2.114). This numerical method is fast, stable and the small amount of "undershooting" that results from the backward difference is inconsequential in that the characteristic time associated with Eq.(2.113) attaining steady state is short in comparison to a typical MELCOR time step.

2.10.4 User Suggestions Concerning Use of the Hygroscopic Model

MELCOR uses Eq.(2.114) to predict the growth of a representative particle in each of the size sections, and from this determines a section to section mass transfer that reflects this growth. MELCOR uses MAEROS to perform other aerosol dynamics calculations including agglomeration and deposition. Understanding the overall model requires understanding a little about MAEROS. The user is encouraged to review the sections in this manual pertaining to the MAEROS model. For convenience, the following review is given. MELCOR of course uses a **Class** grouping to represent fission product species which have common physical/chemical characteristics such as volatility. MELCOR's aerosol mechanics model (MAEROS) recognizes and operates on the aerosol portions of these fission product (radioactive and non-radioactive) classes. For the purposes of performing more economic aerosol mechanics calculations, MELCOR allows the user to define aerosol **Components**, which are groupings of one or more fission product **Classes**. These components are allowed to have distinct size distributions. The size distributions are characterized by the amount of aerosol mass within a range of aerosol particle sizes. These size ranges are referred to as **Sections**, or sometimes as size bins. MAEROS homogenizes the section populations of aerosol *classes* that are members of the same aerosol *component*, even if the user sources in the classes with different size distributions.

The hygroscopic growth model operates on the section populations without any consideration of the component definition. That is to say that all particles of all RN classes within a given *section* (regardless of their component assignment) are used to determine the mean activity using Eq. (2.110), which in turn is used to determine particle growth by condensation. As a result, all aerosol mass associated with all radionuclide *classes* that reside in a given size *section* are transferred to larger (or smaller) size sections proportionally by the hygroscopic growth routines.

This means that non-hygroscopic particles residing in a size section that is dominated by hygroscopic particles will be moved to different size sections along with their hygroscopic companions, and conversely, hygroscopic particles residing in a size section that is dominated by non-hygroscopic particles will be retained in the section to the extent determined by their non-hygroscopic companions. However, if hygroscopic and non-hygroscopic particles reside in different size sections (which can only be represented by MAEROS if they are assigned to different aerosol components), the two particle populations will behave independently. The hygroscopic particles will grow or shrink, depending on the relative humidity, while the non-hygroscopic ones will remain the same size (after losing any water that they may have contained). This makes it important that water and non-water aerosol components be assigned to different aerosol classes. The MELCOR 1.8.5 code release has a default configuration of 2 aerosol components, one for water class aerosol which will subsume fog droplets formed as a results of thermodynamic conditions in the atmosphere into the smallest size section, and one for non-water class aerosols. Three aerosol components are recommended if it is desired to track hygroscopic and non-hygroscopic aerosols that have different size distributions.

2.11 Iodine Pool Model

2.11.1 Introduction

The potential release of radioactive iodine as a result of a core damage accident in a nuclear power plant has long been a principal concern of reactor safety and consequence analyses. Iodine in particular is a concern because of its major contribution to the radiological hazard to the environment. A specific model devoted to the chemistry of iodine in reactor containments under accident conditions is needed in the MELCOR computer code because of the unique chemical properties of iodine and the severe consequence attributed to the release of the radioactive isotopes of iodine to the environment. Possible release of iodine has always played a significant role in the regulation of nuclear reactors. In early assessments of iodine consequences, it was assumed that iodine would be released to the reactor containment as a gaseous species. About one quarter of the initial core inventory was assumed to remain in the containment atmosphere, available for release to the environment. However, research over the last 15 years has shown it to be more likely that most of the iodine will be released to the containment atmosphere as aerosol particles, principally CsI. The Revised Accident Source Term (NUREG-1465) [38] assumes that at least 95% of the iodine reaching the containment is in aerosol form. Iodine within the containment atmosphere is able to pass through containment leak paths to the environment, thereby resulting in a dose to the public with ensuing consequences. Reduction of releases therefore requires control of atmospheric iodine concentration. This can be accomplished by causing the iodine to remain confined in aqueous forms in pools and sumps. Advanced reactor designs may incorporate chemical systems to keep the atmospheric concentration of iodine low by trapping iodine in aqueous forms and hence limit risk. An important use for MELCOR will be to assess the adequacy of these designs and identify processes and mechanisms that may defeat the intent of these systems.

Light water reactor containment temperatures can be expected to condense any residual cesium iodide vapors and form aerosols. These containments will also contain substantial quantities of water that can trap aerosol particles during severe accidents. For example, the condensation of steam formed during the core degradation processes will take place to a large extent within the containment. Trapping of most radionuclides in water effectively removes these radionuclides from further consideration in the analysis of the public consequences of reactor accidents by removing them from the containment atmosphere. However, radioactive iodine may not remain trapped in water because of its relatively dynamic chemical behavior. Engineered safety systems, such as sprays and suppression pools, are still effective mechanisms for scrubbing particulate iodine from the system and trapping it in the aqueous phase. However, there are important processes that can regenerate gaseous forms of iodine that release into the containment atmosphere from the water, thus becoming available for release to the environment for long times after the accident initiation.

The chemical and radiolytic oxidation of iodine in the pool can lead to the formation of a variety of chemical forms of iodine, such as elemental iodine and volatile organic iodides. The formation of volatile iodine in the pool is followed by a "partitioning" of the iodine between the pool and the atmosphere. This partitioning is important primarily in the longer term phases of the accident after the natural and engineered safety features have removed the other radioactive aerosols released during the accident. The formation of volatile forms of iodine in solution is dependent not only upon the dose rate to the aqueous phase but also on temperature, the hydrogen ion concentration (conventionally expressed as pH), and the total iodine concentration. It has been shown experimentally that large fractions of the iodine released from the reactor core can be expected to reside within the containment atmosphere in a volatile form when pH is not controlled to an alkalinity level greater than 7 [38]. It has also been observed that irradiation induced release of acids from the wall surface coatings, cable insulation, and the containment air lowers the pH [39]. However, the combination of high pH and high irradiation has not been thoroughly tested. In addition, the effect of other materials on the pool chemistry is not well established. Consequently, any model must be adaptable to the results of ongoing research. This fact is considered in the design of the MELCOR model, and provision is made to accommodate new information as it becomes available.

2.11.2 Features of Iodine Pool Model

The iodine pool model addresses these concerns. It embodies the current state of knowledge in a form that can be easily modified as current research yields results. It uses the known chemistry to predict what factors affect the iodine concentration in the atmosphere, while allowing for additional chemical reactions. In the containment atmosphere, where gas-phase behavior is important, there are submodels relating the radiolysis of the air and cable insulation to the generation of nitric acid and hydrochloric acid, respectively. On the structural surfaces, provision is made to account for the type of surface, thus allowing the extension to treat the effects of different paints and other surface coatings on iodine behavior. In the water pool, where liquid phase behavior is important, the model determines the pH based upon the user controlled boric acid and phosphate buffering, the effects of cesium hydroxide, cesium iodide and control rod silver released by the accident scenario chosen, and the effects of the acids introduced from the containment atmosphere due to radiolysis. The aqueous pool chemistry model then determines the speciation of iodine, particularly the important elemental, molecular, and organic forms, over the full range of pH. Thus, chemical systems that control pool pH can be examined as well as pools and films on surfaces that have no pH controls. With this combination of features, the iodine pool model allows for the ability to conduct sensitivity studies and incorporate new effects found in the course of ongoing research.

2.11.3 Criteria for Application of the Model

A MELCOR calculation typically involves several volumes with differing properties. When the model is invoked, it will be applied everywhere. The full model is used only in volumes with a pool, atmosphere, and iodine. Acid generation by radiolysis is still calculated in volumes with only an atmosphere, as these acids can be transported by MELCOR to other connected volumes. However, the aqueous chemistry model was designed for volumes where the pressure is less than 10 atm and the liquid temperature is less than 423 K, corresponding to conditions in a commercial reactor containment. If these limits are exceeded, the pool model becomes invalid. In such cases, the aqueous chemistry model is not used.

The effects of partitioning of iodine between the aqueous and gaseous phases is typically only important in the late term phases of an accident (after about 10 hours for the NUREG-1465 severe accident [38]). By this time, most of the iodine in a MELCOR calculation will have been transported to volumes where the pool model is valid. At earlier times, radionuclide behavior will be dominated by other phenomena. Thus, the limitations on the applicability of the aqueous chemistry model should have little impact on the ability to calculate the important phenomena in reactor accident sequences.

2.11.4 Detailed Description of the Model

The model involves four areas of modeling as shown schematically in Figure 2.2. The area labeled as one (1) indicates the transport of iodine species among the walls, the bulk gas, and the pool. This part of the model interacts directly with the MELCOR intra-cell mass transport coefficient (TRAP-MELT like) solution, and contributes to determining the structural surface concentration of the chemically and physically bound iodine species by using kinetic reactions to determine a transport rate. The change in pool depth from timestep to timestep changes in heat structure surface area, and transfer of iodine between pools and films is handled by existing MELCOR coding. The area labeled as two (2) is the containment atmosphere part of the model. It determines the radiolytic formation of acids and the gas-phase destruction and formation of iodine species. Species of iodine added to the cell atmosphere come from the pool, the structural surfaces, and adjacent cells (e.g., the reactor coolant system break location.) The area labeled as three (3) is concerned with the hydrogen ion concentration (i.e., pH), and accounts for the effects of the acids and bases introduced into the pool as well as the removal of iodine due to silver. The pH solution is typically dominated by the effect from the initial buffering of the pool. Thus, the model does not currently account for the hydrolysis of the other materials that may be in the pool, for example, cadmium, sludge, iron, and uranium. The area labeled as four (4) is the aqueous iodine chemistry model where the iodine, hydrogen, oxygen, carbon, iron, and electron balance equations are solved.

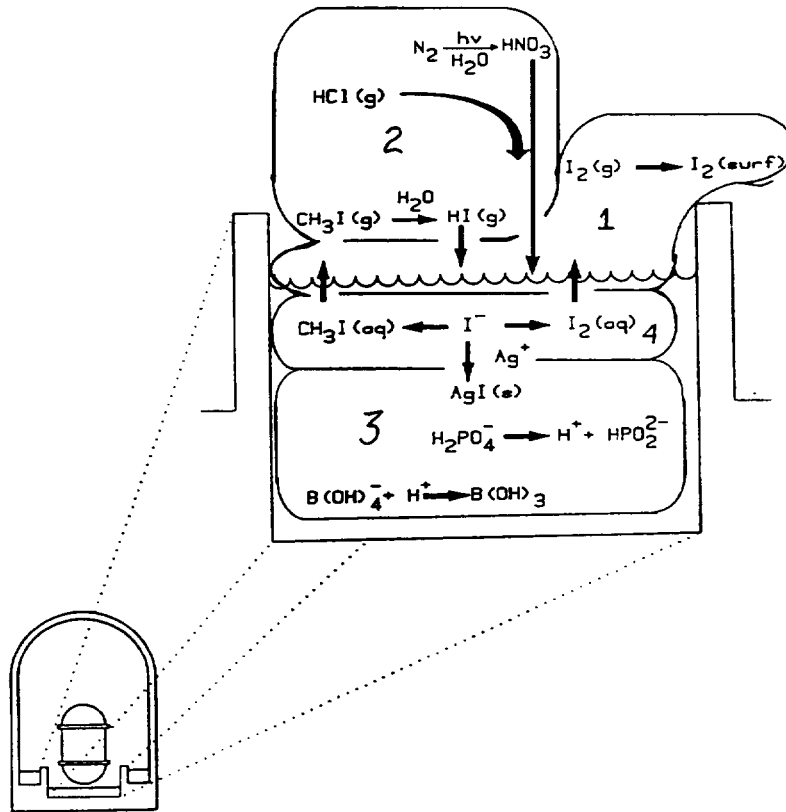


Figure 2.2 Schematic Representation of the Iodine Transformations Considered

The formulation chosen uses a dilute solution approximation that allows the effect of water radiolysis and radiolytic reactions to be explicitly included and should allow the results of current experimental studies to be compared. The approach adopted by Weber et al. [40] is modified here to include a more comprehensive set of chemical reactions and to explicitly include dose rate effects for the radiolysis while retaining the quasi-steady approximations for the dynamic equations.

2.11.5 Interaction with MELCOR

In MELCOR, intra-cell transport processes, for example condensation and aerosol deposition in a volume, is followed by inter-cell transport of material, for example silver and iodine moving from the reactor coolant system to the containment. The iodine chemistry model can be thought of in terms of intra-cell transport. The iodine model processes affect the distribution of iodine among the pool, the atmosphere, and the heat structures in

various control volumes. Thus, for a PWR, after a mix of water and radionuclides has been removed from the containment by deposition or through the action of the sprays and placed into the sump, this model allows MELCOR to distribute the iodine among the sump, the containment open volume, and the walls. Similarly, in a BWR, after the radionuclides have been placed in the wetwell, this model allows MELCOR to distribute the iodine among the suppression pool, the vapor space above it, and the wetwell walls.

Figure 2.3 shows the relationship between the iodine models and the balance of the MELCOR code. Volumes 1 and 2 are typical MELCOR hydrodynamic control volumes where a variety of processes take place. As shown for volume 1, these include scrubbing of aerosols from the atmosphere by sprays, deposition of aerosols onto structural surfaces with water films draining into the pool, and interface transport between pool and atmosphere. MELCOR also accounts for the transport of material between volumes. Not all MELCOR processes are shown; for example, the heat transfer processes are not indicated. None of these MELCOR processes will be affected by adding the iodine model. The iodine model performs aqueous chemistry calculations within existing pool regions of MELCOR control volumes. That is, based upon a species distribution and the radiation environment it determines the local pH and the quantity of elemental and organic iodine available at the pool-atmosphere interface. The model also performs vapor chemistry calculations within the existing atmosphere regions of MELCOR control volumes. That is, based upon a species distribution and the radiation environment, it determines the radiolytic formation of acids and destruction of iodine. These submodels are shown as the two add-on boxes above and below volume 1 in Figure 2.3. The model determines the transport and partitioning of the iodine species between the pool and atmosphere regions, allowing MELCOR to determine the late phase concentration of iodine in the atmosphere.

MELCOR determines the flux of important species into and out of all volumes within the inter-volume transport calculation. For the purposes of this model, important transported species include: the original thirteen (13) MELCOR radionuclide classes, used to determine the distribution of radiation sources in the control volume (xenon, cesium hydroxide, barium, elemental iodine, tellurium, ruthenium, molybdenum, cerium, lanthanum, uranium dioxide, cadmium, tin, and boron classes), four (4) species to control the hydrogen ion concentration in the pool (boric acid, cesium iodide, and phosphate are new; cesium hydroxide can be represented by existing class 2), four (4) in the atmosphere (methyl iodine, hydrochloric acid, and nitric acid are new; iodine is represented as class 4), two (2) deposited species (non-volatile form of iodine and methyl iodine to allow for surface chemistry), one (1) pool species which acts as a sink for iodine (silver, represented as existing class 12), and three (3) water pool chemistry species (silver iodine and methyl iodine are new; aqueous iodine is represented as class 4). There are many more species included in the aqueous pool chemistry model, including the two main species, elemental and molecular iodine; however, due to the equilibrium nature of the chemistry model, these species do not all need to be transported—the model is initialized at the beginning of a timestep by a small subset of the species, principally iodine, and creates the speciation for the conditions existing in the pool during that timestep. Obviously, these new species are

not all radionuclides and do not need to be examined in all code modules, i.e., they do not all need to be full RN classes. Table 2.5 shows some of the main and secondary species available from the model.

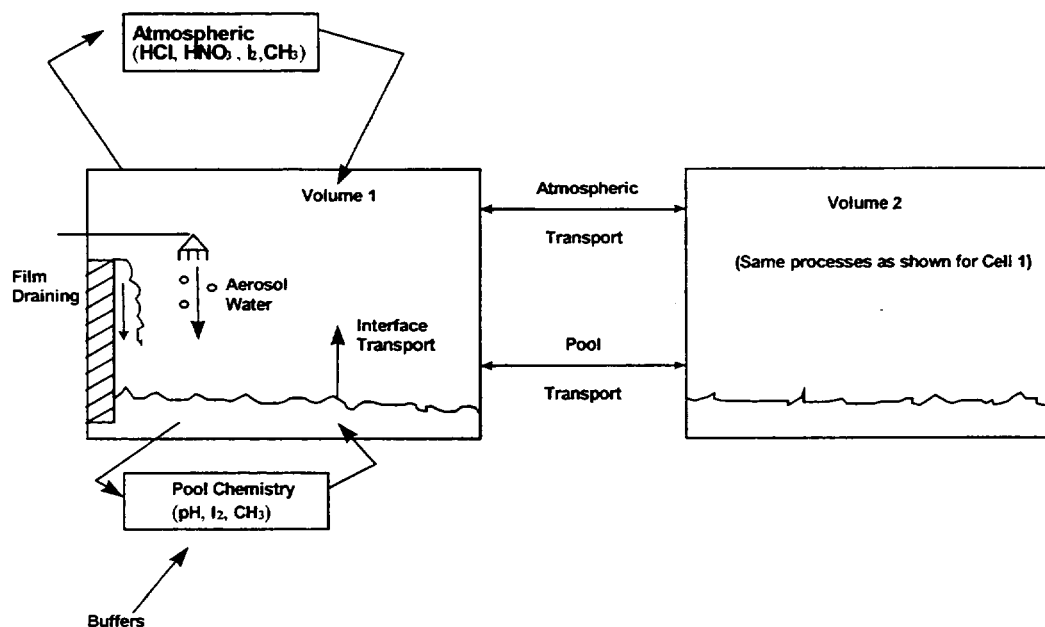


Figure 2.3 Interface between MELCOR and Iodine Pool Model

Table 2.5 Representative Species in Iodine Pool Model

Species	RN Class (Y/N)?	Species	RN Class (Y/N)?
I ₂	Y (4)	HOI-	N
I-	Y (4 or 16)	H ₂ O ₂	N
I ₃ -	N	O ₂ -	N
IO-	N	HO ₂ -	N
IO ₃ -	N	CH ₃ I	Y
I ₂ OH	N		

Classes 14 (water) and 15 (concrete) are included in the original RN list—even though they are not “radionuclides”—because they form aerosols. Many current calculations include cesium iodide as a user-defined 16th class. CsI has been changed as part of the iodine pool model update to be a default RN class.

RN Package Reference Manual

Transport of air and water, also used by the iodine pool model, is done by the MELCOR hydrodynamics module CVH. To use the pool model, it is necessary that the atmosphere components hydrogen, methane, and carbon dioxide be initialized in MELCOR input, as well as the usual atmosphere constituents (nitrogen, oxygen, and steam).

MELCOR determines the liquid, vapor, and heat structure surface temperatures and vapor pressure within the volume, within the energy transport calculation. With this information, the iodine models determine the intra-cell transport coefficients for the iodine species, that is, those coefficients determining the transport of elemental and organic iodine between the pool and the vapor space and between the vapor space and the heat structures. The model also determines the change from volatile to non-volatile iodine species on the surfaces, the change from one iodine species to another in the pool (including silver iodide), and the homogeneous destruction of iodine species in the atmosphere.

2.11.6 Order of Calculation of Model

The order of calculation in a control volume for the model is shown in Figure 2.4. This figure shows that the main functions of the model are carried out in a simple consecutive order, starting with the check for atmosphere volume in the upper left corner (Block 1) and continuing to the output block in the lower right corner (Block 14). Starting with the check for atmosphere volume, Block 1 in Figure 2.4, the calculation proceeds as follows:

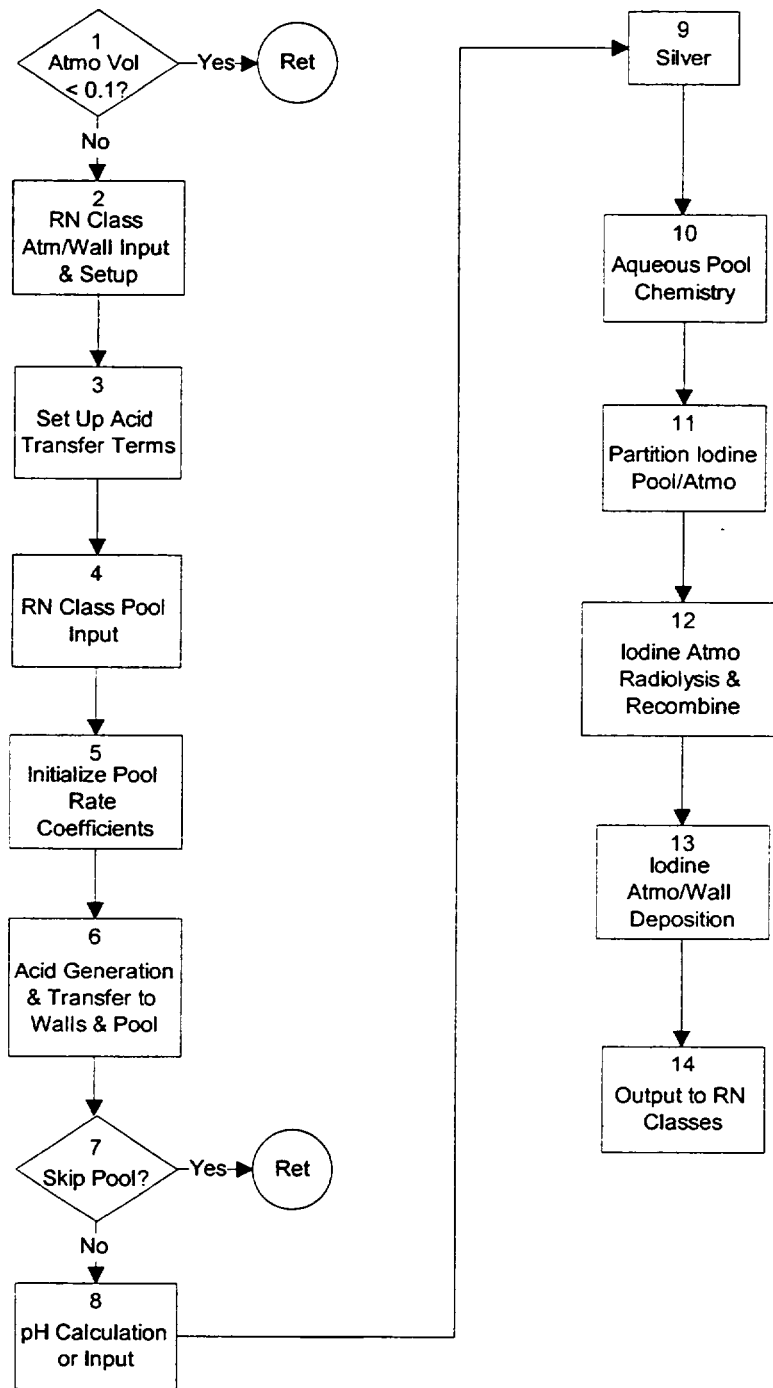


Figure 2.4 Calculation Flow of MELCOR Iodine Pool Model

RN Package Reference Manual

- (1) The atmosphere volume in the control volume is checked against a limit with a default of 0.1 m^3 . If this test is not satisfied, the rest of the model is skipped for this control volume.
- (2) RN class input and atmosphere/pool setup: the atmosphere and pool driver species are initialized at the beginning of the timestep from the MELCOR RN classes. This is only done for the atmosphere and walls at this point in the calculation. In the atmosphere, these are iodine (class 4), methyl iodine (class 17), hydrochloric and nitric acid (classes 18 and 19), and nitrogen, steam, oxygen, hydrogen, carbon dioxide, and methane (hydrodynamic materials). Atmosphere, pool, and wall areas and volumes are set up. Wall species for physically and chemically bound iodine and methyl iodide, and deposited nitric and hydrochloric acid on wet walls, are initialized from extended MELCOR chemisorption classes.
- (3) The terms in the ordinary differential equations describing mass transport of hydrochloric and nitric acid from the atmosphere to the walls are set up, as are the radiolysis generation terms.
- (4) The pool species are initialized from the MELCOR RN classes. These are iodine (class 4 and 16, CsI), the buffers boric acid (class 20) and phosphate (class 22), hydrochloric and nitric acid (classes 18 and 19), cations (CsI , class 16), silver (class 12), and iron (class 7). Although silver iodide is also transported as an RN class, the pool silver iodide does not need to be initialized, as silver acts only as a sink for iodine, not a source, and hence silver iodide (once formed) plays no further role in the pool chemistry.
- (5) The rate coefficients for the pool chemistry calculation are initialized. These will be used later in the aqueous chemistry routine.
- (6) The calculation of mass transport for hydrochloric and nitric acid is done. This includes the radiolysis generation rates, transport between the atmosphere and wall surfaces, and transport between atmosphere and pool. This last step is necessary to have the updated pool acid concentrations available for the pH calculation.
- (7) The conditions for using the full iodine pool model are checked against limits here. These include the presence of iodine, atmospheric pressure less than 1 MPa, pool present, and pool temperature less than 425 K. If these conditions are not satisfied, then the rest of the pool calculation is skipped. There is a user input flag that will override the iodine criterion, allowing pool hydrolysis calculations to be done.
- (8) The pH calculation is performed based on the relative molar concentrations of acids and bases in the pool. Alternatively, the pH can be directly entered in user input via tabular or control functions, or an external data file.

- (9) A fraction of the silver present (set to 10^{-6}) is assumed chemically active and can remove some of the iodine in the pool as silver iodide, acting as a sink.
- (10) The aqueous pool chemistry solver is called. This is a quasi-equilibrium solver and assumes steady-state conditions. The iodine from the MELCOR RN classes 4 (I_2) and 16 (I^-) is treated as an initial inventory of I^- . The aqueous chemistry model performs the speciation of the iodine each timestep, based on the pH and radiolysis in the pool (see Table 2.5 for major and secondary species available for output in MELCOR).
- (11) The molar concentrations of iodine and methyl iodide in the pool are used to determine a pool surface concentration. This is used together with atmosphere conditions to partition the iodine and methyl iodide between the pool and atmosphere, giving new concentrations in the pool and atmosphere.
- (12) The atmospheric iodine and methyl iodide concentrations are further modified by atmospheric radiolysis and thermal and concentration-dependent destruction rates to form free iodine; the final concentrations are determined by a recombination step using equilibrium coefficients.
- (13) The atmosphere iodine and methyl iodide concentrations are used together with the wall concentrations to determine mass transport between the atmosphere and dry wall surfaces. Radiolysis at painted walls is included.
- (14) Results of the pool model calculation are output. The relevant RN classes are updated, (see block 2 and 4 descriptions), including the silver iodine class. The silver iodide class is necessary to maintain mass conservation. On output, available cations (Cs) is combined with available I^- in the pool to form the new CsI (class 16) mass, and uncombined Cs or I^- are added to the CsOH (class 2) or I_2 (class 4) masses, respectively. The main iodine species, I_2 and I^- , are otherwise output as class 4. Other secondary species are also added into class 4 to maintain mass conservation. Updated wall concentrations are also output. The pH of the pool is available as a MELCOR plot variable. The masses and concentrations of the RN classes for the pool and atmosphere (transported species) are likewise available via control functions. A list of main and secondary species available via control function is shown in Table 2.5.

2.11.7 Submodels in the Iodine Pool Model

There are seven main submodels in the iodine pool model. These are detailed below, starting with the acid generation and transport models.

2.11.7.1 Acid Generation and Transfer to Walls and Pool

Formation of nitric acid in the atmosphere by radiolysis is calculated using the rate

$$\dot{S}_{HNO_3} = 5.45 \times 10^{-7} M_{N_2} \dot{D}_{atm} \quad (2.115)$$

where

\dot{S}_{HNO_3} = formation rate of nitric acid by radiolysis (kg-mole/s)

M_{N_2} = mass of nitrogen in the atmosphere (kg)

\dot{D}_{atm} = atmosphere dose rate (MRad/hr)

and the constant has the appropriate units

Formation of hydrochloric acid is assumed to occur via radiolysis of plastic wire insulation in a control volume and go into the atmosphere instantly. The rate is given as

$$\dot{S}_{HCL} = 2.88 \times 10^{-7} M_{cable} \dot{D}_{cable} \quad (2.116)$$

where

\dot{S}_{HCL} = rate of formation of HCl by radiolysis of wire cable insulation (kg-mole/s)

M_{cable} = mass of cable insulation in control volume (kg)

\dot{D}_{cable} = cable dose rate (MRad/hr)

and the constant has the appropriate units.

Nitric and hydrochloric acids in the atmosphere can be deposited in the water films on wet walls via a non-reversible mass transport equation of the form

$$\frac{dC_{w,acid,n}}{dt} = k_{w,acid,n} C_{atm,acid} \quad (2.117)$$

where

$C_{w,acid,n}$ = moles of acid on wall surface n (kg-mole)

$k_{w,acid,n}$ = transport coefficient from atmosphere to wall n for acid (m/s)

$C_{atm,acid}$ = atmospheric moles of acid (kg-mole)

and the subscript *acid* refers either to nitric or hydrochloric acid. A similar equation is used for transport from the atmosphere to the pool. The new amount of acid in the atmosphere is determined by summing up the transport to all the wet walls in a control volume and the pool (if present) to get

$$\frac{dC_{atm,acid}}{dt} = -C_{atm,acid} \frac{1}{V_{atm}} \left(\sum_n k_{w,acid,n} A_{w,n} + k_{p,acid} A_{pool} \right) + \dot{S}_{acid} \quad (2.118)$$

where

$k_{w,acid,n}$ = transport coefficient from atmosphere to wall surface n for acid (m/s)

$A_{w,n}$ = wall n surface area (m²)

$k_{p,acid}$ = transport coefficient from atmosphere to pool for acid (m/s)

A_{pool} = pool-atmosphere surface area (m²)

V_{atm} = atmospheric volume (m³)

\dot{S}_{acid} = formation rate of acid (kg-mole/s).

This can be solved analytically over the timestep as

$$C_{atm,acid}(t) = C_{atm,acid}(t_0) \exp(-k_{eff,acid}t) + \frac{\dot{S}_{acid}}{V_{atm}k_{eff,acid}} (1 - \exp(-k_{eff,acid}t)) \quad (2.119)$$

where $k_{eff,acid}$ is defined by

$$k_{eff,acid} = \frac{1}{V_{atm}} \left(\sum_n k_{w,acid,n} A_n + k_{p,acid} A_{pool} \right). \quad (2.120)$$

The change in amount of wall acid can be expressed in terms of the change in atmospheric acid as

$$C_{w,acid,n}(t) = C_{w,acid,n}(t_0) + \frac{k_{w,acid,n}}{k_{eff,acid}} \left([C_{atm,acid}(t) - C_{atm,acid}(t_0)] + \dot{S}_{acid}(t - t_0) \right), \quad (2.121)$$

and a similar equation applies for the change in pool acid,

$$C_{p,acid}(t) = C_{p,acid}(t_0) + \frac{k_{p,acid}}{k_{eff,acid}} \left([C_{atm,acid}(t) - C_{atm,acid}(t_0)] + \dot{S}_{acid}(t - t_0) \right). \quad (2.122)$$

Acids deposited in wall films are transported to the pool or other surfaces using the MELCOR film transport model.

2.11.7.2 Pool pH Calculation

The pool pH is determined either from an acid-base balance or set via user input. The pH calculation is done by first performing a charge balance of the acids and bases to estimate pH, and then performing an iteration over the species and charge balance to get the final pH.

The first step is to estimate the hydrogen ion concentration (or pH) from a charge balance on the phosphate (Na_3PO_4), cation (Cs), nitric and hydrochloric acid concentrations, as

$$\Delta Z = 3x_{NaP} + x_{Cs} - x_{HNO_3} - x_{HCl}$$

where (kmole= 10^3 mole)

- ΔZ = charge balance (kmole/ m^3)
- x_{NaP} = phosphate concentration (Na_3PO_4), (kmole/ m^3)
- x_{Cs} = cation concentration (cesium), (kmole/ m^3)
- x_{HNO_3} = nitric acid concentration (kmole/ m^3)
- x_{HCl} = hydrochloric acid concentration (kmole/ m^3)

If ΔZ is greater than 0, then the pH is estimated as

$$x_{OH^-} = \min(0.0001, \Delta Z)$$

$$x_{H^+} = \frac{K_{eq,H_2O}}{x_{OH^-}}$$

$$pH = \log_{10}(x_{OH^-}).$$

If ΔZ equals 0, then

$$x_{H^+} = 10^{-7}$$

$$pH = 7$$

If ΔZ is less than 0, then

$$x_{H^+} = \min(0.0001, |\Delta Z|)$$

$$pH = \log_{10}(x_{H^+})$$

The activities are then initialized. Activities are calculated using Davies modification of the Debye-Huckel equation [41],

$$\log_{10} \gamma(i) = -AZ(i)^2 \left[\frac{\sqrt{I}}{1 + \sqrt{I}} - b I \right]$$

where

$\gamma(i)$ = activity coefficient for ion i

$Z(i)$ = absolute value of the charge on ion i

b = empirical constant = 0.2

I = ionic strength, defined as

$$I = \frac{1}{2} \sum_{\text{all ions}} C(j)Z(j)^2$$

$C(j)$ = concentration of the j^{th} ion in solution

A = $1.825 \times 10^6 \rho_w^{1/2} / (\epsilon T)^{3/2}$

RN Package Reference Manual

ρ_w = density of water (g/cm³)

ϵ = dielectric constant of water.

The initial strength is estimated using the initial buffer species along with the OH⁻ and H⁺ concentrations

$$I = 0.5(3x_{NaP} + x_{Cs} + x_{HNO_3} + x_{HCl} + x_{OH^-} + x_{H^+}).$$

The equations to be solved are:

- (1) the phosphate mole balance:

$$M(P) = [H_3PO_4] + [H_2PO_4^-] + [HPO_4^{2-}] + [PO_4^{3-}],$$

where $M(P)$ is the total kmoles of phosphate per m³ of water and is user input,

- (2) the borate mole balance:

$$M(B) = [B(OH)_4^-] + [B(OH)_3]$$

where $M(B)$ is the input kmoles of borate per m³ of water,

- (3) the CO₂ hydrolysis balance:

$$M(C) = [HCO_3^-] + [CO_3^{2-}]$$

where $M(C)$ is the moles of dissolved CO₂ per m³ of water, and

- (4) the charge balance:

$$\begin{aligned} [NO_3^-] + [Cl^-] + [OH^-] + [H_2PO_4^-] + 2[HPO_4^{2-}] + 3[PO_4^{3-}] + [B(OH)_4^-] \\ + [HCO_3^-] + 2[CO_3^{2-}] = [H^+] + [A^+] + 3M(P) \end{aligned}$$

where $[A^+]$ is the kmoles of alkali per m³ added to adjust for boric acid and the kmoles/m³ of phosphate added is assumed to be in the form Na₃PO₄. Also needed is the ionization constant for water, written in the form:

$$K_w = [H^+] \gamma(1) [OH^-] \gamma(1)$$

where the activity coefficients have been included. The ionization constant is determined from the formula

$$\log_{10} K_{w,p} = 2(7.2 + 2.5\rho_w) \log_{10} \rho_w - \frac{3108}{T} - 3.55$$

where

$K_{w,p}$ = ionization constant of water in units of (moles/kg)²

ρ_w = density of water in g/cm³.

To get the ionization constant in units of (kmole/m³)², multiply by the density of water squared:

$$K_w = K_{w,p} \rho_w^2.$$

The concentrations of the derived species are determined from equilibrium constants:

$$k_4 = \frac{[H^+] [B(OH)_4^-]}{[B(OH)_3]} \gamma(1)^2$$

$$\log_{10} k_4 = \frac{1573}{T} + 28.8397 + 0.11748T - 13.2258 \log_{10} T + \log_{10} K_w$$

$$k_5 = \frac{[HPO_4^{2-}]}{[H^+] [PO_4^{3-}]} \frac{\gamma(2)}{\gamma(1)\gamma(3)}$$

$$\log_{10} k_5 = \frac{-675}{T} + 1.793 + \log_{10} K_w$$

$$k_6 = \frac{[OH^-] [H_2PO_4^-]}{[HPO_4^{2-}]} \frac{\gamma(1)^2}{\gamma(2)}$$

$$\log_{10} k_6 = \frac{-17156.9}{T} - 37.7345 \ln T + 0.0322082 T + \frac{8.97579 \times 10^5}{T^2} + 246.045$$

RN Package Reference Manual

$$k_7 = \frac{[OH^-][H_3PO_4]}{[H_2PO_4^-]} \gamma(n)$$

$$\log_{10} k_7 = \frac{-17655.8}{T} - 39.4277 \ln T + 0.0325405 T + \frac{810134}{T^2} + 253.198$$

$$k_2 = \frac{[H^+][HCO_3^-]}{[CO_{2aq}]} \gamma(1)^2$$

$$\log_{10} k_2 = \frac{2518}{T} - 0.7566 + \log_{10} K_w$$

$$k_3 = \frac{[H^+][CO_3^{2-}]}{[HCO_3^-]} \gamma(2)$$

$$\log_{10} k_3 = \frac{2142}{T} - 3.523 + \log_{10} K_w$$

The iteration proceeds by

- (1) setting the activities, and mass ratios of the acid and CO₂ total masses to the principal species,
- (2) get new species concentrations from the ratios and mole balances,
- (3) recalculate the strength and activities including all species in the charge balance, and
- (4) use the charge balance to calculate the pH. This process is repeated until the pH converges to within 0.0001. The iteration is accelerated by using the gradient of the change in pH after the first 5 iterations.

2.11.7.3 Silver-Iodine Model

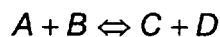
Silver in the pool can act to trap iodine. This is modeled in the iodine pool model by assuming a fixed fraction of the silver present in the pool (default set at 1×10^{-6}) is available to react with iodine, forming AgI sludge. The iodine thus reacted is assumed trapped and does not participate in the pool aqueous chemistry. The silver is assumed to be provided by RN class 12, and AgI is given its own RN class.

2.11.7.4 Iodine Aqueous Pool Chemistry

The aqueous iodine chemistry model is a semi-mechanistic model based primarily on the INSPECT equation set [42,43] plus work by Powers [44]. The model includes the effects of radiolysis, take-up of iodine by silver, metal ions (represented by iron), and acid-base buffers. Equations are included for organic iodine, represented as methyl iodine.

2.11.7.4.1 Chemical Reaction Equations

The chemical equations in the set are of the general form



with forward reaction rate k_f and reverse rate k_r . These are used to set up chemical reaction kinetic equations for each chemical species in the set. Using the above equation as an example, the reaction rate equation for species C would include terms from this equation plus perhaps a source from radiolysis:

$$\frac{d[C]}{dt} = k_f[A][B] - k_r[C][D] + \dot{S}$$

where the brackets [] indicate concentration of the species and the \dot{S} is the source of C from radiolysis. The set of chemical reaction kinetics equations form a coupled set of nonlinear ordinary differential equations, which are solved using a standard stiff differential equation solver [45] to get the pool speciation. Initial conditions are set up by assuming some species, termed driver species, are given and constant over a calculational timestep. There are five driver species in the current equation set. These are aqueous O₂, H₂, CH₄, OH⁻, and H⁺. Some driver species are set by assuming equilibrium with the atmosphere via a Henry's law relationship; these are aqueous O₂, H₂, and CH₄. The OH⁻ and H⁺ are set by determining the pool pH.

The initial total iodine concentration is specified at the beginning of the timestep as species I, and the iron ion concentration is specified as Fe³⁺. Other species in the pool, such as silver, nitric and hydrochloric acids, and phosphate and borate buffers, do not actually participate in the calculation of speciation other than to set the initial pH and iodine level (silver, by removing some iodine). Pool pH is determined either from an acid-base balance or is read in directly via user input.

The current chemical equation set consists of 276 equations as given in Table 2.7 through Table 2.10 and includes 39 species.

RN Package Reference Manual

Table 2.6 Kinetic Equations for Water Radiolysis

Number	Reaction	Rate Constant*
M1	$\text{OH}^\circ + \text{H}_2(\text{aq}) \rightarrow \text{H}^\circ + \text{H}_2\text{O}$	4.2×10^7
M2	$\text{OH}^\circ + \text{H}_2\text{O}_2 \rightarrow \text{HO}_2^\circ + \text{H}_2\text{O}$	2.7×10^7
M3	$\text{OH}^\circ + \text{O}_2^- \rightarrow \text{O}_2(\text{aq}) + \text{OH}^-$	8×10^9
M4	$\text{H}^\circ + \text{O}_2(\text{aq}) \rightarrow \text{HO}_2^\circ$	1.2×10^{10}
M5	$\text{H}^\circ + \text{O}_2^- \rightarrow \text{HO}_2^-$	2×10^{10}
M6	$e^- + \text{O}_2(\text{aq}) \rightarrow \text{O}_2^-$	1.9×10^{10}
M7	$e^- + \text{H}_2\text{O}_2 \rightarrow \text{OH}^\circ + \text{OH}^-$	1.2×10^{10}
M8	$e^- + \text{O}_2^- + \text{H}_2\text{O} \rightarrow \text{HO}_2^- + \text{OH}^-$	1.3×10^{10}
M9	$e^- + \text{H}^+ \rightarrow \text{H}^\circ$	2.3×10^{10}
M10	$e^- + \text{H}_2\text{O} \rightarrow \text{H}^\circ + \text{OH}^-$	19
M11	$e^- + \text{HO}_2^- \rightarrow \text{O}^- + \text{OH}^-$	3.5×10^9
M12	$\text{OH}^\circ + \text{HO}_2^\circ \rightarrow \text{O}_2(\text{aq}) + \text{H}_2\text{O}$	6×10^9
M13	$2 \text{OH}^\circ \rightarrow \text{H}_2\text{O}_2$	5.5×10^9
M14	$\text{H}^\circ + \text{HO}_2^\circ \rightarrow \text{H}_2\text{O}_2$	2×10^{10}
M15	$\text{H}^\circ + \text{H}_2\text{O}_2 \rightarrow \text{OH}^\circ + \text{H}_2\text{O}$	5×10^7
M16	$\text{OH}^- + \text{H}^\circ \rightarrow e^- + \text{H}_2\text{O}$	2.5×10^7
M17	$\text{HO}_2^\circ + \text{O}_2^- \rightarrow \text{O}_2(\text{aq}) + \text{HO}_2^-$	9.7×10^7
M18	$2 \text{HO}_2^\circ \rightarrow \text{H}_2\text{O}_2 + \text{O}_2(\text{aq})$	2.35×10^6
M19	$\text{H}^+ + \text{O}_2^- \rightarrow \text{HO}_2^\circ$	5×10^7
M20	$\text{HO}_2^\circ \rightarrow \text{H}^+ + \text{O}_2^-$	(7.93×10^5)
M21	$\text{H}^+ + \text{HO}_2^- \rightarrow \text{H}_2\text{O}_2$	2×10^{10}
M22	$\text{H}_2\text{O}_2 \rightarrow \text{H}^+ + \text{HO}_2^-$	(0.0413)
M23	$\text{OH}^\circ + \text{OH}^- \rightarrow \text{H}_2\text{O} + \text{O}^-$	1.3×10^{10}
M24	$\text{O}^- + \text{H}_2\text{O} \rightarrow \text{OH}^\circ + \text{OH}^-$	(1.47×10^8)
M25	$\text{HO}_2^\circ + \text{OH}^- \rightarrow \text{O}_2^- + \text{H}_2\text{O}$	(1×10^9)
M26	$\text{O}_2^- + \text{H}_2\text{O} \rightarrow \text{HO}_2^\circ + \text{OH}^-$	(0.639)
M27	$\text{H}^\circ + \text{OH}^\circ \rightarrow \text{H}_2\text{O}$	7×10^9
M28	$2 \text{H}^\circ \rightarrow \text{H}_2(\text{aq})$	5×10^9
M29	$e^- + \text{H}^\circ + \text{H}_2\text{O} \rightarrow \text{OH}^- + \text{H}_2(\text{aq})$	2.4×10^{10}
M30	$2e^- + 2\text{H}_2\text{O} \rightarrow 2\text{OH}^- + \text{H}_2(\text{aq})$	5.5×10^9
M31	$e^- + \text{OH}^\circ \rightarrow \text{OH}^-$	3×10^{10}

Number	Reaction	Rate Constant*
M32	$O^- + O_2(aq) \rightarrow O_3^-$	3.5×10^9
M33	$H_2(aq) + O^- \rightarrow H^0 + OH^-$	1×10^8
M34	$H_2O_2 + O^- \rightarrow H_2O + O_2^-$	5×10^8
M35	$OH^0 + HO_2^- \rightarrow HO_2^0 + OH^-$	7.5×10^9
M36	$HO_2^- + O^- \rightarrow OH^- + O_2^-$	8×10^8
M37	$O_3^- + H_2O_2 \rightarrow O_2^- + O_2(aq) + H_2O$	1.6×10^6
M38	$O_3^- + HO_2^- \rightarrow O_2^- + O_2(aq) + OH^-$	8.9×10^5
M40	$O_3^- + H_2 \rightarrow H^0 + O_2(aq) + OH^-$	2.5×10^5
M102	$H_2O_2 \rightarrow 2 OH^0$	2.33×10^{-7} ($6.4 \times 10^5 \exp(-8540/T)$)

*Rate constants are in units $m^3/kmole-s$ and s^{-1} . Most rate constants were taken from [42]. Rate constants within parentheses were estimated as part of this work.

Table 2.7 Reactions of Iodine

Number	Reaction	Rate Constant*
M53	$I^0 + e^- \rightarrow I^-$	2.4×10^{10}
M54	$I_2(aq) + e^- \rightarrow I_2^-$	5.1×10^{10}
M55	$IO_3^- + e^- \rightarrow IO_3^{2-}$	7.8×10^9
M56	$I_2^- + e^- \rightarrow 2I^-$	1.3×10^{10}
M57	$I_3^- + e^- \rightarrow I^- + I_2^-$	3.5×10^{10}
M59	$IO_3^0 + e^- \rightarrow IO_3^-$	13.5×10^{10}
M60	$IO_2^- + e^- \rightarrow IO^- + O^-$	11×10^{10}
M61	$IO^- + e^- \rightarrow I^- + O^-$	22.9×10^{10}
M62	$IO^0 + e^- \rightarrow IO^-$	21×10^{10}
M63	$HOI^- + e^- \rightarrow I^- + OH^-$	1.9×10^{10}
M65	$I^0 + H^0 \rightarrow H^+ + I^-$	2.7×10^{10}
M66	$I_2(aq) + H^0 \rightarrow I_2^- + H^+$	3.5×10^{10}
M67	$I_2^- + H^0 \rightarrow 2I^- + H^+$	1.8×10^7

1 Rate from Wren

2 Rate from Karasawa

RN Package Reference Manual

Number	Reaction	Rate Constant*
M68	$I_3^- + H^0 \rightarrow I^- + I_2^- + H^+$	8×10^9
M69	$I^- + H^0 \rightarrow HI^-$	5.3×10^6
M70	$HOI^- + H^0 \rightarrow I^- + H_2O$	4.4×10^{10}
M72	$HOI^0 + H^0 \rightarrow I^0 + H_2O$	1×10^9
M73	$IO_2^- + O_2^- + H_2O \rightarrow IO^0 + O_2(aq) + 2OH^-$	1×10^7
M74	$I_2(aq) + O_2^- \rightarrow I_2^- + O_2(aq)$	21×10^9
M75	$HOI^0 + O_2^- \rightarrow I^0 + O_2(aq) + OH^-$	1×10^6
M76	$I_3^- + O_2^- \rightarrow I_2^- + I^- + O_2(aq)$	22.5×10^8
M77	$I_2^- + O_2^- \rightarrow 2I^- + O_2(aq)$	27.5×10^9
M78	$IO^0 + O_2^- \rightarrow IO^- + O_2(aq)$	8×10^7
M79	$IO_3^- + O_2^- \rightarrow IO_3^{2-} + O_2(aq)$	8×10^9
M80	$I_2^- + HO_2^0 \rightarrow I_2(aq) + HO_2^-$	1×10^{10}
M81	$HOI^0 + HO_2^0 \rightarrow I^0 + O_2(aq) + H_2O$	1×10^5
M82	$IO_2^- + HO_2^0 \rightarrow IO^0 + O_2(aq) + OH^-$	1×10^7
M83	$I_2(aq) + HO_2^0 \rightarrow I_2^- + O_2(aq) + H^+$	1.8×10^7
M84	$I^0 + OH^0 \rightarrow HOI^0$	1.6×10^{10}
M85	$HOI^0 + OH^0 \rightarrow IO^0 + H_2O$	7×10^9
M86	$IO^0 + OH^0 \rightarrow HIO_2^0$	11×10^{10}
M87	$IO_2^0 + OH^0 \rightarrow IO_3^- + H^+$	11×10^{10}
M88	$I^- + OH^0 \rightarrow HOI^-$	1.8×10^{10}
M89	$I_2(aq) + OH^0 \rightarrow HOI^0 + I^0$	1.1×10^{10}
M90	$IO_3^- + OH^0 \rightarrow IO_3^0 + OH^-$	21×10^6
M91	$HOI^- + OH^0 \rightarrow HOI^0 + OH^-$	2.7×10^{10}
M92	$I_2^- + OH^0 \rightarrow I_2(aq) + OH^-$	3.8×10^{10}
M93	$I_3^- + OH^0 \rightarrow I_2(aq) + I^0 + OH^-$	2×10^{10}
M94	$I^- + O^- + H_2O \rightarrow I^0 + 2OH^-$	24.7×10^7
M95	$IO^- + O^- + H_2O \rightarrow IO^0 + 2OH^-$	21.1×10^8
M96	$IO_3^- + O^- + H_2O \rightarrow IO_3^0 + 2OH^-$	15.23×10^6
M97	$I^- + H_2O_2 \rightarrow IO^- + H_2O$	10.014
M100	$IO_3^0 + H_2O_2 \rightarrow IO_3^- + HO_2^0 + H^+$	1×10^9
M101	$I^0 + H_2O_2 \rightarrow I^- + HO_2^0 + H^+$	3000

RN Package Reference Manual

Number	Reaction	Rate Constant*
M103	$\text{HIO}_2^\circ \rightarrow \text{IO}_2^- + \text{H}^+$	21×10^{10}
M104	$\text{I}^\circ + \text{I}^- \rightarrow \text{I}_2^-$	21.1×10^{10}
M105	$\text{HOI}^- \rightarrow \text{I}^- + \text{OH}^\circ$	2.25×10^6
M106	$\text{I}^- + \text{HOI}^- \rightarrow \text{I}_2^- + \text{OH}^-$	2.5×10^4
M107	$\text{HOI}^- \rightarrow \text{I}^\circ + \text{OH}^-$	1.2×10^8
M108	$2\text{I}_2^- \rightarrow \text{I}_3^- + \text{I}^-$	4.5×10^9
M109	$\text{I}_2^- + \text{O}_2(\text{aq}) + \text{H}^+ \rightarrow \text{HO}_2^\circ + \text{I}_2(\text{aq})$	6×10^5
M110	$\text{I}_2^- + \text{I}^\circ \rightarrow \text{I}_3^-$	4.5×10^9
M111	$2\text{I}^\circ \rightarrow \text{I}_2(\text{aq})$	1×10^{10}
M112	$\text{I}_2^- + \text{HOI}^\circ \rightarrow \text{IO}^\circ + 2\text{I}^- + \text{H}^+$	1×10^5
M113	$\text{IO}_3^{2-} + \text{H}_2\text{O} \rightarrow \text{HIO}_3^- + \text{OH}^-$	1×10^8
M114	$\text{IO}_3^\circ + \text{I}^- \rightarrow \text{IO}_2^- + \text{IO}^\circ$	11×10^6
M115	$\text{IO}_2^\circ + \text{I}^- \rightarrow \text{I}_2(\text{aq}) + \text{O}_2^-$	1×10^{10}
M116	$\text{HI}^- + \text{H}_2\text{O} \rightarrow \text{I}^\circ + \text{H}_2(\text{aq}) + \text{OH}^-$	1000
M117	$\text{HI}^- + \text{H}^+ \rightarrow \text{I}^\circ + \text{H}_2(\text{aq})$	11×10^{10}
M118	$\text{I}_2^- + \text{HOI}^- \rightarrow \text{I}_3^- + \text{OH}^-$	1.8×10^{10}
M119	$\text{HOI}^- + \text{I}^\circ \rightarrow \text{I}_2(\text{aq}) + \text{OH}^-$	2.3×10^{10}
M120	$2\text{HOI}^- \rightarrow \text{I}_2(\text{aq}) + 2\text{OH}^-$	2×10^{10}
M121	$\text{HOI}^\circ + \text{e}^- \rightarrow \text{HOI}^-$	2×10^{10}
M122	$\text{HOI}^\circ + \text{O}_2^- \rightarrow \text{HOI}^- + \text{O}_2(\text{aq})$	11×10^9
M123	$2\text{IO}^\circ \rightarrow \text{I}_2\text{O}_2$	1.5×10^9
M124	$\text{I}_2\text{O}_2 + \text{H}_2\text{O} \rightarrow \text{IO}_2^- + \text{HOI}^\circ + \text{H}^+$	11000
M125	$\text{IO}^\circ + \text{IO}_2^- \rightarrow \text{IO}_2^\circ + \text{IO}^-$	11×10^{10}
M126	$\text{IO}_2^\circ + \text{H}_2\text{O} \rightarrow \text{HIO}_3^- + \text{H}^+$	11000
M127	$2\text{HIO}_3^- \rightarrow \text{IO}_3^- + \text{IO}_2^- + \text{H}_2\text{O}$	25.2×10^9
M128	$\text{IO}_3^\circ + \text{HIO}_3^- \rightarrow 2\text{IO}_3^- + \text{H}^+$	11×10^{10}
M129	$\text{IO}_3^\circ + \text{IO}_3^{2-} \rightarrow 2\text{IO}_3^-$	11×10^{10}
M130	$\text{IO}_2^- + \text{H}_2\text{O}_2 \rightarrow \text{IO}^- + \text{O}_2(\text{aq}) + \text{H}_2\text{O}$	1×10^8
M131	$\text{I}_2(\text{aq}) + \text{H}_2\text{O} \rightarrow \text{I}_2\text{OH}^- + \text{H}^+$	*
M132	$\text{I}_2\text{OH}^- + \text{H}^+ \rightarrow \text{I}_2(\text{aq}) + \text{H}_2\text{O}$	1×10^{10}
M133	$\text{I}_2(\text{aq}) + \text{OH}^- \rightarrow \text{I}_2\text{OH}^-$	1×10^{10}

RN Package Reference Manual

Number	Reaction	Rate Constant*
M134	$I_2OH^- \rightarrow I_2(aq) + OH^-$	13×10^5
M135	$I_2OH^- \rightarrow I^- + HOI^0$	1963
M136	$I^- + HOI^0 \rightarrow I_2OH^-$	1×10^6
M137	$IO^- + I_2OH^- \rightarrow IO_2^- + 2I^- + H^+$	6
M138	$IO_2^- + I_2OH^- \rightarrow IO_3^- + 2I^- + H^+$	26
M139	$2HOI^0 \rightarrow IO_2^- + I^- + 2H^+$	16.7
M141	$HOI^0 + IO_2^- \rightarrow IO_3^- + I^- + H^+$	1×10^7
M144	$HOI^0 + OH^- \rightarrow IO^- + H_2O$	1×10^9
M145	$IO^- + H_2O \rightarrow HOI^0 + OH^-$	2750
M146	$2I^- + 1/2O_2(aq) + 2H^+ \rightarrow I_2(aq) + H_2O$	347
M147	$I_2(aq) + H_2O \rightarrow 2I^- + 1/2O_2(aq) + 2H^+$	1×10^{-10}
M148	$I_2(aq) + I^- \rightarrow I_3^-$	
M149	$I_3^- \rightarrow I_2(aq) + I^-$	*
M150	$I^- + IO_2^- + 2H^+ \rightarrow 2HOI^0$	$10^{12} \times R139$
M151	$IO_3^- + 2I^- + 2H^+ \rightarrow H_2I_3O_3^-$	6.72×10^8
M152	$H_2I_3O_3^- + 3I^- + 4H^+ \rightarrow 3I_2(aq) + 3H_2O$	1×10^{10}
M153	$I_2^- \rightarrow I^0 + I^-$	1.1×10^5
M154	$HOOI + I^- \rightarrow I_2(aq) + HO_2^-$	4.5×10^5
M155	$I_2(aq) + HO_2^- \rightarrow HOOI + I^-$	R154 / 0.04119
M156	$HOI^0 + HO_2^0 \rightarrow HOOI + OH^0$	2.1×10^9
M157	$HOOI + OH^- \rightarrow I^- + O_2 + H_2O$	2×10^9
M158	$HOI^0 + H_2O_2 \rightarrow HOOI + H_2O$	37
M159	$HOOI \rightarrow I^- + O_2 + H^+$	0.2

Number	Reaction	Rate Constant*
Footnotes to table:		
*INSPECT selects a rate constant based on the equilibrium constant and the rate constant for the back reaction.		
**See Powers [44].		
$\frac{d[I_2(aq)]}{dt} = -\frac{1}{2} \frac{d[I^-]}{dt} = -\frac{1}{2} \frac{d[H^+]}{dt} = -2 \frac{d[O_2(aq)]}{dt} = 34[I^-]^2[H^+][O_2(aq)]$ $+ \frac{7.14 \times 10^4 [I^-][B(OH)_3][H^+][O_2(aq)]}{(1 + 1.47 \times 10^8 [H^+])}$		
***See Powers [44].		
$\frac{d[IO_3^-]}{dt} = -\frac{d[I^-]}{dt} = -\frac{2}{3} \frac{d[O_2(aq)]}{dt} = 3.2 \times 10^{-5} [I^-][O_2(aq)]$		

Table 2.8 Reactions of Ferrous and Ferric Ions

Number	Reaction	Rate Constant
M259	$Fe^{2+} + O_2(aq) \rightarrow Fe^{3+} + O_2^-$	$\frac{d[Fe^{2+}]}{dt} = k[Fe^{2+}][O_2(aq)][OH^-]^2$ $k = 3.10^{21} \exp(-3557/T)$
M260	$Fe^{3+} + H_2O_2 \rightarrow Fe^{2+} + HO_2^0 + H^+$	$2 \times 10^{-3} / (1 + x/[H^+])$
M261	$Fe^{3+} + HO_2^- \rightarrow Fe^{2+} + HO_2^0$	$1.1 \times 10^{24} \exp(-14090/T) / (1 + x/[H^+])$
M262	$Fe^{3+} + H_2^0 \rightarrow Fe^{2+} + O_2(aq) + H^+$	3×10^5
M263	$Fe^{3+} + O_2^- \rightarrow Fe^{2+} + O_2(aq)$	$5040 \exp(3294/T)$
M264	$Fe^{3+} + e^- \rightarrow Fe^{2+}$	2.3×10^{10}
M265	$Fe^{3+} + H^0 \rightarrow Fe^{2+} + H^+$	9.6×10^7
M266	$Fe^{2+} + H^0 + H^+ \rightarrow Fe^{3+} + H_2$	7.5×10^6
M267	$Fe^{3+} + OH^0 + H_2O \rightarrow Fe^{2+} + H_2O_2 + H^+$	$1.5 / (1 + y/[H^+])$ Ref. 184
M268	$Fe^{2+} + O^- + H_2O \rightarrow Fe^{3+} + 2OH^-$	3.8×10^9
M269	$Fe^{2+} + OH^0 \rightarrow Fe^{3+} + OH^-$	3×10^8
M270	$Fe^{2+} + H_2O_2 \rightarrow Fe^{3+} + OH^- + OH^0$	77
M271	$Fe^{2+} + HO_2^0 \rightarrow Fe^{3+} + HO_2^-$	3×10^7
M272	$Fe^{2+} + HO_2^- \rightarrow Fe^{3+} + OH^- + O^-$	770
M273	$Fe^{2+} + O_2^- \rightarrow Fe^{3+} + 2O^-$	7.2×10^6
M274	$Fe^{3+} + H_2O_2 \rightarrow Fe^{2+} + O_2^- + 2H^+$	$2 \times 10^{-3} \times / ([H^+] + x)$
M275	$Fe^{3+} + HO_2^- \rightarrow Fe^{2+} + O_2^- + H^+$	$1.1 \times 10^{24} \exp(-14090/T) \times / ([H^+] + x)$

RN Package Reference Manual

Number	Reaction	Rate Constant
M276	$\text{Fe}^{3+} + \text{OH}^{\circ} + \text{H}_2\text{O} \rightarrow \text{Fe}^{2+} + \text{HO}_2^- + 2\text{H}^+$	$1.5 y / ([\text{H}^+] + y)$ Ref. 184
$x = \text{equilibrium constant for } \text{HO}_2^{\circ} \rightarrow \text{H}^+ + \text{O}_2^- = 10^{-1431/T}$ $y = \text{equilibrium constant for } \text{H}_2\text{O}_2 \rightarrow \text{H}^+ + \text{HO}_2^- = 10^{-3484/T}$		

Table 2.9 Organic Reactions

Number	Reaction	Rate Constant
M377	$\text{CH}_4(\text{aq}) + \text{OH}^{\circ} \rightarrow \text{CH}_3 + \text{H}_2\text{O}$	1.21×10^8
M378	$\text{CH}_4(\text{aq}) + \text{I}_2(\text{aq}) \rightarrow \text{CH}_3\text{I} + \text{I}^- + \text{H}^+$	4
M379	$\text{CH}_4(\text{aq}) + \text{IO}^- \rightarrow \text{CH}_3\text{I} + \text{I}^- + \text{OH}^-$	1×10^8
M380	$\text{CH}_4(\text{aq}) + \text{HOI}^{\circ} \rightarrow \text{CH}_3\text{I} + \text{H}_2\text{O}$	1×10^8
M381	$2 \text{CH}_3 \rightarrow \text{products}$	1.24×10^9
M382	$\text{CH}_3 + \text{OH}^{\circ} \rightarrow \text{CH}_3\text{OH}$	1×10^8
M383	$\text{CH}_3 + \text{H}_2\text{O}_2 \rightarrow \text{CH}_3\text{OH} + \text{OH}^{\circ}$	3.5×10^7
M384	$\text{CH}_3 + \text{O}_2(\text{aq}) \rightarrow \text{products}$	4.9×10^9
M385	$\text{CH}_3 + \text{HOI}^{\circ} \rightarrow \text{CH}_3\text{I}(\text{aq}) + \text{OH}^{\circ}$	1×10^9
M386	$\text{CH}_3 + \text{e}^- + \text{H}_2\text{O} \rightarrow \text{CH}_4 + \text{OH}^-$	1×10^{10}
M387	$\text{CH}_3 + \text{H}^{\circ} \rightarrow \text{CH}_4(\text{aq})$	1×10^{10}
M388	$\text{CH}_3 + \text{I}^{\circ} \rightarrow \text{CH}_3\text{I}(\text{aq})$	1×10^{10}
M389	$\text{CH}_3 + \text{IO}_3^{\circ} \rightarrow \text{CH}_2\text{O} + \text{HIO}_2^{\circ}$	1×10^8
M390	$\text{CH}_3 + \text{IO}_2^{\circ} \rightarrow \text{CH}_2\text{O} + \text{HOI}^{\circ}$	1×10^8
M391	$\text{CH}_3 + \text{IO}^{\circ} \rightarrow \text{CH}_3\text{OH} + \text{HOI}^{\circ}$	1×10^8
M392	$\text{CH}_3 + \text{HOI}^{\circ} \rightarrow \text{I}^{\circ} + \text{CH}_3\text{OH}$	1×10^8
M393	$\text{CH}_3 + \text{I}_2(\text{aq}) \rightarrow \text{CH}_3\text{I}(\text{aq}) + \text{I}^{\circ}$	6×10^9
M394	$\text{CH}_3 + \text{HIO}_3^- \rightarrow \text{CH}_2\text{O} + \text{HOI}^{\circ} + \text{OH}^-$	1×10^8
M395	$\text{CH}_3\text{I}(\text{aq}) + \text{OH}^{\circ} \rightarrow \text{CH}_3\text{OH} + \text{I}^{\circ}$	1×10^8
M396	$\text{CH}_3\text{I} + \text{H}_2\text{O} \rightarrow \text{CH}_3\text{OH} + \text{H}^+ + \text{I}^-$ $\log_{10} k = 93.14585 - 9661.274/T - 24.42937 \log_{10} T$	
M397	$\text{CH}_3\text{I} + \text{OH}^- \rightarrow \text{CH}_3\text{OH} + \text{I}^-$	6.5×10^{-5}
M398	$\text{CH}_3\text{I}(\text{aq}) + \text{e}^- \rightarrow \text{CH}_3 + \text{I}^-$	1.6×10^{10}
M399	$\text{CH}_3\text{I}(\text{aq}) + \text{H}^{\circ} \rightarrow \text{CH}_3 + \text{H}^+ + \text{I}^-$	1×10^{10}
M400	$\text{CH}_3\text{I}(\text{aq}) + \text{OH}^{\circ} \rightarrow \text{CH}_4\text{OI}$	1.4×10^9

Number	Reaction	Rate Constant
M401	$\text{CH}_4\text{OI} \rightarrow \text{CH}_3\text{I}^+ + \text{OH}^-$	3.1
M402	$\text{CH}_4\text{OI} + \text{I}^- \rightarrow \text{I}_2^- + \text{CH}_3\text{OH}$	2×10^9
M403	$\text{CH}_3\text{I}^+ + \text{OH}^- \rightarrow \text{CH}_4\text{OI}$	1×10^{10}
M404	$\text{CH}_3\text{I}^+ + \text{I}^- + \text{H}_2\text{O} \rightarrow \text{CH}_3\text{OH} + \text{I}_2 + \text{H}^+$	7.7×10^9
M405	$\text{CH}_2\text{O} + \text{OH}^\circ \rightarrow \text{HCO} + \text{H}_2\text{O}$	1×10^9
M406	$\text{Fe}^{3+} + 2\text{I}^- \rightarrow \text{Fe}^{2+} + \text{I}_2^-$	21
M407	$\text{CH}_3\text{OH} + \text{OH}^\circ \rightarrow \text{CH}_3\text{O} + \text{H}_2\text{O}$	1×10^9
M408	$2\text{CH}_3\text{O} \rightarrow \text{product}$	1×10^9
M409	$\text{Fe}^{3+} + \text{CH}_3\text{O} \rightarrow \text{Fe}^{2+} + \text{product}$	1×10^9
M410	$\text{H}^+ + \text{CH}_3\text{O} + \text{Fe}^{2+} \rightarrow \text{Fe}^{3+} + \text{CH}_3\text{OH}$	1×10^9
M411	$\text{CH}_3\text{OH} + \text{H}^\circ \rightarrow \text{CH}_3\text{O} + \text{H}_2$	5×10^8
M412	$\text{CH}_3\text{OH} + \text{e}^- \rightarrow \text{H}^\circ + \text{CH}_3\text{O}$	1×10^4
M413	$\text{CH}_3 + \text{CH}_3\text{OH} \rightarrow \text{CH}_4(\text{aq}) + \text{CH}_3\text{O}$	2×10^5
M414	$\text{CH}_3\text{O} + \text{H}_2\text{O}_2 \rightarrow \text{CH}_2\text{O} + \text{OH}^\circ + \text{H}_2\text{O}$	4×10^4
M415	$\text{CH}_3\text{O} + \text{O}_2 \rightarrow \text{products}$	4.2×10^9
M416	$\text{CH}_2\text{O} + \text{e}^- + \text{H}_2\text{O} \rightarrow \text{CH}_3\text{O} + \text{OH}^-$	1×10^7
M417	$\text{CH}_2\text{O} + \text{H}^\circ \rightarrow \text{H}_2 + \text{HCO}$	5×10^6
M418	$\text{CH}_2\text{O} + \text{CH}_3 \rightarrow \text{CH}_4(\text{aq}) + \text{HCO}$	5×10^6
M419	$\text{CH}_2\text{O} + \text{O}^- \rightarrow \text{OH}^- + \text{HCO}$	1×10^9

Table 2.7 is the basic water hydrolysis set from INSPECT [42]. Table 2.7 is the iodine reaction set from INSPECT [42,43] and Powers [44]; Table 2.10 is the iron reaction set [44]. Table 2.9 is the organic iodine set [44]. The framework for the organic reactions is in place, but the equations have not been entered, due to a lack of data to compare results. When data becomes available, the organic reactions can be activated by entering the equations into the EQINIT routine. The numbers for the reactions in the first column of the tables corresponds to the reactions as labeled in Powers [44]. The column labeled "Rate Constant" in the tables gives either a constant rate or refers to a calculated rate as given in Table 2.10.

Table 2.10 Variable Rates

M10	$\text{e}^- + \text{H}_2\text{O} \rightarrow \text{H}^\circ + \text{OH}^-$	$\text{R16} * \text{K}_{\text{H}_2\text{O}} / \text{K}_{\text{H}_0}$
M20	$\text{HO}_2^\circ \rightarrow \text{H}^+ + \text{O}_2^-$	$\text{R19} * \text{K}_{\text{HO}_2}$
M22	$\text{H}_2\text{O}_2 \rightarrow \text{H}^+ + \text{HO}_2^-$	$\text{R21} * \text{K}_{\text{H}_2\text{O}_2}$

RN Package Reference Manual

M24	$O^- + H_2O \rightarrow OH^0 + OH^-$	$R23 * K_{H2O} / K_{OH0}$
M26	$O_2^- + H_2O \rightarrow HO_2^0 + OH^-$	$R25 * R19 * K_{H2O} / R20$
M102	$H_2O_2 \rightarrow 2OH^0$	$6.4 \times 10^5 \exp(-8540/T)$
M134	$I_2OH^- \rightarrow I_2(aq) + OH^-$	$R132 * R133 * K_{H2O} / R131$
M145	$IO^- + H_2O \rightarrow HOI^0 + OH^-$	$R144 * R152 * K_{H2O} / R151$
M149	$I_3^- \rightarrow I_2(aq) + I^-$	$R148 / K_3$

The K_n in the third column of Table 2.10 are equilibrium constants, and the R_n are reaction rates for equation number n. Also needed are the acid dissociation constants (Table 2.11)

Table 2.11 Acid Dissociation Constants

$OH^0 \Leftrightarrow O^- + H^+$	$\log_{10} K_{OH0} = -4893.6/T + 60.701 - 22.629 \log_{10} T$
$H_2O_2 \Leftrightarrow HO_2^- + H^+$	$\log_{10} K_{H2O2} = -3789.7/T + 56.284 - 16.473 \log_{10} T$
$HO_2^0 \Leftrightarrow O_2^- + H^+$	$\log_{10} K_{HO2} = -519/T - 3.06$
$H^0 + OH^- \Leftrightarrow e^- + H_2O$	$\log_{10} K_{H0} = -2317/T - 1.816$
$I_3^- \Leftrightarrow I_2 + I^-$	$\log_{10} K_{I3-} = 945.5/T - 0.282$
$HOI \Leftrightarrow IO^- + H^+$	$\log_{10} K_{HOI} = -80670/T + 0.7335 T + 2800 - 1115.1 \log_{10} T$

The solution of the equation set proceeds as follows (box 10 in Figure 2.4):

- (1) If this is the initial calculation of speciation (indicated by all species being zero other than the drivers), an initialization is performed to set the initial speciation. At present, this consists of solving for the iodine ion concentration from a set of five equations; these can be reduced to a cubic equation in I^- , which is then solved for directly. The other species in the five equations (I_{2aq} , HOI , IO_3^- , and I_3^-) could also be initialized, but this does not seem to be necessary. In actuality, iodine ion is approximately equal to the total iodine concentration over most of the pH range and only differs at low pHs.
- (2) If the pool speciation calculation has been done previously (on the last timestep), the speciation from the last timestep is used as the initial speciation.
- (3) The set of chemical reaction equations is solved via a stiff ODE solver [45]. As implemented in MELCOR, the equations are advanced in "time" using a default "timestep" of 2.0s until equilibrium is reached, indicated by the changes in the species concentrations being less than an error criterion, or 2000 steps are taken. This result is then taken as the pool speciation. This equilibrium approach is used, rather than advancing the equations in real time, because of the uncertainty in the actual time history of the pool. That is, the pool initial conditions are set to a

simplified starting point when the pool model becomes activated. This initial starting point does not necessarily reflect the actual pool speciation at pool model activation time, and it is unknown to the pool model how long the pool has actually been in existence. Therefore, the time advancement of the pool equations is treated as an advancement in iteration time to equilibrium, rather than advancement in real time. The "iteration timestep", the number of steps, and the convergence criteria are adjustable via sensitivity coefficients 7181.

2.11.7.4.2 Aqueous Radiolysis

The radiolysis model for the pool uses a set of temperature-dependent yields based on values recommended by Buxton et al. [46] at 298 K and Elliot et al. [47] at 573 K, as listed in Table 2.12.

Table 2.12 Primary Products of Water Radiolysis

Species	G (molecules/100 ev)
$e^- = H^+$	$0.9204 + 5.364 T/1000$
H	$0.0798 + 1.7454 T/1000$
OH^0	$1.3238 + 4.6182 T/1000$
H_2	$0.2658 + 0.6182 T/1000$
H_2O_2	$0.1040 + 2.000 T/1000$

This set of yields is used with the user-specified pool dose to calculate the radiolysis source terms for the aqueous chemistry reaction set, as

$$\dot{S}_i = G(i) 2.88 \times 10^{-7} \dot{D}_{pool}$$

where

\dot{S}_i = radiolysis source for species i in pool (kmole/m³-s)

$G(i)$ = yield factor for species i

\dot{D}_{pool} = dose rate to pool (MRad/hr)

2.11.7.4.3 Speciation Initialization

The initialization of the pool species is done by combining a set of five iodine equations to eliminate all but the I^- concentration. This gives a cubic equation in the I^- concentration, which can be solved directly. The equation set does not include the effects of H_2O_2 on iodine, so is not a particularly good guess at high pHs.

2.11.7.5 Pool-Atmosphere Mass Transfer

Once the pool speciation is determined by the aqueous chemistry model, the mass exchange of iodine and methyl iodine with the atmosphere is calculated (see Figure 2.4). This is done via a two-film model, in which the concentration of iodine species in the pool at the pool surface is assumed to be in equilibrium via a partition coefficient with the species in the atmosphere in a film next to the pool surface at local saturation conditions. Mass transfer is then done between this surface film and the bulk atmosphere based on the surface-bulk species concentration difference and a mass transfer coefficient. Transfer rates between the bulk pool and pool surface are ignored (the pool is assumed to be well-stirred). Partition coefficients are included for I_2 , CH_3I , I^0 , and HOI . The mass transfer equation for iodine is written as

$$\frac{d[I_{2atm}]}{dt} = k_{pool} \frac{A_{pool}}{V_{atm}} ([I_{2aq}] / PC_{I_2} - [I_{2atm}])$$

where

$[I_{2atm}]$ = atmospheric iodine concentration (kmole/m³)

$[I_{2aq}]$ = bulk pool iodine concentration (kmole/m³)

k_{pool} = mass transfer coefficient from pool surface to atmosphere (m/s)

PC_{I_2} = partition coefficient for iodine.

The above equation can be written several ways, so care must be taken when comparing between codes.

The partition coefficient is defined as $PC_i = (\text{concentration of species } i \text{ in aqueous phase}) / (\text{concentration of species } i \text{ in gas-phase})$. The most important species released from the pool to the atmosphere is molecular iodine. The partition coefficient for iodine used in MELCOR is given as [48]

$$\log_{10} PC_{I_2} = 13.5467 - 0.0605142T + 7.166 \times 10^{-5}T^2$$

where T is in °K. The partition coefficients for I^0 and HOI in MELCOR are both the same and are given as

$$PC_{I^0} = 0.0238 PC_{I_2}$$

This is derived by taking the ratio of the *PC* for I^0 (1.9) [43] and that for I_2 at room temperature and pressure, and assuming the same temperature dependence for I^0 as for I_2 . The partition coefficients for I^0 and HOI should be used with caution, as there is little proof for the contention that either can be released from the pool. Although a number of researchers have suggested partition coefficients for HOI, researchers have failed to measure its presence [49], and the partition coefficient for HOI should be regarded as a placeholder. Likewise, release of atomic iodine is controversial. These two *PCs* are defaulted to **OFF** in the iodine model but can be turned on via user input. The *PC* for methyl iodine is [50]

$$PC_{CI} = 9.4 \times 10^{-4} \exp\left(\frac{2641}{T}\right)$$

2.11.7.6 Iodine Atmospheric Radiolysis and Recombination

The atmospheric radiolysis model considers homogeneous radiolytic decomposition of iodine species, and subsequent recombination reactions.

The atmospheric reduction of iodine is represented by reactions with hydrogen and ozone, and radiolytic reduction. The thermal reduction reaction with hydrogen is

$$\frac{d[I_{2atm}]}{dt} = -k_{TIH} [I_{2atm}] [H_2]$$

where the reaction rate is [51]

$$k_{TIH} = 1 \times 10^{11} \exp\left(-\frac{20131}{T}\right)$$

And,

k_{TIH} = reaction coefficient with hydrogen ($m^3/kMol-s$)

T = atmospheric temperature (K).

The reaction with ozone is

$$\frac{d[I_{2atm}]}{dt} = -k_{TIO} [I_{2atm}] [O_3]$$

RN Package Reference Manual

where the reaction coefficient is [52]

$$k_{TIO} = 2.42 \times 10^6 \exp\left(-\frac{2050}{T}\right).$$

The radiolytic reduction effect is given as [53]

$$k_{RI} = 0.028 \dot{D}_{atm}$$

where

k_{RI} = radiolytic reduction coefficient, and

\dot{D}_{atm} = atmospheric dose rate (MRad/hr).

The organic iodine is similarly reduced using an oxidation and a radiolytic reaction [54]. The oxidation reaction is

$$\frac{d[CH_3I_{atm}]}{dt} = -k_{TCIO}[CH_3I_{atm}][O_2]$$

where

$[CH_3I_{atm}]$ = atmospheric methyl iodide concentration (kmole/m³),

k_{TCIO} = oxidation reaction rate, given as

$$k_{TCIO} = 10^9 \exp\left(-\frac{13235}{T}\right).$$

The radiolytic reduction rate is

$$K_{RCL} = 0.00164 \dot{D}_{atm}$$

where, k_{RCL} is the radiolytic reduction coefficient for CH₃I. The effect of the decomposition is to increase the amount of elemental iodine in the atmosphere, decreasing the amount of I₂ and CH₃I.

The recombination reaction is assumed to be in equilibrium, using the new concentrations of I_2 and I^0 . An equilibrium coefficient,

$$K_{I_2I} = \frac{p(I_2)}{p(I)^2}$$

$$K_{I_2I} = 5.44 \times 10^{-6} \exp\left(\frac{18163}{T}\right)$$

and a mole balance on the iodine in the atmosphere as I_2 and I^0

$$M(I) = 2[I_2] + [I^0]$$

where $M(I)$ is the molar concentration of I , is used to calculate the recombination of elemental iodine into I_2 . Combining the equilibrium coefficient K_{I_2I} with the mole balance gives the new concentration of I^0 as

$$[I^0] = \frac{1}{4K_{I_2I}RT} \left[-1 + \sqrt{1 + 8K_{I_2I}M(I)RT} \right].$$

Since I^0 is not tracked in MELCOR, the I^0 is added to the I_2 for purposes of transport. The net effect of the decomposition-recombination reactions is to deplete CH_3I from the atmosphere and form I_2 .

where

$[I_{2wall}]$ = wall surface iodine concentration (kmole/m²)

k_{ad} = adsorption coefficient (m/s)

k_{de} = desorption coefficient (s⁻¹).

Default values for steel walls were selected to match results of RTF tests [55]. The coefficients are adjustable via sensitivity coefficients 7180. If the dry wall surfaces subsequently become wet, the water film is assumed to completely dissolve the adsorbed iodine and the film can drain to other surfaces or the pool via the MELCOR film model. The same model is used for steel or painted surfaces, although there is some evidence for a second stage chemical reaction process on painted adsorbing surfaces. There is not enough data presently available to determine the terms for such a model, so the physical model is used by itself.

2.11.7.7 Iodine Atmosphere-Wall Deposition

Iodine species in the atmosphere are allowed to deposit on dry wall surfaces via a physical adsorption-desorption model similar to the one in LIRIC [55]. The model is given as

$$\frac{d[I_{2wall}]}{dt} = k_{ad}[I_{2atm}] - k_{de}[I_{2wall}]$$

where

$[I_{2wall}]$ = wall surface iodine concentration (kmole/m²)

k_{ad} = adsorption coefficient (m/s), and

k_{de} = desorption coefficient (s⁻¹).

Default values for steel walls were selected to match results of RTF tests [55]. The coefficients are adjustable via sensitivity coefficients 7180. If the dry wall surfaces subsequently become wet, the water film is assumed to completely dissolve the adsorbed iodine and the film can drain to other surfaces or the pool via the MELCOR film model. The same model is used for steel or painted surfaces, although there is some evidence for a second stage chemical reaction process on painted adsorbing surfaces. There is not enough data presently available to determine the terms for such a model, so the physical model is used by itself.

2.11.8 Data Base Supporting Model Validation

There are three series of experiments that can be used for validating these models, the wide ranging Radioiodine Test Facility (RTF) experiments that are part of the Advanced Containment Experiments (ACE) performed at (AECL) Whiteshell Nuclear Research Establishment [56], small scale radiolysis tests performed at (CEA) Cadarache [57], and the hydrolysis experiments performed at Oak Ridge National Laboratory (ORNL) [40]. In the RTF experiments, tests 2 and 3 varied the pH over a wide range and measured the iodine partition coefficient, that is, the ratio of the aqueous iodine to the airborne iodine concentrations. Qualitatively, they were able to show that as the pH increases, the partition coefficient increases, and the atmospheric iodine concentration decreases. In the CEA tests, a solution of iodine was exposed to a 0.4 MR/hr source and the iodine speciation was measured. The present MELCOR iodine model was used in a recent participation in International Standard Problem (ISP) 41.

In the ORNL experiments, the temperature and pH of a pool was varied from 25 to 90 degrees Centigrade and from 3 to 9, respectively. In these tests, the end product iodine speciation was measured.

Development and testing of the model initial testing was based on comparison with the results from other codes, in particular radiolysis results from the INSPECT code. Testing against ISP41 results validated the iodine pool-atmosphere partitioning variation with pH and the coefficients for the wall deposition on steel walls [58]. As mentioned, sufficient data to validate the organic reaction set is not yet available, so the organic reactions are not implemented, although all the framework is present.

In later testing, the model will be compared with the available experimental data discussed previously, that is, the Canadian, French, and Oak Ridge data for validation. Finally, the effect of iodine chemistry on a late phase accident will be evaluated.

3. Discussion and Development Plans

3.1 RCS Deposition

The MELCOR Peer Review also placed the omission of some aerosol deposition processes, principally inertial impaction and turbulent deposition, on the list of the most important missing models in MELCOR. These processes, which are not generally important in containment and which therefore are not included in MAEROS, may assume primary importance in the reactor coolant system. As discussed in the MELCOR Peer Review, experimental data and calculations using more comprehensive aerosol deposition models indicate that the neglect of these processes may result in a significant underestimate of the retention of aerosols in the primary system, especially for low-pressure sequences in which gas velocities are high. However, the Marviken assessment calculations [59] showed good agreement with primary system retention data for both aerosols and fission product vapors, indicating the possibility of compensating processes.

3.2 Chemical Reactions with Surfaces

The MELCOR Peer Review also identified the lack of explicit modeling in MELCOR for chemical reactions between deposited fission products and structures in the primary system as one of the most important missing models. Such reactions can greatly affect deposition (chemisorption) and revaporization rates. Although a framework exists in the RN package for allowing user specification of chemical reactions, it is largely untested and unused. Because user input is basically unconstrained, the generation of errors through unexpected reactions is quite possible. The MELCOR Peer Review noted that the lack of explicit modeling applies to all accident sequences and is particularly serious for cesium hydroxide and tellurium compounds. This has been addressed in release 1.8.4 via the surface chemisorption model.

3.3 Aqueous Chemistry

The MELCOR Peer Review separately identified fission product chemistry in water pools as a less critical but still important modeling omission. The chief concern expressed in the MELCOR Peer Review was that release of iodine to the environment may be understated because MELCOR neglects processes that can occur in water pools to transform cesium iodide into more volatile forms of iodine (e.g., reaction with methane to form methyl iodide). The MELCOR 1.8.5 code release includes a detailed iodine pool chemistry model, based largely on the INSPECT code and on work by Powers. The model has received limited testing and verification against the ISP-41 test data [58]. Future assessment against other experimental data is recommended in order to further evaluate and refine other important aspects of iodine chemistry including organic compounds and silver.

**This front page
intentionally left blank**

Appendix A: RN Package Sensitivity Coefficients

This appendix gives the sensitivity coefficients associated with various correlations and modeling parameters described in this reference manual.

Equation or Section	Coefficient	Value	Units
Sec. 2.4.2.3	C7000(1)	1.0E-18	-
	C7000(2)	0.001	-
	C7000(3)	0.1	-
	C7000(4)	0.1	-
	C7000(5)	1.0E-12	kg/m ³

Aerosol Coefficient Criteria			
	C7001(1)	1.0E-18	-
	C7001(2)	0.001	-

Fission Product Decay Beta Range			
Sec. 2.6	C7002(1)	1.2	Kg/m ²

COR Material Release Multipliers			
Sec. 2.3.1	C7100(1)	1.0	-
	C7100(2)	0.0	-
	C7100(3)	0.0	-
	C7100(4)	0.0	-
	C7100(5)	0.0	-
	C7100(6)	0.0	-
	C7100(7)	0.0	-

CORSOR Coefficients			
2.3.1	C7101(1,1,k), k ≠ 5	900.0	K
	C7101(2,1,k), k ≠ 5	1400.0	K
	C7101(3,1,k), k ≠ 5	2200.0	K
	C7101(1,1,5)	900.0	K
	C7101(2,1,5)	1600.0	K
	C7101(3,1,5)	2000.0	K
	C7101(1,2,1)	7.02E-9	min ⁻¹
	C7101(2,2,1)	2.02E-7	min ⁻¹
	C7101(3,2,1)	1.74E-5	min ⁻¹
	C7101(1,3,1)	0.00886	°C ⁻¹
	C7101(2,3,1)	0.00667	°C ⁻¹

CORSOR Coefficients			
	C7101(3,3,1)	0.00460	°C ⁻¹
	C7101(1,2,2)	7.53E-12	min-1
	C7101(2,2,2)	2.02E-7	min-1
	C7101(3,2,2)	1.74E-5	min-1
	C7101(1,3,2)	0.0142	°C ⁻¹
	C7101(2,3,2)	0.00667	°C ⁻¹
	C7101(3,3,2)	0.00460	°C ⁻¹
	C7101(1,2,3)	7.50E-14	min-1
	C7101(2,2,3)	8.26E-9	min-1
	C7101(3,2,3)	1.38E-5	min-1
	C7101(1,3,3)	0.0144	°C ⁻¹
	C7101(2,3,3)	0.00631	°C ⁻¹
	C7101(3,3,3)	0.00290	°C ⁻¹
	C7101(1,2,4)	7.02E-9	min-1
	C7101(2,2,4)	2.02E-7	min-1
	C7101(3,2,4)	1.74E-5	min-1
	C7101(1,3,4)	0.00886	°C ⁻¹
	C7101(2,3,4)	0.00667	°C ⁻¹
	C7101(3,3,4)	0.00460	°C ⁻¹
	C7101(1,2,5)	1.62E-11	min-1
	C7101(2,2,5)	9.04E-8	min-1
	C7101(3,2,5)	6.02E-6	min-1
	C7101(1,3,5)	0.0106	°C ⁻¹
	C7101(2,3,5)	0.00552	°C ⁻¹
	C7101(3,3,5)	0.00312	°C ⁻¹
	C7101(1,2,6)	1.36E-11	min-1
	C7101(2,2,6)	1.36E-11	min-1
	C7101(3,2,6)	1.40E-6	min-1
	C7101(1,3,6)	0.00768	°C ⁻¹
	C7101(2,3,6)	0.00768	°C ⁻¹
	C7101(3,3,6)	0.00248	°C ⁻¹
	C7101(1,2,7)	5.01E012	min-1
	C7101(2,2,7)	5.93E-8	min-1
	C7101(3,2,7)	3.70E-5	min-1
	C7101(1,3,7)	0.0115	°C ⁻¹
	C7101(2,3,7)	0.00523	°C ⁻¹
	C7101(3,3,7)	0.00200	°C ⁻¹
	C7101(1,2,8)	6.64E-12	min-1

RN Package Reference Manual

CORSOR Coefficients			
	C7101(2,2,8)	6.64E-12	min-1
	C7101(3,2,8)	1.48E-7	min-1
	C7101(1,3,8)	0.00631	°C ⁻¹
	C7101(2,3,8)	0.00631	°C ⁻¹
	C7101(3,3,8)	0.00177	°C ⁻¹
	C7101(1,2,9)	5.00E-13	min-1
	C7101(2,2,9)	5.00E-13	min-1
	C7101(3,2,9)	5.00E-13	min-1
	C7101(1,3,9)	0.00768	°C ⁻¹
	C7101(2,3,9)	0.00768	°C ⁻¹
	C7101(3,3,9)	0.00768	°C ⁻¹
	C7101(1,2,10)	5.00E-13	min-1
	C7101(2,2,10)	5.00E-13	min-1
	C7101(3,2,10)	5.00E-13	min-1
	C7101(1,3,10)	0.00768	°C ⁻¹
	C7101(2,3,10)	0.00768	°C ⁻¹
	C7101(3,3,10)	0.00768	°C ⁻¹
	C7101(1,2,11)	1.90E-12	min-1
	C7101(2,2,11)	5.88E-9	min-1
	C7101(3,2,11)	2.56E-6	min-1
	C7101(1,3,11)	0.0128	°C ⁻¹
	C7101(2,3,11)	0.00708	°C ⁻¹
	C7101(3,3,11)	0.00426	°C ⁻¹
	C7101(1,2,12)	1.90E-12	min-1
	C7101(2,2,12)	5.88E-9	min-1
	C7101(3,2,12)	2.56E-6	min-1
	C7101(1,3,12)	0.0128	°C ⁻¹
	C7101(2,3,12)	0.00708	°C ⁻¹
	C7101(3,3,12)	0.00426	°C ⁻¹
	C7101(1,2,13:20)	0.0	min-1
	C7101(2,2,13:20)	0.0	min-1
	C7101(3,2,13:20)	0.0	min-1
	C7101(1,3,13:20)	0.0	°C ⁻¹
	C7101(2,3,13:20)	0.0	°C ⁻¹
	C7101(3,3,13:20)	0.0	°C ⁻¹

CORSOR-M Coefficients			
2.3.2	C7102(1,1)	2.0E5	min ⁻¹

CORSOR-M Coefficients			
	C7102(2,1)	63.8	kcal/mole
	C7102(1,2)	2.0E5	min ⁻¹
	C7102(2,2)	63.8	kcal/mole
	C7102(1,3)	2.95E5	min ⁻¹
	C7102(2,3)	100.2	kcal/mole
	C7102(1,4)	2.0E5	min ⁻¹
	C7102(2,4)	63.8	kcal/mole
	C7102(1,5)	2.0E5	min ⁻¹
	C7102(2,5)	63.8	kcal/mole
	C7102(1,6)	1.62E6	min ⁻¹
	C7102(2,6)	152.8	kcal/mole
	C7102(1,7)*	23.15	min ⁻¹
	C7102(2,7)*	44.1	kcal/mole
	C7102(1,8)	2.67E8	min ⁻¹
	C7102(2,8)	188.2	kcal/mole
	C7102(1,9)**	1.46E7	min ⁻¹
	C7102(2,9)**	143.1	kcal/mole
	C7102(1,10)	1.46E7	min ⁻¹
	C7102(2,10)	143.1	kcal/mole
	C7102(1,11)**	5.95E3	min ⁻¹
	C7102(2,11)**	70.8	kcal/mole
	C7102(1,12)	5.95E3	min ⁻¹
	C7102(2,12)	70.8	kcal/mole
	C7102(1,13)	0.0	min ⁻¹
	C7102(2,13)	0.0	kcal/mole

Note. The CORSOR-M model does not consider release from Class 7 (Moly), Class 9 (La) or Class 11 (Cd) to be significant. Previous versions of MELCOR used zero values for these classes when using CORSOR-M. In MELCOR 1.8.5 non-zero release coefficients are supplied as described.

* Coefficients for CORSOR-M class 7 (Moly) are based on a curve fit to the CORSOR release model for Class 7.

** Coefficients for CORSOR-M Class 7 are set identical to the CORSOR-M Class 8 values, following the same assumption as used in the CORSOR model for Class 7. Likewise for Class 11 and 12.

CORSOR-Booth Class Scaling Factors: Nominal Values			
	C7103(1)	1.0	-
	C7103(2)	1.0	-
	C7103(3)	3.33E-3	-
	C7103(4)	1.0	-
	C7103(5)	1.0	-
	C7103(6)	1.0E-4	-
	C7103(7)	1.0E-3	-
	C7103(8)	3.34E-5	-

RN Package Reference Manual

CORSOR-Booth Class Scaling Factors: Nominal Values			
	C7103(9)	1.0E-4	-
	C7103(10)	1.0E-4	-
	C7103(11)	5.0E-2	-
	C7103(12)	5.0E-2	-
	C7103(13:20)	0.0	-

Release Surface-to-Volume Ratio			
	C7104(1)	422.5	m ⁻¹

Modification of Release Rates for Tellurium			
Sec. 2.3.1	C7105(1)	5.0	-
	C7105(2)	0.7	-
	C7105(3)	0.025	-

CORSOR-Booth Coefficients for Cesium			
2.3.3	C7106(1)	5.0E-8	m ² /s
	C7106(2)	2.5E-7	m ² /s
	C7106(3)	3.0E4	MWD/MTU
	C7106(4)	3.8E5	J/kg-mole
	C7106(5)	1.0E-5	m

CORSOR-Booth Class Scaling Factors: Oxidation Modified			
	C7107(6,3)	0.05	-
	C7107(7,3)	0.05	-
	C7107(6,5)	0.70	-
	C7107(7,5)	0.025	-
	C7107(1,6)	0.75	-
	C7107(2,6)	2300.0	K
	C7107(3,6)	1.06792E-20	-
	C7107(4,6)	0.0159923	K ⁻¹
	C7107(5,6)	2700.0	K
	C7107(6,9)	0.05	-
	C7107(7,9)	0.10	-
	C7107(1,11:12)	0.75	-
	C7107(2,11:12)	2000.0	K
	C7107(3,11:12)	3.194E-9	-
	C7107(4,11:12)	0.008283	K ⁻¹
	C7107(5,11:12)	2300.0	K
	otherwise		

RN Package Reference Manual

CORSOR-Booth Class Scaling Factors: Oxidation Modified			
	C7107(1,i)	1.1	-
	C7107(2,i)	0.0	K
	C7107(3,i)	0.0	-
	C7107(4,i)	0.0	K ⁻¹
	C7107(5,i)	0.0	K
	C7107(6,i)	-1.0	-
	C7107(7,i)	0.0	-

Vapor Pressure			
2.5.22	C7110(1,1,1)	0.0	K
	C7110(1,2,1)	-1.0	K
	C7110(2,1,1)	10000.0	K
	C7110(1,1,2)	600.0	K
	C7110(1,2,2)	9400.0	K
	C7110(1,3,2)	21.59	-
	C7110(1,4,2)	-3.75	-
	C7110(2,1,2)	1553.0	K
	C7110(2,2,2)	6870.778	K
	C7110(2,3,2)	7.994503	-
	C7110(2,4,2)	0.	-
	C7110(1,1,3)	1000.0	K
	C7110(1,2,3)	7836.0	K
	C7110(1,3,3)	6.44	-
	C7110(1,4,3)	0.	-
	C7110(2,1,3)	10000.	K
	C7110(1,1,4)	298.0	K
	C7110(1,2,4)	3578.0	K
	C7110(1,3,4)	17.72	-
	C7110(1,4,4)	-2.51	-
	C7110(2,1,4)	387.0	K
	C7110(2,2,4)	3205.0	K
	C7110(2,3,4)	23.66536	-
	C7110(2,4,4)	-5.18	-
	C7110(3,1,4)	457.0	K
	C7710(3,2,4)	2176.912045	K
	C7110(3,3,4)	7.63735266	-
	C7110(3,4,4)	0.	-
	C7110(1,1,5)	298.0	K
	C7110(1,2,5)	13940.0	K
	C7110(1,3,5)	23.51	-

RN Package Reference Manual

Vapor Pressure			
	C7110(1,4,5)	-3.52	-
	C7110(2,1,5)	10000.0	K
	C7110(1,1,6)	1500.0	K
	C7110(1,2,6)	33200.0	K
	C7110(1,3,6)	10.6088	-
	C7110(1,4,6)	0.0	-
	C7110(2,1,6)	10000.0	K
	C7110(1,1,7)	1500.0	K
	C7110(1,2,7)	32800.0	K
	C7110(1,3,7)	9.68	-
	C7110(1,4,7)	0.0	-
	C7110(2,1,7)	10000.0	K
	C7110(1,1,8)	1500.0	K
	C7110(1,2,8)	21570.0	K
	C7110(1,3,8)	8.74	-
	C7110(1,4,8)	0.0	-
	C7110(2,1,8)	10000.0	K
	C7110(1,1,9)	1500.0	K
	C7110(1,2,9)	21800.0	K
	C7110(1,3,9)	8.683	-
	C7110(1,4,9)	0.0	-
	C7110(2,1,9)	10000.0	K
	C7110(1,1,10)	1500.0	K
	C7110(1,2,10)	32110.0	K
	C7110(1,3,10)	11.873	-
	C7110(1,4,10)	0.0	-
	C7110(2,1,10)	10000.0	K
	C7110(1,1,11)	1000.0	K
	C7110(1,2,11)	13730.0	K
	C7110(1,3,11)	8.43	-
	C7110(1,4,11)	0.0	-
	C7110(2,1,11)	10000.0	K
	C7110(1,1,12)	1000.0	K
	C7110(1,2,12)	15400.0	K
	C7110(1,3,12)	8.15	-
	C7110(1,4,12)	0.0	-
	C7110(2,1,12)	10000.0	K
	C7110(1,1,13)	1000.0	K
	C7110(1,2,13)	19520.0	K
	C7110(1,3,13)	11.125	-

RN Package Reference Manual

Vapor Pressure			
	C7110(1,4,13)	0.0	-
	C7110(2,1,13)	10000.0	K
	C7110(1,1,14:15)	3000.0	K
	C7110(1,2,14:15)	18000.0	K
	C7110(1,3,14:15)	8.875	-
	C7110(1,4,14:15)	0.	-
	C7110(2,1,14:15)	10000.	K
	C7110(1,1,16)	600.0	K
	C7110(1,2,16)	10420.0	K
	C7110(1,3,16)	19.70	-
	C7110(1,4,16)	-3.02	-
	C7110(2,1,16)	894.0	K
	C7110(2,2,16)	9678.0	K
	C7110(2,3,16)	20.34569	-
	C7110(2,4,16)	-3.52	-
	C7110(3,1,16)	1553.0	K
	C7110(1,1,17:20)	3000.0	K
	C7110(1,2,17:20)	18000.0	K
	C7110(1,3,17:20)	8.875	-
	C7110(1,4,17:20)	0.	-
	C7110(2,1,17:20)	10000.	K

Vapor Diffusivity Constants			
2.5.20	C7111(1,1)	4.055	Å
	C7111(2,1)	229.0	K
	C7111(1,2:3)	3.617	Å
	C7111(2,2:3)	97.0	K
	C7111(1,4)	4.982	Å
	C7111(2,4)	550.0	K
	C7111(1,5:20)	3.617	Å
	C7111(2,5:20)	97.0	K

Class Molecular Weights			
Sec. 2.1	C7120(1,1)	131.3	kg/kg-mole
	C7120(2,1)	131.3	kg/kg-mole
	C7120(1,2)	132.905	kg/kg-mole
	C7120(2,2)	149.913	kg/kg-mole
	C7120(1,3)	137.34	kg/kg-mole

RN Package Reference Manual

Class Molecular Weights			
	C7120(2,3)	137.34	kg/kg-mole
	C7120(1,4)	253.8008	kg/kg-mole
	C7120(2,4)	253.8008	kg/kg-mole
	C7120(1,5)	127.6	kg/kg-mole
	C7120(2,5)	143.6	kg/kg-mole
	C7120(1,6)	101.07	kg/kg-mole
	C7120(2,6)	101.07	kg/kg-mole
	C7120(1,7)	95.94	kg/kg-mole
	C7120(2,7)	95.94	kg/kg-mole
	C7120(1,8)	140.12	kg/kg-mole
	C7120(2,8)	140.12	kg/kg-mole
	C7120(1,9)	138.91	kg/kg-mole
	C7120(2,9)	138.91	kg/kg-mole
	C7120(1,10)	238.03	kg/kg-mole
	C7120(2,10)	270.03	kg/kg-mole
	C7120(1,11)	112.4	kg/kg-mole
	C7120(2,11)	112.4	kg/kg-mole
	C7120(1,12)	118.69	kg/kg-mole
	C7120(2,12)	118.69	kg/kg-mole
	C7120(1,13)	69.622	kg/kg-mole
	C7120(2,13)	69.622	kg/kg-mole
	C7120(1,14)	18.016	kg/kg-mole
	C7120(2,14)	18.016	kg/kg-mole
	C7120(1,15)	28.97	kg/kg-mole
	C7120(2,15)	28.97	kg/kg-mole
	C7120(1,16)	259.8054	kg/kg-mole
	C7120(2,16)	259.8054	kg/kg-mole
	C7120(1,17:20)	28.97	kg/kg-mole
	C7120(2,17:20)	28.97	kg/kg-mole

Solubility of RN Classes in Water Films			
Sec. 2.4.2.2	C7136(1:20)	1.0	-

Not Used with LWR COR Package			
7140 - Release from Molten U-Al Pools			
7141 - Solubility of Classes in Al-U Alloy			
7142 - Debris Particle of Average Surface Area			
7143 - Molten Fraction Criterion for Release from U-Al Pools			
7144 - Temperature Criterion for Release from Intact Fuel			

7150 - SPARC-90 Model Parameters			
Appendix E	7150(1)	10.	-
	7150(2)	5.	-
	7150(3)	1.E-4	-
	7150(4)	25.	-
	7150(5)	1.E-4	-
	7150(6)	25.	-
	7150(7)	1.E-3	-
	7150(8)	25.	-
	7150(9)	1.E12	-
	7150(10)	1.0	-

7151 - SPARC-90 Globule Size Correlation			
Appendix D	7151(1,1)	3.45	-
	7151(2,1)	0.46	-
	7151(1,2)	0.0891	-
	7151(2,2)	0.616	-
	7151(1,3)	0.857	-
	7151(2,3)	0.73	-

7152 - SPARC-90 Bubble Size/Shape Model			
E-1	7152(1)	0.007	m
	7152(2)	-0.2265	-
	7152(3)	0.0203	-
	7152(4)	0.0313	-
	7152(5)	0.5	-
E-2	7152(6)	0.817	-
	7152(7)	1.13466	cm ⁻¹
	7152(8)	-0.3795	cm ⁻²

7153 - SPARC-90 Bubble Rise Velocity Model			
E-3	7153(1)	7.876	cm/s
	7153(2)	0.5	cm
	7153(3)	1.40713	-
	7153(4)	0.49275	-

7154 - SPARC-90 Swarm Velocity Model			
E-5	7154(1)	5.33	liter/s
	7154(2)	3.011E-3	liter-s/cm ²
	7154(3)	0.5	-
	7154(4)	-3.975E-4	cm ⁻¹

RN Package Reference Manual

7154 - SPARC-90 Swarm Velocity Model			
	7154(5)	170.	cm/s

7155 - SPARC-90 Particle Impaction Model			
D-11	7155(1)	1.79182	-
	7155(2)	3.3437E-11	-
	7155(3)	5.9244E-3	-
	7155(4)	0.65868	-
D-12	7155(5)	1.13893	-
	7155(6)	1.4173E-6	-
	7155(7)	4.25973E-3	-
	7155(8)	0.99	-

7156 - SPARC-90 Solute Ionization Correlations			
E-12	7156(1)	1.79417	-
	7156(2)	-3.34363	-
	7156(3)	0.021	-
	7156(4)	1.63439	-
	7156(5)	4.30022	-
	7156(6)	1.75467	-
	7156(7)	20.7974	-
	7156(8)	-0.002321	-
	7156(9)	25.	C
	7156(10)	2.0	-

7157 - SPARC-90 Settling Velocity Correlation			
E-19	7157(1)	9.6	-
	7157(2)	27.00	-
	7157(3)	1./1.130	-
	7157(4)	93.6	-
	7157(5)	24.32	-
	7157(6)	1./1.227	-
	7157(7)	410.	-
	7157(8)	15.71	-
	7157(9)	1./1.417	-
	7157(10)	1.07E4	-
	7157(11)	6.477	-
	7157(12)	1./1.609	-
	7157(13)	2.45E5	-
	7157(14)	1.194	-
	7157(15)	1./1.867	-

7158 - SPARC-90 HOI Correlation			
F-4	7158(1)	-1388.89	K
	7158(2)	6.461	-

7159 - SPARC-90 I ₂ Chemistry Model Parameters			
Appendix F	7159(1)	1.3882E-3	-
	7159(2)	3279.3	K
	7159(3)	7.7606	moles ⁻¹
	7159(4)	1370.	K
	7159(5)	1.0423E-2	moles ²
	7159(6)	-7148.	K
	7159(7)	4.2271E-9	moles
	7159(8)	-1748.5	K
	7159(9)	1.56531E-13	moles ²
	7159(10)	5462.81	K
	7159(11)	-1.87376E6	K ²
	7159(12)	1.E-6	moles/cm ³
	7159(13)	1.E-3	-

7160 - Chemisorption Rate Coefficients			
2.9.2	C7160(1,1)	0.139	m/s
	C7160(2,1)	5.96e7	J/kg
	C7160(1,2)	0.035	m/s
	C7160(2,2)	5.96e7	J/kg
	C7160(1,3)	2.0e-7	m/s
	C7160(2,3)	0.0	J/kg
	C7160(1,4)	2.0e-6	m/s
	C7160(2,4)	0.0	J/kg
	C7160(1,5)	5.5e-7	m/s
	C7160(2,5)	2.49e7	J/kg
	C7160(1,6)	9.0e-10	m/s
	C7160(2,6)	3.39e7	J/kg

7170 Hygroscopic Aerosol Sensitivity Coefficients			
Reference	Coefficient	Value	Units
	C7170(1,1)	273.0	K
	C7170(2,1)	373.0	K
	C7170(3,1)	0.0	Kg/kg H ₂ O
	C7170(4,1)	0.0	Kg/kg H ₂ O
	C7170(5,1)	600.0	K
	C7170(6,1)	647.0	K

RN Package Reference Manual

7170 Hygroscopic Aerosol Sensitivity Coefficients			
Reference	Coefficient	Value	Units
	C7170(7,1)	2	ions/molecule
	C7170(8,1)	0	ions/molecule
	C7170(9,1)	1.0	Kg/m ³
	C7170(1,2)	273.0	K
	C7170(2,2)	373.0	K
	C7170(3,2)	3.95	Kg/kg H ₂ O
	C7170(4,2)	3.95	Kg/kg H ₂ O
	C7170(5,2)	600.0	K
	C7170(6,2)	647.0	K
	C7170(7,2)	2	ions/molecule
	C7170(8,2)	0	ions/molecule
	C7170(9,2)	3675.0	Kg/m ³
	C7170(1,3)	273.0	K
	C7170(2,3)	373.0	K
	C7170(3,3)	0.0	Kg/kg H ₂ O
	C7170(4,3)	0.0	Kg/kg H ₂ O
	C7170(5,3)	600.0	K
	C7170(6,3)	647.0	K
	C7170(7,3)	2	ions/molecule
	C7170(8,3)	0	ions/molecule
	C7170(9,3)	5720.0	Kg/m ³
	C7170(1,4)	273.0	K
	C7170(2,4)	373.0	K
	C7170(3,4)	0.0	Kg/kg H ₂ O
	C7170(4,4)	0.0	Kg/kg H ₂ O
	C7170(5,4)	600.0	K
	C7170(6,4)	647.0	K
	C7170(7,4)	2	ions/molecule
	C7170(8,4)	0	ions/molecule
	C7170(9,4)	1.0	Kg/m ³
	C7170(1,5)	273.0	K
	C7170(2,5)	373.0	K
	C7170(3,5)	0.0	Kg/kg H ₂ O
	C7170(4,5)	0.0	Kg/kg H ₂ O
	C7170(5,5)	600.0	K
	C7170(6,5)	647.0	K
	C7170(7,5)	2	ions/molecule
	C7170(8,5)	0	ions/molecule
	C7170(9,5)	5680.0	Kg/m ³
	C7170(1,6)	273.0	K

RN Package Reference Manual

7170 Hygroscopic Aerosol Sensitivity Coefficients			
Reference	Coefficient	Value	Units
	C7170(2,6)	373.0	K
	C7170(3,6)	0.0	Kg/kg H ₂ O
	C7170(4,6)	0.0	Kg/kg H ₂ O
	C7170(5,6)	600.0	K
	C7170(6,6)	647.0	K
	C7170(7,6)	2	ions/molecule
	C7170(8,6)	0	ions/molecule
	C7170(9,6)	6970.0	Kg/m ³
	C7170(1,7)	273.0	K
	C7170(2,7)	373.0	K
	C7170(3,7)	0.0	Kg/kg H ₂ O
	C7170(4,7)	0.0	Kg/kg H ₂ O
	C7170(5,7)	600.0	K
	C7170(6,7)	647.0	K
	C7170(7,7)	2	ions/molecule
	C7170(8,7)	0	ions/molecule
	C7170(9,7)	7440.0	Kg/m ³
	C7170(1,8)	273.0	K
	C7170(2,8)	373.0	K
	C7170(3,8)	0.0	Kg/kg H ₂ O
	C7170(4,8)	0.0	Kg/kg H ₂ O
	C7170(5,8)	600.0	K
	C7170(6,8)	647.0	K
	C7170(7,8)	2	ions/molecule
	C7170(8,8)	0	ions/molecule
	C7170(9,8)	7000.0	Kg/m ³
	C7170(1,9)	273.0	K
	C7170(2,9)	373.0	K
	C7170(3,9)	0.0	Kg/kg H ₂ O
	C7170(4,9)	0.0	Kg/kg H ₂ O
	C7170(5,9)	600.0	K
	C7170(6,9)	647.0	K
	C7170(7,9)	2	ions/molecule
	C7170(8,9)	0	ions/molecule
	C7170(9,9)	6510.0	Kg/m ³
	C7170(1,10)	273.0	K
	C7170(2,10)	373.0	K
	C7170(3,10)	0.0	Kg/kg H ₂ O
	C7170(4,10)	0.0	Kg/kg H ₂ O
	C7170(5,10)	600.0	K

RN Package Reference Manual

7170 Hygroscopic Aerosol Sensitivity Coefficients			
Reference	Coefficient	Value	Units
	C7170(6,10)	647.0	K
	C7170(7,10)	2	ions/molecule
	C7170(8,10)	0	Ions/molecule
	C7170(9,10)	10960.0	Kg/m ³
	C7170(1,11)	273.0	K
	C7170(2,11)	373.0	K
	C7170(3,11)	0.0	Kg/kg H ₂ O
	C7170(4,11)	0.0	Kg/kg H ₂ O
	C7170(5,11)	600.0	K
	C7170(6,11)	647.0	K
	C7170(7,11)	2	ions/molecule
	C7170(8,11)	0	Ions/molecule
	C7170(9,11)	8150.0	Kg/m ³
	C7170(1,12)	273.0	K
	C7170(2,12)	373.0	K
	C7170(3,12)	0.0	Kg/kg H ₂ O
	C7170(4,12)	0.0	Kg/kg H ₂ O
	C7170(5,12)	600.0	K
	C7170(6,12)	647.0	K
	C7170(7,12)	2	ions/molecule
	C7170(8,12)	0	Ions/molecule
	C7170(9,12)	6446.0	Kg/m ³
	C7170(1,13)	273.0	K
	C7170(2,13)	373.0	K
	C7170(3,13)	0.0	Kg/kg H ₂ O
	C7170(4,13)	0.0	Kg/kg H ₂ O
	C7170(5,13)	600.0	K
	C7170(6,13)	647.0	K
	C7170(7,13)	2	ions/molecule
	C7170(8,13)	0	Ions/molecule
	C7170(9,13)	2520.0	Kg/m ³
	C7170(1,14)	273.0	K
	C7170(2,14)	373.0	K
	C7170(3,14)	0.0	Kg/kg H ₂ O
	C7170(4,14)	0.0	Kg/kg H ₂ O
	C7170(5,14)	600.0	K
	C7170(6,14)	647.0	K
	C7170(7,14)	2	ions/molecule
	C7170(8,14)	0	Ions/molecule
	C7170(9,14)	1000.0	Kg/m ³

7170 Hygroscopic Aerosol Sensitivity Coefficients			
Reference	Coefficient	Value	Units
	C7170(1,15)	273.0	K
	C7170(2,15)	373.0	K
	C7170(3,15)	0.0	Kg/kg H ₂ O
	C7170(4,15)	0.0	Kg/kg H ₂ O
	C7170(5,15)	600.0	K
	C7170(6,15)	647.0	K
	C7170(7,15)	2	ions/molecule
	C7170(8,15)	0	ions/molecule
	C7170(9,15)	2250.0	Kg/m ³
	C7170(1,16)	273.0	K
	C7170(2,16)	373.0	K
	C7170(3,16)	0.44	Kg/kg H ₂ O
	C7170(4,16)	2.25	Kg/kg H ₂ O
	C7170(5,16)	600.0	K
	C7170(6,16)	647.0	K
	C7170(7,16)	2	ions/molecule
	C7170(8,16)	0	ions/molecule
	C7170(9,16)	4510.0	Kg/m ³

Appendix B: Agglomeration Kernels

The agglomeration kernels currently implemented in the MELCOR implementation of MAEROS are summarized in this appendix. These kernels are those that are recommended by Powers, Sprung, and Leigh [1].

Brownian

$$\beta = 2\pi (D_i + D_j)(\gamma_i d_i + \gamma_j d_j)/F \quad (\text{B.1})$$

$$D_i = \frac{kT}{3\pi d_i \mu \chi_i} C_i \quad (\text{B.2})$$

$$C_i = 1 + Kn_i [c_m + 0.4 \exp(-1.1 / Kn_i)] \quad (\text{B.3})$$

$$F = \frac{d_i + d_j}{d_i + d_j + 2g_{ij}} + \frac{8(D_i + D_j)}{v_{ij} (d_i + d_j) c_s} \quad (\text{B.4})$$

RN Package Reference Manual

$$g_{ij} = (g_i^2 + g_j^2)^{1/2} \quad (\text{B.5})$$

$$v_{ij} = (v_i^2 + v_j^2)^{1/2} \quad (\text{B.6})$$

$$g = \frac{1}{3 d_i l_i} [(d_i + l_i)^3 - (d_i^2 + l_i^2)^{3/2}] - d_i \quad (\text{B.7})$$

$$l = \frac{8D_i}{\pi v_i} \quad (\text{B.8})$$

$$v = \left(\frac{8kT}{\pi m_i} \right)^{1/2} \quad (\text{B.9})$$

$$Kn_i = 2\lambda / d_i \quad (\text{B.10})$$

$$\lambda = \frac{\mu}{\rho_g} (1.89 \times 10^{-4} M_{w,g} / T)^{1/2} \quad (\text{B.11})$$

$$\rho_g = 1.21 \times 10^{-4} P M_{w,g} / T \quad (\text{B.12})$$

μ = values for air; from the Material Properties (MP) package

Gravitational

$$\beta = \epsilon_g \frac{\pi}{4} c_s (\gamma_i d_i + \gamma_j d_j)^2 |V_{Ti} - V_{Tj}| \quad (\text{B.13})$$

$$V_{Ti} = \frac{\rho_{pi} g d_i^2 C_i}{18 \mu \chi_i} \quad (\text{B.14})$$

$$\varepsilon_g = 1.5 \left[\frac{\min(d_i, d_j)}{(d_i + d_j)} \right]^2 \quad (B.15)$$

Turbulent

$$\beta = c_s (\beta_{T1}^2 + \beta_{T2}^2)^{1/2} \quad (B.16)$$

$$\beta_{T1} = \left(\frac{\pi \varepsilon_T \rho_g}{120 \mu} \right)^{1/2} (\gamma_i d_i + \gamma_j d_j)^3 \quad (B.17)$$

$$\beta_{T2} = \frac{0.04029 \rho_g^{1/4} \varepsilon_T^{3/4}}{\mu^{5/4}} (\gamma_i d_i + \gamma_j d_j)^2 \left| \frac{\rho_{p1} C_1 d_1^2}{\chi_1} - \frac{\rho_{p2} C_2 d_2^2}{\chi_2} \right| \quad (B.18)$$

Nomenclature	
c_m	particle slip coefficient
c_s	particle sticking coefficient
c_t	thermal accommodation coefficient
C	particle mobility
d	particle diameter
D	diffusion coefficient
k	Boltzmann constant
k_g/k_s	ratio of thermal conductivity of the gas over that for the particle
Kn	Knudsen number
m	particle mass
M_w	molecular weight
P	pressure
T	temperature
V	volume

Greek:	
β	coagulation kernel (m ³ /s)
ε_T	turbulence dissipation density
ρ	density
μ	viscosity
λ	mean free path

RN Package Reference Manual

Greek:	
γ	agglomeration shape factor
χ	dynamic shape factor

Subscripts	
b	bulk
g	gas (air assumed)
i, j	particle identifier
p	particle
s	steam

Appendix C: Aerosol Surface Area

The aerosol surface area is used for fission product vapor condensation and evaporation of aerosols. The general equation for the surface area is:

$$A_T = \int_{x_1}^{x_2} n(x)A(x)dx \quad (C.1)$$

where

A_T	total surface area
$A(x)$	area of a particle as a function of x
$n(x)$	number of particles as a function of x

MAEROS assumes that the aerosol size distribution in each section is constant with respect to the natural log of the mass, so the number density can be expressed as (Gelbard [7]):

$$n(x) = \frac{M}{m (\ln m_2 - \ln m_1)} d(\ln m) \quad (C.2)$$

A and m can be expressed in terms of $\ln m$ as follows:

$$m = e^{\ln m} \quad (C.3)$$

$$A = 4\pi r^2 \quad (C.4)$$

$$= 4\pi \left(\frac{3m}{4\pi\rho} \right)^{2/3} \quad (C.5)$$

$$= 4\pi \left(\frac{3e^{\ln m}}{4\pi\rho} \right)^{2/3} \quad (C.6)$$

Equation (C.1) becomes

RN Package Reference Manual

$$A_T = 4 \pi \left(\frac{3}{4\pi\rho} \right)^{2/3} \frac{M}{\ln(m_2/m_1)} \int_{\ln m_1}^{\ln m_2} \exp\left(-\frac{1}{3} \ln m\right) d(\ln m) \quad (C.7)$$

and, after integration,

$$A_T = 12\pi \left(\frac{3}{4\pi\rho} \right)^{2/3} \frac{M}{\ln(m_2/m_1)} [m_1^{-1/3} - m_2^{-1/3}] \quad (C.8)$$

Appendix D: Pool Scrubbing Vent Exit Region Modeling

D.1 Globule Formation

The initial globules formed have a unique size given by a correlation relating the normalized globule volume to the Weber number for each vent type considered. The correlation is

$$v_n = a \cdot We^b \quad (D.1)$$

$$D_{g,o}^3 = \frac{3}{2} v_n D_o^2 \left(\frac{\sigma}{\rho_l g} \right)^{1/2} \quad (D.2)$$

where

$$We = \frac{\rho_l D_o V_o^2}{\sigma} \quad (D.3)$$

and

ρ_l	pool liquid density,
σ	pool liquid surface tension,
D_o	vent equivalent diameter, and
V_o	exit velocity of the gas.

It is assumed that $Q = V_o (\pi/4) D_o^2$, where Q is the gas volumetric flow rate at the vent in equilibrium with the pool conditions at the vent depth. The default correlation constants implemented in sensitivity coefficient array 7151 are:

Vent	a	b	Source
Multiple small holes	3.45	0.46	EPRI program
Downcomer	0.0891	0.616	PNL with EPRI data
Horizontal vent	0.857	0.73	EPRI program

These correlations only apply to inlet gases containing noncondensable gases. Very high steam fractions provide for residual bubbles. High steam fractions have a "cone"-shaped region that does not detach from the vent.

RN Package Reference Manual

The globule diameter decreases linearly to zero over a distance of twelve times its initial value:

$$D_g = D_{g,o} \left[1 - \frac{x}{12D_{g,o}} \right] \quad (D.4)$$

where x has a value of zero at the elevation of the vent exit.

D.2 Vent Exit Region Scrubbing Models

In the vent exit region, aerosol capture occurs because of:

- (1) Stefan flow from steam condensation during gas equilibration to pool conditions,
- (2) inertial impaction of aerosol particles in rapidly decelerating gas flow, and
- (3) centrifugal, diffusional and gravitational particle deposition during gas injection through small orifice, multihole vents.

D.2.1 Steam Condensation

It is assumed that the fraction of particles removed by steam condensation during globule breakup at the vent exit is simply equal to the fractional loss in gas volume caused by condensation at the temperature and pressure of the pool at the vent depth:

$$DF_{EC} = \frac{X_o}{X_i} \quad (D.5)$$

where X_i is the mole fraction of noncondensable gas in the inlet gas and X_o is the mole fraction of noncondensable gas in the gas after equilibration. X_i is determined from the flow composition in the vent provided by the FL package, and X_o is given by

$$X_o = 1 - \frac{P_{sat}(T_p)}{P_{surf} + \rho_l g h_p} \quad (D.6)$$

where T_p , P_{surf} and h_p are the pool temperature, pressure at the pool surface and pool depth at the vent exit, respectively. DF_{EC} is limited to a minimum value of one.

For iodine vapor scrubbing the value of DF_{EC} calculated above may need to be reduced significantly. The concentration of iodine in the condensate may not exceed the product of the equilibrium partition coefficient and the concentration of iodine in the vapor state remaining in the bubbles. Hence, if the concentration of iodine in the condensate would exceed the equilibrium value consistent with the partition coefficient when iodine removal is assumed to be proportional to the volumetric reduction factor (DF_{EC}), then iodine vapor scrubbing will not occur to the extent given by DF_{EC} . Rather, the decontamination factor for vapor scrubbing will be given by

$$DF_{EC,vap} = 1 + \min \left[H_{vap} \left(\frac{\rho_v}{\rho_l} \right), 1 \right] (DF_{EC} - 1) \quad (D.7)$$

so that $DF_{EC,vap}$ is less than DF_{EC} if $H_{vap} (\rho_v / \rho_l) < 1$, and equal to DF_{EC} otherwise. (Additional vapor diffusion into the aqueous phase is considered to be too slow with respect to the time scale of steam condensation to increase $DF_{EC,vap}$ above DF_{EC} in those cases where $H_{vap} (\rho_v / \rho_l)$ exceeds unity.)

D.2.2 Inertial Impaction

If gas leaves the vent exit at a high velocity, the initial globules rapidly lose that velocity. The forward globular interface, as it slows and stops, can capture particles if they have sufficient inertia. Inertia of particle size i is represented by the Stokes number

$$Stk_i = \frac{\rho_i V_e d_i^2}{9\mu D_o} \quad (D.8)$$

where

d_i	particle diameter
ρ_i	particle density
V_e	vent exit gas velocity (before equilibration with pool)
μ	gas viscosity
D_o	vent exit orifice diameter

The DF for this impaction process is

$$DF_{II,i} = \frac{1}{1 - \alpha_i} \quad (D.9)$$

RN Package Reference Manual

where

$$\alpha_i = 1.79182 \left(3.3437 \times 10^{-11} \right)^{\left(5.9244 \cdot 10^{-3} \right)^{\sqrt{Stk_i}}} \quad \text{if } \sqrt{Stk_i} \leq 0.65868 \quad (\text{D.10})$$

and

$$\alpha_i = 1.13893 \left(1.4173 \times 10^{-6} \right)^{\left(4.25973 \cdot 10^{-3} \right)^{\sqrt{Stk_i}}} \quad \text{if } 0.65868 < \sqrt{Stk_i} \quad (\text{D.11})$$

The constants in these correlations have been implemented in sensitivity coefficient array 7155, and the maximum value of α_i permitted is constrained to 0.99, which is also included in sensitivity coefficient array 7155. The importance of inertial impaction is minimal unless near-sonic values of V_e occur.

D.2.3 Centrifugal, Diffusional and Gravitational Deposition

Centrifugal, diffusional and gravitational particle deposition are only evaluated in the vent exit region for small orifice, multihole vents (MVENT=1 on input record RN2PLSXX). The bases for the model are assumptions about the vent injection bubble geometry and velocity relative to pool liquid.

Particle scrubbing is evaluated in two connected time intervals. The injection interval is defined as the time it takes to fill the globule and is given by

$$\tau_{fill} = \frac{\frac{\pi}{6} D_g^3}{\frac{\pi}{4} D_o^2 V_o} \quad (\text{D.12})$$

During the detached globule interval, which follows the injection interval, the globule is slowed by drag forces. This interval is assumed to be three times the characteristic stopping time, which is the time required for the drag force to nullify the bubble momentum

$$\tau_{stop} = \frac{4 \rho_g D_g}{3 f \rho_l V_o} \quad (\text{D.13})$$

where f , the friction factor, has a hard-wired value of 0.2. It is assumed that the final detached injection globule is spherical (of diameter D_g) and during globule formation, the

forming globule is elongated with a hemispherical front of diameter D_o (orifice diameter) moving at velocity V_o relative to the bulk liquid.

For each particle size, denoted by subscript i , the centrifugal deposition velocity is calculated by scaling the gravitational settling velocity by the ratio of the centrifugal acceleration to the gravitational acceleration. The gas circulation velocity is assumed to equal the injection velocity and the radius of curvature is equal to the circular vent radius. The decontamination factors during the injection and detached globule periods are proportional to the ratio of the volumes swept to the globule surface by centrifugal velocity to the total globule volume. The values are given by

$$DF_{C,i} = \exp(V_{C,i}/V_o) \quad \text{during injection}$$

$$DF_{C,i} = \exp\left(\frac{V_o V_{g,i} \rho_g}{9D_o f g \rho_l}\right) \quad \text{after detachment}$$
(D.14)

where $V_{C,i}$ is given by Equation (E.20) with $r_c = D_o/2$ and $V_s = V_o$. The method used to determine the settling velocity, $V_{g,i}$, is also described in Section E.3 below.

Particle deposition from Brownian diffusion during the injection and detached globule periods is modeled using film penetration theory, which is discussed in Section E.2 below. The decontamination factor during each period is proportional to the ratio of the volume swept to the globule surface by Brownian diffusion to the total globule volume. For each particle size, the decontamination factors are given by

$$DF_{D,i} = \exp\left[\frac{16\tau_{fil}}{3D_o} \left(\frac{D_i}{\pi\tau_{fil}}\right)^{1/2}\right] \quad \text{during injection}$$

$$DF_{D,i} = \exp\left[\frac{12\tau_{stop}}{D_o} \left(\frac{V_o D_i}{\pi D_o}\right)^{1/2}\right] \quad \text{after detachment}$$
(D.15)

Particle deposition from gravitational settling during the injection and detached globule periods both use a settling velocity based on Stokes's law for small particles and an empirical correlation based on the Reynolds number for larger particles. These correlations are presented in Section E.3 below. For each particle size, the decontamination factors are given by

RN Package Reference Manual

$$DF_{g,i} = \exp\left(\frac{\bar{A}_s V_{g,i} \tau_{fill}}{(\pi/6)D_{g,o}^3}\right) \text{ during injection} \quad (D.16)$$
$$DF_{g,i} = \exp\left(\frac{3V_{g,i}(3\tau_{stop})}{2D_{g,o}}\right) \text{ after detachment}$$

where the average settling area, \bar{A}_s , during injection is equal to one half the final settling area of the horizontally oriented bullet-shaped globule given by

$$A_{s,o} = \frac{2D_{g,o}^3}{3D_o} + D_o^2\left(\frac{\pi}{8} - \frac{1}{3}\right) \quad (D.17)$$

The overall decontamination factor resulting from centrifugal, diffusional and gravitational deposition, $DF_{ER,i}$, which is used in Equation 2.7.3 in Section 2.7.1, is given by

$$DF_{ER,i} = DF_{c,i} \cdot DF_{D,i} \cdot DF_{g,i} \quad (D.18)$$

Appendix E: Pool Scrubbing Swarm Rise Region Modeling

The primary modeling objective in the swarm rise region is to determine how evolving thermal-hydraulic conditions within the bubbles affect the removal of particulate aerosols and iodine vapors from the bubble. This is achieved by dividing the total rise height (the distance between the vent exit and the pool surface) into several equal sections (given by XNRISE implemented in sensitivity coefficient array 7150 with a default value of 10.), and then marching upward to update the thermal-hydraulic conditions in each section to evaluate the incremental removal in each section. In this procedure it is assumed that the swarm velocity is constant, so that the bubbles spend the same amount of time in each section.

E.1 Bubble Characteristics

The bubbles are modeled as oblate spheroids with an equivalent spherical diameter, d_{vm} , of 0.7 cm (this default value can be adjusted through sensitivity coefficient array C7152), if they contain no steam initially. The presence of steam reduces d_{vm} as follows

$$d_{vm} = 0.7 \cdot 10^{-0.2265 + (0.0203 + 0.0313 x_{rc})^{1/2}} \quad (\text{E.1})$$

The constants in Equation (E.1) re implemented in sensitivity coefficient array 7152. The shape of the bubble is calculated using the following correlation

$$\frac{a}{b} = 0.84107 + 1.13466 d_{vm} - 0.3795 d_{vm}^2 \quad (\text{E.2})$$

where a and b are the lengths of the major and minor axes of the oblate spheroid, respectively. (NOTE: The SPARC-90 documentation erroneously had a/b inverted as b/a .) This correlation was established for $0.15 \leq d_{vm} \leq 1.3$ cm. All bubbles smaller than 0.15 cm are spheres ($a/b = 1$), and bubbles larger than 1.3 cm have $a/b = 1.675$. The constants in Equation (E.2) are implemented in sensitivity coefficient array 7152.

The bubble rise velocity relative to the liquid is given by the following correlation

$$V_r = 7.876 (\sigma / \rho_l)^{1/4} \text{ (cm/s) for } d_{vm} \leq 0.5 \text{ cm} \quad (\text{E.3})$$

$$V_r = 1.40713 d_{vm}^{0.49275} V_r(d_{vm} = 0.5) \text{ (cm/s) otherwise}$$

RN Package Reference Manual

The constants in Equation (E.3) have been implemented as sensitivity coefficient array 7153. The swarm rise velocity is given by the average of the correlation value at the depth of the vent exit and at the pool surface

$$\bar{V}_s = 0.5 \cdot [V_s(x=0) + V_s(x=h_p)] \quad (\text{E.4})$$

where

$$V_s(x) = \left[(\dot{Q}_s + 5.33) / 3.011 \cdot 10^{-3} \right]^{1/2} [1 - 3.975 \cdot 10^{-4} x] \quad (\text{cm/s}) \quad (\text{E.5})$$

where \dot{Q}_s is the total gas volumetric flow rate (liter/s) at depth $h_p/2$, and the depth, x , is measured in cm. (NOTE: In the SPARC-90 documentation, Equation (E.4) is erroneous.) \bar{V}_s is limited to a maximum value of 170. cm/s, which is implemented in sensitivity coefficient array 7154 along with the constants that appear in Equation (E.5).

E.2 Bubble Heat and Mass Transfer

During each spatial step the change in the internal energy of the gas in the bubbles is tracked by evaluating iteratively the work performed by bubble expansion and the heat and mass transfer from the pool to the bubble across the bubble boundary. Because the stable size of the bubbles is assumed to remain constant, as the bubbles expand as the static pressure decreases during their ascent, they are assumed to multiply by splitting. The particle concentration (g/cm^3) in the bubbles decreases as a result of bubble multiplication to conserve mass. Bubble expansion during each step is evaluated by assuming that the bubble is isothermal and that the increase in volume is inversely proportional to the decrease in static head (i.e., by assuming ideal gas behavior).

The work done by the expanding bubble during each step is also evaluated by assuming ideal gas behavior and is given by

$$\begin{aligned} Pdv &= P \left[\left(\frac{\partial V}{\partial P} \right)_T dP + \left(\frac{\partial V}{\partial T} \right)_P dT + \Delta V_{\text{evap}} \right] \\ &= R \left[M_t T_1 \ln \left(\frac{P_1}{P_2} \right) + (T_2 - T_1) M_t + T_1 \Delta M_{\text{evap}} \right] \end{aligned} \quad (\text{E.6})$$

where ΔM_{evap} is the net increase in vapor mass from evaporation into the bubble minus condensation onto particles in the bubble during the spatial step and M_t is the sum of the steam and noncondensable mass in the bubble.

Heat and mass transfer rates between the pool and rising bubbles are based on penetration theory, in which it is assumed that the top-to-bottom gas circulation in the bubble establishes a quasi-steady boundary layer with the leading edge at the top of the bubble. The transport velocity through the boundary layer at a distance ℓ from the leading edge of the boundary layer is then given by

$$V_\phi = \left(\frac{D_\phi V_t}{\pi \ell} \right)^{1/2} \quad (\text{E.7})$$

where $D_\phi = \alpha$ (thermal diffusivity of boundary layer fluid) for heat transfer, $D_\phi = D_i$ (mass diffusivity or diffusion coefficient of species i through the boundary layer) for mass transfer, V_t is the gas circulation velocity parallel to the boundary layer and $T_e = \ell / V_t$ is commonly termed the "exposure" time of the surface. The heat transfer coefficients from the pool and bubble to the pool/bubble interface are

$$h_p = \rho_l C_l (\alpha_l / \pi \tau_e)^{1/2} \quad (\text{E.8})$$

$$h_b = \rho_g C_g (\alpha_g / \pi \tau_e)^{1/2}$$

respectively; and the rate of evaporation at the pool/bubble interface is

$$N_s = \left(\frac{P}{R T_s} \right) \left(\frac{D_s}{\pi \tau_e} \right)^{1/2} \log_e \left[\frac{P - P_{\text{sat}}(T_b)}{P - P_{\text{sat}}(T_s)} \right] \quad (\text{E.9})$$

where the subscript s indicates that the term is evaluated at the pool/bubble interface.

The rates of condensation and evaporation of water on aerosol particles will be determined by using the Mason equation

$$r \frac{dr}{dt} = \frac{S - S_r}{a + b} \quad (\text{E.10})$$

RN Package Reference Manual

which gives the time rate of change of the radius, r , of the aerosol particle as a function of the difference between the actual saturation ratio, S (defined as $P_v/P_{sat}(T)$ inside the bubble), and its equilibrium value, S_r . a , b and S_r in Equation (E.10) are given by

$$a = \frac{\rho_l M_w h_{fg}^2}{k_v R T^2}$$
$$b = \frac{\rho R T}{P_{sat} D_v M_w} \quad (E.11)$$
$$S_r = A_i \exp\left[\frac{2\sigma M_w}{r R \rho_l T}\right]$$

The heat and mass transfer equations are solved iteratively during each spatial step in the bubble's ascent. During each iteration, the heat and mass transfer rates over the bubble surface are numerically integrated by dividing the surface from 0° at the top of the bubble to 180° at the bottom of the bubble into a number (XNCIRC, with a default value of 5. implemented in sensitivity coefficient array 7150) of equally spaced latitudinal strips. The heat and mass transfer over all the strips are summed to obtain the integral values, and the exposure time, τ_e , associated with each strip is saved for use in calculating decontamination factors after the thermal-hydraulic calculations. There are actually three separate iterations to determine the end-of-step values of saturation ratio, S , and the vapor/aerosol temperature, T_b , inside the bubbles. The error tolerances and iteration limits associated with these calculations for saturation, energy and temperature are implemented in sensitivity coefficient array 7150, and have default values that normally yield reasonable accuracy with acceptable computational cost.

E.3 Particle Scrubbing in the Bubbles

Particle scrubbing in the bubbles is the result of a net flux of particles to the bubble boundary, where they are assumed to be absorbed into the pool with perfect efficiency. The decontamination factor during a time interval is defined to be the mass of particles in the bubble at the beginning of the interval divided by the mass of particles in the bubble at the end of the interval. It is assumed that particle removal in the bubble can be modeled as a first-order process as follows:

$$\frac{d c_i}{d t} = - \left[\frac{1}{v_b} \int A_{surf} V_{n,i} d A \right] c_i \quad (E.12)$$

where c_i is the concentration of particles of size i in the bubble, v_b is the bubble volume and $V_{n,i}$ is the velocity of the particles normal to (toward) the surface of the bubble, A_{surf} . The decontamination factor during a time interval, Δt , is obtained from the solution to this equation and is given by

$$DF_{BB,i} = \exp\left[\frac{\Delta t}{v_b} \int A_{surf} V_{n,i} dA\right] \quad (E.13)$$

The particle velocity normal to the surface is given by the normal component of the vector sum of the velocities associated with the individual deposition mechanisms

$$V_{n,i} = V_{c,i} + V_{D,i} - V_{g,i} \cos \beta - V_v \quad (E.14)$$

where β is the angle between the normal vector and vertical. For the assumed elliptical geometry (the cross section of an oblate spheroid), β is given by

$$\beta = \tan^{-1}\left[\frac{b^2 \tan \theta}{a^2}\right] \quad (E.15)$$

where θ is the polar angle between the vertical and the ray that runs from the origin to the given point on the ellipse (θ runs from 0 to π from the top to the bottom of the bubble).

For particles with a diameter less than about 70 microns, the gravitational settling velocity, $V_{g,i}$, follows Stokes's law and is given by

$$V_{g,i} = \frac{\rho_i g S_i d_i^2}{18 \mu} \quad (E.16)$$

where S_i is the Cunningham slip correction factor. For larger particles, a set of empirical correlations is used to determine the Reynolds number, from which $V_{g,i}$ follows

$$f(\text{Re}) = \frac{4 \rho_i \rho_g g d_i^3}{3 \mu^2} \quad (E.17)$$

$$\begin{aligned}
 Re &= [f(Re)/27.00]^{1/1.130} \text{ if } 9.6 < f(Re) < 93.6 \\
 &= [f(Re)/24.32]^{1/1.227} \text{ if } 93.6 \leq f(Re) < 410. \\
 &= [f(Re)/15.71]^{1/1.417} \text{ if } 410. \leq f(Re) < 1.07 \times 10^4 \\
 &= [f(Re)/6.477]^{1/1.609} \text{ if } 1.07 \times 10^4 \leq f(Re) < 2.45 \times 10^5 \\
 &= [f(Re)/1.194]^{1/1.867} \text{ if } 2.45 \times 10^5 \leq f(Re)
 \end{aligned}
 \tag{E.18}$$

$$V_{g,i} = \frac{\mu Re}{\rho_g d_i}
 \tag{E.19}$$

The centrifugal capture velocity, $V_{c,i}$, can be obtained from the gravitational settling velocity by scaling it by the ratio of the centrifugal acceleration to the acceleration of gravity (even though the original derivation is based on the concept of particle mobility)

$$V_{c,i} = V_{g,i} \left(\frac{V_s^2 / r_c}{g} \right)
 \tag{E.20}$$

The local surface velocity, V_s , is calculated by assuming that flow around the rising bubbles is essentially steady three-dimensional, axisymmetric, inviscid, incompressible, irrotational (potential) flow around an oblate spheroid. The stream function, ψ , for this flow can be found by solving the irrotational vorticity equation ($\nabla \times V = 0$) with $V = \nabla \times (0, 0, \Psi/\sigma)$ chosen to satisfy the continuity equation ($\nabla \cdot V = 0$) identically. The solution is effected by using a conformal mapping to transform the equations from cylindrical (radial coordinate σ) to elliptical coordinates. (It can be shown that the equations reduce to those for flow around a sphere as $a/b \rightarrow 1$.) V_s and the radius of curvature of the surface, r_c , which are used to calculate centrifugal acceleration in Equation (E.20) above are given by the following

$$V_s = \frac{-V_r (r \sin \theta / a)}{\left[(r \cos \theta / b)^2 + \sinh^2 \xi_o \right]^{1/2}} \frac{1}{\left[\sinh \xi - \cosh^2 \xi_o \cot^{-1}(\sinh \xi_o) \right]} \quad (E.21)$$

$$r_c = \frac{1}{a b} \left[\frac{a^4 \cos^2 \theta + b^4 \sin^2 \theta}{a^2 \cos^2 \theta + b^2 \sin^2 \theta} \right]^{3/2}$$

where

$\sinh \xi_o$	$[(a/b)_2 - 1]^{-1/2}$
$\cosh \xi_o$	$[1 - (b/a)^2]^{-1/2}$
r	$[(\sin \theta / a)^2 + (\cos \theta / b)^2]^{-1/2}$ (radial coordinate)
θ	spherical polar coordinate ($0 \leq \theta \leq \pi$)

Note that V_s is presented in spherical coordinates rather than the elliptical coordinates used in the derivation.

The local diffusional deposition velocity, $V_{D,i}$, from Brownian diffusion can be estimated from penetration theory of mass transfer

$$V_{D,i} = \left(\frac{D_i}{\pi \tau_e} \right)^{1/2} \quad (E.22)$$

where the diffusion coefficient for the aerosol particles, D_i , can be calculated using the Stokes-Einstein equation

$$D_i = \frac{k_B T S_i}{3 \pi \mu D_i} \quad (E.23)$$

where k_B is the Boltzmann constant and T is the gas temperature in the bubble. The exposure time of the moving surface, τ_e , in Equation (E.22) is the integrated value of the arc length divided by the local surface velocity starting from $\tau_e = 0$ at the top of the bubble. When evaporation is occurring at the surface of the bubble, the diffusion velocity from Equation (E.22) is reduced as follows

$$V'_{D,i} = \xi_i V_{D,i} \quad (E.24)$$

where

$$\xi_i = \frac{\exp(-\phi_i^2)}{2 - \exp(-1.85\phi_i)} \quad (\text{E.25})$$

and the parameter ϕ is equal to $V_w/V_{D,i}$.

The normal component of the deposition velocity given by Equation (E.14) is limited to a minimum value of $V_{D,i}$ and then integrated over the entire bubble surface in Equation (E.13) to get $DF_{BB,i}$, which is used in Equation 2.7.2 in Section 2.7.1.

Appendix F: Iodine Vapor Scrubbing in the Swarm Rise Region

In the swarm rise region, the scrubbing of I_2 and CH_3I is controlled by diffusion of those species. The resistance to diffusion on both sides of the pool/bubble interface is considered to evaluate effective diffusion velocities through the gas and through the liquid. As discussed in Appendix D, in the swarm rise region it is assumed that bubble circulation continually renews the bubble interface and that the film theory of mass transfer resistance holds on both sides of the interface. Because the boundary layer thickness and mass transport through it are functions of the angular position around the rising bubbles, the decontamination factors for each spatial rise step must be evaluated by numerically integrating diffusion velocity over the polar angle of the assumed spherical bubble geometry. Hence, the decontamination factors are given by Equation (E.13) with the particle deposition velocity, $V_{n,i}$, replaced by the gaseous diffusion velocities for I_2 and CH_3I , $V_{D,j}$ ($j = I_2$ or CH_3I), given by (brackets refer to concentrations)

$$V_{D,j} = V'_{D(g),j} \left\{ \frac{\exp\left[-\left(V_v / V'_{D(g),j}\right)^2\right]}{2 - \exp\left[-1.85 \left(V_v / V'_{D(g),j}\right)\right]} \right\}$$

$$V'_{D(g),j} = \frac{1}{[i(g)]} \left\{ V''_{D(g),j} \left([i(g)] - [i(g)]_i \right) \right\} \quad (F.1)$$

$$V''_{D(g),j} = \left(\frac{D_{g,j} V_\ell}{\pi \ell} \right)^{\frac{1}{2}}$$

where the subscript i indicates the concentration is evaluated at the gas/liquid interface. $[i(g)]_i$ is determined by equating the concentration flux from the gas to the interface with the flux from the interface to the pool as follows

$$V''_{D(g),j} \left([i(g)] - [i(g)]_i \right) = V''_{D(l),j} \left(H(l_j) [i(g)]_i - \sum [i(aq)] \right) \quad (F.2)$$

where (g) and (l) indicate the diffusion coefficient applies to the gas and liquid phase, respectively, and $H(l_j)$ is the partition coefficient for species j . Gaseous concentrations in the bubble are updated after each spatial step. However, it is assumed that the total iodine concentration in the pool does not change significantly during the transit time of bubbles (vent depth divided by average swarm velocity) so that its value is updated only at the beginning of each MELCOR system timestep.

RN Package Reference Manual

The total liquid molar concentration of iodine is given by

$$\sum [I_{2(aq)}] = 0.5 [I^-] + 1.5 [I_3^-] + [I_{2(aq)}] + 0.5 [HIO] + 0.5 [H_2OI^+] \quad (F.3)$$

CH₃I is the only organic iodine species considered, and its temperature-dependent partition coefficient is given by the following correlation:

$$H_{IO} = \frac{T}{10^{-1388.89/T + 6.461}} \quad (F.4)$$

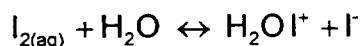
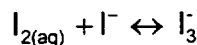
and the constants in the exponent of the denominator have been implemented as sensitivity coefficient array 7158. The partition coefficient of inorganic iodine, H(I₂), is updated during each spatial step by determining the pool equilibrium inorganic iodine species concentrations and solving for H(I₂) as follows

$$H(I_2) = \frac{\sum [I_{2(aq)}]_{(eq)}}{\sum [I_{2(aq)}]_{(eq)}/K_1} = \frac{\sum [I_{2(aq)}]_{(eq)}}{[I_{2(aq)}]_{(eq)}} \quad (F.5)$$

where K₁ is the equilibrium constant for the first reaction listed in Equation (F.6) below.

Hence, in the SPARC-90 treatment of I₂ vapor scrubbing, the major task involves determining the equilibrium concentrations of inorganic iodine species, which can be used to calculate an appropriate value of H(I₂) from Equation (F.5). The equilibrium concentrations of the inorganic iodine species are obtained by considering a limited set of chemical reactions involving inorganic iodine. At equilibrium, this set of reactions yields a set of simultaneous algebraic equations that relate the equilibrium concentrations of the various reactants and products to one another. The solution of this set of equations determines the required equilibrium concentrations of the inorganic iodine species.

In SPARC-90 it is assumed that the equilibrium concentration of the most important inorganic iodine species is determined by the equilibrium solution for the following set of fast reactions



Slow aqueous reactions that affect the concentrations of these species, including radiation-induced pH changes, are not modeled in SPARC-90. However, if accident sequences provide excess CsOH as expected (pH remains high), the models might still be adequate.

At equilibrium the relationship between the reactants and products in Equation (F.6) is given by

$$[I_{2(aq)}]_{(eq)} = K_1 [I_{2(g)}]_{(eq)} \quad (F.7)$$

$$[I_3^-]_{(eq)} = K_2 [I_{2(aq)}]_{(eq)} [I^-]_{(eq)} \quad (F.8)$$

$$[H^+]_{(eq)} [I^-]_{(eq)} [HIO]_{(eq)} = K_3 [I_{2(aq)}]_{(eq)} \quad (F.9)$$

$$[H_2OI^+]_{(eq)} [I^-]_{(eq)} = K_4 [I_{2(aq)}]_{(eq)} \quad (F.10)$$

$$[H^+]_{(eq)} [OH^-]_{(eq)} = K_5 \quad (F.11)$$

When Equation (F.10) is solved for $[H_2OI^+]_{(eq)}$ and the result is substituted into Equation (F.3) along with Equation (F.8) for $[I_3^-]_{(eq)}$ the result is [where subscript (eq) is henceforth suppressed]

RN Package Reference Manual

$$\begin{aligned} \Sigma [I_{2(aq)}] = & 0.5 [I^-] + 1.5 K_2 [I_{2(aq)}] [I^-] + [I_{2(aq)}] \\ & + 0.5 [HIO] + 0.5 \frac{K_4 [I_{2(aq)}]}{[I^-]} \end{aligned} \quad (F.12)$$

The electric charge balance between the reactants and products of Equation (F.6) can be reduced to

$$([I^-] - [I^-]_p) + [I_3^-] - [H_2OI^+] - [H^+]^* = 0 \quad (F.13)$$

where the first term in parentheses is $[I^-]$ exclusive of those ions associated with dissolved CsI particles, $[I^-]_p$ which is known and balanced by $[Cs^+]$, and $[H^+]^*$ are protons released by the third reaction in Equation (F.6) (since protons released by the fifth reaction are always balanced by the simultaneous release of $[OH^-]$). Since $[H^+]^*$ must be equal to $[HIO]$ because of the stoichiometry of the third reaction in Equation (F.6), Equation (F.13) reduces to

$$([I^-] - [I^-]_p) + [I_3^-] - [H_2OI^+] - [HIO] = 0 \quad (F.14)$$

Equation (F.14) can be written as

$$([I^-] - [I^-]_p) + K_2 [I_{2(aq)}] [I^-] - \frac{K_4 [I_{2(aq)}]}{[I^-]} - [HIO] = 0 \quad (F.15)$$

by using the same substitutions that were used to reduce Equation (F.3) to Equation (F.12). From Equation (F.9) $[HIO]$ becomes

$$HIO = \frac{K_3 [I_{2(aq)}]}{[H^+] [I^-]} \quad (F.16)$$

where $[H^+]$ is given by

$$[H^+] = [HIO] + ([OH^-] - [OH^-]_p) \quad (F.17)$$

The first term on the right-hand side ($[HIO]$) are protons released by the third reaction in Equation (F.6) and the term in parentheses are protons released by the fifth reaction, which also releases that portion of $[OH^-]$ exclusive of the $[OH^-]$ associated with dissolved

CsOH ($[\text{OH}^-]_p$ which is known). Substituting Equation (F.11) into Equation (F.17) and rearranging the result yields

$$[\text{H}^+]^2 - ([\text{HIO}] - [\text{OH}^-]_p)[\text{H}^+] - K_5 = 0 \quad (\text{F.18})$$

This quadratic equation for $[\text{H}^+]$ has the solution

$$[\text{H}^+] = \frac{1}{2} \left\{ ([\text{HIO}] - [\text{OH}^-]_p) + \left\{ ([\text{HIO}] - [\text{OH}^-]_p)^2 + 4 K_5 \right\} \right\} \quad (\text{F.19})$$

which may be substituted into Equation (F.16) to give

$$[\text{HIO}] = \frac{2K_3[\text{I}_{2(\text{aq})}]/[\text{I}^-]}{([\text{HIO}] - [\text{OH}^-]_p) + \left\{ ([\text{HIO}] - [\text{OH}^-]_p)^2 + 4 K_5 \right\}^{1/2}} \quad (\text{F.20})$$

Equation (F.20) can be put in the form of a quadratic equation for $[\text{HIO}]$ and solved to give

$$[\text{HIO}] = \frac{[\text{OH}^-]_p + \left\{ [\text{OH}^-]_p^2 + 4 \left(K_5 + \frac{K_3[\text{I}_{2(\text{aq})}]}{[\text{I}^-]} \right) \right\}^{1/2}}{2 \left(1 + \frac{K_5[\text{I}^-]}{K_3[\text{I}_{2(\text{aq})}]} \right)} \quad (\text{F.21})$$

Equation (F.21) can be substituted into Equations (F.12) and (F.15) to yield two equations in two unknowns, $[\text{I}^-]$ and $[\text{I}_{2(\text{aq})}]$, which may be solved iteratively to determine the desired equilibrium concentrations.

A simplification to the procedure just described arises if $[\text{OH}^-]$, including $[\text{OH}^-]_p$, is very large ($\text{pH} > 9$ because of large amounts of dissolved CsOH). Then $[\text{OH}^-]$ remains essentially constant so that $[\text{H}^+]$ is given from Equation (F.11) as

$$[\text{H}^+] = \frac{K_5}{[\text{OH}^-]_p} \quad (\text{F.22})$$

and Equation (F.15) becomes

RN Package Reference Manual

$$([\text{I}^-] - [\text{I}^-]_p) + K_2 [\text{I}_{2(\text{aq})}] [\text{I}^-] - \frac{K_4 [\text{I}_{2(\text{aq})}]}{[\text{I}^-]} - \frac{K_3 [\text{I}_{2(\text{aq})}]}{[\text{H}^+] [\text{I}^-]} = 0 \quad (\text{F.23})$$

which may be written as a quadratic in $[\text{I}^-]$ as follows

$$(1 + K_2 [\text{I}_{2(\text{aq})}]) [\text{I}^-]^2 - [\text{I}^-]_p [\text{I}^-] - \left(K_4 + \frac{K_3}{[\text{H}^+]} \right) [\text{I}_{2(\text{aq})}] = 0 \quad (\text{F.24})$$

Equation (F.24) has the solution

$$[\text{I}^-] = \frac{[\text{I}^-]_p + \left\{ [\text{I}^-]_p^2 + 4(1 + K_2 [\text{I}_{2(\text{aq})}]) \left(K_4 + \frac{K_3}{[\text{H}^+]} \right) [\text{I}_{2(\text{aq})}] \right\}^{1/2}}{2(1 + K_2 [\text{I}_{2(\text{aq})}])} \quad (\text{F.25})$$

in terms of an assumed $[\text{I}_{2(\text{aq})}]$. Then $[\text{HIO}]$ follows immediately from Equation (F.16) and the assumed $[\text{I}_{2(\text{aq})}]$. Now if the resulting $[\text{I}^-]$, $[\text{HIO}]$ and assumed $[\text{I}_{2(\text{aq})}]$ are substituted into the right-hand side of Equation (F.12), the result may be compared to the known value of $\sum [\text{I}_{2(\text{aq})}]$ (obtained from the MELCOR RN data base at the beginning of each system timestep). If the discrepancy is significant, then a new value of $[\text{I}_{2(\text{aq})}]$ is assumed and the procedure is repeated until convergence is obtained.

Hence, at each spatial step in the rise of the bubbles from the vent exit region to the pool surface, the equilibrium concentrations of all the species in Equation (F.6) are updated. This is accomplished iteratively (with an error tolerance implemented in sensitivity coefficient array 7159) using the equilibrium constants for each reaction (which are temperature dependent and also implemented in sensitivity coefficient array 7159) and requiring conservation of the total iodine mass and electric charge.

References

1. D. A. Powers, J. L. Sprung, and C. D. Leigh, "Isotopes, Elements, and Chemical Classes," in Fission Product Behavior During Severe LWR Accidents: Recommendations for the MELCOR Code System, Sandia National Laboratories, Albuquerque, NM (1988).
2. D. E. Bennett, SANDIA-ORIGEN User's Manual, NUREG/CR-0987, SAND79-0299, Sandia National Laboratories, Albuquerque, NM (October 1979).
3. R. M. Ostmeyer, An Approach to Treating Radionuclide Decay Heating for Use in the MELCOR Code System, SAND84-1404, NUREG/CR-4169 (May 1985).
4. M. R. Kuhlman, D. J. Lehmicke, and R. O. Meyer, CORSOR User's Manual, BMI-2122, NUREG/CR-4173 (March 1985).
5. M. Ramamurthi and M. R. Kuhlman, Final Report on Refinement of CORSOR—An Empirical In-Vessel Fission Product Release Model, Battelle Memorial Institute (October 31, 1990).
6. D. A. Powers, J. E. Brockmann, and A. W. Shiver, Vanessa: A Mechanistic Model of Radionuclide Release and Aerosol Generation During Core Debris Interactions with Concrete, SAND85-1370, NUREG/CR-4308 (September 1985) Draft.
7. F. Gelbard, MAEROS User Manual, SAND80-0822, NUREG/CR-1391 (December 1982).
8. H. Jordan and M. R. Kuhlman, TRAP-MELT2 User's Manual, BMI-2124, NUREG/CR-4205 (May 1985).
9. B. J. Mason, The Physics of Clouds, Clarendon, Oxford, UK (1971).
10. P. C. Owczarski and K. W. Burk, SPARC-90: A Code for Calculating Fission Product Capture in Suppression Pools, NUREG/CR-5765, PNL-7723, Pacific Northwest Laboratory, Richland, WA (October 1991).
11. S. E. Dingman, A. L. Camp, C. C. Wong, D. B. King, and R. D. Gasser, HECTR Version 1.5 User's Manual, NUREG/CR-4507, SAND86-0101, Sandia National Laboratories, Albuquerque, NM (February 1986).
12. R. A. Lorenz, E. C. Beahm, and R. P. Wichner, "Review of Tellurium Release Rates from LWR Fuel Elements Under Accident Conditions," Proceedings International Meeting on Light Water Reactor Severe Accident Evaluation (1983).

RN Package Reference Manual

13. T. Nakamura and R. A. Lorenz, "Effective Diffusion Coefficients Calculated from ORNL FP Release Test Results," Oak Ridge National Laboratory Research Paper (April 1989).
14. T. Nakamura and R. A. Lorenz, "A Study of Cesium and Krypton Releases Observed in HI and VI Tests Using a Booth Diffusion Model," Oak Ridge National Laboratory Research Paper (May 1987).
15. J. A. Gieseke, P. Cybulskis, R. S. Denning, M. R. Kuhlman, K. W. Lee, and H. Chen, Radionuclide Release Under Specific LWR Accident Conditions, BMI-2104 (July 1984).
16. R. K. Cole, Jr., D. P. Kelly, and M. A. Ellis, CORCON-Mod2: A Computer Program for Analysis of Molten-Core Concrete Interactions, SAND84-1246, NUREG/CR-3920, Sandia National Laboratories, Albuquerque, NM (August 1984).
17. I. H. Dunbar and S. N. Ramsdale, "Improvements in the Modeling of Sedimentation and Gravitational Agglomeration," CSNI Specialists' Meeting on Nuclear Aerosols in Reactor Safety, Karlsruhe, Germany (September 4-6, 1984).
18. D. C. Williams, K. D. Bergeron, P. E. Rexroth, and J. L. Tills, "Integrated Phenomenological Analysis of Containment Response to Severe Core Damage Accidents," Progress in Nuclear Energy, Vol. 19 (1987).
19. F. Gelbard, "Modeling Aerosol Growth by Vapor Condensation," Aerosol Science and Technology, 12, p. 399 (1990).
20. W. C. Hinds, Aerosol Technology, John Wiley & Sons, New York (1982).
21. L. F. Shampine and H. A. Watts, Practical Solution of Ordinary Differential Equations by Runge-Kutta Methods, SAND76-0585, Sandia National Laboratories, Albuquerque, NM (1976).
22. J. R. Welty, C. E. Wicks, and R. E. Wilson, Fundamentals of Momentum, Heat, and Mass Transfer, John Wiley & Sons, New York (1984).
23. R. B. Bird, W. E. Stewart, and E. N. Lightfoot, Transport Phenomena, John Wiley & Sons, New York (1960).
24. A. K. Postma, et al., Models for Predicting the Removal of Airborne Contaminants by Reactor Containment Sprays, BNWL-B-417 (1975).
25. A. K. Postma, et al., Technological Bases for Models of Spray Washout of Airborne Contaminants in Containment Vessels, NUREG/CR-0009 (1978).

26. A. E. J. Eggleton, Theoretical Examination of Iodine-Water Partition Coefficients, AERE-R-4887 (1967).
27. A. K. Postma and W. F. Pasedag, A Review of Mathematical Models for Predicting Spray Removal of Fission Products in Reactor Containment Vessels, WASH-1329 (1973).
28. A. E. J. Eggleton, Theoretical Examination of Iodine-Water Partition Coefficients, AERE-R-4887 (1967).
29. N. Frossling, Gerlands Beitr. Geophys., 52, p. 170 (1938), as cited in Ref. [23] p. 409.
30. V. Griffiths, The Removal of Iodine from the Atmosphere of Sprays, Report No. AHSB(S)R45, UKAEA, London, England (1963).
31. D. R. Grist, Spray Removal of Fission Products in PWR Containments, Report SRD R267, Safety and Reliability Directorate, UKAEA, England (1982).
32. N. A. Fuchs, The Mechanics of Aerosols, Pergamon Press, New York (1964).
33. I. Langmuir, J. Meteor, 5, 175 (1948).
34. T. J. Heames and R. M. Summers, "Fission Product Surface Chemistry Model Preliminary Design Report," (1995).
35. Pruppacher, H.R. and J.D. Klett, *Microphysics of Clouds and Precipitation*, D. Reidel Publishing Co. Dordrecht, Holland (1980).
36. Gauntt, R.O., et al, "MELCOR Computer Code Reference Manual," NUREG/CR-6119, Vol. 2, Rev. 1 (May 1998).
37. Murata, K.K. et al, "Code Manual for CONTAIN 2.0," p. 7-20, NUREG/CR-6533, Dec 1997.
38. L. Soffer et al., "Accident Source Terms for Light Water Nuclear Power Plants," NUREG-1465 (1995).
39. E. C. Beahm, R.A. Lorenz, and C.F. Weber, "Iodine Evolution and pH Control," NUREG/CR-5950, TI93-005714 (1992).
40. C. F. Weber, E. C. Beahm, T. S. Kress, "Models of Iodine Behavior in Reactor Containments," ORNL/TM-12202 (1992).
41. J. N. Butler, *Ionic Equilibrium, a Mathematical Approach*, Addison Wesley (1964).

RN Package Reference Manual

42. H. Sims et al., "Iodine Code Comparison," EUR 16507 EN, European Commission, Luxembourg (1995).
43. S. Dickinson and H. E. Sims, "Modifications to the INSPECT Model", Proc. 4th OECD Workshop on Iodine Chemistry in Reactor Safety, Paul Scherrer Institute, Switzerland (1996).
44. D. A. Powers, R. K. Cole, and T. J. Heames, "A Simplified Model of Iodine Chemistry for MELCOR," submitted as part of the Preliminary Design Report for Iodine Aqueous Chemistry: Task 1.2 W6203, Sandia National Laboratories, Albuquerque, NM (1998).
45. K. H. Haskell, W. H. Vandevender, and W. L. Walton, "The SLATEC Common Mathematical Subprogram Library: SNLA Implementation," SAND80-2792, Sandia National Laboratories, Albuquerque, NM (1980).
46. G. V. Buxton et al., *J. Phys. Chem. Ref. Data*, Vol. 17, p. 513 (1988).
47. A. J. Elliott, M. P. Chenier, and D. C. Ouellette, *Canadian J. Chemistry*, Vol. 68, p. 712 (1990).
48. R. A. Barton and H. E. Sims, "A Comparison of the Predictions of the INSPECT Reaction Set with Experimental Data", Proc. Third CSNI Workshop on Iodine Chemistry, p. 346, JAERI-M-92-012. NEA/CSNI/R(91)15, Japan Atomic Energy Research Institute, Tokai-mura, Naka-gun, Ibaraki-ken, Japan (1992).
49. L. M. Toth, K. D. Pannell, and O. L. Kirkland, "The Aqueous Chemistry of Iodine", Proc. Fission Product Behavior and Source Term Research, NP-4113-SR, American Nuclear Society, Utah (1984).
50. M. Furrer, R. C. Cripps, and E. Frick, "Iodine Severe Accident Behavior Code IMPAIR 2", PSI Bericht Nr. 25, Paul Scherrer Institute, CH-5232 Villigen/PSI, Switzerland (1989).
51. A. A. Frost and R. G. Pearson, *Kinetics and Mechanism*, 2nd Edition, John Wiley & Sons (1961).
52. A. C. Vikis and R. MacFarlane, *J. Phys. Chem.*, Vol. 89, p. 812 (1985).
53. N. H. Sagert, "Radiolysis of Iodine in Moist Air: A Computer Study", Proc. 2nd CSNI Workshop on Iodine Chemistry in Reactor Safety, AECL-9923, CSNI-149, Atomic Energy of Canada Ltd., Toronto, Canada (1989).
54. A. M. Deane, "Organic Iodine Chemistry Relevant to Nuclear Reactors: A Review", AERE-R-12359, Harwell, Oxfordshire, UK (1988).

55. J. C. Wren, G. A. Glowa, and J. M. Ball, "Modeling Iodine Behaviour Using LIRIC 3.0," Proc. Fourth CSNI Workshop on the Iodine Chemistry in Reactor Safety, Wurenlingen, Switzerland, pp.507 – 530 (1996).
56. G. J. Evans et al., "Preliminary Results from the ACE/RTF Tests 1, 2, and 3", ACE-TR-B3 (1991).
57. C. Hueber, M. Lucas, and J. Gauvain, "Validation of the IODE Code on Analytical Experiments", in "Third CSNI Workshop on Iodine Chemistry in Reactor Safety", JAERI-M-92-012 (1991).
58. M. F. Young, and R. O. Gauntt, "Simulation of the ISP41 Iodine Test Problem with the MELCOR Iodine Model", in ISP-41 Containment Iodine Computer Code Exercise Based on a Radioiodine Test Facility Experiment, NEA/CSNI/R(2000)6/Vol.1 and 2 (1999).
59. L. N. Kmetyk, MELCOR 1.i.1 Assessment: Marviken-V Aerosol Transport Tests ATT-2b/ATT-4, SAND92-2243, Sandia National Laboratories, Albuquerque, NM (January 1993).

Containment Sprays (SPR) Package Reference Manual

The Containment Sprays (SPR) package models the heat and mass transfer between spray water droplets and the containment building atmosphere. The SPR package models were extracted from the HECTR 1.5 code.

This reference manual describes the models employed in the SPR package. Detailed descriptions of the user input requirements can be found in the SPR Package Users' Guide.

Contents

1. Introduction5

2. Model Description5

References9

1. Introduction

Where possible, MELCOR uses a generic building-block approach to modeling engineered safety features (ESFs) through use of control volumes, flow paths, heat structures, and control functions. However, for containment sprays, separate models tailored to this system have been implemented in MELCOR.

The MELCOR Containment Sprays (SPR) package models the heat and mass transfer resulting from operation of containment spray systems. The removal of fission product vapors and aerosols by ESFs is modeled within the RadioNuclide (RN) package. See the RN Package Reference Manual for details on this modeling.

2. Model Description

The Containment Sprays (SPR) package models the heat and mass transfer between spray droplets and the containment building atmosphere. The modeling in the SPR package was taken virtually intact from the HECTR 1.5 code [1], following the recommendations of the MELCOR phenomena assessment on modeling containment spray systems [2]. The model assumes, among other things, that spray droplets are spherical and isothermal and that they fall through containment atmospheres at their terminal velocity with no horizontal velocity components.

An arbitrary number of spray sources may be placed at various heights in any containment control volume. The source of water for each spray may be associated with the pool in any CVH control volume or it may be left unspecified. If a CVH pool is specified as the spray source reservoir, then input ("dryout" pool depth) may be specified to determine whether there is sufficient water in the pool to permit spray operation. Input (resumption pool depth) may also be specified to determine when spray operation may resume following "dryout". If the pool depth for spray source resumption exceeds the pool depth for spray source "dryout", then there will be hysteresis in the spray operation curve that will prevent excessive cycling between episodes of spray operation. In a special application, the spray model also receives water from the Heat Structures (HS) package film-tracking model whenever rain from inverted HS surfaces enters the containment atmosphere.

For each spray source, except for sources associated with rain from the HS film-tracking model, the user must specify an initial droplet temperature and flow rate, each of which may be controlled by a control function. The user may turn the sprays on and off with a separate control function for each spray source. A droplet size distribution also may be input for each spray source. In other words, the spray droplets for each source may be divided into a number of different size bins, with individual drops representing the average droplet size being tracked during their fall through the control volume; the total heat and mass transfer for the spray source is obtained by summing the heat and mass transfer calculated for each size.

SPR Package Reference Manual

For each droplet type in each control volume, the following differential equations are solved to determine the heat and mass transfer rates and the terminal fall velocity as a function of drop size:

$$\frac{dm}{dt} = -2\pi \rho_g D (1 + 0.25 \text{Re}^{1/2} \text{Sc}^{1/3}) D_c \ln(1 + B) \quad (2.1)$$

$$\frac{dT}{dt} = \frac{1}{m c_{pl}} \left[\frac{c_{pv} (T - T_{cv})}{(1 + B)^{1/Le} - 1} + h_{fg} \right] \frac{dm}{dt} \quad (2.2)$$

$$\frac{dz}{dt} = \left[\frac{4(\rho_d - \rho_g) g D}{3\rho_g C_d} \right]^{1/2} \quad (2.3)$$

In these equations, the terms are defined as

- m = droplet mass,
- T, T_{cv} = droplet, control volume atmosphere temperatures,
- z = droplet fall height,
- ρ_d, ρ_g = droplet, atmosphere densities,
- c_{pl} = droplet specific heat capacity,
- c_{pv} = control volume atmosphere specific heat capacity,
- h_{fg} = latent heat of vaporization,
- D = droplet diameter,
- Re = Reynolds number,
- Sc = Schmidt number,
- Le = Lewis number,
- D_c = diffusion coefficient,
- C_d = drag coefficient,

and B is the mass transfer driving force

$$B = \frac{x_b - x_i}{x_i - 1} \tag{2.4}$$

where x_b and x_i are H₂O mass fractions in the bulk atmosphere and at the liquid-gas interface (corresponding to saturation). Equations (2.1) through (2.4) are based on forced convection heat transfer and evaporation and condensation correlations that have been formulated specifically for high temperature atmospheres, such as might be encountered during a hydrogen burn [3]. The constants in Equation (2.1) have been implemented in sensitivity coefficient array 3001.

Correlations for the drag coefficient of spheres, C_d , are used for the following Reynolds number regimes, with the various constants implemented in sensitivity coefficient array 3000:

$$c_d = 27\text{Re}^{-0.84} \quad \text{for } \text{Re} < 78 \tag{2.5}$$

$$c_d = 0.271\text{Re}^{0.217} \quad \text{for } 78 < \text{Re} < 10000 \tag{2.6}$$

$$c_d = 2 \quad \text{for } 10,000 < \text{Re} \tag{2.7}$$

The transfer rates given by Equations (2.1) through (2.3) are integrated by a Runge-Kutta method over the fall height of the spray droplet to obtain the final droplet mass and temperature. By comparing the droplet mass and temperature at the bottom of the compartment to the inlet conditions, the heat transfer and mass transfer to a given droplet are computed. Total heat and mass transfer rates are calculated by multiplying the rates for one droplet by the total number of droplets of that size and summing over all droplet sizes. It is assumed that this total heat and mass transfer rate is constant over a given timestep, and it is also assumed that the containment atmosphere conditions do not change significantly during the fall time of the drop.

The user can describe how droplets falling from one control volume are to be carried over to lower volumes. A control volume may be designated as the containment spray sump. Droplets leaving designated control volumes and not carried over to other volumes will be placed in the pool of the sump. Droplets reaching the bottom of a control volume and not being carried over to other volumes or placed in the sump are put into the pool of the control volume.

It should be noted that the SPR package does not model interactions between spray droplets and other structures (nor does any other MELCOR package). Thus, it is not possible to model either core sprays or steam generator auxiliary feed water sprays properly using the SPR package.

SPR Package Reference Manual

The SPR package is coupled to the RadioNuclide (RN) package for the calculation of aerosol washout and atmosphere decontamination by the sprays. Current limitations of this interface require some restrictions on the input to the SPR package to avoid nonphysical results associated with multiple calculations in the same control volume. When the SPR and RN packages are both active, the user should limit the spray input so that only one spray train passes through each control volume and only a single drop size is used in this spray train.

References

1. S. E. Dingman, A. L. Camp, C. C. Wong, D. B. King, and R. D. Gasser, HECTR Version 1.5 User's Manual, NUREG/CR-4507, SAND86-0101, Sandia National Laboratories, Albuquerque, NM (February 1986).
2. G. G. Weigand, ed., Thermal-Hydraulic Process Modeling in Risk Analysis: An Assessment of the Relevant Systems, Structures, and Phenomena, SAND84-1219, NUREG/CR-3986, Sandia National Laboratories, Albuquerque, NM (August 1984).
3. F. A. Williams, Combustion Theory, Addison-Wesley, Reading, MA (1965).

BIBLIOGRAPHIC DATA SHEET

(See instructions on the reverse)

1. REPORT NUMBER
(Assigned by NRC, Add Vol., Supp., Rev.,
and Addendum Numbers, if any.)

NUREG/CR-6119, Vol. 2
Rev. 2
SAND2000-2417/1

3. DATE REPORT PUBLISHED

MONTH | YEAR

December | 2000

4. FIN OR GRANT NUMBER

W6203

6. TYPE OF REPORT

Technical

7. PERIOD COVERED (Inclusive Dates)

TITLE AND SUBTITLE

MELCOR Computer Code Manuals

Reference Manuals
Version 1.8.5

5. AUTHOR(S)

R.O. Gauntt, R.K. Cole, C.M. Erickson, R.G. Gido,
R.D. Gasser, S.B. Roderiguez, M.F. Young

8. PERFORMING ORGANIZATION - NAME AND ADDRESS (If NRC, provide Division, Office or Region, U.S. Nuclear Regulatory Commission, and mailing address; if contractor, provide name and mailing address.)

Sandia National Laboratories
Albuquerque, NM 87185-0739

9. SPONSORING ORGANIZATION - NAME AND ADDRESS (If NRC, type "Same as above"; if contractor, provide NRC Division, Office or Region, U.S. Nuclear Regulatory Commission, and mailing address.)

Division of Systems Analysis and Regulatory Effectiveness
Office of Nuclear Regulatory Research
U.S. Nuclear Regulatory Commission
Washington, DC 20555-0001

10. SUPPLEMENTARY NOTES

11. ABSTRACT (200 words or less)

MELCOR is a fully integrated, engineering-level computer code that models the progression of severe accidents in light water reactor nuclear power plants. MELCOR is being developed at Sandia National Laboratories for the U.S. Nuclear Regulatory Commission as a second-generation plant risk assessment tool and the successor to the Source Term Code Package. A broad spectrum of severe accident phenomena in both boiling and pressurized water reactors is treated in MELCOR in a unified framework. These include thermal-hydraulic response in the reactor coolant system, reactor cavity, containment, and confinement buildings; core heatup, degradation, and relocation; core-concrete attack; hydrogen production, transport, and combustion; fission product release and transport behavior. This publication of the MELCOR computer code manuals corresponds to MELCOR 1.8.5. Volume 1 contains a primer that describes MELCOR's phenomenological scope, organization (by package), and documentation. The remainder of Volume 1 contains the MELCOR User's Guides, which provide the input instructions and guidelines for each package. Volume 2 contains the MELCOR Reference Manuals, which describe the phenomenological models that have been implemented in each package.

12. KEY WORDS/DESCRIPTORS (List words or phrases that will assist researchers in locating the report.)

Severe Accident, probabilistic risk assessment (PRA), source term, computer code, fission product transport, core melt progression, core meltdown, containment response, Level-2 PRA

13. AVAILABILITY STATEMENT

unlimited

14. SECURITY CLASSIFICATION

(This Page)

unclassified

(This Report)

unclassified

15. NUMBER OF PAGES

16. PRICE



Federal Recycling Program